



ALMA MATER STUDIORUM  
UNIVERSITÀ DEGLI STUDI DI BOLOGNA  
Facoltà di Scienze Matematiche Fisiche e Naturali

Dottorato di Ricerca in Geofisica  
XXI Ciclo  
Settore scientifico disciplinare: GEO/10

***TECTONICS AND KINEMATICS OF CURVED  
MOUNTAIN BELTS: EXAMPLES FROM THE ALPS  
AND THE ANDES***

*Ph.D. Thesis by:*  
**Marco Maffione**

*Tutor:*  
**Dr. Fabio Speranza**

*Co-tutor:*  
**Dr. Rubén Somoza**

*Supervisor:*  
**Prof. Claudio Faccenna**

*Coordinator:*  
**Prof. Michele Dragoni**

# TABLE OF CONTENTS

<b>PART I. INTRODUCTION TO THE CURVED MOUNTAIN BELTS.....</b>	<b>1</b>
<b>CHAPTER 1. General features, kinematics, and mechanisms of formation.....</b>	<b>2</b>
1. Introduction and aim of the study.....	3
2. Methods.....	6
2.1. Paleomagnetism: potentialities and restrictions.....	6
2.2. Structural analysis.....	9
3. Brief history of the orocline concept.....	10
4. The oroclinal test.....	13
5. Different geometries of orogenic bends.....	18
6. Kinematics of orogenic bends.....	20
6.1. Marshak’s classification of kinematic patterns.....	20
6.1.1. Primary arcs.....	21
6.1.2. Secondary arcs.....	22
7. Mechanisms of orogenic bends formation.....	24
7.1. Nonrotational arcs related to “indenters”.....	25
7.1.1. The problem of tangential extension.....	27
7.1.2. The example from the Carpathian Arc.....	29
7.2. Nonrotational arcs formed along irregular continental margins.....	34
7.2.1. The example from the Appalachian (Pennsylvania, North America).....	34

7.3. Salients associated with obstacles.....	37
7.3.1. The example from the Maghrebian thrust belt of Sicily (Italy).....	38
7.4. Basin-controlled orogenic bends.....	40
7.4.1. The example from the Jura Arc (Northern Alps).....	42
7.5. Topography-driven arcs.....	45
7.5.1. The example from the Hellenic Arc.....	48
7.6. Orogenic arcs linked to the bending of “ribbon continent”.....	53
7.6.1. The example from the Great Alaskan Terrane Wreck.....	53
7.7. Subduction-related arcs.....	56
7.7.1. The example from the Calabrian Arc (southern Italy).....	59
7.8. Oroclines formed by orogen-parallel compression (buckling).....	63
7.8.1. The example from the Cantabria-Asturias Arc (northern Spain).....	64
<b>PART II. THE EXAMPLES FROM THE ALPS AND THE ANDES.....</b>	<b>68</b>
<b>CHAPTER 2. The Western Alpine Arc.....</b>	<b>69</b>
A synchronous Alpine and Corsica-Sardinia rotation.....	70
1. Introduction.....	70
2. Tectonic setting of the Alpine-Apenninic chain in the Mediterranean domain: interplay between Africa-Eurasia convergence and Tertiary roll-back of subducting slab fragments.....	73
3. Previous paleomagnetic evidence from the western Alpine-northern Apennine chain, the Adria and Corsica-Sardinia (micro) plates, and the Tertiary Piedmont Basin.....	73

4. Geological setting of the Tertiary Piedmont Basin.....	75
5. Samplings and methods.....	76
6. Results.....	76
6.1. Biostratigraphy.....	76
6.2. Magnetic mineralogy.....	78
6.3. Anisotropy of magnetic susceptibility.....	80
6.4. Paleomagnetism.....	80
7. Discussion.....	83
7.1. Local vs. uniform rotations at the TPB.....	83
7.2. Magnitude and timing of rotations.....	86
7.3. Rotation of the TPB in the frame of Alpine-Appennine tectonics.....	87
7.4. No paleomagnetic rotation of Adria after mid Miocene times.....	89
7.5. The enigmatic nature of the TPB: information from anisotropy of magnetic susceptibility data.....	89
7.6. The connection between Alps and the Apennines: insight into the mechanism of the Mediterranean Arc formation.....	90
8. Conclusions.....	91
References.....	91
<b>CHAPTER 3. The Bolivian Orocline.....</b>	<b>95</b>
Bending of the Bolivian orocline and growth of the Central Andean plateau: paleomagnetic and structural constraints from the Eastern Cordillera (22-24°S, NW Argentina).....	96
Abstract.....	96

1. Introduction.....	97
2. Background.....	100
2.1. Regional geology.....	100
2.2. Timing of deformation within the Eastern Cordillera and the surrounding regions.....	101
2.3. Previous paleomagnetic studies from the Central Andes and their tectonic implications.....	103
3. Geological setting of the study area.....	105
4. Sampling and methods.....	109
5. Results.....	110
5.1. Magnetic mineralogy.....	110
5.2. Paleomagnetic characteristic directions.....	112
5.3. Structural analysis.....	115
6. Discussion.....	122
6.1. Paleomagnetic rotation pattern from the Eastern Cordillera.....	122
6.2. Oroclinal test: implications for the structural style and deformation timing.....	126
6.3. Style and timing of deformation in the Eastern Cordillera: interplay between compressive and strike-slip tectonics.....	128
6.4. A southward lateral growth of the Puna plateau?.....	132
7. Conclusions.....	134
8. Acknowledgements.....	135
Table 1.....	136
Table 2.....	138

Tables 3.....	139
Tables 4.....	139
<b>CHAPTER 4. THE PATAGONIAN OROCLINE.....</b>	<b>140</b>
Paleomagnetic evidence for a pre-early Eocene (~50 Ma) bending of the Patagonian orocline (Tierra del Fuego, Argentina): paleogeographic and tectonic implications.....	141
Abstract.....	141
1. Introduction.....	142
2. Background.....	146
2.1. Geology of the Patagonian and Fuegian Andes, and structural setting of the Magallanes belt of Tierra del Fuego.....	146
2.2. Previous paleomagnetic data from the Patagonian orocline and the Antarctic Peninsula.....	150
3. Sampling and methods.....	152
4. Results.....	154
4.1. Magnetic mineralogy.....	154
4.2. Anisotropy of magnetic susceptibility.....	156
4.3. Paleomagnetism.....	158
5. Discussion.....	161
5.1. Rotational nature of the Patagonian orocline, and relations with Scotia plate spreading and Drake Passage opening.....	161
5.2. Unravelling the relative relevance and timing of thrust vs. strike-slip tectonics in the Fuegian Andes: evidence from magnetic fabric.....	164

6. Conclusions.....	167
7. Acknowledgements.....	168
Table 1.....	169
Table 2.....	170
<b>PART III. CONCLUSIONS.....</b>	<b>171</b>
<b>Chapter 5. Results, implications, and concluding remarks.....</b>	<b>172</b>
1. Main results and implications from the studied curved belts.....	173
2. Concluding remarks about curved mountain belts and their study.....	175
<b>REFERENCES.....</b>	<b>177</b>

# **PART I**

## **INTRODUCTION TO CURVED MOUNTAIN BELTS**

# **CHAPTER 1**

*General features,  
kinematics,  
and mechanisms of formation*

## 1. Introduction and aim of the study

Curved mountain belts have always fascinated geologists and geophysicists because of the complexities arising from their peculiar structural setting and geodynamic mechanisms of formation. Generally, during the convergence of two lithospheric plates, the mountain building process results in a relatively straight orogenic belt parallel to the plates margins. Thus, the question arises as to why curved mountain belts formed. Since the beginning of the past century, well before the plate tectonics theory was formulated, *Argand* [1924] first, and *Carey* [1955] after, tried to explain the significance of these great-scale curved orogenic structures, being aware of their geodynamic importance.

A huge amount of structural, paleomagnetic, seismological, analogue modelling, and geophysical studies carried out during the last 50 years, have dealt with curved orogenic belts, trying to answer to the following questions: what are the mechanisms governing orogenic bends formation? Why do they form? Do they develop under particular geological conditions? And if so, what are the most favourable conditions to their genesis? What are their relationships with deformational history of the belt? Why is the shape of arcuate orogens in many parts of the Earth so different? What are the factors controlling the shape of orogenic bends?

Relevant contributions to the understanding of the curved mountain belts have been given through time, though several aspects remain still obscure because of the geological complexities of particular orogenic domains. In fact, as we will show in this study, many factors can control arc formation, and only a detailed multidisciplinary approach, not always and everywhere possible, can contribute to the unravelling of the tectonic and geodynamic evolution of complex orogens.

Likely, arcuate structures are not uncommon features in a mountain belt, but rather a logical and simple consequence of the orogenesis. This implies that the answers to the above questions about curved mountain belts can help scientists to understand some basic (and probably not still fully understood) mechanisms of mountain building.

With this study I wish to give a little contribute to the knowledge of orogenic arc formation from different geological contexts. To reach this goal I investigated three very relevant orogenic bends: the Western Alpine Arc (NW Italy), the Bolivian Orocline (Central Andes, NW Argentina), and the Patagonian Orocline (Tierra del Fuego, south Argentina). These regions were selected because of the still open debate on the timing and kinematics of their formation. Also, the geodynamic mechanisms governing the development of bending at these regions are still subject to different, and sometimes contrasting, speculations.

I mainly used paleomagnetism, and, where possible, structural analysis, as research tools. Paleomagnetism is the unique technique able to document the deformation of a belt from the point of view of the pattern of vertical axis rotations. In fact, only paleomagnetism can document the occurrence and timing of a possible bending process. Contextually, a structural analysis was carried out to definite the strain pattern of the area, including tectonic transport directions on fault planes. Brittle fault plane directions, and relative kinematic indicators (i.e., slickensides, mineral fibers growth, SC-structures) were measured in order to unravel the features of the tectonic regime responsible of the mountain building.

I will not discuss in this work the fundamentals of these two techniques because it is out of the aim of this study, and furthermore, paleomagnetism and structural geology

analysis are two well known and extremely diffuse methods. Conversely, I will show how these tools can be properly used in the study of curved mountain belts.

The thesis is composed by three parts: parts I, II, and III. In the first part, I will show the different types of orogenic bends, their classification and kinematics, and their mechanisms of formation, reporting for each one of them a natural example from previous studies. Part II is composed by one published and two submitted papers relative to paleomagnetic investigations I carried out in three different orogens: the Alps, the Central Andes, and the Southernmost Andes. I report on paleomagnetism and structural geology of three striking orogenic bends, the Western Alpine Arc, the Bolivian Orocline, and the Patagonian Orocline, inferring tectonic and geodynamic implications for their evolution.

Finally, in part III I will conjointly discuss the results of this study, also taking into account literature data, making concluding remarks about general aspects of curved mountain belts and their study.

## 2. Methods

### 2.1. Paleomagnetism: potentialities and restrictions

This paragraph does not contain presentation of the paleomagnetic technique, as it is a well known and widely diffuse method in tectonic studies. For the knowledge of fundamentals of paleomagnetism I suggest specific books, such as those by *Tarling* [1983], *Tauxe* [1998], and *Butler* [2004]. On the contrary, I consider more useful showing potentialities and limitations of paleomagnetism in the study of curved mountain belts.

During the past few decades, paleomagnetism has been used as a primary tool to assess kinematic models of curved orogenic systems around the world because of its great potential in quantifying rotations along vertical axes [*Carey*, 1955; *Eldredge et al.*, 1985; *Marshak*, 1988; *Van der Voo et al.*, 1997; *Weil and Sussman*, 2004]. On the basis of the spatial and temporal relationships between deviations in structural trend and the vertical axis rotations observed in a given belt, it has been possible to unravel the tectonic evolution of arcuate belts. In fact, only paleomagnetic data can assess when, how, and how much different segment of an orogenic bend rotated during deformation. In the specific case of the study of curved mountain belts paleomagnetism represents the only possible technique to distinguish between different types of orogenic arcs, depending on magnitude and timing of their bending process.

On the other hand, few basic assumptions, determining together its limitations, are needed by paleomagnetism. The first assumption is that rotations in an orogenic belt occur within rigid crustal blocks separated by discontinuities (i.e., faults). In this way it is neglected the inner deformation of rocks. However, *Lowrie et al.* [1986] have demonstrated that in very deformed rocks paleomagnetic directions can be influenced by the local strain, resulting in spurious rotations. Thus, the applicability of the paleomagnetic

method is restricted to weakly deformed rocks in brittle deformation context. Lithology is the other great limitation in paleomagnetism: depending on the type and amount of mineral magnetic carrier content, only a limited percentage of rocks yields a stable and measurable Natural Remanent Magnetization (NRM) by which vertical axis rotations are computed. Generally, among sedimentary rocks, the most suitable lithologies are fine-grained muddy formations, while among igneous rocks, both effusive and intrusive lithologies can yield reliable results. In particular, volcanic rocks are generally characterized by a strong magnetic signal due to the high content of ferromagnetic mineral (i.e., magnetite). Finally, metamorphic rocks can record a NRM, but paleomagnetic directions suffer of strong uncertainties linked to both the age of magnetization and the lack of paleo-horizontal control needed for computing of the tectonic rotations.

With paleomagnetism we can infer tectonic rotations occurred in a given region and relate them to an accurate time interval. This can be made if two conditions are satisfied: (1) the age of the sampled rock is well known, and (2) the NRM recorded by the rock is a primary remanent magnetization. The rock age can be inferred by paleontology (in sedimentary rocks), or radiometric data (in igneous-metamorphic rocks). If the NRM constitutes a primary magnetization, then the ages of magnetization and of rock formation are coincident. In this way we can choose the correct paleopole (see *Besse and Courtillot* [2002]) when computing the rotation values by the paleomagnetic declinations. Then, we can correlate the computed tectonic rotations to the time interval that follows to the acquisition age of the NRM. Nevertheless, if a NRM is not a primary magnetization it is possible to infer the magnetization age relying on the knowledge of the timing of the main deformation phase.

Also, rocks sampling procedure can affect paleomagnetic results. In fact, spacing of single cores sampled within a site (or locality) should be made in order to average out the secular variation of the geomagnetic field. Because the paleosecular variation is averaged within several millennia, just a single core ~2 cm height sampled from a sedimentary formation characterized by a low sedimentation rate (i.e., 0.01 mm/a) could have recorded an averaged geomagnetic field. Yet, rock samples are commonly gathered within two 1-2 m (or more) spaced outcrops. Generally, sampling from volcanic formations, that acquire their NRM instantaneously after cooling below the blocking temperature of the main magnetic carriers, should be carried out collecting samples relative to different eruptive episodes.

A peculiar problem in paleomagnetic studies applied to tectonics is found when sampling rocks from high latitudes. Having the geomagnetic field vector a high dip value, up to 90°, magnetic declination which represent the projection of the vector onto the horizontal plane will yield a wide error bar near the geomagnetic poles. This is easy to understand looking at the equation (1) showing the declination error ( $\Delta D$ ):

$$\Delta D = \alpha_{95} / \cos(I) \quad (1)$$

Where  $\alpha_{95}$  is the *Fisher's* [1955] statistical parameter estimating precision of the mean paleomagnetic direction (in degrees) on a spherical distribution, and  $I$  is the magnetic inclination, given by the projection of the geomagnetic field vector onto the vertical plane. It can be noted from equation (1) that for high values of  $I$  also the declination error ( $\Delta D$ ) is high. The declination error coincides to the  $\alpha_{95}$  only when the geomagnetic field vector is horizontal (i.e., near equatorial latitude).

Finally, it should be taken into account that an intrinsic restriction to the paleomagnetic technique exists, due to natural paleomagnetic scattering, errors induced

during sampling, instrumental errors, or local magnetic anomalies. This implies that the normal resolution of paleomagnetism is about  $10^\circ$  in declination, as also suggested by *Lowrie and Hirt* [1986], and thus rotations lower than  $10^\circ$  can hardly be considered as significant.

## 2.2. Structural analysis

Many authors who tackled the study of curved mountain belts have evidenced the need of an integrated paleomagnetic and structural investigation [e.g., *MacDonald*, 1980; *Lowrie and Hirt*, 1986]. In fact, paleomagnetic data should be interpreted according to the structural framework of a given region, but, on the other hand, structural data require a paleomagnetic control. Thus, paleomagnetism and structural analysis are two complementary tools for studies in orogenic settings.

Kinematic analysis reveals to be the most useful method in structural investigations, because it can supply information on the evolutionary history of an orogenic belt. Kinematic analysis is based on the study of finite strain of a deformed area and, in particular, on the measuring of kinematic indicators on fault planes. This allows us to calculate the tectonic transport direction at a local scale, indicating the movement of the hanging wall, and, through an extensive analysis, draw the displacement trajectories path within the entire belt. Through the study of temporal and spatial variation of transport directions in orogenic arcuate systems it is possible to infer on the tectonic evolution of the bend [e.g., *Nur et al.*, 1986; *Allerton*, 1994].

There are several kinematic indicators used for kinematic analysis in brittle deformation settings, but the most common and easy to recognize is represented by fault lineations (or slickensides) [*Allerton*, 1998]. These are represented by the growth of

elongated mineral fibers (quartz, calcite, etc.), or abrasion features originated on the fault plane during slip motion. Direction of fault lineations constitutes a strong constrain to the real displacement of the hanging wall on a fault plane. The sense of shear is usually inferred by other kinematic indicators, such as SC-structures and quartz/calcite steps.

One simple and powerful tool in the analysis of rotational thrust systems involves comparison of fault lineation directions with amount of paleomagnetic rotations over a series of thrust sheets [Allerton, 1998]. Three alternative situations can be considered (Figure 2.1): (1) the thrust lineations post-date rotation. In this case a plot of lineation vs. paleomagnetic declination will show constant lineation directions for a range of declinations. (2) The thrust lineations pre-date rotation. In this case, the lineations vs. paleomagnetic declinations plot on a unitary slope line. (3) The thrust lineations are synchronous with rotation, so the lineations and declinations plot in a region bounded by a line of constant lineation, and a line with a slope of unity. The intersection of the two lines marks the true transport direction and the paleomagnetic reference direction.

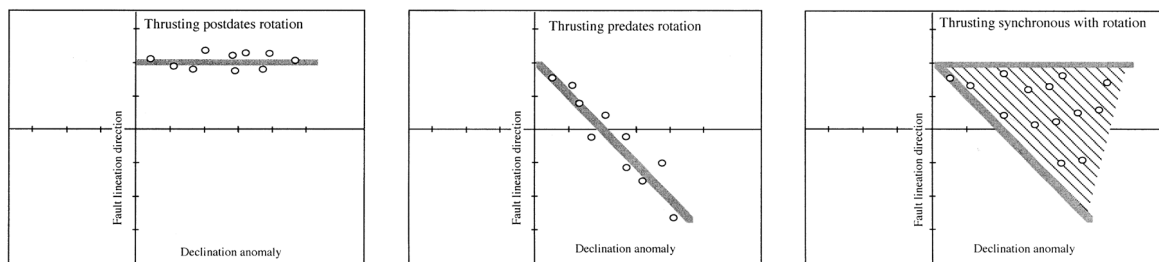


**Figure I 2.1. Fault lineation direction vs. paleomagnetic declination for three different cases. (left), thrust postdates rotation. (Center), thrusting predates rotation. (Right), thrusting synchronous with rotation. Modified from Allerton [1998].**

### 3. Brief history of the orocline concept

Well before the plate tectonics theory was diffused (1960s) several ideas, sometimes contrasting, were proposed about the origin and the geologic significance of

curved mountain belts. Indicating simply geometric aspect, *Miser* [1932] coined the terms “salient” and “recess” to distinguish between arcuate shape orogens with curvature convex and concave toward the foreland, respectively. In this meaning, the terms salient or recess were used to indicate any curved orogenic system regardless to their kinematics and mechanisms of formation.

With the diffusion of the plate tectonics theory it was clear that the understanding of curved belts could be the key to reveal the fundamentals of the orogenesis. The term “orocline” was introduced for the first time by *Carey* [1955] and its etymology comes from Greek and means both mountain and bend. The *Carey*'s definition of orocline was used to indicate an initially straight fold-thrust belt that acquired curvature during a second deformation event. However, during the following years, the term orocline have been erroneously used to indicate any curved belt, thus yielding only a geometric meaning. This was due to the concrete difficulties in inferring the timing of formation of the arc. *Carey* distinguished oroclines by primary bends, which, on the contrary, formed when younger orogens were molded onto the irregular margins of preexisting cratons.

The orocline concept was following redefined by *Marshak* [1988] who linked the term to a specific kinematics. In fact he distinguishes between oroclines, that formed by the bending of an originally linear mountain belt, and “nonrotational arcs”, which represent curved fold-thrust belts that initiate in their present curved form and their curvature does not increase during subsequent deformation. As a result, nonrotational arcs are discerned by oroclines by the fact that the formers preserve their shape during deformation, and no segment of the arc undergoes vertical axis rotations. Conversely, oroclines are characterized by opposite rotations of the limbs of the bend during its formation, according to a mechanism which is called oroclinal bending. Oroclines and nonrotational arcs have

also been called primary and secondary arcs, respectively, while the term “bend” started to be used to indicate any generic fold-thrust belt with a curved shape.

Many years later, *Weil and Sussman* [2004] proposed a new classification scheme of curved belts relying on the timing relationship between thrusting and vertical axis rotations. According to this classification, nonrotational arcs and oroclines represent two end-members models among possible curved mountain belts. In nonrotational arcs, no vertical axis rotations occur and the formation of the curvature predates deformation, while in oroclines, rotations accompanying arc formation postdate thrusting. Among these, *Weil and Sussman* [2004] considered an intermediate type of bend whose arcuate shape develops contemporaneously with growth of the belt, called progressive arc. A progressive arc is defined as an orogenic belt that either acquires its curvature gradually throughout the belt’s deformation history, or a belt that acquires a portion of its curvature during a subsequent deformation phase of the belt.

### ***Used nomenclature***

In order to better understand the following discussions, I introduce some specific terms used to geometrically describe an orogenic bend [*Marshak*, 1988; *Macedo e Marshak*, 1999]. Figure 3.1 shows the main geometric features cited below.

The leading edge (LE) is the line that defines the boundary between the curved fold-thrust belt and the foreland basin (“marker line” in *Marshak* [1988]). The apex (A) is the point where the leading edge has the smallest radius of curvature. As such, the apex corresponds to the hinge point on a fold profile. The hinge zone represents the region along the leading edge, surrounding the apex. The endpoints (EP) are the points at either end of the salient at which it terminates, while the reference line (RL) constitutes the straight line

connecting the two endpoints. The limbs are the regions between the hinge zone and the endpoints. The midpoint (M) is the point halfway between the two endpoints, as measured along the reference line. The amplitude (AMP) is the shortest distance between the reference line and the apex. The midline (ML) represents the line that connects the midpoint to the apex. The interlimb angle ( $\alpha$ ) is the angle between the two legs of a triangle, in which the salient can be inscribed. The degree of asymmetry (DA) constitutes the ratio between the midline and the amplitude. It describes the inclination of the midline with respect to the amplitude, and thus can also be represented by the angle between the midline and the reference line. Finally, the area ratio (AR) is the ratio between the approximate area of the salient and the area of the interlimb triangle.

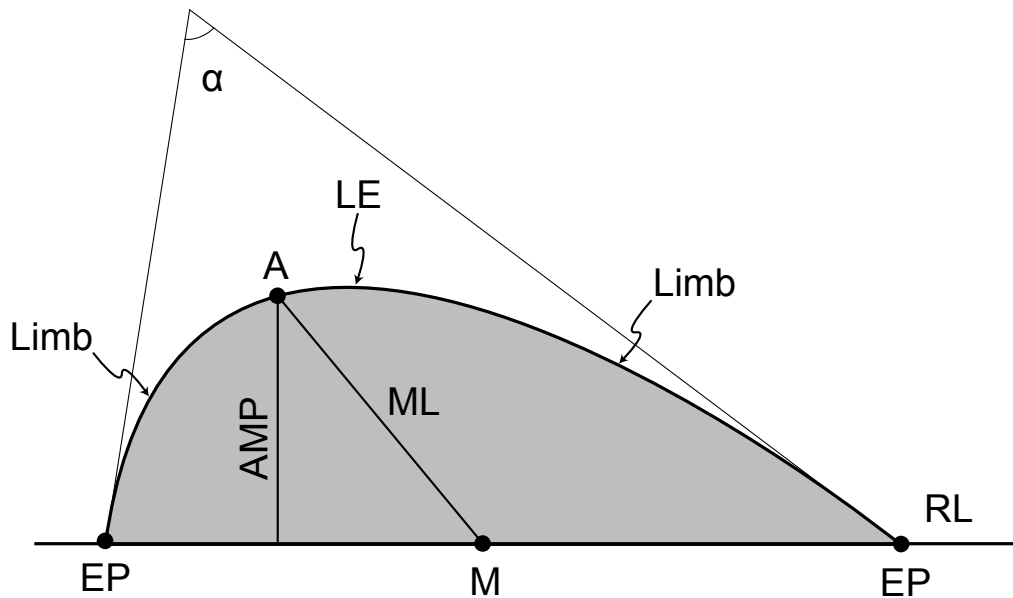


Figure 3.1. Simplified scheme showing the main geometric elements of orogenic bends.

#### 4. The oroclinal test

Since the 1980s, when paleomagnetism started to be used in the study of orogenic bends [Van der Voo and Channell, 1980], it was possible to unravel the deformation

history of a curved fold-thrust belt, and distinguish between primary and secondary curves. After the first studies it became soon clear that paleomagnetism could represent a very strong constraint to the kinematics of an orogenic bend.

Paleomagnetic analysis in the study of orogenic bends is based on the fundamental principle that bending of an initially straight structure is accompanied by a variation in the direction of magnetic declinations within different sectors. Necessary condition is that the natural remanent magnetization of rocks be a primary magnetization. This variation is proportional to the deviation of the direction of the main structural features in the belt (i.e., fold axes). Conversely, in a primary arc, the direction of magnetic declinations does not change along the entire arc.

Yet, some studies have documented intermediate paleomagnetic directions with respect to those expected, according to the structural deviation observed in the belt [*Bachtadse and Van der Voo, 1986; Miller and Kent, 1986*]. This could imply an oroclinal bending of an already partially curved belt. But, how can we quantify the real correlation between paleomagnetic and structural directions? Opposite vertical axis rotations within the limb of a curved orogenic belt, in fact, do not necessarily indicate that it represent an orocline.

Commonly, two analogueous statistical tests (oroclinal test) are used in order to estimate the degree of correlation between paleomagnetic and structural directions in a curved fold-thrust belt. In the first test, proposed by *Schwartz and Van der Voo [1983]* a linear regression is performed on a data population plotted in an orthogonal diagram where the X and Y coordinate for each point is represented by the difference between the local strata direction (S) and the mean value of the strata directions ( $S_0$ ), and the difference between the site mean declination (D) and a reference declination ( $D_0$ ), respectively

(Figure 4.1). In the second test, proposed by *Eldredge et al.* [1985], the X and Y coordinate of each point from data population is given by the difference between the reference structural direction ( $S_r$ ) (considered as the initial direction of the orogen before bending) and local strike of fold axes ( $S_o$ ), and the difference between a reference declination value ( $D_r$ ) (which is generally the declination value from the foreland area) and the site mean declination ( $D$ ) (Figure 4.2).

An essential condition is that rocks used for an oroclinal test must have a similar age, otherwise, different reference declinations ( $D_r$ ) should be considered for each group of sites with similar age. Conversely, the choice of the reference declination for similar age rocks does not influence the result of the test.

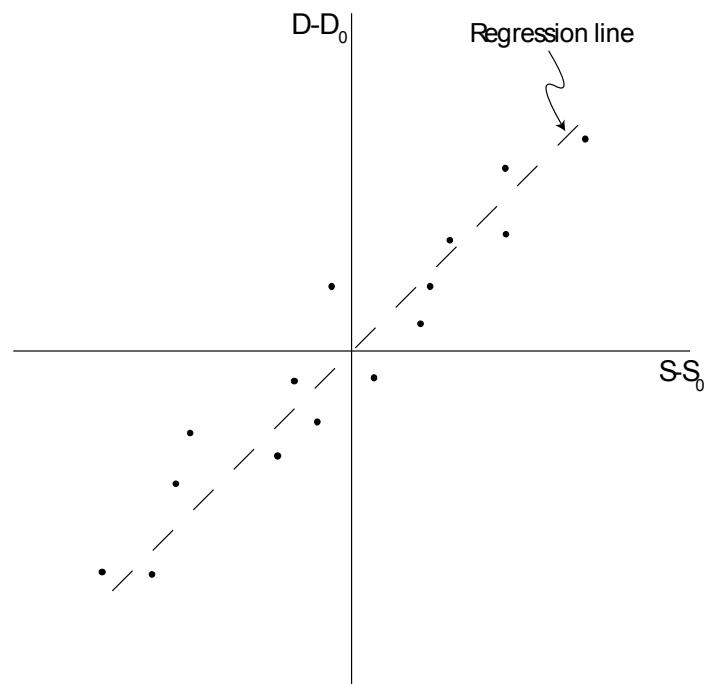
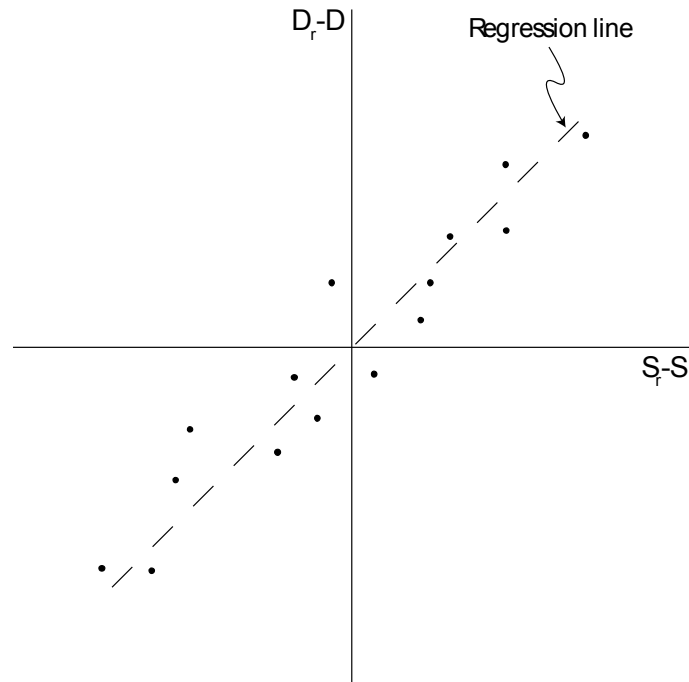


Figure I 4.1. Oroclinal test according to the method by *Schwartz and Van der Voo* [1983].



**Figure 4.2.** Oroclinal test according to the method by *Eldredge et al. [1985]*.

Results from the linear regression can show three end-member situations, depending on its angular coefficient ( $m$ ) (Figure 4.3):

- a) ( $m = 1$ ): paleomagnetic declinations are 1:1 correlated with structural directions, and the orogenic bend represents a perfect orocline.
- b) ( $m = 0$ ): declination values are constant over the curvature and there is no correlation between paleomagnetic and structural directions. The bend is a primary feature and represents a nonrotational arc.
- c) ( $0 < m < 1$ ): variation of paleomagnetic directions is lower than variation of structural directions. This means that the orogenic bend, formed originally curved (as a primary arc), was bent during following tectonic events.

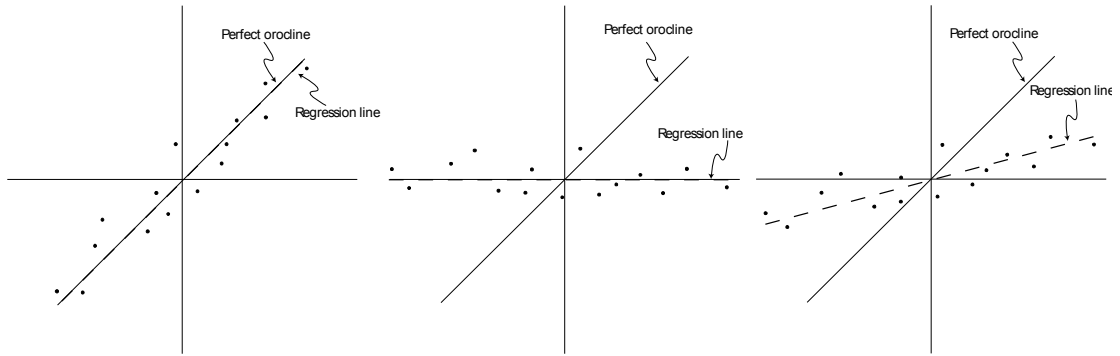


**Figure 4.3.** Sketch showing possible results from the oroclinal test, indicating a perfect orocline (left), a primary arc (center), and a primary arc subsequently affected by some amount of oroclinal bending, or a progressive arc (right).

At this point, the statistical significance of the slope of the regression line must be quantitatively estimated comparing it with the zero or the unitary slope line. In the first works by *Schawartz and Van der Voo* [1983] and *Eldredge et al.* [1985] the correlation coefficient ( $C$ ) was considered in order to estimate the significance of the linear regression. Yet, this estimate was usually very subjective, and a coefficient major than 0.8 was always considered indicative for a reliable correlation of data. After few years, a more objective tool was proposed for oroclinal tests: the statistical  $t$ -test [*Lowrie and Hirt*, 1986]. The  $t$ -test is used to assess if the slope of the regression line calculated by linear regression is statistically different from a give slope, which can be zero or one if we consider the end-member situations for a perfect orocline or a nonrotational arc. The value of  $t$  is given by the following equation:

$$t = m \cdot \sqrt{(N-2) \frac{\sum (S_o - S_R)^2}{\sum ((D_o - D_R) - D_P)^2}} \quad (1)$$

where:

- ( $m$ ) is the relative angular coefficient of the regression line with respect to the reference slope. In example, for a regression line with an angular coefficient of 0.2 the

value  $m$  in the equation (1) is equal to 0.2 when compared to the zero slope line, but it is equal to 0.8 ( $1-0.2=0.8$ ) if compared to the unitary slope line;

- ( $N$ ) is the number of observations (data);
- ( $S_o$ ) and ( $S_R$ ) are the observed and reference local structural directions, respectively;
- ( $D_o$ ) and ( $D_R$ ) are the observed and reference declination, respectively;
- ( $D_p$ ) is given by the following equation (2):

$$D_p = m (S_o - S_r) + c \quad (2)$$

where,  $m$  and  $c$  are the parameters of the regression line.

Result from equation (1) is then compared with critical values of  $t$  depending on the value of  $N$  and the confidence (or significance) level we choose. Usually, confidence levels of 5% and 1% are used. If the  $t$  value resulted by the oroclinal test is lower than the critical value, then the regression line and the reference line are not statistically different.

So, in an ideal case where our regression line is close (but not coincident) to the zero slope line, the  $t$ -test is used to define if some oroclinal bending occurred or not.

## 5. Different geometries of orogenic bends

Curved mountain belts from different part of the Earth show a great variability in their geometric features, such as amplitude (AMP), interlimb angle ( $\alpha$ ), degree of asymmetry (DA) (Figure 5.1), and pattern of structural trend-line (Figure 5.2).

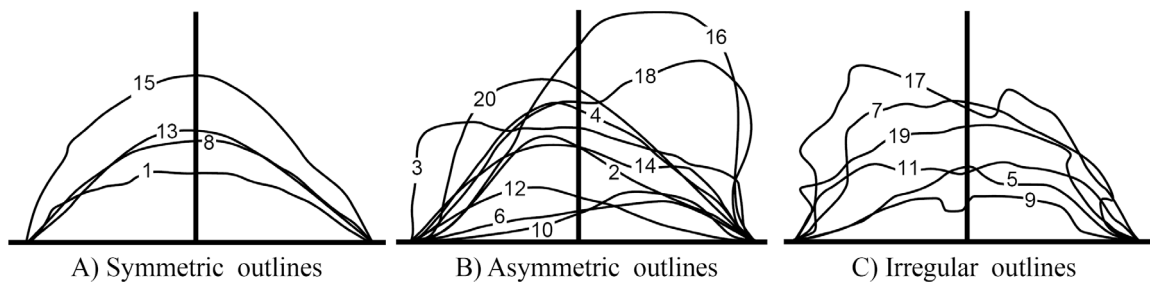


**Figure 5.1.** Shapes of salient leading edges, normalized to the same reference line length. Numbers indicate specific regions where salients are present. After *Macedo and Marshak [1999]*.

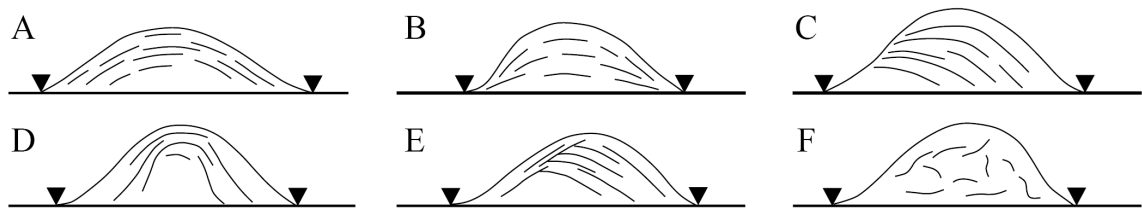


**Figure 5.2.** Types of structural trend-line patterns observed in salients. The continuous curved line represents the leading edge of the salient, whereas the broken lines represent structural trend lines. The straight line represents the reference line, and the inverted triangles define the end points of the curve. (A) Parallel trend-line pattern. (B) Convergent trend-line pattern with trend lines converging to both end points. (C) Convergent trend-line pattern with trend lines converging to one end point. (D) Divergent trend-line pattern. (E) Truncated trend-line pattern. (F) Chaotic trend-line pattern. After *Macedo and Marshak [1999]*.

Besides these substantial differences, several studies have demonstrated that both primary and secondary arcs can show identical final geometric features. For that reason, factors or boundary conditions common to both types of bends should exist and be independent from the mechanisms of arc formation. This consideration, once again, stresses the importance of a multidisciplinary approach (paleomagnetic and structural) in the study of the orogenic bends.

*Macedo e Marshak [1999]* proposed a preliminary classification for different bend geometries based on the degree of asymmetry, dividing most of the existing curved structures into three main groups: symmetric, asymmetric, and irregular arcs. In symmetric arcs, the Amplitude (AMP) coincides with the Midline (ML), while in an asymmetric arc they form an angle which increases as the degree of asymmetry increases. In irregular arcs the Leading Edge (LE) can form small-scale secondary bends. The authors, after having checked most of the existing orogenic bends, concluded affirming that asymmetric arcs are the most frequent structures.

In the following sections the possible factors/boundary conditions controlling the final shape of an orogenic bend will be discuss.

## 6. Kinematics of orogenic bends

The first intuitive interpretations of arcuate fold belts consisted in “virgations du premier genre” [e.g., *Argand*, 1924] and were interpreted to be characterized by fanning transport directions. However, although widely diffused, orogenic bends are still not fully understood from the point of view of their kinematics. Usually, a geologist who studies an orogenic belt has to resolve an inverse problem, which is unravelling its kinematics starting from an observed finite strain. This can be made through structural analysis, and in particular with kinematic analysis on fault planes, the study of balanced cross sections, and with paleomagnetism.

During the evolution of an orogenic bend in a brittle tectonic setting, depending on the mechanism governing its formation and, thus, the type of bend (primary or secondary), individual points within the belt can show different displacement path trajectories. The first classification of kinematic patterns in curved fold-thrust belt was proposed by *Marshak* [1988] who demonstrated that a number of different kinematics can lead to the development of primary and secondary arcs.

### 6.1. Marshak’s classification of kinematic patterns

*Marshak*’s [1988] classification relies on 14 different kinematic patterns characterizing both primary and secondary arcs. The evolution of an orogenic bend can be described through: (1) the displacement paths, (2) the amount and variation of the arc-parallel extension, (3) the displacement of the endpoints, and (4) the movement of the reference line.

In the next paragraph I will discuss the possible kinematic patterns for primary and secondary arcs.

### 6.1.1. Primary arcs

Nonrotational arcs are bends in which the strike of a segment of the fold-thrust belt does not change during the formation of the arc. Three distinct displacement path trajectory patterns can lead to the development of a nonrotational arc, such as (Figure 6.1.1.1):

- Pattern AA: the displacement path trajectories have zero length, the leading edge is fixed in position with respect to adjacent crust, and no horizontal translation occurs. Such a pattern would be characteristic of primary bends that have been subjected only to vertical movement.
- Pattern AB: the displacement path trajectories along the length of the bend are equal in magnitude and are parallel to one another. For such bends there is no tangential extension, no rotation of segments of the orogen, and no change in the curvature of the belt during its evolution.
- Pattern AC/AD: the displacement path trajectories are nearly orthogonal (AC) or orthogonal (AD) to the trend of the orogenic belt and are unequal in length. Different segments of the belt do not change strike as they translate into the foreland, while tangential extension, of variable amount along the arc, must occur during the evolution of the orogen.

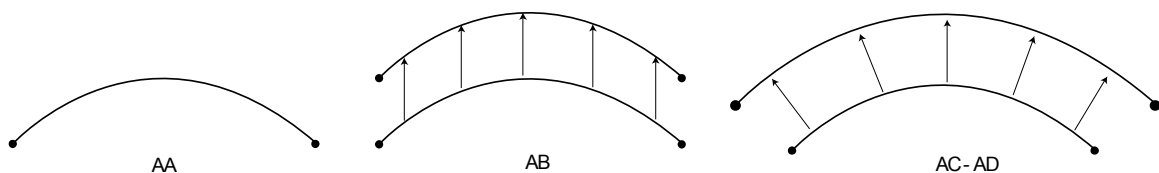


**Figure 6.1.1.1. Sketch displaying displacement path trajectory patterns for nonrotational arcs.**

In the following paragraph we will show that patterns AA and AB have never been recognized in primary arcs, whereas pattern AC-AD were found to be the most diffused in nature, and a common results in numerous analogue experiments [e.g. *Zweigel, 1998*].

### 6.1.2. Secondary arcs

If the orientation or magnitude of displacement path trajectories varies around a bend in such a way that the segments of the bend change strike with time, then the bend is an orocline. The possible kinematic patterns are (Figure 6.1.2.1):

- Pattern OA: as the leading edge moves into the foreland, the bend remains a segment of a circle with the same radius of curvature. The endpoints are not fixed and there is tangential extension. The displacement path trajectories are straight lines forming a diverging fan.
- Pattern OB: the displacement path trajectories are perpendicular to the strike of the belt but vary in length around the arc. The endpoints translate into the foreland during deformation and tangential extension varies along the length of the bend.
- Pattern OC: the endpoints are fixed and the leading edge undergoes uniform tangential extension. The displacement path trajectories form a diverging fan and decrease in length toward the endpoints.
- Pattern OD: the displacement path trajectories are parallel to one another but their lengths vary continuously and decrease toward the endpoints. There must be tangential extension, but it is not uniform along the length of the arc. Endpoints are fixed.
- Pattern OE: the positions of the endpoints are fixed and no tangential extension occurs. In this case, rock must slide or flow past the endpoints. The displacement path trajectories define a convergent fan.
- Pattern OF: as the leading edge migrates into the foreland the endpoints approach one another along the reference line.

- Pattern OG: the displacement path trajectories are approximately perpendicular to the trend of the orogen and decrease in length toward the crest. Therefore the curvature of the orogen in plan view decreases as it propagates into the foreland. There is tangential extension.
- Pattern OH: one endpoint is fixed and no tangential extension occurs during development of the bend. The development of the bend involves rotation around a single vertical axis located at some point along the orogen, and the displacement path trajectories are segments of circular arcs. There is no tangential extension. A variation to this pattern is that the displacement path trajectories are parallel to one another, and perpendicular to the reference line.

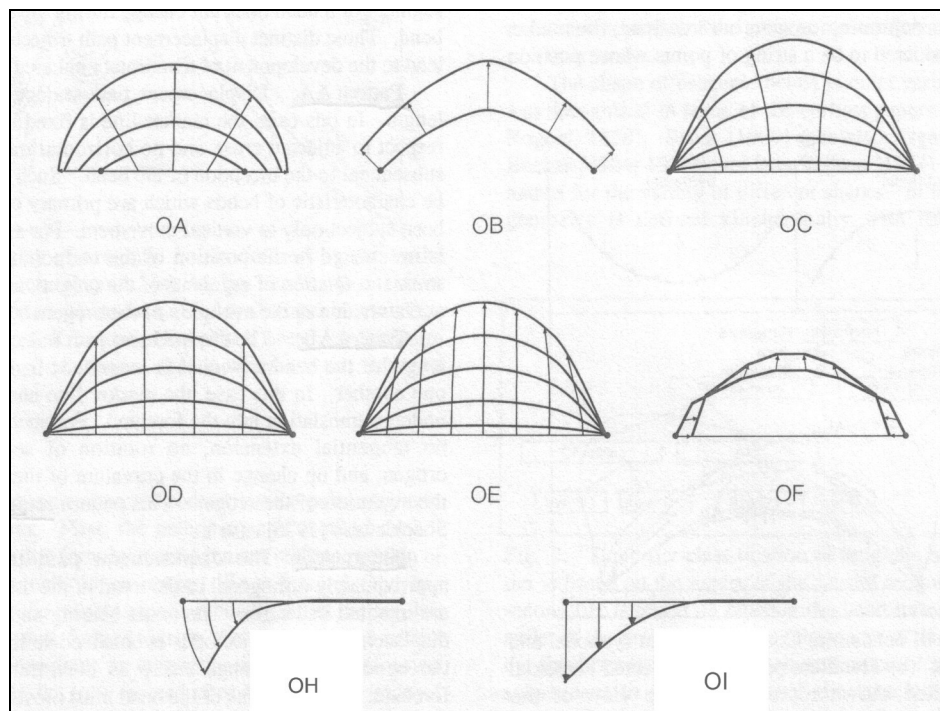


Figure 6.1.2.1. Displacement path trajectory patterns for oroclines. After *Marshak* [1988].

## 7. Mechanisms of orogenic bends formation

Hitherto, the most representative geometries and kinematic patterns of curved belts have been exposed. But, the occurrence of bending in a fold-thrust belt and its main features depend on the geodynamic processes controlling their developing. As I have already said previously, paleomagnetic, structural, and geophysical data should be integrated in order to document the geodynamic framework of a curved belt, and unravel its formation mechanisms.

Numerous orogens in the Earth show arcuate systems (Figure 7.1). Numerous geologic factors that can control the developing of a bend exist, such as: geologic and mechanical features of the orogenic wedge and the foreland, the original shape of the sedimentary basin before deformation, the geometry and kinematic of the subducting slab, the shape of continental margins before the collision, and the presence of obstacles (or buttress), among many others.

In the next paragraphs the main orogenic bend formation mechanisms will be discussed, reporting, for each one of them, a natural example.

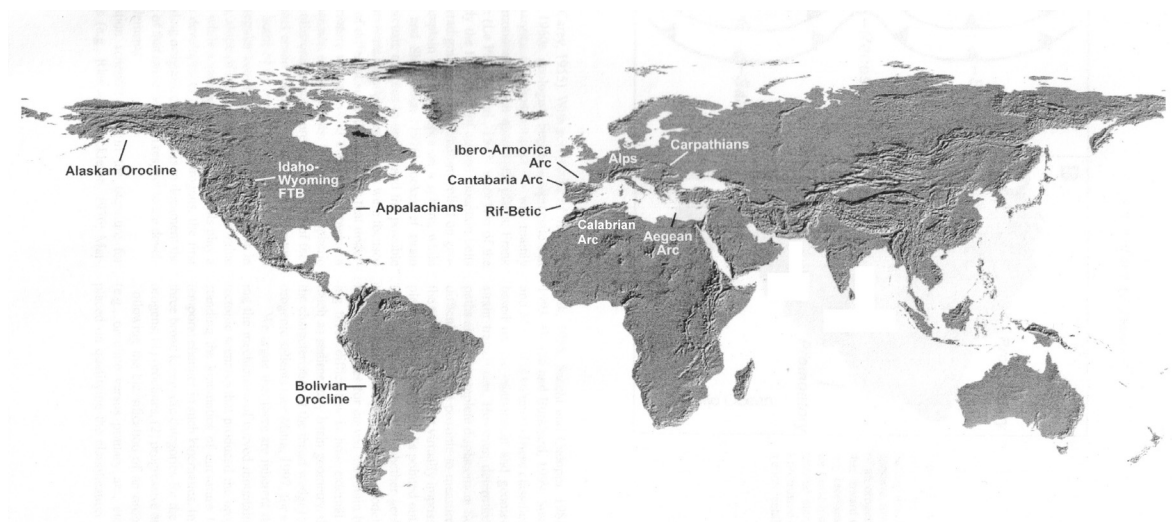


**Figure 7.1. Digital elevation model of the Earth showing location of the main orogenic bends. Adapted from Weil and Sussman [2004].**

### 7.1. Nonrotational arcs related to “indenters”

The term “indenter” has been used in the past to indicate any rigid block that can collide with a continental margin. In nature, an indenter can be represented by a continental promontory or an exotic terrane (i.e., island arcs, or microplates). The effects of the convergence of indenters into a deformable material have been documented by numerous analogue experiments performed during the last two decades [Tapponnier *et al.*, 1982; Davy and Cobbold, 1988; Marshak, 1988; Marshak *et al.*, 1992; Lu and Malavieille, 1994; Macedo and Marshak, 1999; Zweigel, 1998; Costa e Speranza, 2003].

The main result from these experiments is that nappes, created in front of an indenter, have curved thrust traces and fold axes in map view. Marshak *et al.* [1992] demonstrated that a spoon-shaped detachment surface forms following to indentation, determining the development of an initially curved structure in the hanging wall. The detachment surface has low inclination in the frontal part and becomes subvertical near the lateral edges of the indenter. During the initial phase of convergence, the displacement path trajectories in the deformed wedge show divergent fanning directions that are suborthogonal to the strike of the fold axes. In the following phase, when indentation prosecutes, a new detachment surface forms in front of the former one, and a new curved nappe develops. The displacement path trajectories in the first developed nappe are now parallel to one another, being the internal region uniformly transported toward the foreland, whereas the frontal part of the bend shows again divergent fanning displacement path trajectories.

Similar results have been documented by Costa and Speranza [2003], who performed a “magnetized analogue experiment” using sand mixed with magnetite-dominated powder. Before deformation, the model was magnetized by means of two

permanent magnets generating a quasi-linear magnetic field. After deformation, cylindrical specimens were sampled within thrust sheets, and vertical axis rotations were calculated. Their results indicate that an indenter pushing into deforming belts generally forms nonrotational curved outer fronts, while the more internal fronts show oroclinal-type rotations. This would represent a composite curved belt consisting of an orocline in the inner part and a nonrotational arc in the outer one. According to the new classification of orogenic bends by *Weil and Sussman* [2004], the bend formed in the inner part of the deforming wedge would represent a progressive arc, rather than an orocline.

Many analogue experiments have demonstrated that material deformed in front of the central part of the indenter is characterized by pure shear, while simple shear affects material located near its corners. This implies that the frontal part of arcs formed by indentation of a rigid block is also affected by a different amount of tangential extension (the extension parallel to the strike). The topic of tangential extension will be treated more in detail in paragraph 7.1.1. Conversely, at two limbs of the bend, clockwise and counterclockwise vertical axis rotations occur in front of the right and left corner of the indenter, respectively. Rotations are induced by internal deformation of the rock, without implying a rotation of the thrust surfaces [e.g., *Zweigel*, 1998]. In fact, rotation amount occurring within these portions of the bend is always minor than the structural trend variation within the arc. Therefore, the angle between a trend line and the reference line of the salient does not necessarily indicate the amount of rotation of a limb.

*Zweigel* [1998] suggested that several features of indenter-related bends are controlled by the indentation angle (i.e., the angle between the indentation direction and the normal to the frontal face of the indenter). *Zweigel* observed that: (a) the ratio between the widths of the lateral and frontal parts of the wedge increases linearly with increasing

indentation angle, thus influencing on the final shape of the bend. (b) Tangential extension in the corner area decreases with increasing indentation angle. (c) Tangential extension in the corner area is initially high, decreases during progressive convergence, and attains a stable level during the advanced stages of the experiments when self-similarity conditions are reached. (d) Displacement vectors of accreted material exhibit fanning around the arc, but in oblique indentation the spread of their orientation is smaller than the change of structural strike (nappe traces and fold axes). In fact, displacement vectors trend mainly orthogonal to the structural grain of the belt when indentation is parallel, conversely, they rotate clockwise and counterclockwise in the left and right limb of the arc, respectively, when convergence is oblique.

Analogue experiments have also demonstrated that the final shape of the bend is controlled by different factors, such as the shape of the indenter and the shape of the sedimentary basin over which the curved structure develops [*Macedo and Marshak, 1999*]. The shape of the salient leading edge closely reflects the shape of the indenter: a rectangular-shaped indenter yields a flat-crested salient, a symmetric parabolic-shaped indenter yields a parabolic salient, and an asymmetric rounded indenter yields an asymmetric salient. Furthermore, these authors proposed that a salient, formed by indentation of a rigid block, can be recognized by a divergent structural trend-line pattern (see paragraph 5).

In conclusion, it can be asserted that the indentation of a rigid block within a deformable material generally produces primary arcs.

### **7.1.1. The problem of tangential extension**

Kinematic models proposed by *Marshak* [1988] have evidenced that tangential extension can affect both primary and secondary arcs, though it is not a necessary consequence of bend development. The origin of the arc-parallel stretching is different in the two types of bend: in primary arcs, it is mainly associated to the pure shear generated in front of the central part of the indenter, whereas in oroclines tangential extension results as a consequence of the increasing in the curvature radius of the outer part of the arc with respect to the inner part. In examples, in oroclinal bending due to buckling, the outer and inner part of the bend undergoes arc-parallel extension and compression, respectively.

Nevertheless, how tangential extension occur in curved belts is not still fully understood. *Marshak* [1988], proposed two types of fracture arrays accommodating tangential extension: a multiple set of nonparallel fractures and a single parallel array. The first type has been recognized by *Marshak et al.* [1982] in the northern Apennines (Italy), where a widespread array of mesoscopic strike-slip faults, which roughly define a conjugate system, permitted arc-parallel extension, without implying a rotation of mesoscopic-scale blocks (Figure 7.1.1.1).

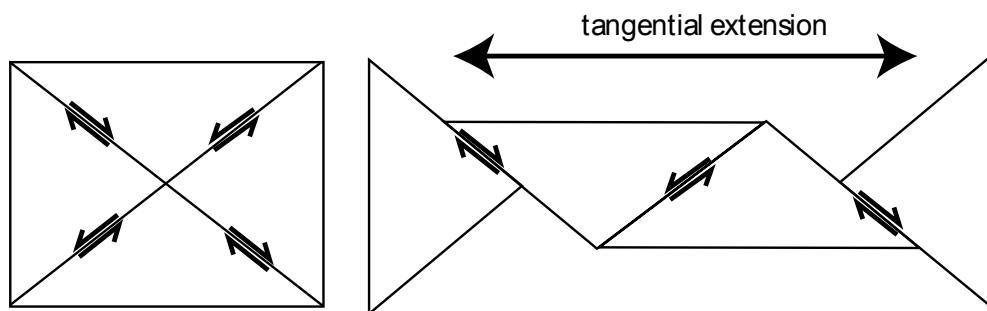


**Figure 7.1.1.1. Sketch showing kinematics for tangential extension through a non-parallel fault array.**

However, conjugate fault arrays associated to tangential extension need, not always involve strike-slip faults. For example, *Ramsay* [1981] documented the occurrence of tangential extension in the Helvetic nappes accommodated by conjugate normal faulting.

The second type of fracture array has been documented from the Makran Mountains (Pakistan) by *Marshak* [1988] and consists on a set of parallel faults produced in a region characterized by simple shear in a direction parallel to the transport direction of the belt.

### **7.1.2. The example from the Carpathian Arc**

The Carpathians represent a 700-km long fold-thrust belt with a striking curved structure formed during the Late Cenozoic by the convergence of the Adriatic microplate and other continental fragments (such as the Tisia-Dacia block), with respect to Europe [*Burchfiel*, 1980]. The Carpathians are divided into an inner part, consisting of crystalline basement nappes and their Mesozoic sedimentary cover (Tisia-Dacia block, Inner Carpathians), and an outer part of Cretaceous to Tertiary flysch and molasse nappes (Outer Carpathians). The Outer Carpathians form a continuous, curved belt from the Western Carpathians to the southern end of the Eastern Carpathians, and continue below the Miocene to Recent sedimentary cover along the front of the Southern Carpathians (Figure 7.1.2.1).

Structures are convex towards the foreland and show outward tectonic vergence. In the Western Carpathians the orogen grain strikes ~NE-SW, then it makes curves of ~90° showing, in the Eastern Carpathians, a general NNW-SSE trending, and finally it changes to a roughly E-W direction in the Southern Carpathians [*Morely*, 1986; *Linzer et al.*, 1998; *Zweigel*, 1998]. The hinterland of the orogenic belt, consisting of basement units which underwent their major deformation in the early Cretaceous (145-99 Ma) together with an accretionary wedge, exhibits a convex right-angled corner and constitutes the Tisia-Dacia block.

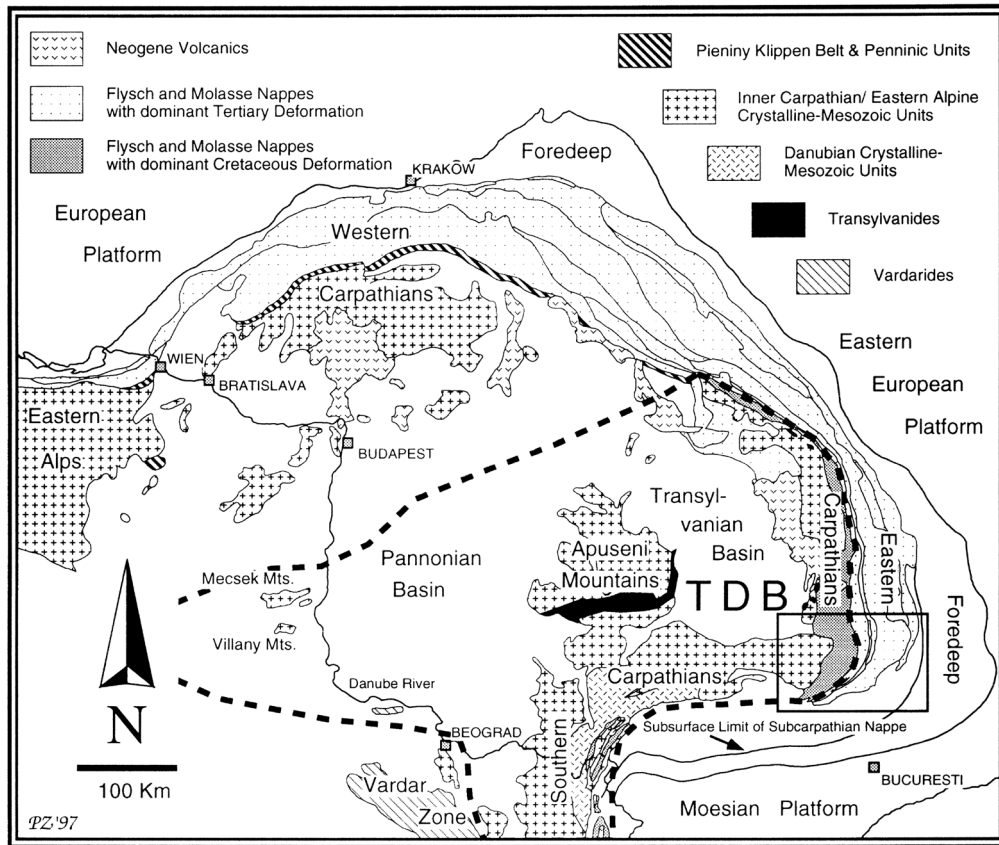


Figure 7.1.2.1. Geological map of the Carpathians arc system. After *Zweigel et al.* [1998].

Thrusts transport directions, inferred by fault lineations, exhibit a fanning distribution around the arc (Figure 7.1.2.2) [*Linzer et al.*, 1998], and their spread is systematically smaller than the change of strike of fold-thrust structures [*Zweigel et al.*, 1998]. According to these evidence, convergence in the Eastern Carpathians is almost normal to orogenic strike, whereas movements in the Southern Carpathians are almost pure right-lateral strike-slip to the west and right-lateral transpressive to the east [*Ratschbacher et al.*, 1993; *Morley*, 1996; *Zweigel*, 1997; *Linzer et al.*, 1998]. This model is in agreement with the increasing shortening components normal to orogenic strike of the Southern Carpathians from west to east documented by *Mațenco et al.* [1997].

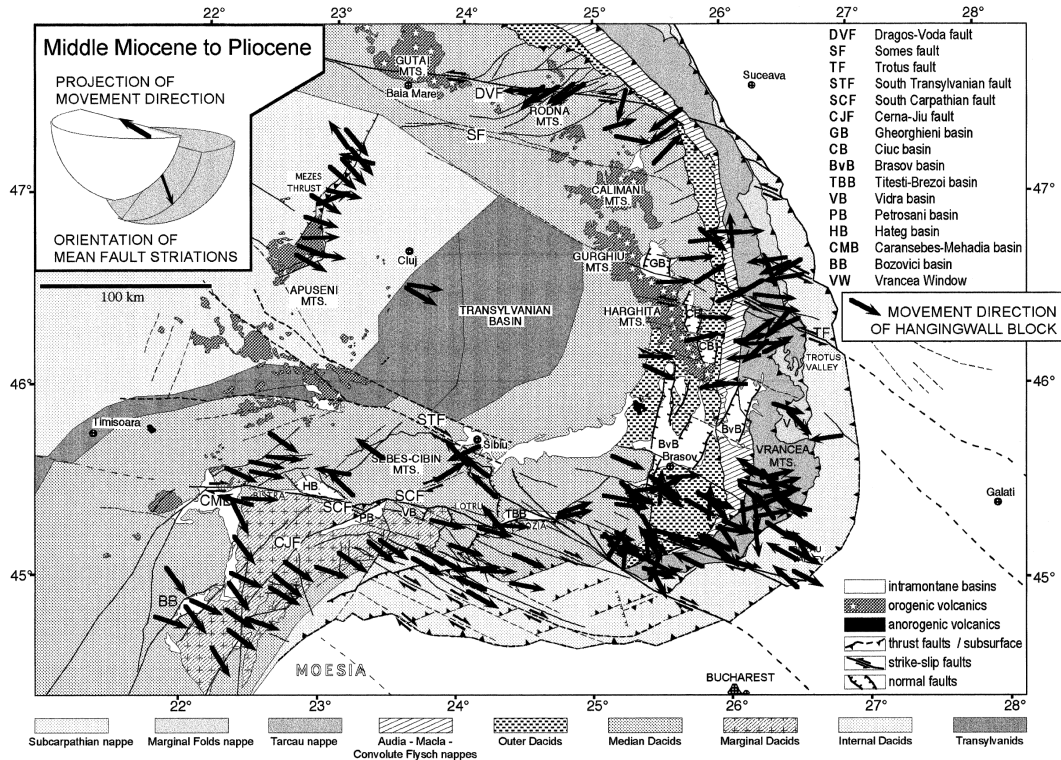
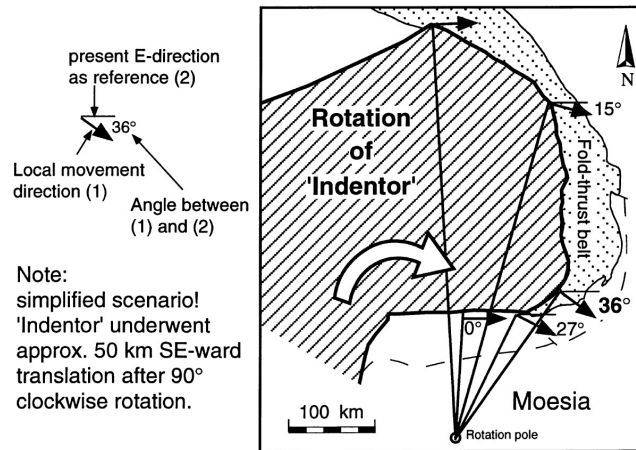


Figure 7.1.2.2. Pleistocene to Holocene displacement orientations of hanging wall block of Eastern and Southern Carpathians. After Linzer *et al.*, 1998.

Paleomagnetic and structural data from the Tisia-Dacia block show that the hinterland did not move straight, but carried out a clockwise rotation [Ratschbacher *et al.*, 1993; Pătrașcu *et al.*, 1994] followed by a small southeastward translation [Zweigel, 1997]. This rotation, resulted in an oblique indentation of the Tisia-Dacia block with the Eastern Carpathians, which is maximum (36°) in the region connecting Eastern and Southern Carpathians (Bend Area) (Figure 7.1.2.3).

Previous paleomagnetic data from the Carpathians evidenced over 90° opposite rotation on both the limbs of the arc, showing the existence of two distinctive tectonic domains: the northwestern Carpatho–Pannonian domain with systematic counterclockwise rotations and the southeastern Carpatho–Pannonian domain with systematic clockwise rotations [e.g., Balla, 1987; Linzer, 1996; Csontos and Voros, 2004; Dupont-Nivet *et al.*, 2005].



**Figure 7.1.2.3. Clockwise rotation of the Tisia-Dacia block around a pole situated in its vicinity in western Moesia (Romania). Angles of convergence relative to the normal to strike of the orogen are shown. After Zweigel [1998].**

*Dupont-Nivet et al.* [2005] showed that no significant rotation has affected the eastern Carpathians since ~9 Ma. In the southern Carpathians, a ~30° clockwise rotation seems to have occurred during the 13-6 Ma time interval. This indicates that a regional tectonic event occurred in this region probably between 13 and 9 Ma.

Further (but less reliable) paleomagnetic data from Cretaceous rocks [*Bazhenov et al.*, 1993] would represent evidence for an early phase of clockwise rotation of 60-100° in Southern Carpathians and 10-50° in Eastern Carpathians.

The development of the Carpathian Arc occurred during Late Cretaceous to Eocene times, when the northwestward movement of the Adriatic plate closed the Penninic oceanic basins. The Tisza–Dacia block was situated in its pre-rotational position SW of the Moesian plate (Romania). During Paleogene times, the Alpine–Carpathian orogenic front moved to the north driven by slab roll back of the oceanic lithosphere [*Balla*, 1987; *Linzer et al.*, 1998]. The Tisza–Dacia block rotated clockwise between 90° and 120° around the Moesian plate from Late Cretaceous to Middle Miocene times, with main rotation occurring in post-Aquitania times (<22 Ma). *Dupont-Nivet et al.* [2005] proposed a 30°–70° clockwise rotation for the Eastern and Southern Carpathians occurring during this time

span. Subsequently, the Middle Miocene to Pliocene deformation was mainly driven by retreat of the subducting slab in the embayment between the Moesian and European plates, and by the eastward escape of the Tisza–Dacia block [*Ratschbacher et al.*, 1993]. Closure of the oceanic embayment and subsequent collision of the Tisza–Dacia block (which acted as an indenter) with the Eastern European and Moesian foreland generated the arc structure of the Carpathians, inducing a further  $\sim 30^\circ$  clockwise rotation in the southern Carpathians [*Dupont-Nivet et al.*, 2005].

Structural data indicate an Early to Middle Miocene E–W contraction, followed by Middle to Late Miocene right–lateral oblique convergence in the southern Carpathians and frontal convergence in the eastern Carpathians [*Morley*, 1996; *Linzer et al.*, 1998; *Zweigel et al.*, 1998]. *Dupont-Nivet et al.* [2005] interpreted the Middle to Late Miocene vertical axis rotations in the Eastern and Southern Carpathians as the result of the indenting of the Tisia-Dacia block within the European margin. A possible mechanism explaining the clockwise rotations in the Southern Carpathians is dextral wrench tectonics affecting this region [*Linzer et al.*, 1998].

The early evolutionary phase of the Carpathians has been clearly controlled by retreat of the subducting slab. Conversely, the final shape of the arc appears to be a primary feature caused by the rotational indentation of the Tisia-Dacia block. The low amount (<20%) of orogen-parallel extension in the Eastern Carpathian arc documented by *Zweigel et al.* [1998], constitutes a proof for the syn-accretionary character of the arc, in contrast to secondary arcs which would require a major orogen-parallel extension [*Marshak et al.*, 1992; *Zweigel*, 1997]. In turn, the movement of the Tisia–Dacia block was attributed to the pull from its front (east) due to the retreating of the subducting slab [e.g.,

Royden, 1993]. Furthermore, the fanning distribution of transport directions is a feature compatible with results obtained from many indentation experiments [e.g., Zweigel, 1998].

## **7.2. Nonrotational arcs formed along irregular continental margins**

Generally, if a straight continental margin is subjected to a uniform compressive stress along strike, a roughly linear fold-thrust belt develops. However, most continental margins are not straight due to many factors linked to their past evolutionary history. The shape of passive margins would determine the distribution of stratigraphic units which could in turn affect the initial geometry of thrust faults. If thrust faults are initially spoon-shaped, then the hanging wall structures will be curved in plan view and the orogen will initiate as a nonrotational arc. Being the kinematics of such structures similar to those for indenter-related primary bends, the displacement path trajectory patterns could correspond to the patterns AB or AC of *Marshak's* [1988] classification (see paragraph 6.1.1).

One of the most commonly cited examples of nonrotational arcs formed as a consequence of the irregularity of continental margins is the Pennsylvania salient.

### **7.2.1. The example from the Appalachian (Pennsylvania, North America)**

Paleozoic rocks within the central Appalachians consist of a nearly continuous section of carbonate and clastic sedimentary rocks deposited on a rifted margin of metamorphic basement [Thomas, 1977]. The Pennsylvania salient of the Valley and Ridge is composed of three roughly linear segments of different trend: a southern (020°–025°), central (055°–060°), and northern segment (065°–085°) (Figure 7.2.1.1). The culmination in the central segment (Juniata Culmination) reflects differences in map scale shortening in

the salient. In fact, rocks have been shortened 30-38% in the south, 38-39% in the north, and ~46% in the central salient [Gray e Stamatakos, 1997].

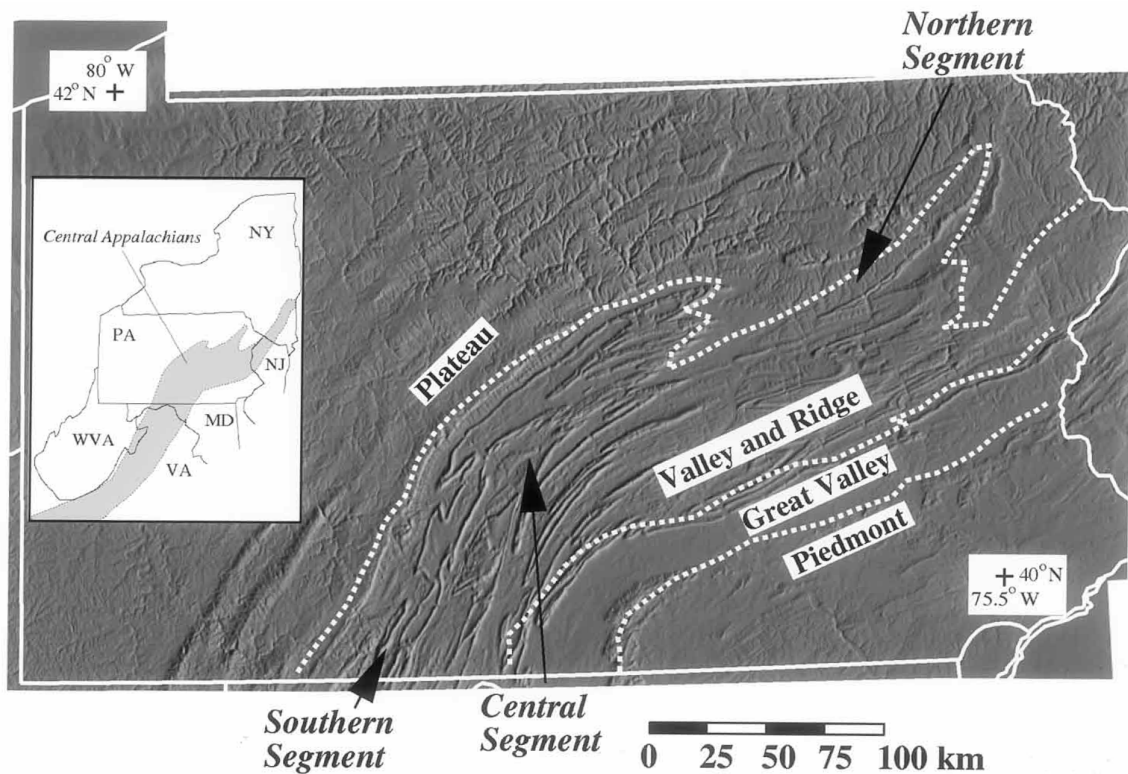


**Figure I 7.2.1.1.** Digital elevation model of the Pennsylvania salient showing the main physiographic features.

Regional shortening directions record as much as 30° clockwise rotation in the northern segment [Gray and Mitra, 1993] and opposite rotation sense in the southern segment [Evans, 1994]. The regional shortening directions on both limbs of the salient were initially subparallel and trended 320°–340°. After the early deformation phase which yielded a layer-parallel shortening, the shortening directions began to diverge. The final stages of deformation exhibit maximum shortening directions of 280°–290° in the southern segment, and 010° in the northern segment [Gray e Stamatakos, 1997].

Paleomagnetic results from previous studies [Schwartz and Van der Voo, 1983; Stamatakos and Hirt, 1994; Stamatakos et al., 1996] reveal the following spatial and

temporal relationships of deformation: (1) Folding in the salient occurred in the Permian. (2) Either prior to or during the earliest stages of deformation, rocks within the salient were rotated about a vertical axis between  $20^\circ$  and  $30^\circ$ . It remains unclear whether all of the rotation took place on one limb of the salient or whether the rotations were evenly distributed on the limbs of the salient. If both limbs of the salient rotated to achieve the overall  $30^\circ$  tightening of the salient, each limb must have rotated  $15^\circ$  in opposite directions during the earliest phase of the orogenesis. (3) Since the onset of folding and thrusting, vertical axis rotations around the salient have been negligible. Compatibly, oroclinal test performed by *Schwartz and Van der Voo* [1983] evidenced that paleomagnetic and structural direction are not correlated, as the best-fit line is not statistically different from zero slope line (see paragraph 4).

This implies that, despite evidence for early vertical axis rotations, curvature is an original feature of the arc. This conclusion is subsequently supported by the shortening directions that rotated in opposite sense to those predicted for an orocline, and precludes tectonic models that explain the curvature of the orogen solely in terms of impact by rigid indenters on the opposing African margin [e.g., *Faure et al.*, 1996].

According to the tectonic model by *Gray e Stamatakos* [1997], lateral differences in the amount of layer-parallel shortening in the lower thrust sheet produced vertical axis rotations in the upper thrust sheet. Imbrication of the lens-shaped lower sheet eventually led to the development of a three-dimensionally tapered wedge. Gravitational spreading of the tapered wedge generated progressively radiating paleostress trajectories (and concordant maximum shortening directions within the wedge) while it inhibited further vertical axis rock rotations.

### 7.3. Salients associated with obstacles

An obstacle is a feature which impedes movement on a detachment fault in a fold-thrust belt. In literature, obstacles have also been indicated by the term “buttress” [e.g., *Horberg et al.*, 1949]. Geologically, an obstacle can be represented by a stratigraphic pinch-out of a glide horizon [*Laubsher*, 1972], a basement massif on the underthrust plate [*Grubbs and Van der Voo*, 1976; *Schwartz e Van der Voo*, 1984], a seamount or an oceanic ridge upon a subducting slab, or rigid carbonate shelf [*Costa and Speranza*, 2003].

If a segment of a fold-thrust belt is pinned at an obstacle while adjacent segment are able to advance, a bend may develop. The obstacle causes systematic reorientation of stress trajectories which leads to along-strike variations in displacement path trajectories [*Laubsher*, 1972; *Beutner*, 1977]. *Marshak* [1988] suggested that oroclines can form in association with buttresses, displaying kinematic patterns OA, OB, OC, or OD (see paragraph 6.1.2).

In the experiments by *Macedo and Marshak* [1999] it has been observed that when the thrust front reach the obstacles, new thrusts that form to the foreland of the obstacles initiate with a curved trace, thus yielding nonrotational arcs. Preexisting thrusts eventually undergo oroclinal bending as they force through the space between the obstacles. These authors also noted that the shape of the salient depends on the spacing between buttresses: for a given amount of shortening, the degree of curve protrusion decreases as the distance between buttresses increases. Similar results were also obtained from magnetized analogue models by *Costa and Speranza* [2003]. Furthermore, the relative amount of shortening, as manifested by the number of thrusts and by the thickness of the thrust wedge, is greater near the end points (EP, see paragraph 3) than near the apex.

*Costa and Speranza* [2003] carried out analogue experiments using different boundary condition for buttress, such as the presence or not of a lateral confinement, the buttress type (surmountable or insurmountable in order to reproduce shallow and deep portions of the deforming sheets, respectively), and its orientation with respect to the shortening direction. Interesting aspects resulting by these experiments are listed below:

- (a) Deforming wedges colliding with obstacles in the foreland, oblique to the shortening direction, display rotations of the outer fronts opposite in sign to the oroclinal rotations.
- (b) The more internal fronts rotate only later, due to both lateral shear strain and interaction with later and more external fronts. They show oroclinal rotations, but the magnitude of rotation is smaller than that expected for a perfect orocline, except for those fronts formed inside the lateral symmetrical obstacles.
- (c) When deforming wedges collide with obstacles, rotations more strongly affect laterally unconfined wedges. Also in thin-skinned tectonics of natural settings rotations are probably easier where rocks are poorly confined laterally or in the shallower structural levels.

In the next paragraph I will report on a natural example of arcuate belt formed in association with a buttress: the Gela nappe of the Maghrebian thrust belt of Sicily (Italy).

### **7.3.1. The example from the Maghrebian thrust belt of Sicily (Italy)**

The Gela Nappe is a striking, southward-verging, salient corresponding to the largest southward advancement of the Sicilian Maghrebian belt over the African foreland (Figure 7.3.1.1). It is formed by a thin-skinned wedge exposing upper Miocene-mid Pleistocene basinal sediments [*Lickorish et al.*, 1999] deformed until mid Pleistocene

times. The Gela Nappe salient develops between two uplifted domains exposing thick and rigid shelf carbonates: the Hyblean plateau to the east, and the Saccense ridges to the west.

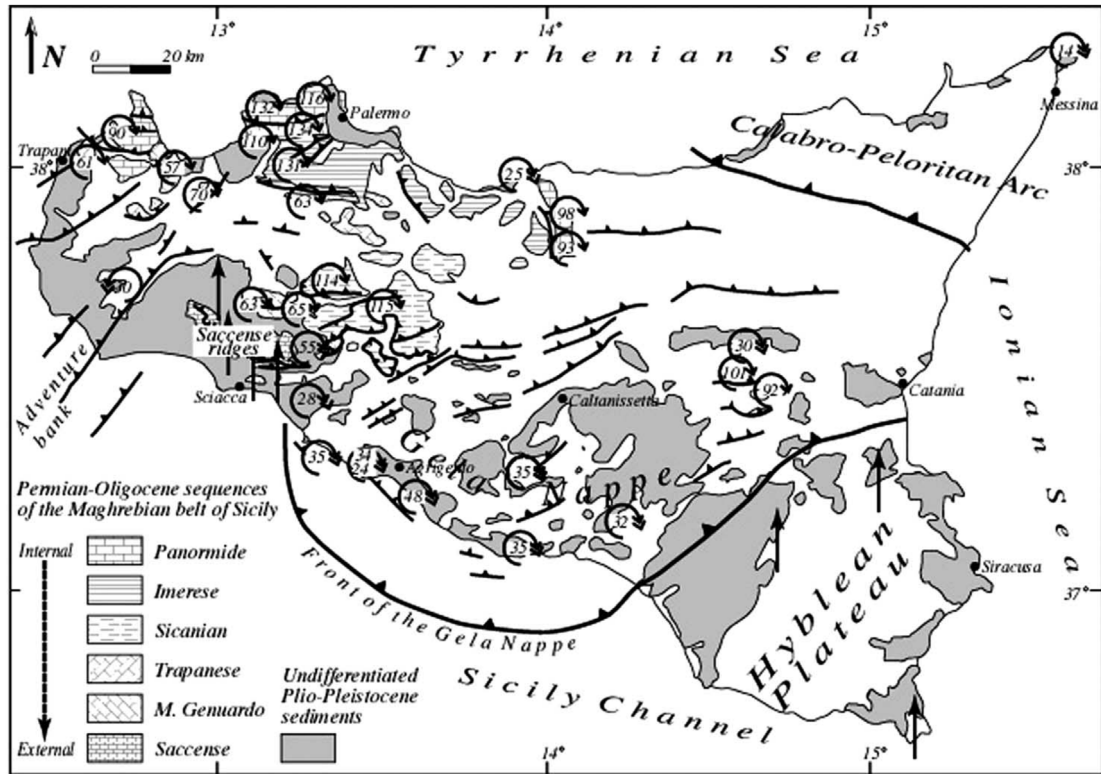


Figure 7.3.1.1. Schematic map of Sicily and paleomagnetic orogenic rotations, after Speranza *et al.* [2003]. Vertical arrows indicate unrotated areas. Circular arrows (and the enclosed angle) indicate the amount of clockwise and counterclockwise rotations calculated for the single sampling localities.

Paleomagnetic studies have shown that in Sicily large-scale clockwise rotations occurred synchronous with thrust sheet emplacement [Channell *et al.*, 1990; Speranza *et al.*, 1999, 2003]. Clockwise rotations seem to have a regional character, and to be genetically related with the spreading of the southern Tyrrhenian Sea, which induced the formation of a large-scale orocline represented by southern Apennines, Calabria, and Sicilian Magherbides belt fragments [e.g., Gattacceca and Speranza, 2002; Speranza *et al.*, 2003]. In Sicily, Speranza *et al.* (2003) have shown that a 70° clockwise rotation occurred in mid Miocene times, followed by a late Miocene-Pleistocene 30° clockwise rotation.

Plio-Pleistocene sediments sampled in several parts of the Gela Nappe show invariantly 10–30° CW rotations [*Speranza et al.*, 1999, 2003]. Older pre-orogenic sediments exposed at the edges of the Gela Nappe itself similarly show a ubiquitous 100° total orogenic rotation, without any major difference between the eastern and western limbs of the salient [*Channell et al.*, 1990; *Speranza et al.*, 2003].

The paleomagnetic data summarized above show that the Gela Nappe salient is an almost perfect nonrotational arc, once the uniform CW rotation of the Sicilian nappes is eliminated. The two platform carbonate domes represented by the Hyblean plateau to the east, and the Saccense ridges to the west, may have represented the foreland obstacles colliding with a southward propagating thrust wedge and causing the formation of a pronounced belt salient. This hypothesis appears to be in good agreement with the results of analogue models by *Costa and Speranza* [2003], who showed that lateral symmetrical obstacles in the foreland colliding with forward propagating wedges produce a nonrotational outer curved front.

#### **7.4. Basin-controlled orogenic bends**

Numerous authors have documented the existence of a spatial association of salients with particularly thick sedimentary basins [*Marshak and Wilkerson*, 1992; *Boyer*, 1995], and that the position of the salient's apex coincides, in many cases, with the location of the precollisional depocenter (i.e., thickest strata) in the basin from which the salient formed [*Macedo and Marshak*, 1999]. Therefore, along-strike variations in the predeformational basin thickness in a sedimentary basin can yield favourable conditions for bends formation. Also, if variation in predeformational sedimentary thickness affect salient location, it can also affect its shape. In fact, several analogue experiments [e.g.,

*Macedo and Marshak, 1999*] have demonstrated that the thickness of sedimentary succession, and thus, the shape of the sedimentary basin, controls the final shape of the bend. Thus, if the basin has a symmetric (asymmetric) shape, the salient will develop with a symmetric (asymmetric) shape. Moreover, if the basin has a flat or spoon-shaped bottom surface, the bend will develop with a flat or rounded crest, respectively. In Figure 7.4.1 possible salient shape based on the shape of the sedimentary basin are shown.

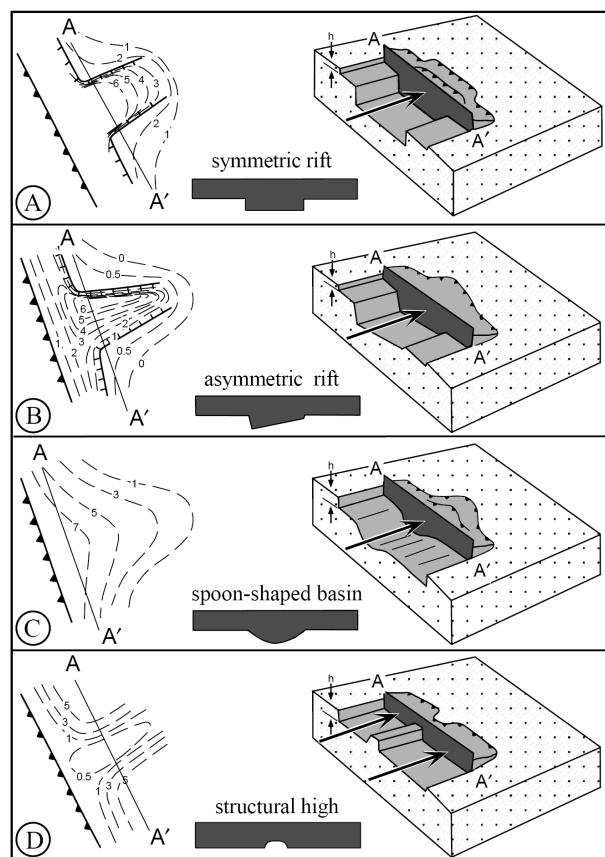


**Figure 7.4.1. Possible bend geometries depending on the shape of the sedimentary basin, (h) Thickness of deforming sedimentary layer. After *Macedo and Marshak* [1999].**

Basin-controlled salients form because, as *Marshak and Wilkerson* [1992] noted, the width of a thrust wedge is linearly proportional to the sediment thickness (Figure 7.4.2), a relationship that reflects volume balance during deformation.

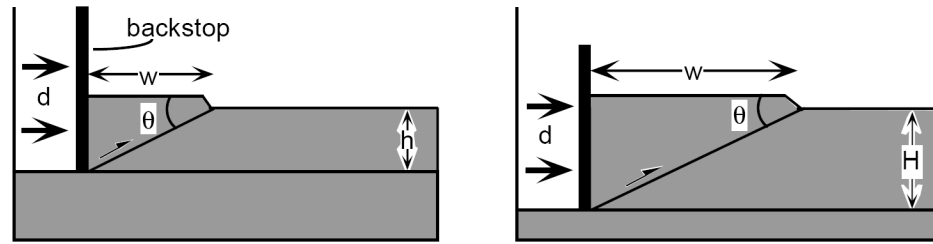


**Figure 7.4.2. Cross-section comparison of the effect of layer thickness on the width of a thrust sheet. Assuming the same thrust angle, the width of thrust sheets must be wider when formed from a thicker layer than from a thinner layer because when the layer is thicker, a greater volume of material must be displaced. After Macedo e Marshak [1999].**

As pointed out by *Marshak et al.* [1992], basin-controlled salients are nonrotational arcs, in the sense that thrusts in these salients initiate with curved trend lines so that the limbs of the salient do not rotate significantly around a vertical axis with progressive deformation. However, the statement that thrust traces do not undergo rotation in basin-controlled salients does not imply that the rock composing thrust sheets are not affected by rotations. In fact, simple shear of rock within thrust sheets on the limbs of the salient could yield a variable amount of rotation. Furthermore, strike-slip faults develop in cases where the transition between thick and thin strata is very abrupt.

Finally, according to the bends geometries classification by *Macedo and Marshak* [1999] (see paragraph 5), the pattern of structural trend lines in basin-controlled salients shows trend lines convergent toward the end points. This is caused by the fact that the sedimentary sequence involved in thrusting thins toward the end points.

In the following paragraph I will show the natural example of basin-controlled salient of the Jura Arc, northern Alps.

#### **7.4.1. The example from the Jura Arc (Northern Alps)**

The Jura fold-thrust belt is an arcuate region of more than 350 km lateral extent, lying northwest of the northern alpine foreland basin (Swiss Molasse). The structural grain

of the Jura arc swings a full 90° from a N-S direction at the southwest end to an E-W direction at the northeast end. The belt is composed of Mesozoic strata detached from a Permo-Carboniferous basement by Triassic evaporite layers. This latest and most external fold-thrust belt of the Alps developed after the middle Miocene (Serravallian) on the external side of the Molasse foredeep [Laubscher, 1992; Burkhard and Sommaruga, 1998]. Bulk shortening perpendicular to the fold trends ranges from more than 35 km in western parts to some 25 km in central parts [Mugnier *et al.*, 1990; Philippe, 1995]. Towards the east, bulk shortening decreases regularly to zero [Burkhard, 1990]. The strain trajectories map in Figure 7.5.1, describe a strongly divergent, radial pattern with NE-N-directed compression at the eastern end of the Jura and W-directed compression behind the western termination of the arc. This gross pattern confirms the large-scale structural trend of the Jura fold-thrust belt as depicted by tectonic maps.

Early paleomagnetic studies from the Jura fold belt [Van der Voo *et al.*, 1979; Eldredge *et al.*, 1985; Lowrie and Hirt, 1986; Gehring *et al.*, 1991], documented only very small and barely significant clockwise rotations of less than 10°. Oroclinal tests performed by Eldredge *et al.* [1985] and Lowrie and Hirt [1986] proved the primary origin of the arc. Conversely, two recent studies in Oligo-Miocene Molasse sandstones from the hinterland of the Jura have identified small but systematic clockwise deviations of paleo-poles from present day geographic north, on the order of  $5 \pm 25^\circ$  [Schlunegger *et al.*, 1996; Kempf *et al.*, 1998]. There are only two published sites from behind the western half of the Jura [Burbank *et al.*, 1992]. The tectonic interpretation of the paleomagnetically determined declinations for Oligocene Molasse sandstones is somewhat hampered by the fact that there are no directly comparable sites available for the undeformed foreland of the Jura. The maximum difference between paleo-pole declinations east and west of the symmetry

axis of the Jura arc is on the order of  $30\pm 35^\circ$  for rocks of the same Oligocene age. Excluding an oroclinal bending mechanism producing these rotations, we can tentatively propose a shear-induced origin along the limbs of the bend for them.

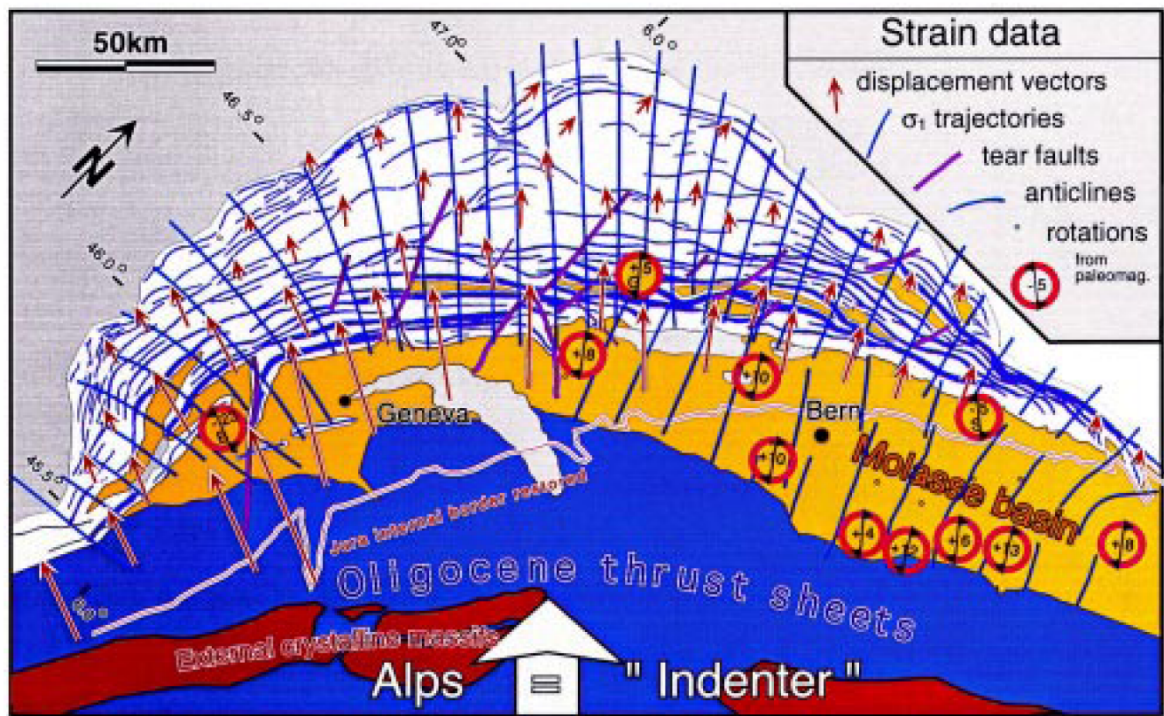


Figure 1. Tectonic overview of the Jura arc in front of the northwestern Alps with compiled strain data. The arcuate shape of the Jura is materialized by the trend of major anticlines. Strain trajectories (in blue) have been computed from a large data set of 180 stations where populations of minor faults have been used to calculate paleo-stress tensors by inversion methods (Homberg, 1996). Displacement vectors (red, to scale) are based on the study by Philippe et al. [1996]. Rotations have been taken by previous studies by Kempf et al. [1998], Gehring et al. [1991], Burbank et al. [1992], and Schlunegger et al. [1996]. After Hindle and Burkhard [1999].

*Laubscher* (1972) and *Hindle et al.* [2000] proposed as mechanism for crustal shortening in the Jura belt the indenting by the western Alps (Helvetic and Prealpine nappes), pushing as a rigid block into the Molasse and Jura (i.e. both are indented but only the Jura shows significant deformation) with a uniform northwestward direction. This mechanism is suitable to explain the overall geometry of total finite displacement in the Jura arc, without requiring divergent transport along strike or secondary bending.

The external border of the Jura arc coincides with the Triassic evaporite (representing the basal detachment surface) pinch-out and the arc mimics directly the original shape of the Triassic basin border. Therefore, it is very likely that the western and eastern limbs of the Jura arc owe their asymmetry to paleogeography [e.g., *Philippe*, 1994]. In addition to lateral variations in the basal décollement level, a lateral increase in total thickness of the folded Mesozoic cover explains a striking westward increase in fold amplitude and wavelength. While the outer curvature of the Jura arc can largely be interpreted in terms of paleogeographic prestructuration, the inner curvature, i.e. the rather abrupt change between virtually undeformed Molasse basin and strongly folded and thrustured Jura, still remains a matter of debate.

In conclusion, according to the geologic, structural and paleomagnetic data available from the Jura fold-thrust belt, we can consider the Jura arc as a basin-controlled primary bend, where an important role has also been played by the presence of a buttress, i.e. the lateral termination of the salt-gypsum level (representing a glide horizon for deformation).

### **7.5. Topography-driven arcs**

According to the gravitational collapse model by *England and Houseman* [1989], shortening and extension are initiated and driven by the potential energy difference between the extending region and the surrounding shortening region. This would result in a region of extension encircled by a region of shortening resulting from radial thrusting. No vertical axis rotations are expected because radial spreading would imply that outward thrusting is always perpendicular to the strike of the arc. Conversely, tangential extension is required.

The origin of the potential energy difference has been generally attributed to a thickened crust [e.g., *Molnar and Tapponnier, 1978*]. The difference in potential energy  $\Delta E_p$  is given by the following equation (1) [*Frank, 1972*]:

$$\Delta E_p = \int_0^{z_c} \int_0^z [\rho(z)g]_T dzdz - \int_0^{z_c} \int_0^z [\rho(z)g]_R dzdz \quad (1)$$

where  $z$  is the depth below the surface,  $\rho(z)$  is the depth-dependent density,  $g$  is the gravity acceleration, T and R denote thickened and reference columns, respectively. The density of crust and lithospheric mantle can be assumed to be constant. Considering that the reference crust has a thickness  $H$ , and the thickened crust has  $(H+h+\Delta H)$ , where  $h$  is the topographic elevation from the reference crust and  $\Delta H$  is the crustal root the equation (1) can be calculated by integrating the equation (1) for  $z=0$  to  $z=h+H+\Delta H$ :

$$\Delta E_p = \frac{1}{2} \rho_{cr} g h^2 + \rho_{cr} g H h + \frac{1}{2} \rho_{cr} g h \Delta H \quad (2)$$

where  $\rho_{cr}$  is the density of the crust. The equation (2) can be rewritten in terms of  $h$  and  $H$ , as follows:

$$\Delta E_p = \frac{1}{2} \rho_{cr} g h^2 + \rho_{cr} g H h + \frac{\rho_{cr}^2 g h^2}{2(\rho_m - \rho_{cr})} \quad (3)$$

where  $\rho_m$  is the density of the mantle.

In summary, it can be observed that, being constant the other parameters, the potential energy increase with the increasing of  $h$ , that is the topographic relief.

In the lithospheric and crustal collapse models, it has generally been assumed [e.g., *Platt and England, 1994*] that collapse will occur when potential energy difference between a thickened column and foreland column (equation 3) is larger than the extensional integrated strength of the thickened column given by the following equation (4):

$$\text{Integrated Strength} = \int_0^{z_l} (\sigma_1 - \sigma_3) dz \quad (4)$$

where  $z_l$  is the base of the lithosphere.

In conclusion, the gravitational collapse model might work for orogenic regions with a very thickened crust and therefore with high potential energy, as also proposed by *Schellart and Lister* [2004].

The importance of topography and gravitational potential, as primary controls on stress distribution within the lithosphere, has long been recognized [e.g., *England and Molnar*, 1997; *Marques e Cobbold*, 2002]. Where there is topographic relief, the stress field will vary horizontally. According to the Critical Taper theory, a wedge of non-cohesive Coulomb material deforms until it reaches a critical angle of taper (including surface slope and basal slope), which depends on the internal and basal coefficients of friction. If these coefficients are constant, the wedge profile becomes triangular [*Dahlen*, 1990]. Where topography was locally higher than that predicted by the theory, no further thickening took place during deformation. Where topography was lower than predicted, thickening occurred preferentially, although not always in the earliest stages of deformation.

Relying on this theory, corroborated by numerous analogue experiments [e.g., *Marques and Cobbold*, 2002], active thrusts tend to be arcuate in map view, forming salients around areas of high topography and recesses across areas of continuing erosion (Figure 7.5.1). Experiments by *Davy and Cobbold* [1991] and *Marques and Cobbold* [2002], evidenced the tendency for that areas subjected to erosion to be more prone to shortening. Therefore, continuing erosion in the hinterland caused repeated reactivation of thrusts, rather than formation of new ones towards the foreland. Conversely, areas of high

topography (plateaux and conical mountains) tend to spread sideways. At the leading edge of a plateau, dip-slip motions on arcuate thrust salients accommodated radial displacements, yielding primary arcs.

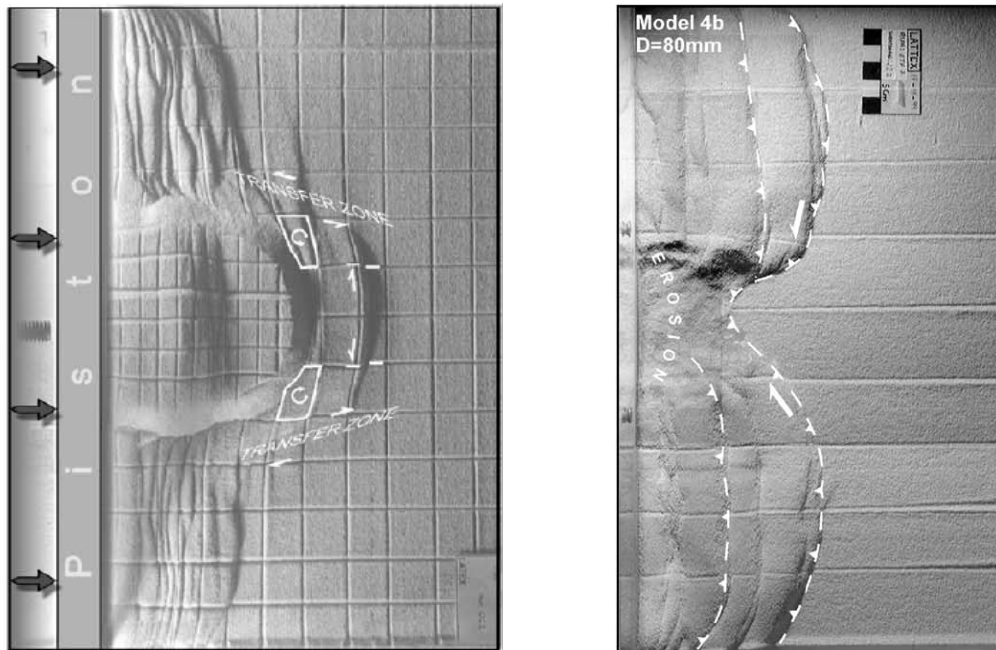


**Figure 7.5.1.** Analogue models by *Marques and Cobbold* [2002] showing the formation of a salient in front of an area of high topography (left), and recess across an area subjected to erosion (right).

At the lateral edges of the plateau, which are affected by a simple shear stress, transfer zones could develop. Deformation in these zones tended to be strongly localized, and accommodated by oblique slip on thrust faults and by block rotations about vertical axes, that are clockwise and counterclockwise in the right and left side of the plateau, respectively (Figure 7.5.1, left).

### 7.5.1. The example from the Hellenic Arc

The Eastern Mediterranean Alpine belt results from the N-S convergence of the Eurasia and Arabia/Africa plates [*Sengör and Vilmaz*, 1981]. The Aegean Sea (southern

Greece) represents a piece of continental lithosphere undergoing widespread ~N-S extension at the rear of a curved subduction zone (South Hellenic subduction zone), beneath which the oceanic lithosphere of the African plate plunges northward (Figure 7.5.1.1). Between Greece and Turkey the Alpine orogen, here constituted by the Dinarides, Cyclades and Taurides, forms a kilometric-scale salient known as the Hellenic Arc [McKenzie, 1978; Le Pichon, 1982; Kissel and Laj, 1988; Duermeijger et al., 1998; Walcott and White, 1998; Gautier et al., 1999; Kissel et al., 2003]. The Aegean Sea and the Hellenic arc together form a classical arc-backarc system.

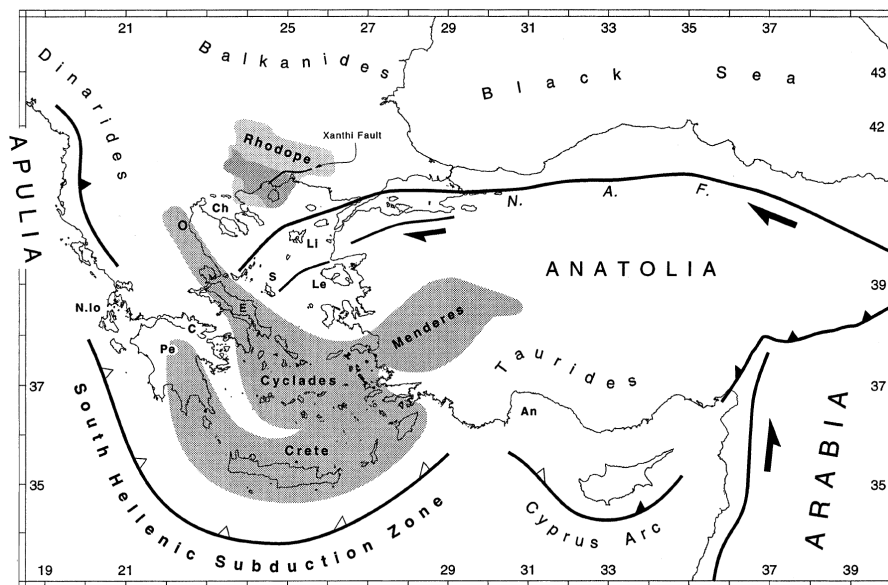


Figure 7.5.1.1. Simplified structural map of the Eastern Mediterranean. After Gautier et al. [1999].

The distribution of stretching directions along the entire Aegean, associated with backarc extension, shows a divergent pattern, being NE-SW and N-S in the eastern and southern regions, respectively [Gautier and Brun, 1994]. However, Lee and Lister [1992] documented a well developed NE-dipping mylonitic foliation, and an ENE-trending mineral elongation lineation in the extension-related exhumed rocks from the backarc

region. These kinematic indicators are consistent with a top-to-NE sense of shear along the major detachment faults of the basin.

Paleomagnetic data from the Aegean reveal the existence of a western (West Aegean) and eastern (East Aegean) region characterized by a general  $\sim 30^\circ$  clockwise and counterclockwise rotation, respectively [Kissel and Laj, 1988; Kissel and Speranza, 1995; Speranza *et al.*, 1995; Morris and Anderson, 1996; Kissel *et al.*, 2003]. The central Aegean, where a mean N-S stretching direction dominates, appears to have undergone no rotation or a small ( $< 20^\circ$ ) counterclockwise rotation [Morris and Anderson, 1996; Duermeijer *et al.*, 1998] (Figure 7.5.1.2). All these rotations occurred after early Miocene times.

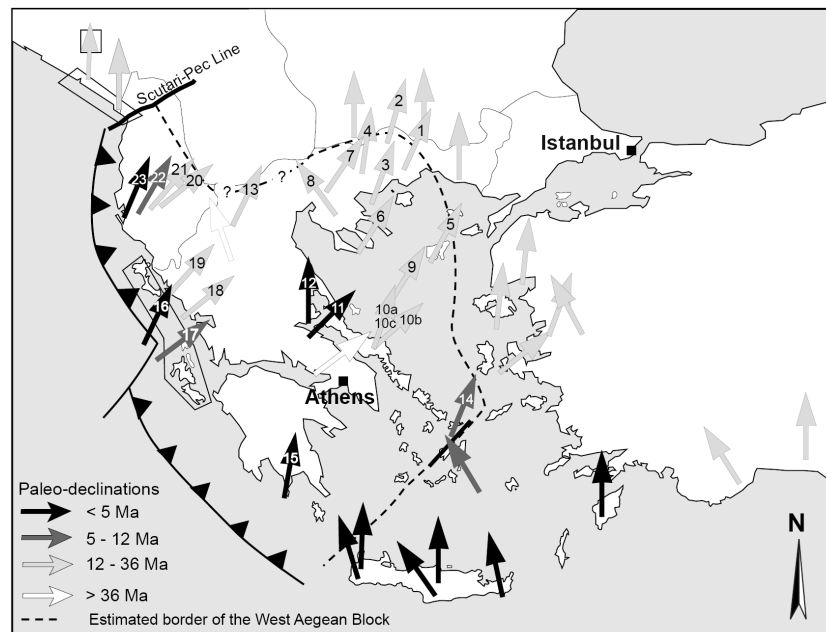
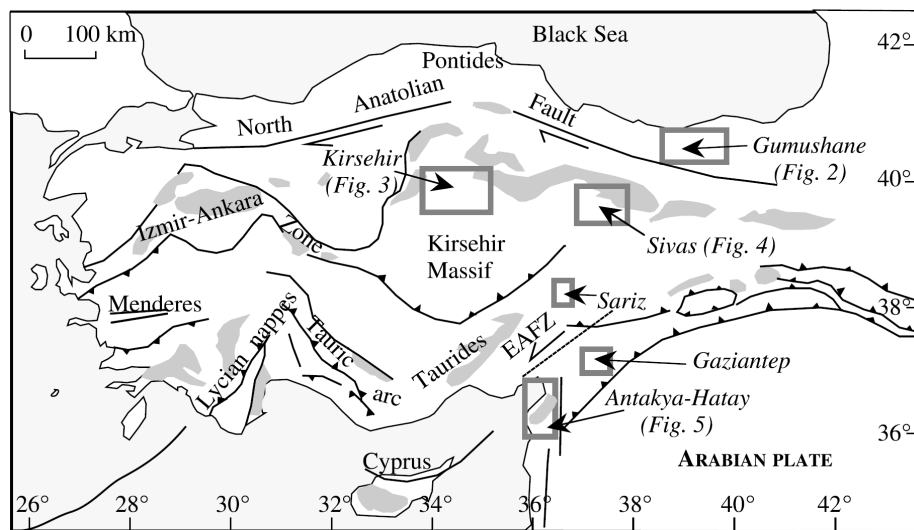


Figure 7.5.1.2. Paleomagnetic declinations of Tertiary rocks in the Aegean. The dotted line marks the boundary of an area of predominantly clockwise rotation. After *Walcott and White* [1998].

The eastern side of the Hellenic Arc is represented by the Anatolian block. In late Miocene to Present times, a major dislocation of entire Anatolia block occurred along two

prominent active structural lines: the dextral North Anatolian and the sinistral East Anatolian strike-slip fault zones (Figure 7.5.1.3). Between these kilometric faults, the Anatolian block moves westward, escaping from the Arabian/Eurasiatic collision zone. Paleomagnetic data from this region [Piper *et al.*, 1996; Gürsoy *et al.*, 1997; Platzman *et al.*, 1998; Kissel *et al.*, 2003] reveal that a large-scale counterclockwise rotation of the Anatolian block of  $\sim 25^\circ$  has occurred during Neogene time ( $< 21$  Ma).



**Figure 7.5.1.3. Tectonic map of Turkey showing the Anatolian block and the North and East (EAFZ) Anatolian Faults. After Kissel *et al.* [2003].**

Many different tectonic scenarios have been drawn so far to explain the evolution of the Aegean area, mainly based on structural and paleomagnetic evidence. Kissel and Laj [1988] suggested that the current curvature of this region was acquired in two major phases starting in the early Miocene from an almost rectilinear E–W-trending of the belt. During the first phase (middle Miocene,  $\sim 15$  Ma) a clockwise rotation in the West Aegean (Dinarides) and a counterclockwise rotation in western Anatolia (Turkey) took place. The second phase, characterizing the last 5 Ma, produced only clockwise rotations for the northwestern part of Greece.

Analogously, *Walcott and White* [1998] suggested that a  $\sim 30^\circ$  clockwise rotation in the West Aegean and a  $\sim 19^\circ$  counterclockwise rotation in the East Aegean occurred between 25 and 3 Ma (Figure 7.5.1.4). They interpreted the bulk rotation of the West Aegean to be the result of pinning and shortening of the northwest margin whilst the southeast Aegean underwent extension. After  $\sim 3$  Ma the West Aegean block subdivided into two portions: the southeastern portion coupled with the SW Cycladic area to form the Central Aegean block and started to translate southwest without any rotations, while the NW margin continued to rotate  $\sim 15^\circ$  clockwise.

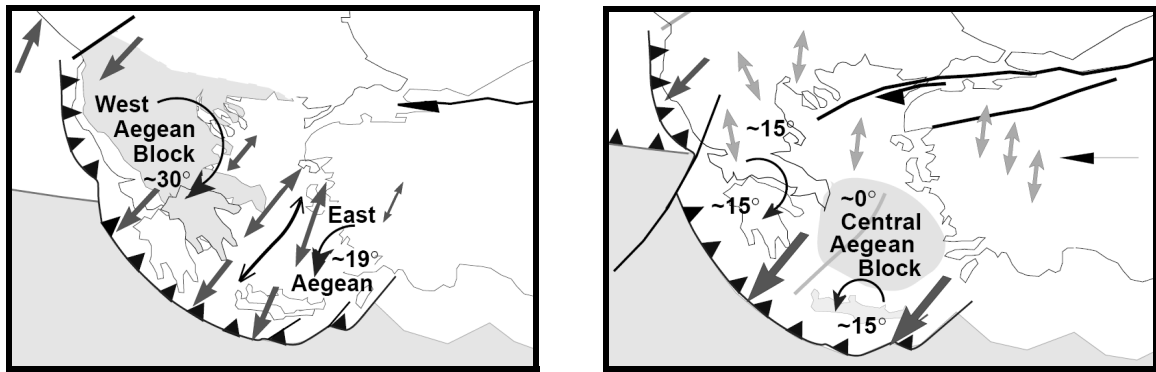


Figure 7.5.1.4. Tectonic evolution during the 25-3 Ma (left) and post-3 Ma (right) phase, as proposed by *Walcott and White* [1998]. After *Walcott and White* [1998].

Three major mechanisms have been proposed to explain the development of the Hellenic arc-backarc system. The first is the southward retreat and rollback of the subducting slab driven by the negative buoyancy of the cold African oceanic lithosphere sinking into the mantle [e.g., *Le Pichon*, 1982]. The second is the westward extrusion of Anatolia block along the North Anatolian fault [e.g., *McKenzie*, 1972], and the third is gravitational collapse of an overthickened crust [e.g., *Gautier et al.*, 1999].

According to the gravitational collapse model by *Gautier et al.* [1999], the tectonic evolution of the Aegean initiates between 21 and 16 Ma with the southward spreading of

the Aegean thickened lithosphere as a result of gravity forces acting along its southern boundary, which provided the arcuate shape of the orogen. After ~16 Ma the westward movement of the Anatolia block resulted in a further deformation of the Aegean domain. Results from analogue models carried out by *Gautier et al.* [1999] are compatible with the structural and paleomagnetic features of the Hellenic arc.

## **7.6. Orogenic arcs linked to the bending of “ribbon continent”**

During phases of accretion of lithospheric blocks against a major pre-existing continental margin, their mechanical properties influence the deformation process. In fact, has been documented how elongated lithospheric blocks, characterized by asymmetric shape, known in literature as “ribbon continents” [e.g., *Johnstone*, 2001] can be more easily deformed and bended than a block with a symmetric shape. Therefore, when a migrating ribbon continent collides with an irregular margin of a major plate it can be bended and form arcuate orogenic systems.

### **7.6.1. The example from the Great Alaskan Terrane Wreck**

One of the most striking example of continental growth due to accretion of terranes to continental margin is represented by the Cordillera of North America. Paleomagnetic data for Cretaceous rocks of the Cordillera imply that the crust containing these units lay far (2000-3000 km) to the south during their formation, and require significant late Cretaceous dextral translation to bring these terranes to their current position [*Irving and Wynne*, 1991]. The continental drift of such blocks were possible because of the strongly

oblique plates convergence which constituted an ideal setting for the entrainment and orogen-parallel translation of crustal blocks.

An E-W-trending, north-verging structural stack of rock sequences underlying the Arctic Alaska region of northern Alaska is continuous over a strike distance major than 4000 km west into Siberia and southeast into Yukon. This mountain chain is composed of several orogenic arcs which *Box* [1985] considered as being primary features of the Paleozoic continental margin of western North America. It suggested that younger terranes draped over this sinuous margin during accretion.

Central and northern Alaska is divisible into the northerly E-W-trending Arctic Alaska, the central SW-trending Ruby, and the southerly E-W-trending Dillinger belts, constituting a Z-shaped bend (Figure 7.6.1.1). The belts are connected through orogenic bends, and both facing and structural vergence directions vary in a consistent and predictable fashion from belt to belt, indicating that they previously formed a coherent linear “ribbon continent”. The Arctic Alaska belt is in fault contact to the east with a Jurassic to Cretaceous molasse deposits, which separate the Arctic Alaska belt to the west from autochthonous Paleozoic continental margin sequences of ancestral North America to the east, and are involved in the North Alaskan orocline. They therefore limit bends formation to the time interval Late Cretaceous-Tertiary.

Paleomagnetic data, though complicated by the lack of primary remanent magnetization, imply that increasingly far-sided paleo-poles characterize the more southerly belts. Thus, displacement of the Arctic Alaska belt (~1320 km) is less than that of the Yukon-Tanana belt and attached strata to the south (3000±500 km south at 85 Ma, and 1900±700 km south at 70 Ma). Rotations required by the paleomagnetic data include counterclockwise rotation of Arctic Alaska, clockwise rotation of strata within the North

Alaskan orocline, significant counterclockwise rotation of the Dillingen belt, and little rotation of the Yukon-Tanana belt.

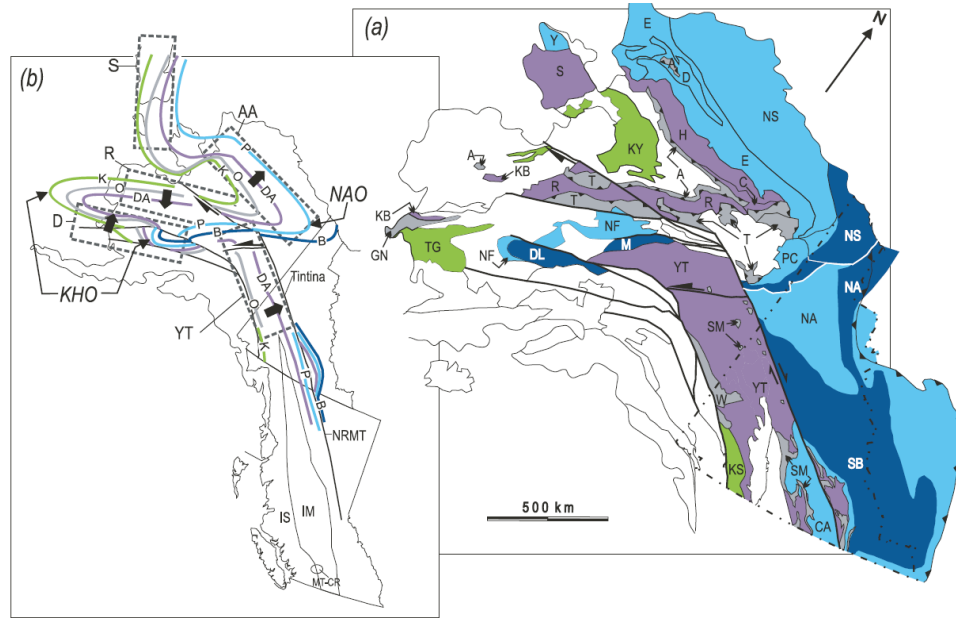


**Figure 7.6.1.1. Geologic map of Alaska and Yukon. After *Johnstone* [2001].**

The geological history, the continuity of the belts, structural relationships (oroclines and escape structures), together with paleomagnetic data, indicate that the belts originated as an elongate linear “ribbon continent”. The current geometry of the orogen is the result of buckling of the ribbon continent, which was over 8000 km long and 500 km wide, about vertical axes of rotation. Northward translation of the ribbon continent initiated at about 85 Ma when the oceanic Farallon plate, which floored most of the northern Pacific basin, rifted into a northerly Kula plate and a southerly Farallon plate. Buckling of the ribbon continent appears to have begun almost immediately after the initiation of northward displacement. Figure 7.6.1.2 shows the evolution of the ribbon continent.

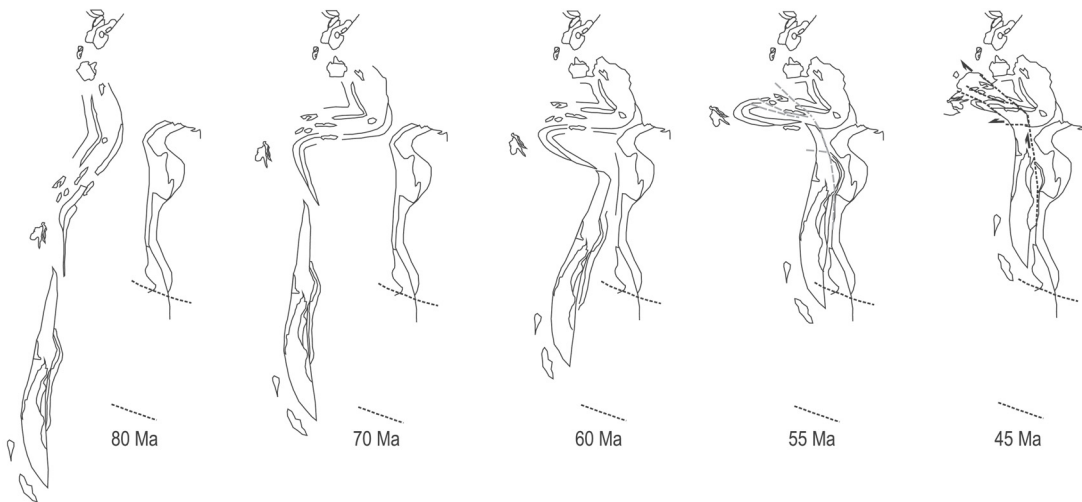


**Figure 7.6.1.2. Schematic paleogeographic maps showing, from left to right, northward migration and buckling of the ribbon continent. After *Johnstone* [2001].**

### 7.7. Subduction-related arcs

In subduction zones an arc can be defined by the geometry of both the trench and the volcanic arc. But the question arises as why is the trench (and slab) shape curved in map view? *Frank's* [1968] model tried to explain this phenomenon invoking the Earth's sphericity. His model implies a direct relationship between slab dip angle ( $\alpha$ ), the central vertex angle ( $\beta$ ) depending on the arc radius, and the arc radius ( $r$ ):

$$\alpha = \beta = 360(r/\pi R)$$

where  $R$  is the Earth's radius. The model predicts that slab dip should increase with increasing central vertex angle, and that slab dip should remain constant along the length of the arc, requirements that are generally not observed in natural examples. Based on these criteria, the model does not account for arcuate subduction zones around the globe.

However, there are several lines of evidence from different disciplines in geology that suggest that most arcs are not initial static geometries but evolve through time from more rectilinear geometries. These can be reassumed in the following points:

- The wide range of arcuate shapes;

- Vertical axis rotations are different in sense along the arc;
- GPS data indicate that different segments of the arc are characterized by different velocities compared to a fixed hinterland;
- The presence of back-arc basins on their concave side which have often experienced a long lasting extension or spreading.

Though not all arc-shaped convergent zones necessarily evolved from initially straighter geometry in an arc-backarc system the possibility of developing curve structure are much higher and strictly linked to the mechanisms associated to, and triggered by the subduction process. In fact, arc-backarc systems develop in an overall convergent tectonic setting, with shortening in the overriding plate close to the subduction interface (fore-arc region) and extension on the concave side of the arc (backarc region).

Different types of tectonic models have been proposed so far to explain the formation of arc-backarc systems that are characterized by progressive arc formation, shortening in the fore-arc region, and extension in the backarc region [*Schellart and Lister, 2004*]. Here we will discuss model dealing with arc-backarc system formation in subduction regimes: the slab rollback model [e.g., *Faccenna et al., 1997*]. In the slab rollback model, deformation results from retreat of the subducting slab which triggers simultaneously compression and extension in the overriding plate. Compression occurs close to the trench due to accretion of ocean sediments [*Malinverno and Ryan, 1986*], while extension characterizes the inner part of the overriding plate behind the trench. In fact, rollback leads to the formation of a potentially vacant zone at the contact between the subducting and overriding plates [*Shemenda, 1993*]. This potentially vacant region will be filled by the overriding plate, which collapses toward the retreating hinge of the subducting plate because it is not strong enough to sustain such a potentially vacant region at the plate

boundary. Extension in the overriding plate will be oriented in a direction perpendicular to the trench.

In this geodynamic context, arc formation results from the lateral change in retreat velocity along the subduction zone and would imply opposite sense of vertical axis rotation (saloon-door type) along the limbs of the arc during progressive slab retreat. One common factor causing arc formation during slab retreat is mantle flow around the slab edges in the case that the slab has a small lateral extension [*Faccenna et al.*, 1997; *Schellart*, 2004; *Cifelli et al.*, 2007].

Several driving mechanisms have been proposed to explain the retreat of the hinge-line of the subducting lithosphere, such as: (1) negative buoyancy of the slab with respect to the sub-lithospheric mantle through which it sinks [*Malinverno and Ryan*, 1986; *Shemenda*, 1993]. (2) The pushing of the overriding plate on the hinge-line of the subducting plate [*Gautier et al.*, 1999] caused by body forces (linked to potential energy) or tectonics. (3) The overall east-directed flow in the asthenosphere or the net westward rotation of the lithosphere which would push west-dipping slabs eastward, increasing its dip angle, and causing a deviatoric tension along the subduction interface [*Moore*, 1973]. *Schellart and Lister* [2004] conclude that the negative buoyancy force is the most likely cause for the slab rollback mechanism, among those proposed. Furthermore, the rollback process is considered the most likely candidate to form arcuate systems as the overriding plate has no option other than to follow the migrating hinge. In fact, if this were not the case, the retreating slab would simply create a lithospheric-scale gap, and of course, no such gaps are found along subduction zones.

In the next paragraphs I will introduce the example from the Calabrian arc (southern Italy).

### 7.7.1. The example from the Calabrian Arc (southern Italy)

The Calabrian Arc defines a mountain belt encircling the Tyrrhenian Sea, from southern Apennine to Sicilian Maghrebides (Figure 7.7.1.1). The Calabrian Arc is presently located on top of a narrow (roughly 200 km) and steeply ( $70^\circ$ ) subducting slab [Anderson and Jackson, 1987; Selvaggi and Chiarabba, 1995; Lucente et al., 1999], 700 km long [Piromallo and Morelli, 2003].

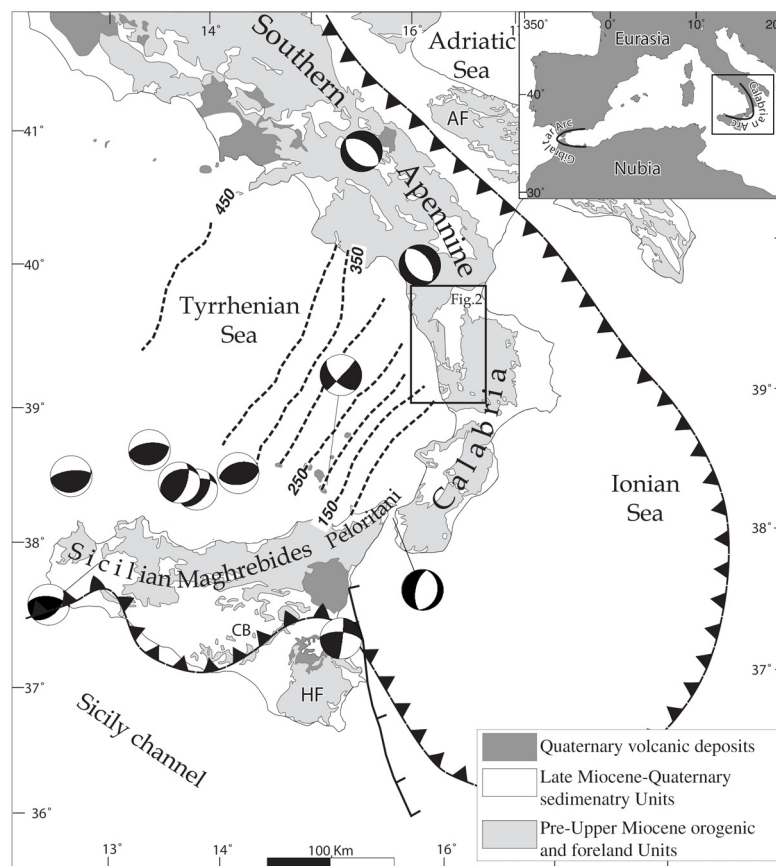


Figure 7.7.1.1. Schematic geologic map of southern Italy. After Cifelli et al. [2007].

Since the mid-late Miocene, back-arc extension and rifting processes in southern Tyrrhenian Basin were synchronous with the outward migration of compressional phases in southern Apennines-Sicilian Maghrebides toward the Apulian foreland. Trench retreat

of the Ionian slab generated the opening of the southern Tyrrhenian Sea back-arc basin and the overprinting of the early Alpine compressional structures by extensional tectonics [e.g., *Rossetti et al.*, 2004]. The fast retreat of the Ionian slab was responsible of the southeastward drifting of the Calabro-Peloritane Domain (CPD), which was finally incorporated in the Apennine-Maghrebian chain, to form the present-day Calabrian Arc. The geological architecture of northern Calabria consists of an Eocene orogenic nappe stack accreted onto the Apulian paleomargin and is made of Hercynian basement rocks and Alpine polymetamorphic sequences derived from the deformation of the southern Tethyan margin. This orogenic pile is unconformably covered by middle Miocene to Recent postorogenic synrift to postrift sediments along the Tyrrhenian side and by a thick Oligocene to Pleistocene forearc sedimentary sequence along the Ionian side [e.g., *Bonardi et al.*, 2001].

Paleomagnetic data collected in southern Italy (Figure 7.7.1.2) evidence two geologic sectors, southern Apennines to the north and Calabria and Sicily to the south, affected by opposite tectonic rotations (counterclockwise and clockwise, respectively) [*Channell et al.*, 1980, 1990; *Gattacceca and Speranza*, 2002; *Mattei et al.*, 2002; *Speranza et al.*, 1999, 2003; *Cifelli et al.*, 2004; *Mattei et al.*, 2004; *Cifelli et al.*, 2007]. Rotations are confined to the orogenic wedge, and do not extend to the Apulia and Hyblean forelands, which did not undergo tectonic rotations. In Sicily, paleomagnetic data from Middle Jurassic sedimentary rocks show a decrease in paleomagnetic rotations from the more internal Panormide-Imerese and Sicanian units (up to 145° clockwise), to the intermediate paleogeographic units of the Trapanese and Internal Saccense (50° clockwise). In the southern Apennines paleomagnetic data from Cretaceous to middle Miocene carbonate platform sediments, and from Jurassic to Cretaceous pelagic

calcareous-marly sediments, evidence a constant amount of counterclockwise rotations (70°–80° in average) which have been measured either in Jurassic to Oligocene units.

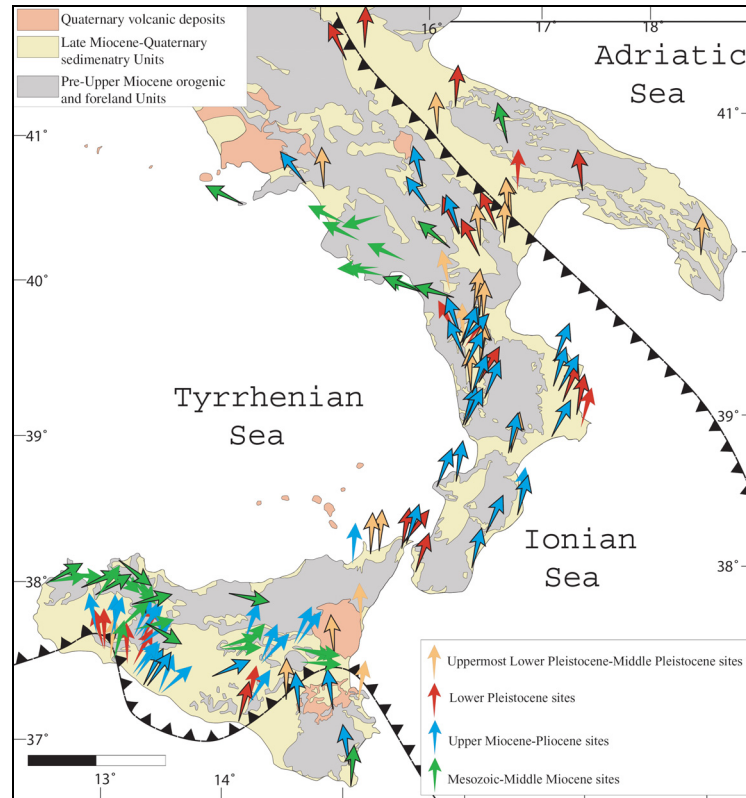


**Figure 7.7.1.2. Paleomagnetic rotations from the southern Apennines, Calabrian Arc and Sicily. After Cifelli *et al.* [2007].**

Finally, both in Sicily and southern Apennines, uppermost lower Pleistocene and middle Pleistocene sediments are substantially not rotated. In the CPD, paleomagnetic data mainly collected in upper Miocene to Pleistocene sedimentary sequences show a post-mid Miocene 20° clockwise rotation, whereas the uppermost lower Pleistocene–middle Pleistocene sediments generally do not show appreciable rotations.

These data evidenced that the tectonic evolution of the Calabrian Arc cannot be explained using classical concepts of primary, secondary or progressive arcs, which do not

account for the complex rotational history of this area. The presence of opposite paleomagnetic rotations in Sicily and southern Apennines demonstrates that the tectonic evolution of the Calabrian Arc does not fit well with a primary arc model. The orocline model is not consistent with the tectonic evolution of the Calabrian Arc curvature as well, because large magnitude vertical axis rotations occurred contemporaneously with fold-thrust belt formation and not during a second phase, when the orogen were already developed. Consequently, as a first approximation the Calabrian Arc could be better described as a progressive arc [*Weil and Sussman, 2004*], which acquired its curvature during the development of the belt. But, the curvature of the arc increased progressively only along its edges, whereas the frontal part, represented by the CPD, did not undergo significant magnitude paleomagnetic rotations during late Miocene and Pliocene, but was mainly affected by SE drifting.

The main factor controlling the bending of the Calabrian Arc is the presence of a small oceanic lithosphere plate (the Ionian Sea), intervening between the Apulia and Africa continental margins [*Malinverno and Ryan, 1986*]. This configuration of the subducting plate caused a differential southeast rollback of the trench during the Neogene and Quaternary, and the progressive drifting of a continental region (CPD), now impinged within the core of the Calabrian Arc.

The tightening of the arc was also accompanied by the decreasing of the width of the active trench through time. In fact, structural and stratigraphic data show that the southern Apennine foredeep basins and the thrust activity progressively shifted toward the southeast, parallel to the front of the chain, during late Pliocene to Pleistocene, and are currently located offshore in the Ionian Sea [*Tropeano et al., 2002*]. The progressive decrease in the width of the trench increased the role of lateral shear along the two edges of

the arc and could be ultimately responsible of the present-day tight curvature of the Calabrian Arc.

In the specific case of the Calabrian Arc, *Cifelli et al.* [2007] speculate that slab retreat could be not sufficient alone to form tight arcs like this, and they suggest that a progressive decrease in the width of the active trench should also be considered as an active mechanism to explain the timing and distribution of crustal rotations in the Calabrian Arc and its huge curvature.

### **7.8. Oroclines formed by orogen-parallel compression (buckling)**

When an orogen-parallel compression is applied to a pre-existing fold-thrust belt, deformation occurs due to compression parallel to the strike of the orogen, resulting in outward bending of the orogen in a direction perpendicular to its long axis. This mechanism, thus, generates a perfect orocline characterized by opposite sense of rotations on either sides of the arc. Outward bending, under specific conditions, may result in formation of a backarc region on the concave side of the orogen and shortening on the convex side. In general the convex side of the bend is affected by a great amount of tangential extension, whereas the inner concave side of the arc could undergoes an orogen-parallel compression.

In the following paragraph I will show the example of an orocline formed by the bending through buckling of a original straight fold-thrust belt: the Cantabrian Arc, northern Spain.

### 7.8.1. The example from the Cantabria-Asturias Arc (northern Spain)

The Cantabria-Asturias Arc (CAA) is the foreland fold-thrust belt of northern Iberia's Variscan orogen and makes up the core of the larger Ibero-Armorican Arc (Figure 7.8.1.1). The CAA is an unusual orogenic belt that curves 180°, with a geometry that is concave towards the foreland; i.e. folds and thrusts verge toward the core of the arc.

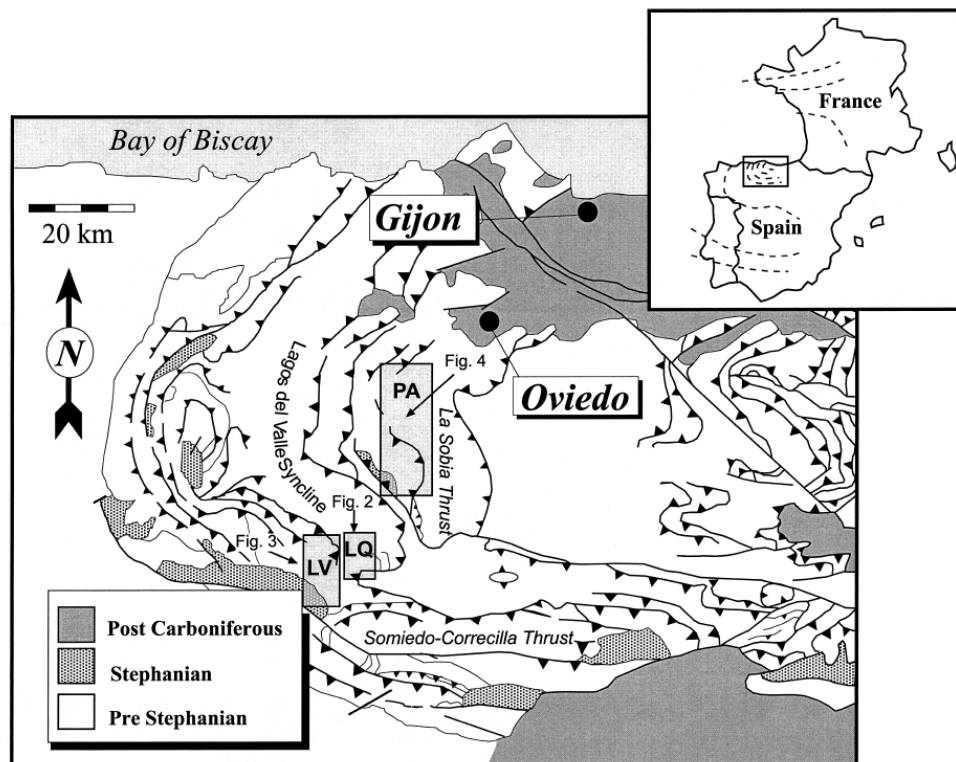


Figure 7.8.1.1. Simplified structural map of the Cantabrian Arc. After *Weil et al., 2000*.

Several structural and paleomagnetic studies, carried out during the last two decades [*Ries et al., 1980; Perroud, 1982, 1983, 1985, 1986; Lowrie and Hirt, 1986; Parés et al., 1994; Van der Voo et al., 1997; Weil et al., 2000, 2001; Weil, 2006*], have evidenced the existence of two main deformation phases responsible for the final shape of the arc. The first deformation phase (D1) resulted in thrusting and folding related to west-to-east tectonic transport (in present-day coordinates) in Westphalian to Stephanian times (315-

290 Ma). Thrusting during this initial phase resulted in locally complex footwall geometries that are characterized by frontal and oblique/lateral ramps. These ramps produced regional folding about horizontal axes, ranging from north-south along frontal ramps to east-west around lateral ramps. This late Variscan (280-256 Ma) deformation phase (D2) buckled originally linear, N-S (in present-day coordinates) trending hanging wall folds, and modified corner folds associated with D1 frontal/lateral/oblique ramp intersections (Figure 7.8.1.2). Modification was accommodated by reactivation of lateral/oblique ramps as frontal ramps, reactivation of frontal ramps as oblique ramps, and overall tightening of D1 corner folds.

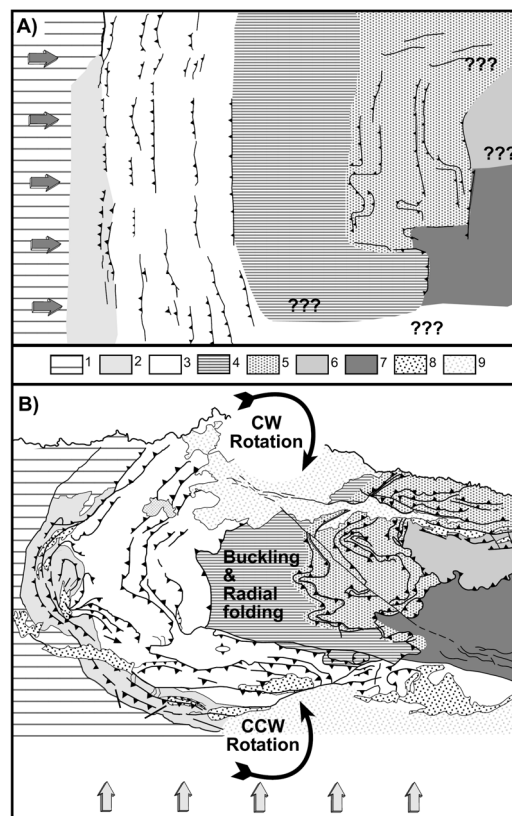
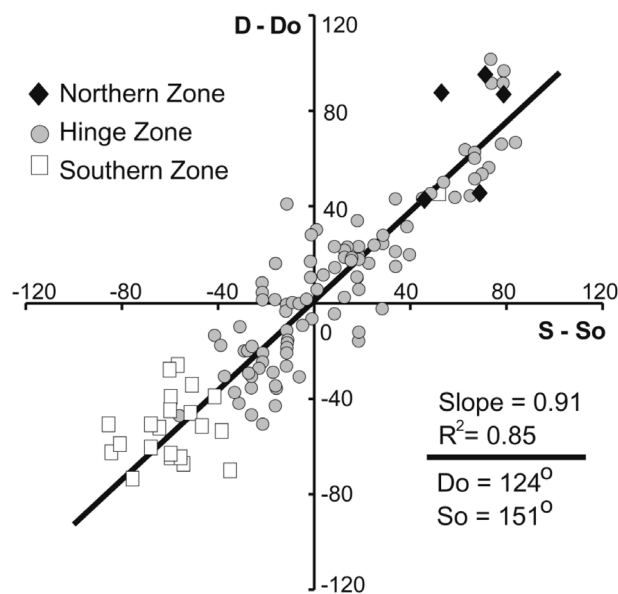


Figure 7.8.1.2. Structural cartoon map of palaeogeographically restored Cantabrian Arc showing (a) the general configuration after initial east-west (in present-day coordinates) compression (D1 deformation phase), and (b) present-day configuration of Cantabrian Arc after oroclinal bending, which resulted in counterclockwise rotation of the southern limb, clockwise rotation of the northern limb and buckling. After *Weil* [2006].

This is confirmed by the result of the oroclinal test performed by *Weil et al.* [2001] (Figure 7.8.1.3), which show a 1:1 correlation between paleomagnetic and structural directions, indicating the secondary origin of the curved shape. Also, displacement vectors along the arc are always sub-orthogonal to the strike of fold axes, suggesting that they formed originally parallel to one another, and were subsequently dispersed during the D2 deformation phase producing buckling of the linear fold-thrust belt.



**Figure 7.8.1.3. Declination deviations vs. strike deviations including data from *Weil et al.* (2000), *Van der Voo et al.* (1997), and *Parés et al.* (1994). After *Weil et al.*, 2001.**

The ultimate change from E-W to N-S compression near the Carboniferous/Permian boundary in the Cantabrian Arc region was likely the result of the final collision of the North African margin of Gondwana with southwestern Europe during the last stages of Pangea amalgamation [*Weil et al.*, 2001; *Weil*, 2006]. This is in contrast to other tectonic models for secondary folding [e.g., *Aller and Gallastegui*, 1995; *Alonso et al.*, 1996], which argue that much of the reactivation and superposed folding in this part of the Cantabrian Arc was due to significant Alpine N-S shortening.

Paleomagnetic data would also suggest that the D2 deformation phase did not produced a further tilting on previously deformed sedimentary formations of the arc. This means that during the D2 phase, rocks only underwent pure vertical axis rotations. Consequently, as proposed by *Weil*, 2006, buckling of the belt may have occurred above a subhorizontal detachment surface, formed at an indeterminate crustal level.

## **PART II**

# **THE EXAMPLES FROM THE ALPS AND THE ANDES**

## **CHAPTER 2**

### ***The Western Alpine Arc***



## A synchronous Alpine and Corsica-Sardinia rotation

Marco Maffione,<sup>1,2</sup> Fabio Speranza,<sup>1</sup> Claudio Faccenna,<sup>3</sup> Antonio Cascella,<sup>4</sup>  
Gianluca Vignaroli,<sup>3</sup> and Leonardo Sagnotti<sup>1</sup>

Received 8 June 2007; revised 10 August 2007; accepted 10 December 2007; published 25 March 2008.

[1] We report on the paleomagnetism of 34 sites from lower Oligocene–middle Miocene sediments exposed in the Tertiary Piedmont Basin (TPB, northern Italy). The TPB is formed by a thick (~4000 m) and virtually undeformed sedimentary succession unconformably lying upon Alpine nappes decapitated by extensional exhumation, which in turn are tectonically stacked over the Adriatic foreland. Paleomagnetic directions from 23 (mostly Oligocene) sites were chronologically framed using new biostratigraphic evidence from calcareous nannoplankton. Our data, along with published paleomagnetic results, show that the TPB rotated ~50° counterclockwise with respect to Africa in Aquitanian-Serravallian times. The rotation was likely driven by underneath nappe stacking and was synchronous with (further) bending of the Alpine chain. Both the rotation magnitude and its timing are similar to those documented for the Corsica-Sardinia microplate. Therefore the formation of the western Alpine arc (or at least part of its present-day curvature) occurred during the rollback of the Apenninic slab and related back-arc spreading of the Liguro-Provençal Basin and drift of the Corsica-Sardinia block. This suggests a common dynamics driving both the Alpine and the Apennine slab motions. Paleomagnetic data also document that the Adriatic plate has undergone no paleomagnetic rotation since mid-late Miocene times. Anisotropy of magnetic susceptibility data suggests that the TPB, an enigmatic basin arising from a controversial tectonic setting, formed in an extensional regime characterized by a stretching direction approximately orthogonal to the main trend of the underlying chain.

**Citation:** Maffione, M., F. Speranza, C. Faccenna, A. Cascella, G. Vignaroli, and L. Sagnotti (2008), A synchronous Alpine and Corsica-Sardinia rotation, *J. Geophys. Res.*, 113, B03104, doi:10.1029/2007JB005214.

### 1. Introduction

[2] The boundary between the Africa-Adria plate and the EurAsia plate in the western Mediterranean region is represented by a diffuse, “S-shaped,” orogenic belt (Figure 1). Complexities arise from the fact that boudins of the older inner “Alpine” chain are fragmented, stretched and drifted apart during the Neogene opening of the back-arc extensional basins [Alvarez *et al.*, 1974]. Because of this intensive late reworking, the three-dimensional (3-D) restoration of the style and geometry of the ancient Alpine chain is complex and disputed. The Alps and the Apennines are an outstanding example of this problem. They presently constitute two apparently independent orogenic segments characterized by opposite tectonic transport oriented roughly perpendicular to their arcuate trends (Figure 1). The western Alpine arc, in particular, is remarkably tight (almost isoclinal) in shape, if compared to the Apennines-Calabria-

Maghrebide arc (Figure 1). The timing for the formation of the horseshoe-shaped alpine arcuate belt is poorly constrained at present, and hence the mechanism of its formation is still a matter of debate. Several paleomagnetic investigations of the southwestern Alpine chain have documented a widespread magnetic overprint affecting both the Subalpine chain and the Penninic zone in late Paleogene-Neogene times [Aubourg and Chabert-Pelline, 1999; Thomas *et al.*, 1999; Katz *et al.*, 2000; Cairanne *et al.*, 2002; Collombet *et al.*, 2002; Kechra *et al.*, 2003]. Some external sectors did not rotate after the remagnetization event [Henry, 1973; Katz *et al.*, 2000; Kechra *et al.*, 2003], while others (both internal and external) underwent different amounts of counterclockwise (CCW) rotations varying locally between 40° and 117° [Aubourg and Chabert-Pelline, 1999; Thomas *et al.*, 1999; Collombet *et al.*, 2002]. These rotations, that were essentially unconstrained in time, have been considered so far as due to a variable interplay of three different causes: (1) northwestward indentation of Adria plate within Europe [e.g., Tapponnier, 1977; Schumacher and Laubscher, 1996; Schmid and Kissling, 2000]; (2) left-lateral shear along major fault(s) [Collombet *et al.*, 2002], and (3) recent and possibly present-day CCW rotation of Adria [Márton *et al.*, 2003; Caporali and Martin, 2000; Calais *et al.*, 2002; Babbucci *et al.*, 2004; D’Agostino *et al.*, 2006].

<sup>1</sup>Istituto Nazionale di Geofisica e Vulcanologia, Rome, Italy.

<sup>2</sup>Dipartimento di Fisica, Università di Bologna, Bologna, Italy.

<sup>3</sup>Dipartimento di Scienze Geologiche, Università degli studi Roma Tre, Rome, Italy.

<sup>4</sup>Istituto Nazionale di Geofisica e Vulcanologia, Pisa, Italy.

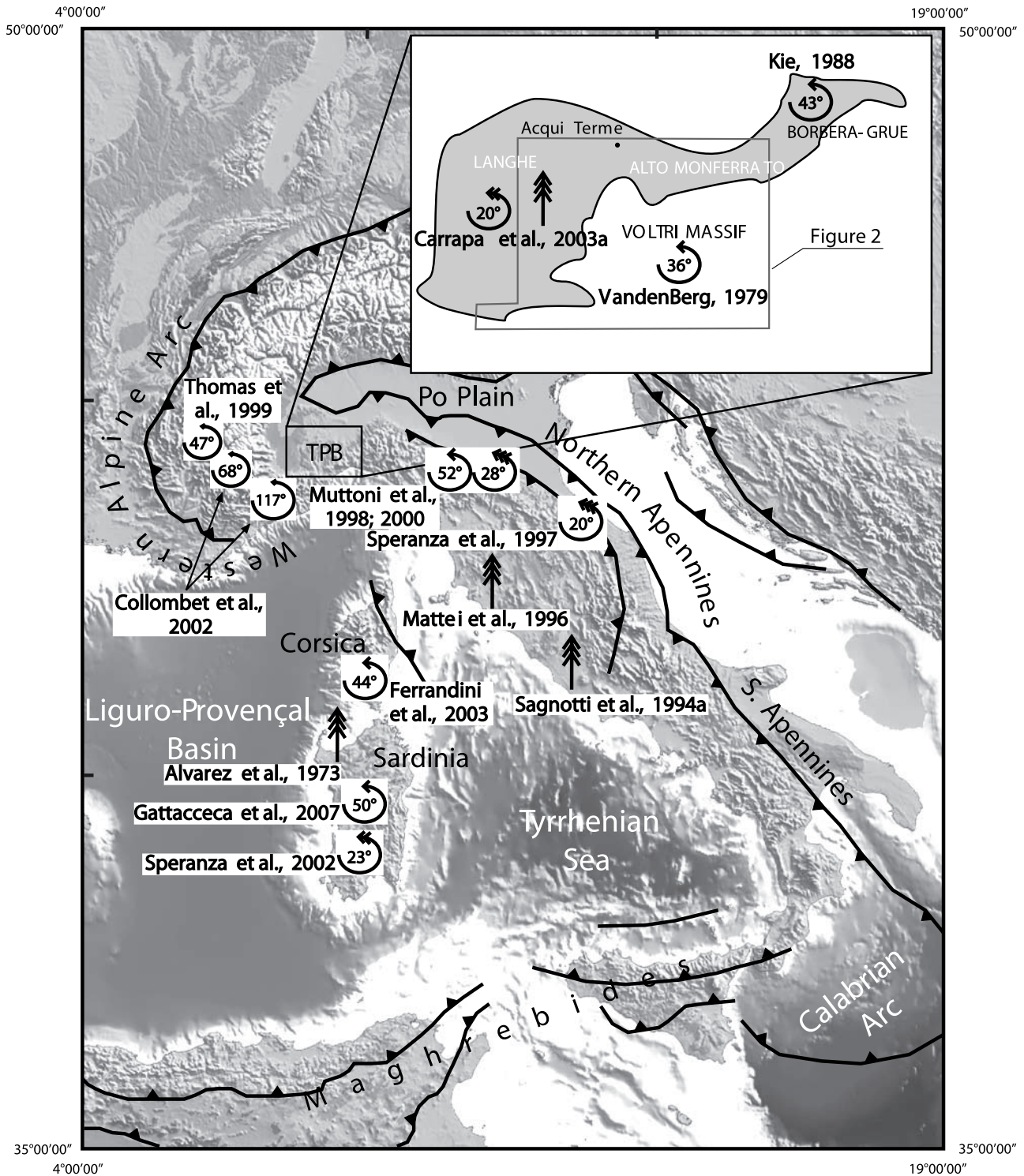


**Figure 1.** Digital elevation model of the central Mediterranean domain and mean paleomagnetic rotation values (within circular arrows) with respect to nearby African/European plates for the internal Western Alps, the northern Apennines, and the Corsica-Sardinia block (see text for details). Circular arrows with simple, double, and triple tips indicate post-Oligocene, post-Burdigalian, and post-Pliocene rotations, respectively. Vertical arrows indicate nonrotated areas after late Miocene-Pliocene times.

[3] The rocks exposed in the Tertiary Piedmont Basin (TPB, Figures 1 and 2) offer the unique opportunity to detail the timing of the CCW rotation affecting the western Alpine arc, and hence to investigate the geodynamics that favored

its bending. The TPB formation is considered to be intimately connected together with the exhumation and the denudation (tectonic and/or erosion) of the neighboring high-pressure/low-temperature (HP/LT) metamorphic do-

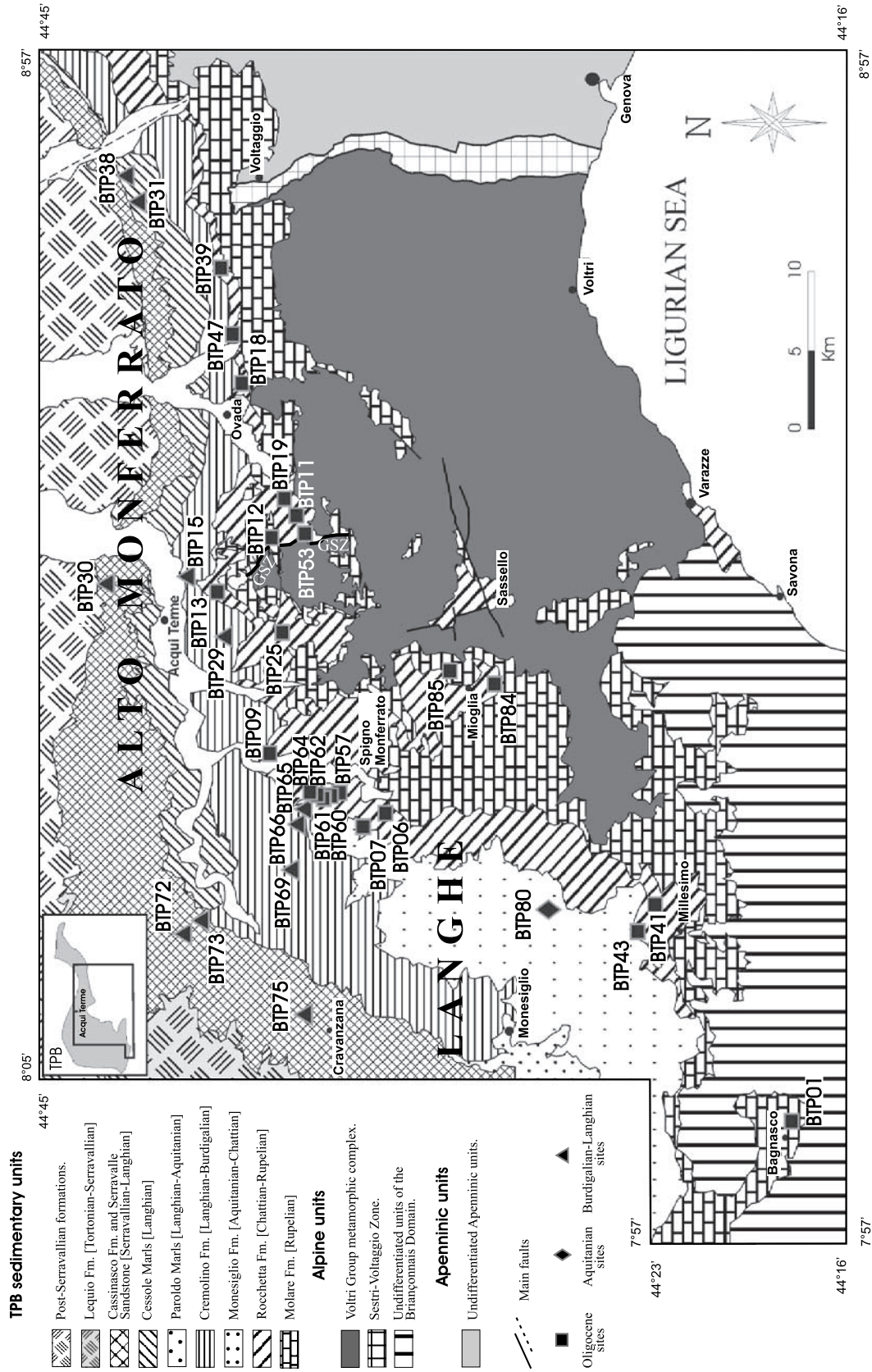


Figure 2. Simplified geological map of the study area and location of the sampling sites. GSZ, Grogno Shear Zone.

main (the Voltri Massif [e.g., *Vanossi et al.*, 1984]). Structurally, the TPB sedimentary succession is characterized by a monoclinale geometry, gently plunging toward the north, lying upon the Voltri Massif units, whose final exhumation has been constrained to the early Oligocene by geochronological data [*Federico et al.*, 2005; *Vignaroli*, 2006]. Recent structural investigation has showed that the tectonic juxtaposition between the sedimentary deposits and the underlying metamorphic units is controlled by extensional features [*Vignaroli et al.*, 2008]. The whole Alpine orogenic pile topped by the TPB is in turn northward stacked over the Adriatic foreland along the Po Plain, where thrust sheet emplacement occurred until late Pliocene times, at least [*Cassano et al.*, 1986]. The TPB sediments have not undergone any metamorphism, and thus are expected to have escaped the widespread magnetic overprint documented so far at all western Alpine nappes.

[4] In this paper, we report on a paleomagnetic investigation of the whole sedimentary succession exposed in the TPB. Our data, together with previous paleomagnetic evidence, reveal the rotation recorded by TPB strata while being passively carried on top of Alpine nappes overthrusting the Adriatic foreland. The detailed reconstruction of the timing and magnitude of the TPB rotation, besides being a definitive proof for a null paleomagnetic rotation of Adria, documents that bending of the western Alpine chain is synchronous (and probably genetically related) with a previously unconsidered fourth geodynamic engine: the back-arc spreading of the Liguro-Provençal Basin and drift rotation of the Corsica-Sardinia microplate.

## 2. Tectonic Setting of the Alpine-Apenninic Chain in the Mediterranean Domain: Interplay Between Africa-Eurasia Convergence and Tertiary Rollback of Subducting Slab Fragments

[5] The central western Mediterranean domain has always received considerable geologic attention, and noteworthy geological-geophysical multidisciplinary investigation. Its geodynamic complexity is related to the presence of the 2000-km-long S-shaped Alpine-Apennine orogenic belt encircling two diachronous Tertiary back-arc basins, the Liguro-Provençal Basin and the Tyrrhenian Sea (Figure 1).

[6] The Alpine orogenic system formed consequently to the approximately N-S collision between the European and African plates, starting in late Cretaceous times after the closure of the small intervening Liguro-Piedmont Ocean [e.g., *Dercourt et al.*, 1986]. Since late Cretaceous the Adriatic plate, acting as a promontory of Africa, has deeply indented Europe, yielding the orogenic building of the Alpine chain [*Platt et al.*, 1989], and even intraplate deformation (the Rhine Graben) within Europe itself. Whether the Adriatic promontory (or “Adria”) has passively followed the African drift, or has been decoupled from nearby plates undergoing independent motion (and rotation), has been a matter of lively and decade lasting debate (see section 3).

[7] The present-day Alpine arcuate shape is considered to be the consequence of frontal Tertiary collision in the central eastern Alps, and oblique indentation and collision associated with sinistral transpression in the western Alps [*Tapponnier*, 1977; *Laubscher*, 1988; *Platt et al.*, 1989;

*Schmid and Kissling*, 2000; *Rosenbaum and Lister*, 2005]. At ~35–30 Ma ago, arc volcanism and back-arc extension occurring at the Provençal-Catalan sectors of the European Alpine margin, is interpreted as the first consequence of the southeastward retreat of NW dipping subducting oceanic lithosphere slabs [*Beccaluva et al.*, 1989; *Faccenna et al.*, 1997]. Tomographic models [*Wortel and Spakman*, 2000; *Piromallo and Morelli*, 2003] image the current position of such ancient suture zones by high-velocity anomaly bodies running parallel to the Alpine chain axis down to 660 km depth.

[8] After 30–35 Ma ago, ongoing slab retreat for the whole Tertiary times caused the eastward (on average) migration of the Alpine-Apennine wedge, microplate (Corsica-Sardinia) and terrain (Calabria) dispersal, and the back-arc spreading of two diachronous oceanic basins, the Liguro-Provençal Basin and the Tyrrhenian Sea [*Alvarez et al.*, 1974; *Malinverno and Ryan*, 1986; *Gorini et al.*, 1993; *Jolivet and Faccenna*, 2000; *Faccenna et al.*, 2001; *Lucente and Speranza*, 2001; *Rosenbaum et al.*, 2002]. The trench progressively rotates from its original NE-SW direction (i.e., parallel to the European passive margin) to approximately N-S [*Faccenna et al.*, 2001]. This geodynamic process occurred along with both exhumation of deep-seated metamorphic units in the Western Alps [e.g., *Jolivet et al.*, 2003], and onset of the eastward (on average) nappe stacking and migration of the Apennine chain [*Patacca et al.*, 1990]. Since mid-late Miocene, the locus of extension jumped east of the Corsica-Sardinia block, giving rise to the Tyrrhenian Sea spreading in late Miocene–early Pleistocene times [*Kastens et al.*, 1986; *Patacca et al.*, 1990; *Faccenna et al.*, 1997, 2001; *Nicolosi et al.*, 2006]. Though the approximately N-S Africa-Europe convergence continued in Tertiary times at a rate of ~1 cm/a [*Faccenna et al.*, 2001], being responsible for ongoing continental collision and nappe stacking along the Alps, tectonic processes related to fast slab rollback events occurred (episodically) at a significantly greater speed (i.e., up to ~20 cm/a [*Nicolosi et al.*, 2006]), obliterating in the central western Mediterranean domain the role of the “slow” Africa-Europe convergence.

[9] Present-day subduction below the southern Tyrrhenian Sea is documented by a continuous 200-km-wide NW dipping Wadati-Benioff seismogenetic zone, plunging downward to a depth of ~450 km with a dip of 70° [*Selvaggi and Chiarabba*, 1995]. Conversely, the available tomographic maps from the northern Tyrrhenian–northern Apennine domain, reveal a slab dipping WSW by ~70°–80° [*Lucente et al.*, 1999], but no associated seismicity below ~100 km depth.

## 3. Previous Paleomagnetic Evidence From the Western Alpine–Northern Apennine Chain, the Adria and Corsica-Sardinia (Micro) Plates, and the Tertiary Piedmont Basin

[10] The strikingly curved western Alpine arc (Figure 1) has been explained invoking a variety of geodynamic models [e.g., *Schmid and Kissling*, 2000], though few are really based upon paleomagnetic evidence. In fact, a wealth of paleomagnetic data has been gathered from the western Alps during the last three decades. At the external sectors of the western Alps (Dauphino-Elvetic cover of the external

crystalline massifs) a paleomagnetic study of Triassic-Liassic lavas from the Pelvoux-Belledonne area [Henry, 1992], integrated with previous results by Westphal [1973, 1976] and Henry [1976, 1980], documented four main regions affected by different amounts of rotation: Region I, southwestern Taillefer (yielding a large CCW rotation of up to  $90^\circ$ ); region II, southern border of Pelvoux (with CCW rotations in the order of  $30^\circ$ ); region III, Rochail (showing no significant rotations); and region IV, northern Belledonne (which rotated clockwise of  $\sim 40^\circ$ ). Similar results are shown by Aubourg and Chabert-Pelline [1999] who performed paleomagnetic investigations on the upper Jurassic black shales from the southern Subalpine Chain, between the Pelvoux and Argentera massifs. They suggested a widespread Neogene remagnetization, followed by a CCW rotation of  $\sim 40^\circ$  with respect to Europe. This pervasive widespread remagnetization, occurred during Tertiary times, seems to be a common feature of sediments from this area. Recently, Cairanne *et al.* [2002], Kechra *et al.* [2003], and Katz *et al.* [2000] proposed a Tertiary magnetic overprint of the lower Jurassic to lower Cretaceous sedimentary units from the Mesozoic Vocontian basin (SE France), invoking different remagnetization mechanisms.

[11] Nevertheless, other studies have documented a non-rotation (with respect to Europe) of several localities from the neighbor Alpine sectors. A paleomagnetic study on Permian red beds from the Dôme de Barrot (SW of Argentera Massif) by Kruijer *et al.* [2000], yielded  $D = 212^\circ$ ,  $I = -17^\circ$  as mean values of the primary magnetization ( $R = 14^\circ \pm 3.8^\circ$ , with respect to stable Europe, recalculated using Permian paleopoles from Van der Voo [1993]). Similar results from Permian sedimentary units from the same area were also reported by Van den Ende [1977], who documented a Permian primary magnetization with a mean direction of  $D = 205.5^\circ$ ,  $I = -13.5^\circ$  ( $R = 7.4^\circ \pm 3.7^\circ$ ), by Cogné and Perroud [1985], who found for the less deformed sites (see group I of Cogné and Perroud [1985]) a mean value of  $D = 198.0^\circ$ ,  $I = -10.5^\circ$  ( $R = -4.7^\circ \pm 6.7^\circ$ ), and by Henry [1973], who measured a mean magnetic declination of  $208^\circ$  and an inclination of  $-10^\circ$  ( $R \approx 18^\circ$ ). Farther south, paleomagnetic data by Bogdanoff and Schott [1977] suggested no significant rotation affecting this area since the Permian with respect to both the surrounding regions (Dôme de Barrot, Esterel), and stable Europe. West of the external Alpine fronts, within the Vocontian basin, Kechra *et al.* [2003] did not find any significant rotation with respect to Europe since the late Eocene ( $D = 354.2^\circ$ ,  $I = 54.6^\circ$ ). Similarly, the mean paleomagnetic direction recalculated by us from the Katz *et al.* [2000] study, yields  $D = 352.1^\circ$ ,  $I = 55.6^\circ$ , indicating no vertical axis rotation after the (likely post-Eocene) chemical remagnetization. Finally, paleomagnetic data by Merabet and Daly [1986] from the Maures Massif (SE France) seem indicating that no substantial rotation relative to the stable Europe occurred since the Permian.

[12] In conclusion, though paleomagnetic results reveal contrasting rotation values at different localities, and therefore make it difficult to provide a precise rotation value for the whole external Alpine sector, it seems that CCW rotations dominate, specially south of the Belledonne Massif.

[13] Instead, paleomagnetic results from the internal nappe of the Western Alpine Arc appear much clearer.

Thomas *et al.* [1999] and Collombet *et al.* [2002] studied the upper Jurassic sediments from the Briançonnais sedimentary cover of the Penninic Zone, documenting a systematic magnetic overprint, likely subsequent to Eocene-late Oligocene Alpine blueschist-greenschist metamorphism, and a subsequent CCW rotation relative to Europe. The rotation values are  $47^\circ \pm 13^\circ$  in the Briançon-Guillestre area [Thomas *et al.*, 1999], and  $68^\circ \pm 15^\circ$  and  $117^\circ \pm 19^\circ$  in the Ubaye and Liguria locality, respectively [Collombet *et al.*, 2002, Figure 1]. Collombet *et al.* [2002] proposed a composite rotation model for the Western Alpine Arc, characterized by three main contributors: (1) a  $20^\circ$ – $25^\circ$  CCW rotation of Adria (with respect to both Africa and Eurasia), corroborated by paleomagnetic data from Eocene sediments from Istria-Dalmatia region [Márton *et al.*, 2003] and GPS evidence [Caporali and Martin, 2000], (2) the large-scale, left-lateral shear along a NW-SE oriented shear zone located at the southern border of the arc, east of the Argentera Massif, and (3) the southward extrusion of the Alps along the curved Frontal Pennine Thrust due to indentation of the Adriatic promontory within Europe [e.g., Tapponnier, 1977; Ménard, 1988]. However, though GPS and seismological data robustly confirm that Adria is at present rotating CCW with respect to the neighbor plates [Caporali and Martin, 2000; Calais *et al.*, 2002; Babbucci *et al.*, 2004; D'Agostino *et al.*, 2006], there is not a consensus on whether such present-day (or older) rotations have been large enough to be confidently detectable by paleomagnetism (i.e., they have reached or exceeded a  $10^\circ$ – $15^\circ$  value).

[14] The paleomagnetic evidence from Adria was gathered from the few exposed parts of it (Istria, Gargano, and Apulia), as well as from the belts encircling it, such as the southern Alps, the Apennines, and the Dinarides (see the comprehensive review from Van der Voo [1993]). In the last years, most paleomagnetists have stressed the first-order agreement of Permian to lower Tertiary paleomagnetic data from the Adriatic region and Africa, implying that Adria has paleomagnetically followed the African drift without any significant rotation [e.g., Van der Voo, 1993; Channell *et al.*, 1992; Channell, 1996; Muttoni *et al.*, 2001]. Such coupling would also imply the lack of a Tertiary rotation of Adria with respect to the geographic north because Africa has undergone a northward drift but no significant rotation during Tertiary times [Besse and Courtillot, 2002]. On the other hand, Márton *et al.* [2003] relying on the paleomagnetism of Eocene sediments from Istria and Dalmatia, suggested a post-Eocene  $24^\circ$  to  $30^\circ$  CCW rotation of Adria with respect to Africa.

[15] In the northern Apennine belt, the paleomagnetic study of the relatively undeformed upper Oligocene–middle Miocene Epiligurian units, unconformably resting upon Liguride nappes, revealed a  $52^\circ$  CCW rotation with respect to Africa [Muttoni *et al.*, 1998, Figure 1]. Further data by Muttoni *et al.* [2000] showed that  $\sim 24^\circ$  of the  $52^\circ$  rotation is Oligocene-Miocene in age, and likely related to the drift (and CCW rotation) of the Corsica-Sardinia block. Conversely, the remaining  $28^\circ$  CCW rotation, observed in upper Miocene to Pliocene sediments, is due to Pliocene shortening episodes occurring at the Apennine chain front. The latter paleomagnetic data confirmed previous results from Speranza *et al.* [1997], who studied upper Messinian clayey deposits from the external northern Apennines, and found a CCW rotation of  $\sim 20^\circ$  in the northern part of the studied

domain. At the rear of the CCW-rotated northern Apennines, paleomagnetic data from the Tuscan-Latium Tyrrhenian margin reveal no rotation since at least late Messinian–early Pliocene times [Sagnotti et al., 1994a; Mattei et al., 1996], implying that rotations are confined to the external compressive front of the northern Apennines.

[16] Further east, the paleomagnetic investigation of the Tertiary and Permian volcanic complexes from Sardinia and Corsica showed, since the 1970s, that the Corsica-Sardinia microplate has undergone a significant CCW Tertiary rotation with respect to Europe [e.g., Montigny et al., 1981]. More recent paleomagnetic and  $^{40}\text{Ar}/^{39}\text{Ar}$  data from Sardinian volcanics [Gattacceca et al., 2007] and sediments [Speranza et al., 2002] (Figure 1) concur for a CCW rotation of  $\sim 50^\circ$  with respect to Europe occurring in early mid-Miocene times, between 20–21 Ma and 15–16 Ma ago. Finally, the paleomagnetism of Plio-Pleistocene basalts from Sardinia [Alvarez et al., 1973] has confirmed the absence of post-mid-Miocene rotations. Paleomagnetic results from southern Corsica by Ferrandini et al. [2003] which testify a post-Chattian CCW rotation of  $\sim 44^\circ$  with respect to Europe (Figure 1) fall in substantial agreement with those from Sardinia.

[17] Within the TPB, various paleomagnetic studies were already carried out in the past. Bormioli and Lanza [1995] studied lower Oligocene–mid-Miocene sediments from the northern part of the TPB, reporting paleodeclinations varying from  $\text{N}260^\circ$  to  $\text{N}330^\circ$  (besides a magnetic overprint at some sites). Upper Oligocene sediments from the eastern margin of the TPB yielded  $\text{N}316^\circ$  paleodeclination [Kie, 1988]. Further south, Vandenberg [1979] documented a  $36^\circ \pm 8^\circ$  CCW rotation with respect to Europe in upper Eocene–lower Oligocene rocks from the Voltri region. More recently, Carrapa et al. [2003a] sampled upper Oligocene to Pliocene sediments from the Langhe basin, (western TPB, Figure 1), documenting a  $\sim 20^\circ$  CCW rotation with respect to Europe occurring before Tortonian times.

#### 4. Geological Setting of the Tertiary Piedmont Basin

[18] The TPB is located between the Po Plain and the Liguro-Provençal Basin (Figure 1). It directly lies on top of the eclogitic domain of the Alpine Voltri Massif [e.g., Vanossi et al., 1984], and partially covers the conventionally defined tectonic contact between the western Alps and the northern Apennines (occurring along the so-called “Sestri-Voltaggio Zone” [e.g., Cortesogno and Haccard, 1984; Dela Pierre et al., 1995; Piana and Polino, 1995; Polino et al., 1995]) (Figure 2). It is divided in three main geographic domain: the Langhe basin to the west, the Alto Monferrato located north of the Voltri Massif and the Borbera Grue, at the eastern margin (Figure 1). It is commonly interpreted as an “episutural basin” situated on top of the alpine edifice [Biella et al., 1988; Polino et al., 1990; Shumacher and Laubscher, 1996; Biella et al., 1997; Schmid and Kissling, 2000]. Nevertheless, the considerable thickness of its sedimentary sequence (up to 4000 m), and the paucity of large-scale faults cutting the whole sedimentary succession remain puzzling and open to debate.

[19] The age of the oldest sediments exposed in the TPB is constrained to the early Oligocene by both biostratigraphic

[Gelati and Gnaccolini, 1982; Gelati et al., 1993; Dela Pierre et al., 1995; Gelati and Gnaccolini, 1998] and geochronological evidence [Carrapa et al., 2003b, 2004; Federico et al., 2005]. Such age turns out to be very similar to the exhumation age of the underlying metamorphic units of the Voltri Massif, which is  $\sim 33$  Ma [Federico et al., 2005; Vignaroli, 2006]. The sedimentary sequence of the TPB displays frequent lateral variations of facies and thickness, likely due to the articulated basement morphology [Gnaccolini et al., 1998]. The first transgressive sediments (Molare Formation) of lowermost Oligocene age display a progressive alluvial to nearshore sedimentation evolution [Gelati et al., 1993, and references therein] (Figure 2). The Molare Formation underlies the Rocchetta Formation (early Oligocene–Aquitainian), which is made by hemipelagic mudstones and testifies the onset of deep basinal sedimentation [Gelati and Gnaccolini, 1996, 1998]. The upper part of this formation contains some turbiditic layers, which become more frequent in the overlying Monesiglio Formation (Aquitainian–Burdigalian) of the Langhe basin. After a short Burdigalian emersion episode documented in the Alto Monferrato [D’Atri, 1995; D’Atri et al., 1997], the TPB was filled by eastward directed (in present-day coordinates) turbiditic fluxes yielding the Cremolino Formation (late Burdigalian–early Langhian) [Ghibaudo et al., 1985; Gelati et al., 1993; Gelati and Gnaccolini, 1998]. During the Langhian, the sedimentation turned again to hemipelagic with the deposition of the Cessole Marls [Ghibaudo et al., 1985, and references therein]. Finally, from Langhian–Serravallian to Tortonian times, the eastern part of the TPB was characterized by shelf slope sedimentation of the Serravalle Sandstones [Caprara et al., 1985; Ghibaudo et al., 1985], while deep-sea turbidites continued infilling the Langhe basin to the west (Cassinasco Formation and Lequio Formation). A recent  $^{40}\text{Ar}/^{39}\text{Ar}$  geochronological analysis of detritic minerals from the TPB has showed that the source area of sediments exposed in the TPB was located in the Ligurian Alps and in the Western Alps during Oligocene and Miocene, respectively [Carrapa et al., 2004].

[20] From a structural point of view, the strata from the TPB plunge northward to northwestward, and to the north are covered by the Neogene succession of the Po Plain [Perotti, 1985; Fossati et al., 1988]. Locally, Gelati and Gnaccolini [1998] and Bernini and Zecca [1990] documented synsedimentary decametric-scale folds (with NW–SE fold axes) in the Rocchetta Formation at two basin localities (Mioglia, Mombaldone). Similar structures were mapped by Carrapa et al. [2003a] in Langhian–Serravallian sediments from the southwestern part of the Langhe basin. Other metric-scale folds were documented in the Oligocene formations from the eastern part of the TPB [Perotti, 1985; Fossati et al., 1988; Marroni et al., 2002]. Along a main ductile-to-fragile thrusting zone (the “Grogardo Shear Zone,” Figure 2 [D’Atri et al., 1997, 2002; Piana et al., 2006]) the metamorphic basement is tectonically stacked over the oldest sedimentary deposits. Both the folds and the thrust were interpreted by Carrapa et al. [2003a] as a result of a northeastward directed compression occurring during Oligocene times. Finally, decametric to centimetric-scale normal and strike-slip fault systems have been described for the whole sedimentary sequence [Mutti et al., 1995;

*Carrapa et al.*, 2003a; *Vignaroli et al.*, 2008]. These structures have been related to a N-S extension affecting the entire basin during Oligocene-Miocene times by *Mutti et al.* [1995], *Gelati and Gnaccolini* [1998], and *Carrapa et al.* [2003a]. Conversely, relying on both the structural evidence (i.e., the progressive ductile-to-brittle evolution of the deformation fabric in the metamorphic pile approaching the TPB) and the kinematic compatibility (i.e., the parallelism between the stretching lineations in the metamorphic units and the abrasion striae in faulted sedimentary deposits) *Vignaroli et al.* [2008] refers the early Oligocene extensional features to the latest stage of the postorogenic exhumation of the Voltri Massif, dated at 33 Ma ago [*Federico et al.*, 2005].

[21] The genesis and development of the TPB have been explained invoking several tectonic models, but in fact remain rather elusive at present. *Mutti et al.* [1995] proposed that (sparse) normal faults of Oligocene age within the TPB, probably linked to the Ligurian Sea opening, testify an extension related mechanism responsible for the first period of subsidence. They also propose an inversion in the stress field (from extensional to compressive) occurring in the late Oligocene–early Miocene times. The main Miocene subsidence of the TPB has been associated by *Gelati et al.* [1993] with compressional tectonics, possibly related to the thrust activity developed at this time in the southwestern Alps [*Roure et al.*, 1990]. The Oligocene–Miocene synsedimentary compressional structures documented in the TPB [*Gelati and Gnaccolini*, 1998; *Bernini and Zecca*, 1990; *Carrapa et al.*, 2003a] and thrusting of the Ligurian Alps (Voltri massif) over the TPB sediments (as documented by *D'Atri et al.* [1997, 2002]), seem to support this hypothesis. Anisotropy of magnetic susceptibility and structural analysis by *Carrapa et al.* [2003a] suggested a NE–SW to NW–SE shortening acting since the Oligocene. However, small-scale normal faults, detected in Rupelian to Tortonian sediments, may also be a proof for a quite homogeneous N–S extension over the entire basin. Finally, *Carrapa and Garcia-Castellanos* [2005] propose for the evolution of the TPB a flexural subsidence from orogenic loading in combination of far-field compressional stresses in the Western Alps (where back thrusts were active), suggesting a complex 3-D interaction between multivergent compressional tectonics.

## 5. Samplings and Methods

[22] We carried out a preliminary sampling campaign in order to select outcrops and lithologies carrying a measurable (and stable during demagnetization) natural remanent magnetization (NRM). We identified sampling localities characterized by fresh cuts and blue-grey clay facies (suggesting the absence of strong weathering alteration). Hand samples were collected from lower Oligocene to upper Langhian sediments exposed at 88 localities, homogeneously spread all over the Alto Monferrato and the easternmost part of the Langhe basin.

[23] All laboratory analyses were performed in the paleomagnetic laboratory at the Istituto Nazionale di Geofisica e Vulcanologia (INGV, Rome, Italy). The NRM of the specimens was measured in a magnetically shielded room with a DC-SQUID cryogenic magnetometer (2G Enterprises,

USA), and its stability was checked by alternating field (AF) cleaning treatment up to a maximum field of 70 mT. After this preliminary sampling, 34 sites revealed suitable magnetic properties, and were sampled in detail using a petrol-powered portable drill, gathering 378 cylindrical cores (25 mm in diameter) oriented in situ with a magnetic compass (Figure 2 and Table 1). The local magnetic field declination value at the TPB was expected to be less than 1° during the sampling campaign, according to *Istituto Nazionale di Geofisica e Vulcanologia* [2001]. Consequently, a magnetic compass was used throughout, and the magnetic declination was considered as negligible. We collected 8–14 cores (11–12 on average) from each site, spaced in at least two outcrops, in order to try to average out the secular variation of the geomagnetic field. At all sites marine clays were sampled, but at site BTP01 (lower Oligocene), where lacustrine mudstones were collected. The sampled sediment ages were defined relying on both the available geological maps [*Servizio Geologico d'Italia*, 1969, 1970a, 1970b, 1970c, 1971], and on new ad hoc analyses of the calcareous nannoplankton content of specimens from each sampling site (see section 6.1, Table 1). The ages of the sites can be grouped in three main groups: Oligocene (22 sites), Aquitanian (1 site) and Burdigalian–Langhian (11 sites). The cores were cut into standard cylindrical specimens of 22 mm height, and a specimen per core was stepwise AF demagnetized in 14–15 steps from 5 to 100 mT. For 8 sites, where the AF cleaning proved to be not effective (due to unstable behavior and/or acquisition of a parasitic remanence in fields higher than 30 mT), twin specimens from the same cores were subjected to thermal demagnetization in 12 steps up to 600°C (Table 1).

[24] Before paleomagnetic analyses, we measured the low-field anisotropy of magnetic susceptibility (AMS) of a specimen per core with a KLY 3 bridge (AGICO). Furthermore, we carried out a series of rock magnetic analyses in order to characterize the nature of the main magnetic carriers at each sampling site. We measured the hysteresis properties of at least one specimen per site, using a Micromag Alternating Gradient Magnetometer (AGM, model 2900) with a maximum applied field of 1 T, and derived the saturation magnetization ( $M_s$ ), saturation remanent magnetization ( $M_{rs}$ ) and coercive force ( $B_c$ ) values. Then, on the same specimens and also with the AGM, we analyzed the acquisition of an isothermal remanent magnetization (IRM) and its subsequent back-field demagnetization (both in a succession of fields up to 1 T), which allowed the evaluation of the coercivity of remanence ( $B_{cr}$ ) values. Finally, one specimen per site was also selected to investigate the thermal change of the magnetic susceptibility during a heating-cooling cycle from room temperature to 700°C, using an AGICO CS-3 apparatus coupled to the KLY 3 bridge.

## 6. Results

### 6.1. Biostratigraphy

[25] The biostratigraphy of the studied sediments was analyzed investigating the calcareous nannofossil assemblages of at least three samples from each site. The analyses were performed on smear slides examined with a light microscope at  $\times 1250$  magnification, under cross-polarized

Table 1. Paleomagnetic Directions From the Tertiary Piedmont Basin<sup>a</sup>

Site	Formation	Geographic Coordinates		Nannofossil Zone	Age	Age (Ma)	Bedding (deg)	Chrons	Cleaning Strategy	Tilt			$\alpha_{95}$ (deg)	n/N	Rotation (deg)	Flattening (deg)		
		Latitude N	Longitude E							Corrected	In Situ	D (deg)					I (deg)	I (deg)
BTP01	Molare	44° 18'35.0"	8° 03'12.2"	-	Rupelian	30.5–33.5	252–14	C12n-C13n	AF; TH	317.4	39.7	308.4	32.8	332.1	4.2	5/12	-38.2 (6.6)	13.6 (5.4)
BTP06	Rocchetta	44° 32'17.4"	8° 18'59.3"	NP24	Rupelian	28.7–29.7	284–11	C10r-C11n1n	AF	124.2	-51.0	130.9	-61.3	94.0	5.3	9/11	-51.3 (0.4)	2.5 (6)
BTP07	Rocchetta	44° 32'26.8"	8° 18'19.6"	NP24	Rupelian-Chattian	28.0–29.4	327–6	C9r-C10r	AF	131.7	-55.7	128.7	-61.8	19.5	12.0	9/10	43.9 (17.7)	-2.2 (1.0)
BTP09	Rocchetta	44° 36'31.4"	8° 21'26.7"	NP24	Rupelian-Chattian	28.0–29.7	18–9	C9r-C11n1r	AF	140.5	-54.6	128.7	-58.5	12.7	14.1	10/11	-35.1 (20.1)	-1 (11.8)
BTP11	Rocchetta	44° 35'34.8"	8° 33'01.5"	NP23	Rupelian	30.0–30.5	319–16	C11r	AF	106.2	-48.7	91.4	-59.2	96.9	8.4	6/9	-74.2 (11)	5.7 (7.8)
BTP12 <sup>b</sup>	Rocchetta	44° 36'38.0"	8° 32'11.6"	-	Rupelian-Chattian	21.6–32.0	23–21	-	AF; TH	-	-	-	-	-	-	-	-	-
BTP13	Rocchetta	44° 38'30.8"	8° 29'52.8"	NP23	Rupelian	29.9–30.9	236–35	C11n2n-C12n	AF	269.2	32.5	296.5	57.8	56.7	6.5	10/12	-86.4 (7.9)	21.1 (6.6)
BTP15	Cremolino	44° 39'47.5"	8° 30'39.1"	MNN4a	Burdigalian	16.5–17.6	359–9	C5Dn-C5Cn3n	AF; TH	0.5	26.4	0.9	38.9	62.1	9.8	5/10	-1.8 (9.1)	32 (8)
BTP18	Rocchetta	44° 37'45.0"	8° 40'08.0"	NP23	Rupelian	30.1–32.3	325–23	C11r-C12r	AF	134.1	-45.1	124.8	-67.5	43.0	9.3	7/8	-51.6 (11.5)	8.5 (8.4)
BTP19 <sup>c</sup>	Rocchetta	44° 36'20.0"	8° 34'0.8"	NP23	Rupelian	29.9–30.9	356–23	C11n2n-C12n	AF; TH	4.4	26.2	7.5	48.9	499.2	2.5	8/8	8.7 (5.5)	27.4 (4.7)
BTP25 <sup>b</sup>	Rocchetta	44° 36'21.4"	8° 27'49.1"	NP23	Rupelian	29.9–30.9	325–23	-	AF; TH	-	-	-	-	-	-	-	-	-
BTP29 <sup>c</sup>	Cremolino	44° 38'54.8"	8° 27'22.0"	MNN5a	Langhian	15.0–15.2	29–12	C5Bn2n	AF	5.5	42.7	359.7	53.2	165.0	3.5	12/13	3.3 (4.9)	15.7 (3.5)
BTP30 <sup>c</sup>	Serravalle	44° 43'44.2"	8° 28'58.6"	MNN4a	Burdigalian-Langhian	16.0–17.6	21–12	C5Cn	AF; TH	10.1	40.9	7.4	52.2	202.0	4.3	7/8	7.8 (5.5)	17.5 (4)
BTP31 <sup>c</sup>	Cessole	44° 41'20.0"	8° 47'38.0"	MNN5b	Langhian	14.2–14.6	336–22	C5ADn	AF	350.5	34.3	357.3	55.2	46.2	6.8	11/11	-11.8 (7.2)	24 (5.7)
BTP38	Rocchetta	44° 41'20.0"	8° 48'38.0"	MNN5a/b	Langhian	14.8–15.2	310–49	C5Bn1n-C5Bn2n	AF	337.3	36.1	35.6	68.4	96.4	4.7	11/11	-25 (5.5)	22.4 (4.3)
BTP39	Rocchetta	44° 38'10.0"	8° 45'53.0"	NP23	Rupelian	30.1–32.3	356–25	C11r-C12r	AF	155.1	-18.5	161.4	-38.7	50.4	7.3	9/9	-20.6 (7.9)	35 (7)
BTP41	Rocchetta	44° 22'35.0"	8° 13'50.0"	NP23	Rupelian	29.9–30.9	38–3	C11n2n-C12n	AF	302.4	41.8	299.5	41.4	79.4	4.9	12/12	-53.2 (7.2)	11.6 (5.8)
BTP43	Rocchetta	44° 22'50.0"	8° 12'28.0"	NP24	Rupelian-Chattian	28.3–29.9	197–7	C10n-C11n1m2n	AF	309.4	65.4	321.4	59.6	38.4	9.4	8/10	-44 (17.2)	-9.6 (8.5)
BTP47	Rocchetta	44° 38'08.0"	8° 41'42.4"	NP23	Rupelian	29.9–30.9	325–18	C11n2n-C12n	AF; TH	312.9	42.1	307.8	58.5	62.1	11.7	4/10	-42.8 (13.4)	11.5 (10)
BTP53	Rocchetta	44° 35'21.9"	8° 32'47.1"	NP23	Rupelian	29.9–30.9	280–12	C11n2n-C12n	AF	311.7	19.4	314.8	29.7	128.9	3.7	13/13	-44 (5.9)	34.2 (5.2)
BTP57	Rocchetta	44° 34'22.8"	8° 19'57.0"	NP23	Rupelian	29.9–30.9	253–17	C11n2n-C12n	AF	287.3	43.5	300.1	56.4	101.2	4.8	10/12	-68.3 (7.3)	10 (5.7)
BTP60	Rocchetta	44° 34'26.7"	8° 19'54.6"	NP23	Rupelian	29.9–30.9	11–9	C11n2n-C12n	AF	343.9	48.6	338.1	56.2	51.3	8.5	7/9	-11.7 (11.3)	4.9 (7.9)
BTP61	Rocchetta	44° 34'28.1"	8° 19'53.6"	NP23	Rupelian	29.9–30.9	245–27	C11n2n-C12n	AF	302.6	52.4	343.2	58.9	86.6	5.6	9/11	-53 (8.8)	1.1 (6.2)
BTP62	Rocchetta	44° 34'33.1"	8° 19'51.2"	NP23	Rupelian	29.9–30.9	276–9	C11n2n-C12n	AF	316.6	44.7	323.6	51.2	119.0	4.2	11/11	-39 (6.9)	8.8 (5.4)
BTP64	Rocchetta	44° 34'43.5"	8° 19'40.6"	NP23	Rupelian	29.9–30.9	257–2	C11n2n-C12n	AF	306.1	55.1	308.6	56.5	64.9	6.9	8/12	-49.5 (10.7)	-1.6 (6.9)
BTP65 <sup>c</sup>	Monesiglio	44° 35'08.7"	8° 19'29.5"	MNN2a	Aquitanian	20.5–20.7	329–10	C6An1n	AF	357.0	49.3	3.7	57.4	72.9	5.1	12/13	-7 (7.5)	7 (5.2)
BTP66	Cremolino	44° 35'25.0"	8° 18'41.2"	MNN2b	Burdigalian	19.2–20.2	308–4	C6n	AF; TH	9.8	36.7	12.3	38.4	226.0	4.5	6/13	5.8 (6.2)	19.6 (4.9)
BTP69 <sup>c</sup>	Cremolino	44° 35'34.6"	8° 15'37.9"	MNN4a	Burdigalian-Langhian	16.0–17.6	247–4	C5Cn-C5Dn	AF	0.6	59.2	5.7	57.7	398.2	3.5	5/11	-1.6 (6.2)	-0.9 (3.6)
BTP72 <sup>c</sup>	Cassinaco	44° 38'17.7"	8° 14'15.9"	MNN5a	Langhian	14.8–15.2	352–9	C5Bn	AF	359.0	43.3	0.4	52.2	111.3	4.6	10/10	-3.2 (5.9)	15.1 (4.2)
BTP73 <sup>c</sup>	Cassinaco	44° 38'15.8"	8° 14'13.8"	MNN5a	Langhian	14.8–15.2	27–4	C5Bn	AF	5.2	49.5	3.2	53.4	97.3	6.8	6/11	3 (8.8)	8.9 (5.8)
BTP75 <sup>c</sup>	Cassinaco	44° 34'46.4"	8° 08'11.4"	MNN5a	Langhian	14.8–15.2	296–10	C5Bn	AF	350.3	48.5	1.0	53.6	139.3	3.7	12/13	-11.9 (5.4)	9.9 (3.7)
BTP80	Monesiglio	44° 26'07.3"	8° 14'0.8"	MNN1c	Aquitanian	22.9–23.8	322–7	C6An2n/C6Cn	AF	320.8	39.2	320.6	45.9	51.9	8.5	7/11	-39.8 (10.1)	18 (7.7)
BTP84	Rocchetta	44° 28'36.2"	8° 24'56.1"	NP23	Rupelian	29.9–30.9	295–9	C11n2n-C12n	AF	334.2	20.0	336.8	27.1	42.6	6.7	12/12	-29.6 (7.5)	33.3 (6.8)
BTP85	Molare	44° 29'54.3"	8° 25'09.2"	-	Rupelian	30.9–33.1	263–5	C12r	AF	110.4	-51.4	113.7	-55.9	280.0	3.6	7/13	-65.2 (6.8)	2.1 (5.1)

<sup>a</sup>The geographic coordinates are referred to ED50 datum. Nannofossil zones are from *Martini* [1971] and *Formaciari and Rio* [1996]. Age in Ma is from the geologic timescale of *Gradstein et al.* [2004] and is inferred considering both the magnetic polarity (chron boundary ages) and our new biostratigraphic data. Bedding is expressed in dip azimuth and dip values. Cleaning strategy is alternating field (AF) and/or thermal (TH); D and I are site-mean declination and inclination calculated before and after tectonic correction; k and  $\alpha_{95}$  are statistical parameters after *Fisher* [1953]; n/N is number of samples giving reliable results/number of studied samples at a site. Site-mean rotation and flattening values (according to *Demarest* [1983]) are relative to coeval D and I African values expected at Tertiary Piedmont Basin (errors are in parentheses). The reference African paleocoles are from *Besse and Courtillot* [2002].

<sup>b</sup>Sites yielding scattered demagnetization diagrams.

<sup>c</sup>Remagnetized sites (see text).

and transmitted light. A semiquantitative analysis characterized the assemblages in terms of abundance and preservation. A quantitative analysis was carried out on the genus *Sphenolithus* and *Helicosphaera*, due to the significant abundance pattern of the sphenoliths and helicoliths for the Oligocene and early Miocene biostratigraphy. Particularly, a counting of 100 sphenoliths was performed to evaluate the abundance of *Sphenolithus ciproensis*, *S. belemnos* and *S. heteromorphus*; *Helicosphaera ampliaperta* and *H. walbersdorfensis* were counted in 50 helicoliths [Backman and Shackleton, 1983; Rio et al., 1990].

[26] The Oligocene biozones were recognized following the standard biostratigraphic scheme of Martini [1971], while the Miocene biozone attribution was according to the Mediterranean biostratigraphic scheme of Fornaciari and Rio [1996] and Fornaciari et al. [1996], which offers a more detailed biostratigraphic resolution than the standard scheme for the Miocene Mediterranean sediments. Moreover, calcareous nannofossil zones (detailed in Table 1) have been correlated to the planktonic foraminifer zones and to the Geomagnetic Polarity Timescale of Gradstein et al. [2004].

[27] Calcareous nannofossils resulted generally common and moderately preserved, and few reworking occurred. The record of some index species allowed us to collocate almost all the studied samples in the adopted biostratigraphic scheme (see Table 1).

[28] The samples from the Molare Formation resulted barren (site BTP01) or bearing taxa referable to a long time interval between middle Eocene and middle Miocene (site BTP85). Consequently, the early Oligocene age attribution for this formation was according to Gelati et al. [1993] and Servizio Geologico d'Italia [1970b, 1971]. The Rocchetta Formation samples were attributed to two biozones, across the early-late Oligocene boundary: the samples characterized by the presence of *H. recta*, *S. distentus*, *Cyclicargolithus abisectus* ( $>10 \mu\text{m}$ ) and the absence of *Reticulofenestra umbilica* and *S. ciproensis* were ascribed to the upper part of NP23 Zone of Martini [1971]; the samples showing the occurrence of *S. ciproensis* together with *S. distentus* were assigned to NP24 Zone. The Monesioglio Formation samples were characterized mainly by taxa with long stratigraphic ranges and few early Miocene index species. The presence of rare *H. carteri*, common *H. euphratis*, the absence of *S. delphix* and *S. disbelemnos* allowed us to attribute some samples to Aquitanian subzones MNN1c (site BTP80). The samples with common *H. carteri*, without *H. euphratis* and *H. ampliaperta* were assigned to MNN2a Zone of Fornaciari and Rio [1996] (site BTP65). Following the distribution of *H. ampliaperta*,

*H. walbersdorfensis* and *S. heteromorphus*, we were able to date with good approximation the remaining lower mid-Miocene formations. The Cremolino Formation samples were attributed to MNN2b and MNN5a Zones; the MNN2b Zone was recognized on the presence of *H. ampliaperta* and the absence of *S. belemnos*. The samples assigned to the MNN5a subzone of Fornaciari et al. [1996] were characterized by the presence of *S. heteromorphus* (40–50%), rare *H. walbersdorfensis*, and the absence of *H. ampliaperta*. For the above reason, the samples from the Cassinasco Formation were assigned to the MNN5a subzone. Concerning the samples from the Cessole Formation, the abundance of *H. walbersdorfensis* ( $>10\%$ ) and *S. heteromorphus* (40%) allowed us to assign them to the younger MNN5b subzone. The samples from the Serravalle Formation contain calcareous nannofossils referable to the MNN4a Zone, due to the absence of *S. belemnos*, and the contemporary occurrence of *S. heteromorphus* and *H. ampliaperta*.

## 6.2. Magnetic Mineralogy

[29] Hysteresis properties investigated in sediments from the TPB show the presence of two main groups of samples. Group 1 is characterized by narrow, multidomain-like, hysteresis loops (Figure 3a), with a saturation remanence to saturation magnetization ratio (Mrs/Ms) in the range 0.08–0.03 and the coercivity of remanence (Bcr) ranging from 16 to 36 mT. To the group 1 belong all the Oligocene sites, except for BTP12, BTP19, and BTP25, the Aquitanian site (BTP80) and the Langhian site BTP38. Group 2, mainly including the Burdigalian-Langhian sites, shows a magnetic behavior dominated by paramagnetic minerals (Figure 3b). The presence of a minor contribution of ferromagnetic minerals in samples from the group 2 appears only after correction of the hysteresis loops for the high-field slope. The lower Oligocene site BTP01 stays apart from the two outlined groups and shows distinct magnetic properties by having an open, single-domain-like, hysteresis loop, higher coercivity (Bcr = 77 mT) and a Mrs/Ms ratio of 0.33; we suppose for this site the presence of ferrimagnetic sulphides (greigite?).

[30] The thermal variation of the low-field magnetic susceptibility reflects the same group distribution. In fact, during the heating-cooling cycle of specimens from the group 1, the susceptibility remains nearly constant with increasing temperature (or has a minor inflection around 320–350°C, that may be due to conversion of a minor amount of maghemite to hematite [Stacey and Banerjee, 1974; Dunlop and Özdemir, 1997]), then it abruptly decreases at the Curie temperature for magnetite ( $\sim 580^\circ\text{C}$ , Figures 3c and 3d). For most of the group 1 samples, the

**Figure 3.** Hysteresis loops (Figures 3a and 3b) and thermomagnetic curves (Figures 3c–3f) of representative specimens from groups 1 and 2 (see text). (a) Hysteresis loop showing a soft-coercivity, multidomain-like, ferromagnetic (in the broad sense) behavior, typical for samples of group 1. (b) Hysteresis loop for a typical sample of group 2, showing a paramagnetic-dominated behavior (line passing through the origin). (c, d) Variation of the low-field magnetic susceptibility (k) during a heating-cooling cycle (black and grey arrow, respectively) from room temperature to 700°C, for two typical samples of group 1. (e, f) Variation of the low-field magnetic susceptibility for a representative sample of group 2 (Figure 3e) and close-up of only heating path (Figure 3f). (g) Day plot [Day et al., 1977] for sediments from group 1 (black squares). Fields for single-domain (SD), pseudosingle-domain (PSD), and multidomain (MD) for (titano)-magnetite grains and the theoretical trend lines for mixture of SD-MD and of SD superparamagnetic (SP) magnetite grains (with numbers indicating the percentage of soft coercivity particles) are shown according to Dunlop [2002].

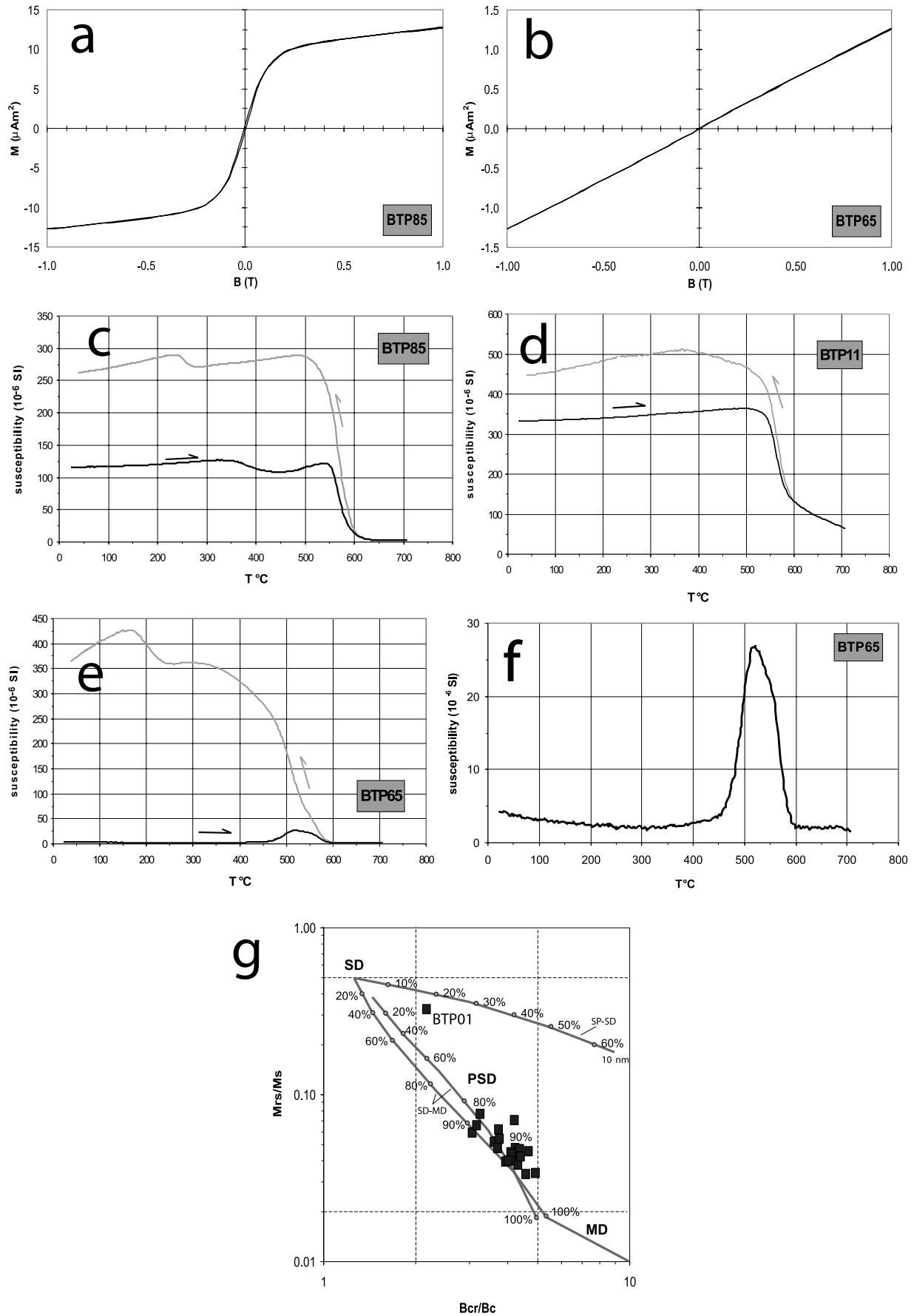


Figure 3

susceptibility continues decreasing after  $\sim 600^{\circ}\text{C}$  up to the Neel temperature of hematite ( $\sim 680^{\circ}\text{C}$ ), suggesting the coexistence of magnetite and hematite grains (Figure 3d). Only the lower Oligocene site BTP85 shows a constant, and almost null, magnetic susceptibility value in the heating path after  $580^{\circ}\text{C}$  (Figure 3c), indicating that hematite is not present at that site. For all sites, the cooling path shows higher susceptibility values with respect to the heating path. This suggests the formation of new magnetite particles from the clayey matrix of the sediment during heating.

[31] In the samples from the group 2, magnetic susceptibility decreases following a hyperbolic trend up to  $\sim 300^{\circ}\text{C}$  during heating (Figure 3f), confirming a prevalent contribution of the paramagnetic fraction to the susceptibility. The paramagnetic versus ferromagnetic contribution may be evaluated according to the method of Hrouda [1994] and is of the order of 80%. In most of the specimens from the group 2, an increase of the susceptibility values occurs between  $400\text{--}450^{\circ}\text{C}$  and  $580^{\circ}\text{C}$  during heating (Figures 3e and 3f), and it is most likely due to the formation of new magnetite from the paramagnetic matrix (pyrite? clay minerals?). In fact, the cooling path is characterized by higher magnetic susceptibility values and a significant increase starting at the Curie temperature of magnetite (Figure 3e).

[32] The ratios of hysteresis parameters for the group 1 samples, plus site BTP01, when plotted in a Day plot [Day *et al.*, 1977] (Figure 3g), fall in the pseudosingle-domain field, and are located along the theoretical trend line for mixtures of single-domain (SD) and multidomain (MD) magnetites [Dunlop, 2002]. Only data from site BTP01 fall apart from the main group.

[33] The analyses of the hysteresis properties and of the low-field magnetic susceptibility thermal variation indicate that in samples from the group 1 the magnetic mineralogy is composed by prevailing PSD magnetite and a subordinate fraction of hematite. On the other hand, the magnetic properties of the sediments from the group 2 are mainly controlled by the paramagnetic clayey matrix. Only a minor fraction of ferromagnetic (in the broad sense) minerals is contained in these sediments, and is responsible of their NRM. IRM acquisition curves and Bcr values for samples of group 2 are compatible with a low-coercivity, magnetite-like, mineral as the main magnetic carrier. Finally, site BTP01 shows magnetic properties different from those of the two groups, pointing to the additional presence of presumably ferrimagnetic iron sulphides.

### 6.3. Anisotropy of Magnetic Susceptibility

[34] The AMS parameters at both the specimen and the site levels were evaluated using Jelinek statistics [Jelinek, 1977, 1978] and are reported in Table 2. The site-mean susceptibility values reveal a time-related evolution (Figure 4a). For sites of the group 1 the mean susceptibility values are very high, ranging from  $948$  to  $30,000 \times 10^{-6}$  SI. Such values strongly suggest a predominant contribution of the ferromagnetic minerals (that is magnetite according to the mineral magnetic results discussed in section 6.2) to the susceptibility [e.g., Rochette, 1987]. Conversely, sites belonging to the group 2 and site BTP01 are characterized by considerably lower susceptibility values, comprised between  $70$  and  $350 \times 10^{-6}$  SI. Susceptibility values as low as  $200\text{--}300 \times 10^{-6}$  SI

are indicative for a major contribution of the paramagnetic matrix to the bulk susceptibility [e.g., Rochette, 1987]. Therefore, the temporal changes of the susceptibility values seem indicating that only the older (Oligocene-Aquitainian) TPB sediments are predominantly made by debris coming from erosion and dispersal of magnetite-rich rocks (likely the Voltri ophiolites). Therefore we propose that a significant change on the sediment feeding system, probably linked to an evolution of the main paleodrainage system, occurred in the TPB between Aquitainian and Burdigalian times, as also radiometric analyses by Carrapa *et al.* [2004] confirm. Alternatively, magnetite may have been dissolved in a sub-oxic/anoxic environment, with high sedimentation rates and a large supply of organic matter during burial upon the iron reduction zone [Karlin and Levi, 1983; Karlin, 1990a, 1990b].

[35] For all sites the shape of the AMS ellipsoid is predominantly oblate, with a shape factor (T)  $> 0.2$  (0.7 on average, Table 2), suggesting a prevailing sedimentary fabric. The magnetic foliation is always well defined, and parallel to the bedding plane (Figure 4b), confirming that the sampled sediments host a predominant sedimentary-compactional magnetic fabric. Moreover, 28 sites are characterized by a well-developed magnetic lineation, as documented by the clustering of  $K_{\text{max}}$  axes from the individual specimens ( $e_{12} \leq 30^{\circ}$ , Figure 4b, 13 sites display an  $e_{12}$  value even  $< 15^{\circ}$ ). All in situ magnetic lineation directions (only for sites characterized by  $e_{12} \leq 30^{\circ}$ ) are shown in Figure 4c. The large majority of the sites show a N-S to NNW-SSE mean magnetic lineation, implying that the sedimentary successions from the TPB are characterized by a magnetic lineation trending parallel to the mean plunge of the strata, and almost orthogonal to the direction (about E-W) of the Alpine thrust fronts buried below the TPB and the Po Plain.

### 6.4. Paleomagnetism

[36] Demagnetization data were plotted on orthogonal demagnetization diagrams [Zijderveld, 1967], and the magnetization components were isolated by principal component analysis [Kirschvink, 1980]. The NRM from all sites was well above the noise level of the magnetometer ( $\sim 5 \mu\text{A/m}$ ). Samples from 26 sites could be efficiently AF cleaned at  $70\text{--}100$  mT (Figures 5c–5f). Conversely, at two sites (BTP01 and BTP66), a parasitic remanence (probably a gyroremanent magnetization [Stephenson, 1980]) was induced after  $\sim 30$  mT (Figures 5a and 5g), while six additional sites (BTP12, BTP15, BTP19, BTP25, BTP30, and BTP47, Figure 5i) revealed an unstable behavior during AF demagnetization treatment. Therefore, twin specimens from cores from these latter eight sites were thermally demagnetized up to  $600^{\circ}\text{C}$  (though several specimens were completely demagnetized at  $330^{\circ}\text{C}$ ). Sites BTP12 and BTP25 definitely yielded only scattered demagnetization diagrams (Table 1).

[37] A viscous component, subparallel to the GAD field direction for the study area, was removed for all specimens at  $10\text{--}20$  mT or at  $120\text{--}180^{\circ}\text{C}$ , while a characteristic remanent magnetization (ChRM) direction was isolated in the  $20\text{--}100$  mT or  $180\text{--}330^{\circ}\text{C}$  AF/temperature intervals (Figure 5). Such coercivity spectra, together with mineral magnetic results (Figure 3), suggest that magnetite is the main magnetic carrier in the 26 AF cleaned sites. Conversely, the two sites showing a significant acquisition of a

**Table 2.** Anisotropy of Magnetic Susceptibility Results From the Tertiary Piedmont Basin<sup>a</sup>

Site	Formation	Age	Age (Ma)	n/N	Km	P'	T	D (deg)	I (deg)	Dtc (deg)	e12 (deg)
BTP01	Molare	Rupelian	30.5–33.5	10/10	70	1.097	0.915	187.3	5.4	229.9	17
BTP06	Rocchetta	Rupelian	28.7–29.7	11/11	5450	1.247	0.371	317.4	9.4	13.2	3
BTP07	Rocchetta	Rupelian-Chattian	28–29.4	11/11	5397	1.270	0.777	334.4	6.2	22.7	10
BTP09	Rocchetta	Rupelian-Chattian	28–29.7	9/11	5715	1.352	0.914	263	3.7	302.5	13
BTP11	Rocchetta	Rupelian	30–30.5	8/9	9794	1.298	0.678	7.3	10.6	81.1	12
BTP12	Rocchetta	Rupelian-Chattian	21.6–32	12/12	115	1.084	0.916	-	-	-	50
BTP13	Rocchetta	Rupelian	29.9–30.9	8/12	7265	1.205	0.652	-	-	-	32
BTP15	Cremolino	Burdigalian	16.5–17.6	10/10	175	1.093	0.836	244	3.9	-	18
BTP18	Rocchetta	Rupelian	30.1–32.3	8/8	4877	1.187	0.792	167.4	21.6	223.3	27
BTP19	Rocchetta	Rupelian	29.9–30.9	10/10	234	1.037	0.697	92	2.5	-	5
BTP25	Rocchetta	Rupelian	29.9–30.9	8/13	140	1.070	0.863	-	-	-	34
BTP29	Cremolino	Langhian	15–15.1	13/13	169	1.075	0.815	12.8	11.3	-	29
BTP30	Serravalle	Burdigalian-Langhian	16–17.6	8/8	150	1.058	0.840	141.5	5.9	-	17
BTP31	Cessole	Langhian	14.2–14.6	10/11	350	1.104	0.574	8.8	18.6	-	8
BTP38	Cessole	Langhian	14.8–15.1	9/11	948	1.150	0.359	13.7	19.8	-	9
BTP39	Rocchetta	Rupelian	30.1–32.3	6/9	30478	1.510	0.675	18.1	12.3	43.0	27
BTP41	Rocchetta	Rupelian	29.9–30.9	10/12	4640	1.139	0.667	337	1.6	34.6	16
BTP43	Rocchetta	Rupelian-Chattian	28.3–29.9	9/10	3292	1.204	0.855	184.5	6.6	236.0	15
BTP47	Rocchetta	Rupelian	29.9–30.9	9/10	5915	1.269	0.890	18.5	10.2	65.6	30
BTP53	Rocchetta	Rupelian	29.9–30.9	11/13	5266	1.302	0.258	335.8	6.9	24.1	6
BTP57	Rocchetta	Rupelian	29.9–30.9	10/12	6833	1.229	0.628	321.8	6.3	24.5	13
BTP60	Rocchetta	Rupelian	29.9–30.9	9/9	4765	1.211	0.472	322.7	5.8	338.8	6
BTP61	Rocchetta	Rupelian	29.9–30.9	9/11	6164	1.205	0.552	324.2	5.7	21.6	17
BTP62	Rocchetta	Rupelian	29.9–30.9	11/11	3178	1.207	0.516	317	6.8	0.4	6
BTP64	Rocchetta	Rupelian	29.9–30.9	10/12	6977	1.220	0.759	280.4	2.1	334.3	10
BTP65	Monesiglio	Aquitanian	20.5–20.7	10/13	167	1.056	0.883	332.3	9.5	-	21
BTP66	Cremolino	Burdigalian	19.2–20.2	8/8	185	1.072	0.930	-	-	-	49
BTP69	Cremolino	Burdigalian-Langhian	16–17.6	10/10	168	1.062	0.799	-	-	-	55
BTP72	Cassinasco	Langhian	14.8–15.2	10/10	157	1.096	0.958	-	-	-	40
BTP73	Cassinasco	Langhian	14.8–15.2	8/8	213	1.085	0.805	348.5	3.3	-	26
BTP75	Cassinasco	Langhian	14.8–15.2	9/13	125	1.037	0.912	262.3	8.2	-	18
BTP80	Monesiglio	Aquitanian	22.9–23.8	10/11	7150	1.271	0.761	20	3.6	59.2	23
BTP84	Rocchetta	Rupelian	29.9–30.9	11/12	7193	1.200	0.748	332.6	7.3	358.4	16
BTP85	Molare	Rupelian	30.9–33.1	13/13	5850	1.214	0.682	335.4	1.6	45	19

<sup>a</sup>Ages are as in Table 1; n/N is number of samples giving reliable results/number of studied samples at a site; Km is mean susceptibility, in  $10^{-6}$  SI; P' and T are corrected anisotropy degree and shape factor, respectively, according to *Jelinek* [1981]; D and I are in situ site-mean declination and inclination, respectively, of the maximum susceptibility axis; Dtc is site-mean declination of the maximum susceptibility axis back-rotated according to the paleomagnetic rotation values listed in Table 1 (only for the Oligocene and Aquitanian sites); e12 is semiangle of the 95% confidence ellipse around the mean  $K_{\max}$  axis in the  $K_{\max} - K_{\text{int}}$  plane.

parasitic remanence during the AF treatment (BTP01, BTP66), and the four sites which are completely demagnetized at 330°C (BTP15, BTP19, BTP30, BTP47), suggest iron sulphides (probably greigite) as likely remanence carriers.

[38] The site-mean directions (evaluated by *Fisher's* [1953] statistics) are generally well defined, the  $\alpha_{95}$  values being lower than  $10^\circ$  in all but three sites (Table 1). The site-mean directions are both of normal and reverse polarity, but the normal polarity is predominant (25 out of 32 sites, Figure 6 and Table 1), and the few reverse-polarity sites are all of Oligocene age. The tilt-corrected declinations are significantly scattered, and are spread from westward to northward direction (when translated all to the normal polarity state).

[39] Field tests were performed for Oligocene-Aquitanian and Miocene sites separately. For Oligocene-Aquitanian sites ( $N = 20$ , excluding site BTP19, see below) we performed an Inclination-only fold test (according to *Enkin and Watson* [1996]), as they underwent different amounts of rotations. Maximum clustering occurs at 5% of unfolding ( $k = 21.42$ ), and it decreases until 100% of complete unfolding ( $k = 15.97$ ). However, the in situ increase of data clustering is not statistically significant ( $k_2/k_1 = 1.31$ , with critical value of  $F_{95\%} = 2.12$  for  $N = 20$  degrees of freedom).

Furthermore, whereas we recognize that the conventional fold test is not suitable for Oligocene-Aquitanian data, the inclination-only fold test may be not fully reliable as well. In fact, our samples are mainly marls and mudstones, and therefore are likely to be affected by a different amount of inclination shallowing, which is determined by the compaction of muddy rocks during diagenesis. Thus, as the in situ directions from Oligocene-Aquitanian sites are far from the geocentric axial dipole (GAD) field direction for the TPB ( $D = 0^\circ$ ,  $I = 63.0^\circ$ , Figure 6), and reveal a pretty homogeneous CCW rotation, we infer that they are not remagnetized and reflect a primary remanent magnetization. Conversely, 8 of the 11 Miocene sites (i.e., excluding sites BTP15, BTP38 and BTP66) show in situ directions very clustered and close to the GAD field direction. The *McFadden* [1990] fold test was performed first on all Miocene sites, resulting indeterminate, then on the 8 grouped sites only, giving a negative result (in situ statistics  $D_{\text{mean}} = 2.3^\circ$ ,  $I_{\text{mean}} = 54.4^\circ$ ,  $k = 771.5$ ,  $\alpha_{95} = 2.0^\circ$ ,  $\xi = 3.054$ , unfolded statistics  $D_{\text{mean}} = 359.6^\circ$ ,  $I_{\text{mean}} = 46.1^\circ$ ,  $k = 79.6$ ,  $\alpha_{95} = 6.3^\circ$ ,  $\xi = 3.690$ ;  $\xi_{95\%}$ critical value = 3.298. Maximum  $k$  and minimum  $\xi$  values occur at 0% unfolding, indicating a postfolding remagnetization).

[40] The reversal test (according to *McFadden and McElhinny* [1990]) performed on the Oligocene-Aquitanian

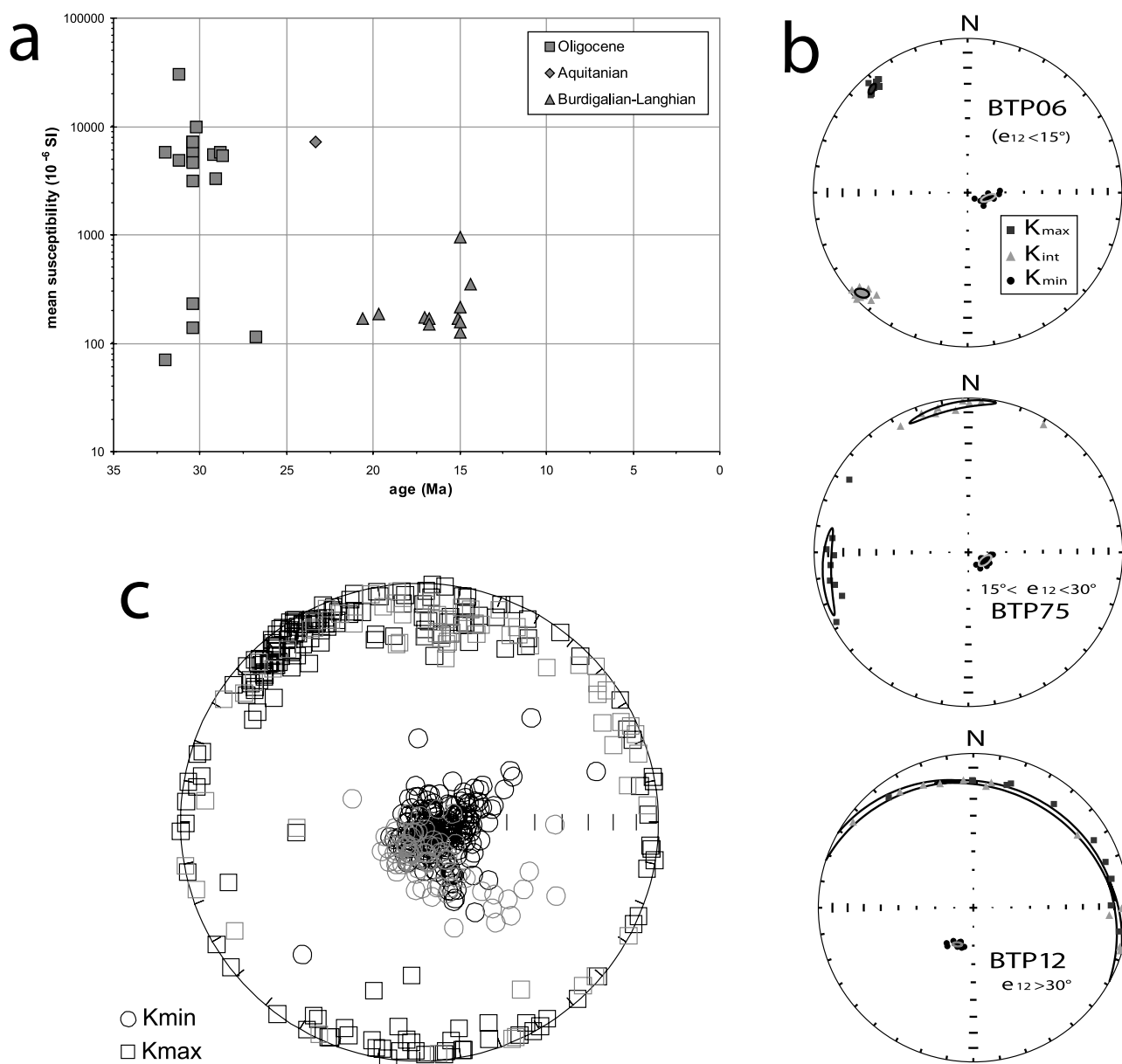


**Figure 4.** AMS results from the TPB. (a) Mean magnetic susceptibility values versus site ages (according to Table 2). (b) Schmidt equal-area projections, lower hemisphere, of the principal axes of the AMS ellipsoid, for three representative sites (in situ coordinates), showing variable degrees of scattering for the magnetic lineation ( $e_{12}$  is the semiangle of the 95% confidence ellipse around the site-mean  $K_{max}$  in the  $K_{max} - K_{int}$  plane). (c) Lower hemisphere equal-area projection of the in situ  $K_{max} - K_{min}$  directions from all cores with  $e_{12} < 30^\circ$  (see also Table 2). Black (grey) symbols are referred to Oligocene (Miocene) samples.

sites (displaying dual polarities) yielded the following results:  $D_{mean} = 310.6^\circ$ ,  $I_{mean} = 43.4^\circ$ ,  $k = 18.12$  for 13 normal polarity sites, and  $D_{mean} = 130.5^\circ$ ,  $I_{mean} = -47.8^\circ$ ,  $k = 21.33$  for 7 reverse polarity sites, resulting positive of class C and suggesting that the adopted magnetic cleaning has efficiently resolved the ChRMs from each specimen.

[41] Concluding, we infer that all Oligocene-Aquitian sites (except site BTP19) host a primary magnetization, and their rotation values are reliable for reconstructing the tectonics of the TPB. Conversely, 8 out of 11 Miocene sites

are remagnetized, as suggested by the negative fold test. The in situ paleomagnetic directions for the remaining 3 Miocene sites stand far from the GAD field direction, suggesting that they retain a primary magnetization.

[42] The direction of the Oligocene site BTP19 (Table 1) is very close to that of the eight remagnetized Miocene sites in in situ coordinates, and it displays a positive paleodeclination ( $D = 4.4^\circ$ ), while all the remaining Oligocene sites yield negative (up to  $-90.8^\circ$ ) declination values. Furthermore, its magnetic/mineralogical properties are similar to

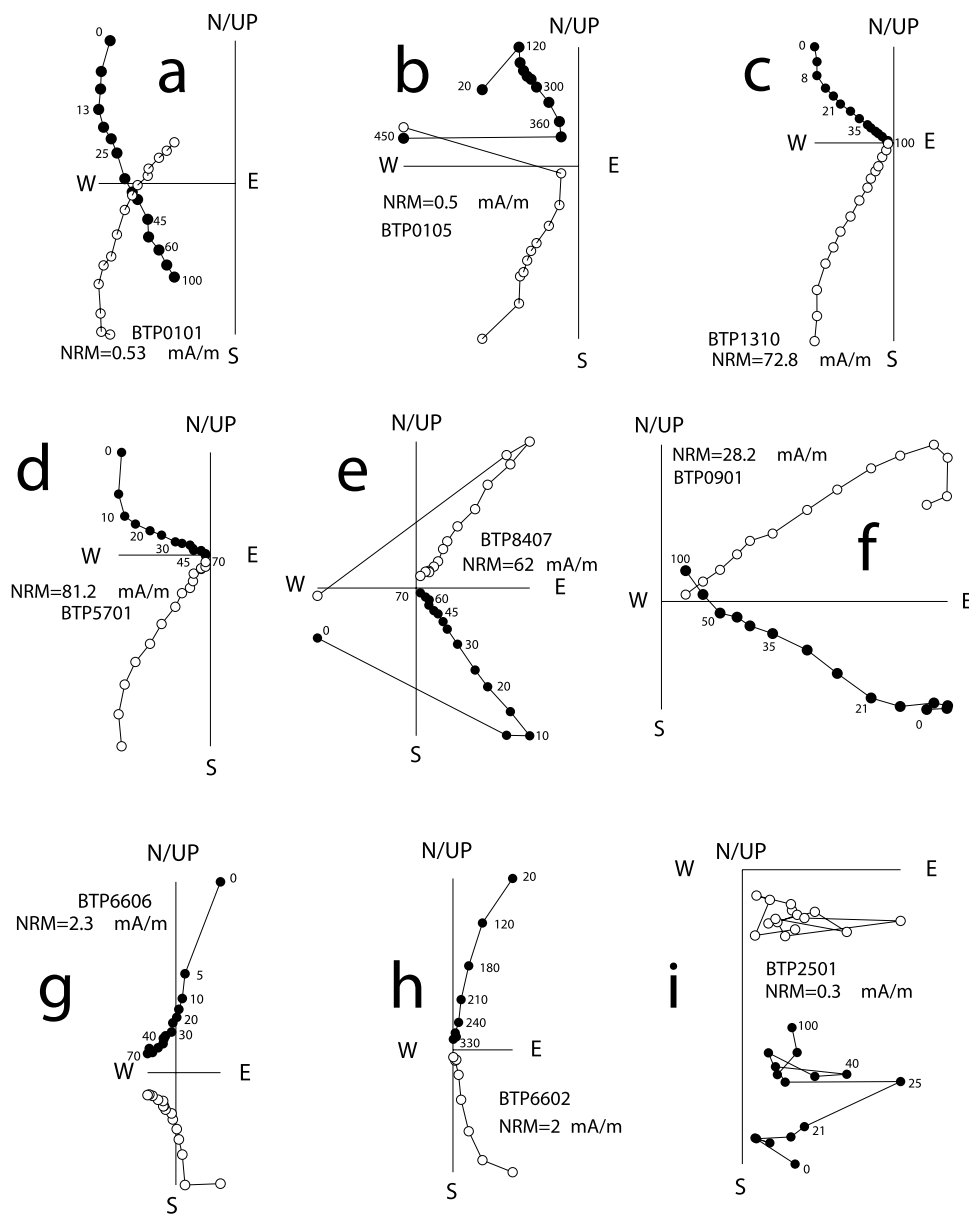


**Figure 5.** Orthogonal vector diagrams of typical demagnetization data, in situ coordinates. Solid and open dots represent projection on the horizontal and vertical planes, respectively. Demagnetization step values are in mT (Figures 5a, 5c, 5d, 5e, 5f, 5g, and 5i) and in °C (Figures 5b and 5h). See text for explanation.

those of the Miocene remagnetized sites. Therefore we infer that also the Oligocene site BTP19 was magnetically overprinted after tilting.

[43] Our evidence of magnetic overprint concurs with previous results from *Bormioli and Lanza* [1995], who documented a posttilting remagnetization for five mid-Oligocene–mid-Miocene sites from the TPB.

[44] To sum up, it appears that the great majority (23 out of 34) of the sedimentary sites paleomagnetically studied in the TPB host a pretilting (and likely primary) remanent magnetization, while nine sites (eight Miocene and one Oligocene in age, Table 1) were remagnetized after tilting (that is post Miocene [e.g., *Lorenz*, 1984]). The magnetically overprinted sites systematically display low natural

remanence ( $\leq 3.6$  mA/m) and low susceptibility ( $\leq 350 \times 10^{-6}$  SI, Table 2), dominated by the paramagnetic fraction (Figures 3b and 3f).

## 7. Discussion

### 7.1. Local Versus Uniform Rotations at the TPB

[45] A considerable spread of paleomagnetic declinations (ranging from  $-16.1^\circ$  to  $-90.8^\circ$ , Figure 6 and Table 1) characterizes the Oligocene sites, which were sampled at sites where the strata predominantly dip northward and westward at the Alto Monferrato and Langhe, respectively (Figure 1 and Table 1). Therefore the question arises as to whether this is simply a paleomagnetic directional scatter, or different sectors of the TPB have undergone differential

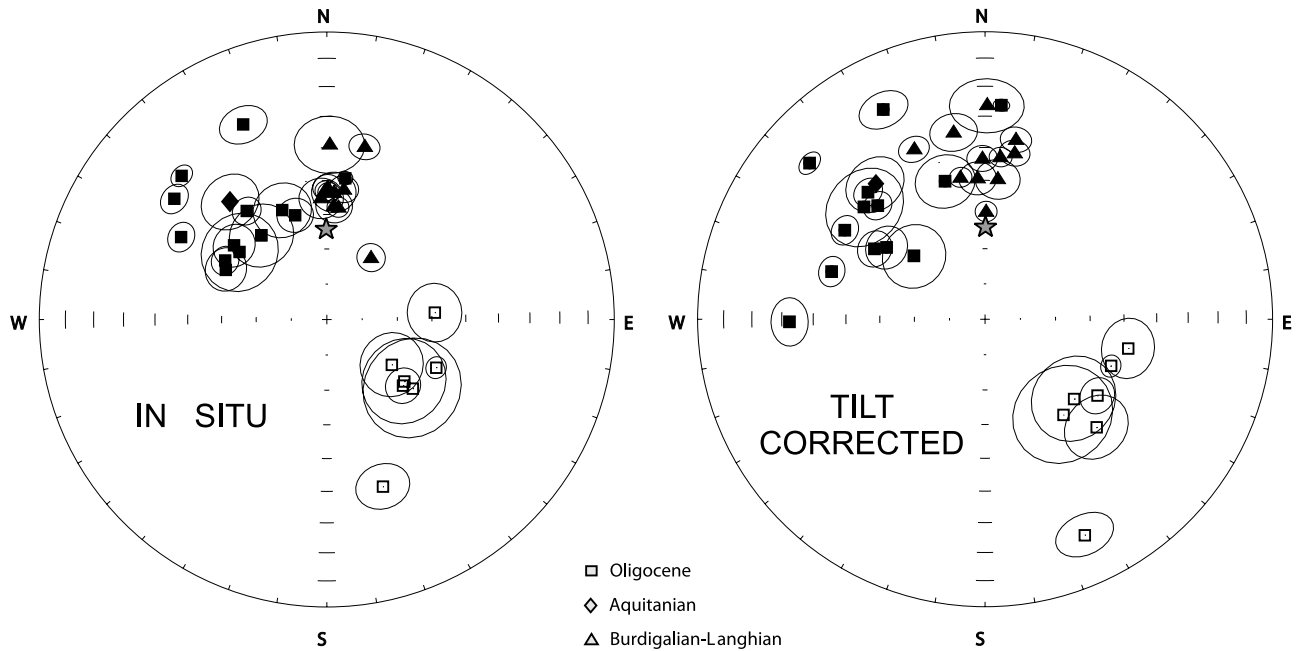


**Figure 6.** Equal-area projections of the site-mean paleomagnetic directions from the TPB. Solid (open) symbols represent projection onto the lower (upper) hemisphere. Open ellipses are the projections of the  $\alpha_{95}$  cones about the mean directions. The star represents the normal polarity geocentric axial dipole (GAD) field direction ( $D = 0^\circ$ ,  $I = 63.0^\circ$ ) for the study area.

rotations. In map view, the TPB formations describe a large-scale salient, formed by E-W and approximately N-S outcrops at the Alto Monferrato and Langhe, respectively (Figure 1). This geologic pattern is more likely to be related to different regional strata tilting occurring in the different basin sectors, rather than to noncoaxial folding characterizing the Alto Monferrato and Langhe. Nonetheless, the

“oroclinal” test [e.g., Schwartz and Van der Voo, 1983; Eldredge et al., 1985; Hirt and Lowrie, 1988] can be used to verify whether a statistically significant rotational difference exists at sites characterized by different “structural” (i.e., fold axis) directions.

[46] In Figure 7 we compare the Oligocene site-mean paleomagnetic declinations to local structural directions

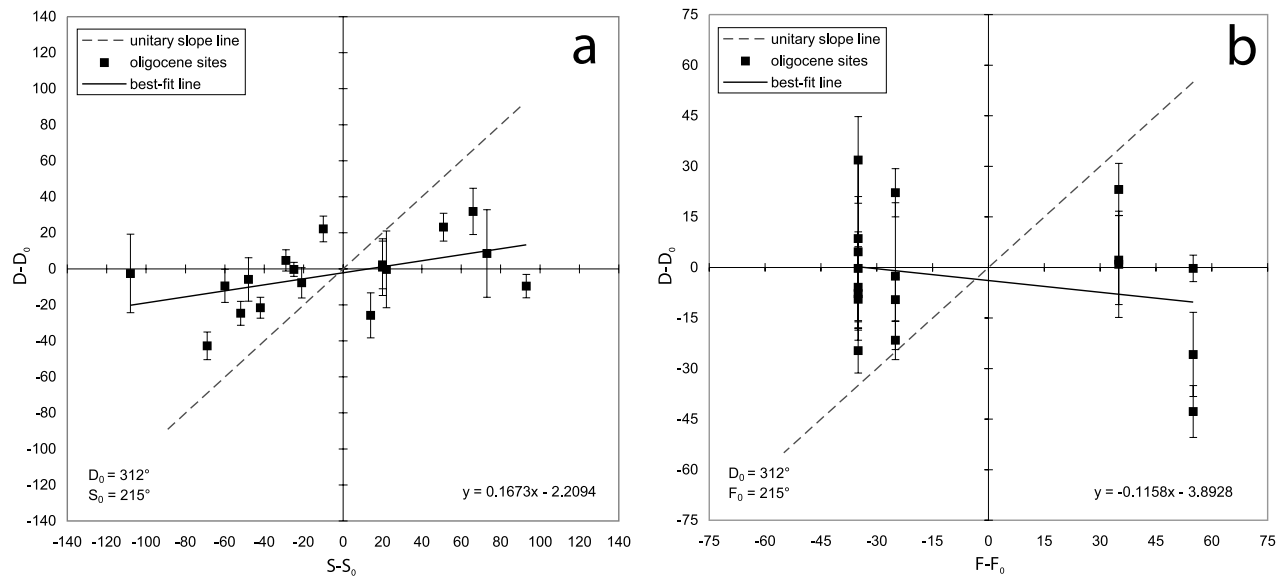


**Figure 7.** Paleomagnetic declination deviations for 18 Oligocene sites (yielding paleomagnetic directions acquired before strata tilting), relative to (a) strike of beds and (b) fold axis deviations [e.g., Schwartz and Van der Voo, 1983].  $D$  is the observed paleomagnetic declination at a site, and  $D_0$  is the reference declination value ( $312^\circ$ ).  $S$  is the observed bed strike at a site and  $F$  is the fold axis direction at a site determined from structural maps (see text). The reference bedding strike ( $S_0$ ) and fold axis ( $F_0$ ) directions are both  $215^\circ$ . Error bars for declination data are the respective  $\alpha_{95}/\cos(I)$  values.

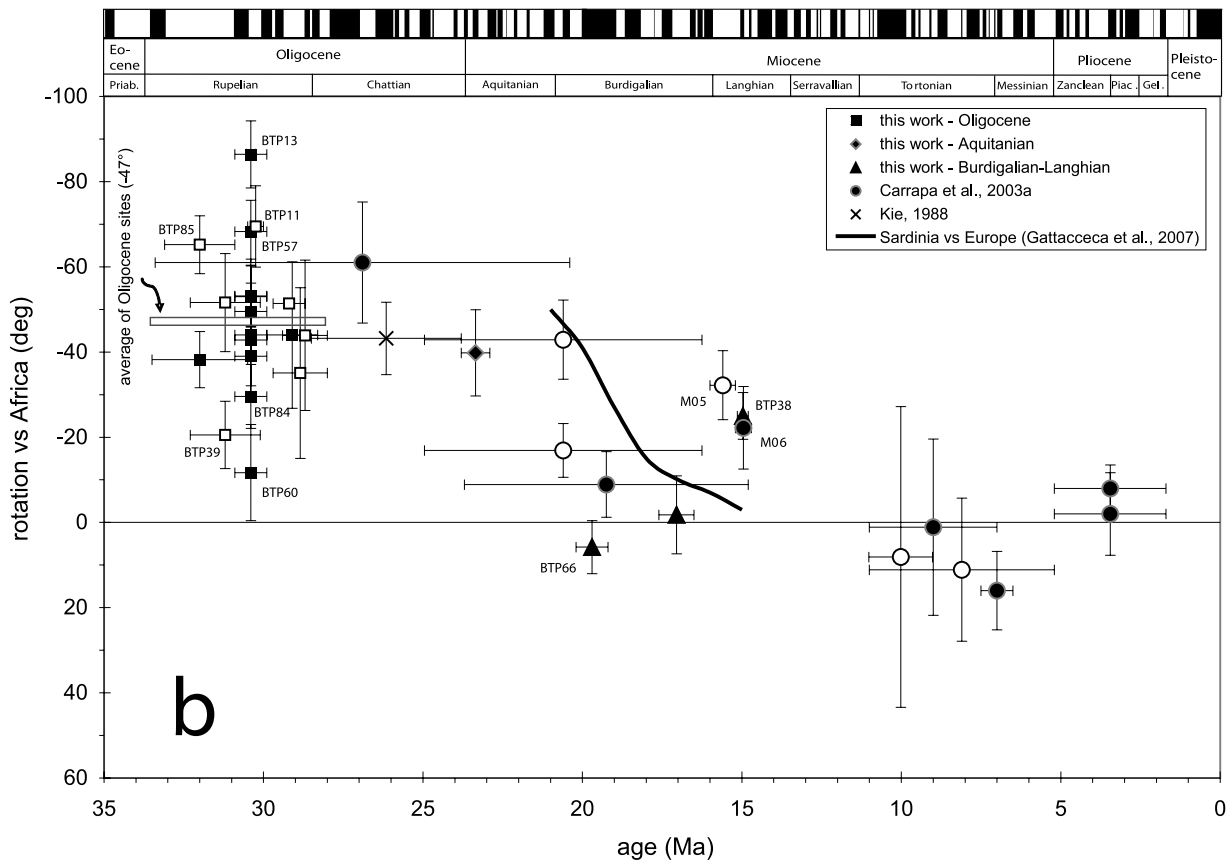
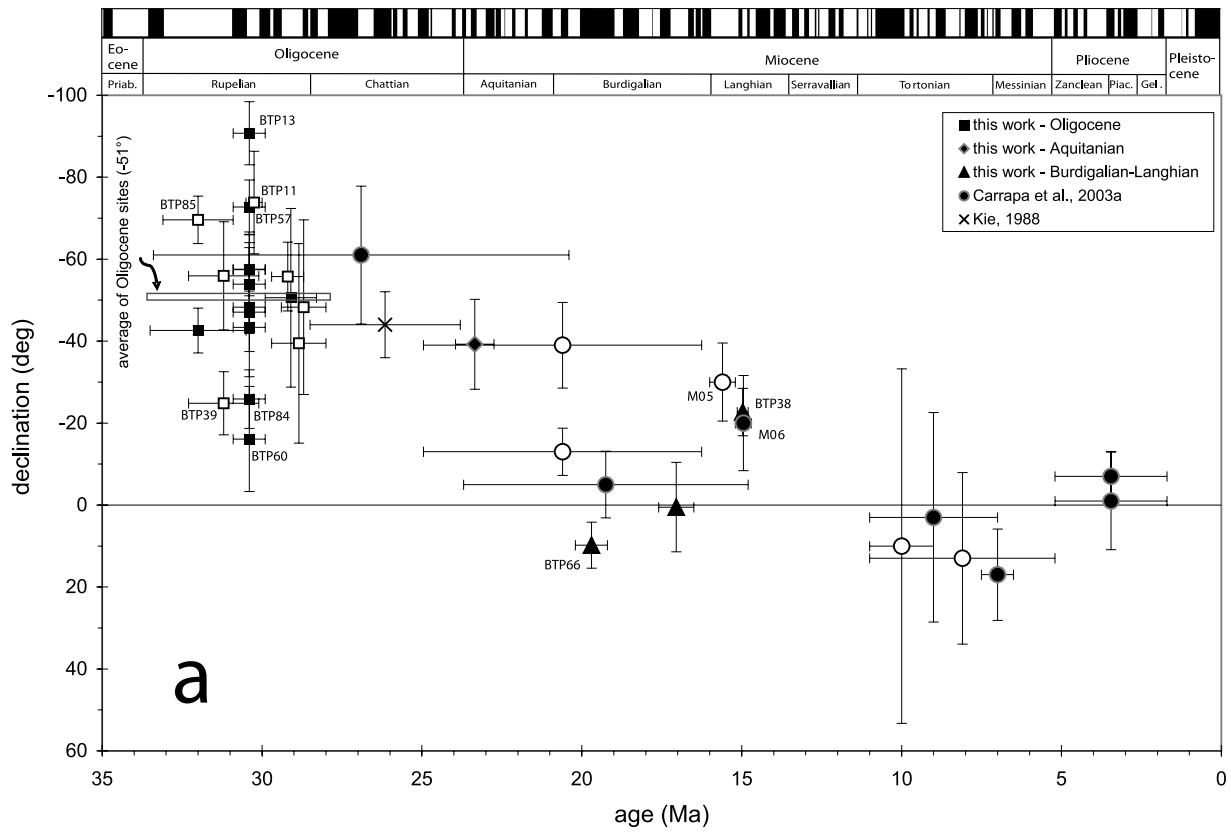


Figure 8

**Table 3.** Previous Paleomagnetic Directions From the Tertiary Piedmont Basins and Updated Rotation Flattening Values With Respect to Africa<sup>a</sup>

Ref.	Site	Formation	UTM		Age (Ma)	Cleaning Strategy	D (deg)	I (deg)	k	$\alpha_{95}$ (deg)	N	R (deg)	F (deg)
			Coordinates Zone 32T	Age									
1	M01	Rocchetta	415635–491086	upper Oligocene-lower Miocene	25.0–16.3	TH	167	–46	147	4	9	–16.9 (6.3)	10.1 (4.6)
1	M03	Rocchetta	413918–491887	upper Oligocene-lower Miocene	25.0–16.3	AF	141	–55	67	6	11	–42.9 (9.3)	1.2 (5.7)
1	M05	-	415000–492038	Langhian	16–15.2	AF	150	–51	84	6	9	–32.2 (8.1)	7.2 (5.2)
1	M06	-	408667–491503	Langhian	15.2–14.7	TH	340	53	167	7	4	–22.2 (9.7)	5.2 (5.9)
1	M07	-	408000–491670	Tortonian	11–9	TH	190	–36	3	35	10	8.1 (35.3)	22.9 (27.4)
1	M08	-	403065–492272	Tortonian-Messinian	7.5–6.5	TH	17	69	141	4	11	16 (9.2)	–9.1 (3.6)
1	M09	-	411303–492559	Miocene	11–5.2	TH	193	–48	23	14	6	11.1 (16.8)	10.9 (11.1)
1	M13	Cortemilia	429767–492761	Aquitanian-Langhian	23.7–14.8	TH	355	52	80	5	11	–8.9 (7.7)	4.2 (5.2)
1	M14	Santa Agata Marls	429653–495209	Tortonian	11–7	TH	3	62	15	12	11	1.1 (20.7)	–3.1 (9.6)
1	M15	Lugagnano Shales	435034–496416	Pliocene	5.2–1.7	TH	353	49	143	4	11	–8.0 (5.5)	10.9 (3.6)
1	M19	Lugagnano Shales	454180–495717	Pliocene	5.2–1.7	TH	359	41	30	9	11	–2.0 (9.7)	18.9 (7.2)
1	M20	Rocchetta-Monesiglio	446547–493557	Oligocene-Aquitanian	33.4–20.4	TH	299	27	10	15	11	–61 (14.2)	30.3 (12.3)
2	Ra	Rocchetta	-	upper Oligocene	28.5–23.8	TH	316	42	99	6	7	–43 (8.5)	15.7 (6)

<sup>a</sup>References (Ref), (1) Carrapa et al. [2003a] and (2) Kie [1988]. Ages are as in Table 1. Cleaning strategy is alternated field (AF) or thermal (TH); D and I are site-mean declination and inclination calculated after tectonic correction; k and  $\alpha_{95}$  are statistical parameters after Fisher [1953]; N is number of samples giving reliable results per site. Updated site-mean rotation (R) and flattening (F) values (according to Demarest [1983]) are relative to coeval D and I African values expected at the Tertiary Piedmont Basin (errors are in parentheses). The reference African paleopoles are from Besse and Courtillot [2002]. The scattered paleomagnetic directions from Bormioli and Lanza [1995] are omitted.

derived from local bed strike (Figure 7a), and regional fold axis direction gathered from structural maps [*Consiglio Nazionale delle Ricerche*, 1991] (Figure 7b). As reference paleodeclination and structural direction, we adopted the mean Oligocene declination ( $312^\circ$ ), and a NNE-SSW trend ( $215^\circ$ ), respectively. The statistical *t* test (according to Hirt and Lowrie [1988]) is used to verify whether the slopes of the best fit lines calculated in Figures 7a and 7b are statistically different from zero slope (indicating no paleomagnetic versus structural correlation).

[47] The *t* test on the slope of the regression lines compared to zero slope gives (for diagrams 7a and 7b, respectively) values  $t = 2.28$  and  $t = 1.16$ , which are both smaller than the critical *t* value at the 99% significance level ( $t_{99} = 2.58$  for number of data  $N = 18$ ), implying that both best fit lines are statistically indistinguishable from zero slope. As a conclusion, the results of the oroclinal test exclude that differential rotations occurred at different TPB sectors, and demonstrate that the basin rotated as a whole.

## 7.2. Magnitude and Timing of Rotations

[48] The declination and rotation versus time evolution of the TPB is shown in Figure 8a and 8b, respectively. Chronologic constraints are provided by the calcareous nannofossil content (see section 6.1 and Table 1) framed

into the timescale of Gradstein et al. [2004], as well as by the paleomagnetic polarity of the 23 reliable sites compared with the geomagnetic polarity timescale of the same authors. Rotations (Figure 8b) were evaluated by comparing TPB paleodeclinations to coeval expected African paleodeclinations from Besse and Courtillot [2002], as the TPB lies on an Alpine wedge stacked onto Adriatic lithosphere, and African poles are routinely used as proxy of Adria poles [e.g., Van der Voo, 1993; Channell et al., 1992; Channell, 1996; Muttoni et al., 2001]. In Figure 8 we also show (1) the mean paleomagnetic direction obtained from seven upper Oligocene sites from the TPB eastern margin, as reported by Kie [1988] and (2) the paleomagnetic data from Carrapa et al. [2003a], who gathered paleomagnetic results from Miocene-Pliocene sediments from the TPB. The use of these formerly published data sets allows a valuable time extension for our study of lower Oligocene–mid-Miocene sediments. The updated rotation values versus Africa, calculated from the formerly published paleodeclination values are also detailed in Table 3.

[49] The data from Figure 8b define a  $47^\circ \pm 17^\circ$  post-Oligocene CCW rotation of the TPB with respect to Africa/Adria, which is consistent with the  $43^\circ \pm 8.5^\circ$  post-Oligocene CCW rotation reevaluated from the data by Kie [1988]. Though the value of  $47^\circ \pm 17^\circ$  of CCW rotation has been

**Figure 8.** Site-mean paleomagnetic declination (Figure 8a) and rotation with respect to Africa (Figure 8b) versus age, for sites from the TPB. Rotations relative to both paleodeclinations from us and from previous works [Kie, 1988; Carrapa et al., 2003a] are evaluated according to Demarest [1983] with respect to coeval African poles from Besse and Courtillot [2002] (see Tables 1 and 3). Solid (open) symbols indicate sites yielding normal (reverse) magnetic polarity. Geologic and geomagnetic polarity timescale are from Gradstein et al. [2004]. Error bars for declination site-mean values are the  $\alpha_{95}/\cos(I)$  values. Error bars for rotations were computed according to Demarest [1983]. Error bars for ages were drawn considering both biostratigraphic information and paleomagnetic polarity (see text and Table 1). The black line in Figure 8b is the Sardinia versus Europe rotation evolution recently proposed by Gattacceca et al. [2007]. The scattered paleomagnetic declinations from Bormioli and Lanza [1995] are omitted.

calculated averaging all Oligocene sites, 7 sites (of both normal and reverse polarity) yield significantly different paleodeclination values (Figure 8a). We think that this simply reflects a normal paleomagnetic data scatter, yet here we provide some possible alternative explanations: (1) site BTP13, which yields the highest rotation value, shows a bedding strike clearly distinct from that of the other sites (Table 1), thus could have undergone a local CCW rotation, besides the regional TPB rotation; (2) sites BTP84 and BTP85 come from the Mioglia locality, where *Bernini and Zecca* [1990] observed a synsedimentary decametric fold, and could thus have undergone a multiphase deformation (Oligocene plus post-Miocene) invalidating a simple paleomagnetic tilt correction; and (3) these sites could have been interested by large-scale sliding processes, not recognized during sampling, but present over the TPB area, which would have introduced spurious rotations.

[50] The results from *Carrapa et al.* [2003a] clearly show that the TPB rotation occurred before Tortonian times and robustly constrain it to the early mid-Miocene. The nine lower mid-Miocene paleomagnetic directions (five from *Carrapa et al.* [2003a], four from this study) indeed show intermediate rotation values, but do not allow a precise determination of the rotation timing. As a rule, lower mid-Miocene reverse-polarity sites yield greater rotation values than roughly coeval normal-polarity sites (Figure 8b) and therefore a magnetic overprint for (at least some of the) Burdigalian-Langhian normal-polarity sites may have occurred. To sum up, our data, integrated with previous results from *Kie* [1988] and *Carrapa et al.* [2003a], consistently reveal that the TPB rotated  $\sim 50^\circ$  CCW with respect to Africa in early mid-Miocene times, between Aquitanian and Serravallian (roughly between 23 and 12 Ma). Additional early mid-Miocene results from the TPB would be needed to further constrain such age window.

[51] When the paleomagnetic inclinations, in tilt corrected coordinates and excluding data from the remagnetized sites, are compared to the coeval expected African inclinations, predominantly positive flattening values are obtained (values range between  $-9.6^\circ$  and  $35^\circ$ , Table 1). Such shallowing of paleomagnetic site-mean directions can be easily explained considering the effect of diagenesis and compaction [e.g., *Deamer and Kodama*, 1990] as observed for similar sediments at different sites from the Italian peninsula [*Speranza et al.*, 1997]. Predominantly positive flattening values are also derived for paleomagnetic inclinations by *Carrapa et al.* [2003a] and *Kie* [1988], when reevaluated using updated African poles (Table 3).

### 7.3. Rotation of the TPB in the Frame of Alpine-Apennine Tectonics

[52] In the Mediterranean domain, the Tertiary back-arc spreading process, and the associated arcuate belt formation and microplate dispersal, have been accompanied by widespread paleomagnetic rotations [*Lonergan and White*, 1997]. The TPB is located just north of the Ligurian Sea, which represents the northern end of the Liguro-Provençal Basin, undergoing back-arc spreading in late Oligocene–mid-Miocene times [*Malinverno and Ryan*, 1986; *Speranza et al.*, 2002] at the rear of the eastward drifting Corsica-Sardinia block. A wealth of paleomagnetic data gathered from Corsican sediments [*Ferrandini et al.*, 2003] and

Sardinian volcanics [e.g., *Gattacceca et al.*, 2007] and sediments [*Speranza et al.*, 2002] have proven that the Corsica-Sardinia microplate drift was accompanied by a CCW rotation with respect to Europe of  $\sim 50^\circ$  occurring in early mid-Miocene, between 20–21 and 15–16 Ma. If the Corsica-Sardinia along-time rotation proposed by *Gattacceca et al.* [2007] is superimposed onto the rotation versus age plot of the TPB (Figure 8b), both the rotation magnitude and its timing from the two data sets appear similar. Some discrepancy between the two data sets can be observed at the age interval of the Corsica-Sardinia rotation, which is early Miocene. In this time interval, there are four sites (two from *Carrapa et al.* [2003a], two from this study, Figure 8) yielding rotation values significantly different than the Corsica-Sardinia rotation path. Among them, site BTP38 shows an anomalously high strata inclination ( $49^\circ$ , Table 1). We may suppose that either bedding attitude measured at site BTP38 is incorrect, or that it reflects a local site rotation superimposed on the regional trend. Conversely, site BTP66 shows magnetic and mineralogical characteristics typical of the remagnetized sites and yields a normal polarity, definitely suggesting a magnetic overprint.

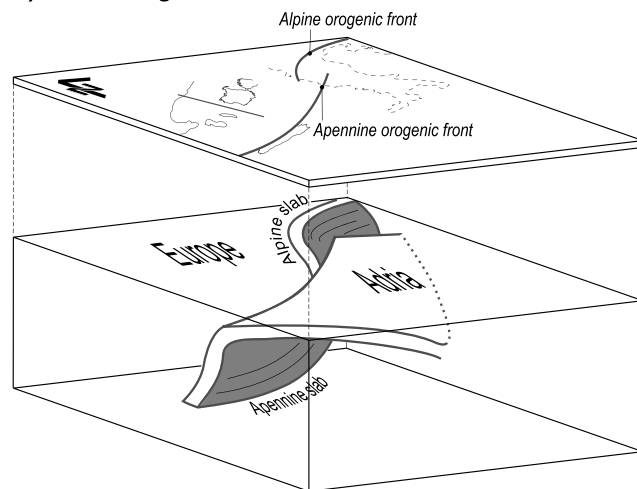
[53] Though rotations from the TPB and Corsica-Sardinia are evaluated with respect to Africa and Europe respectively, they are indeed comparable, as none of the two major plates has undergone significant rotation with respect to the geographic north during Tertiary times [e.g., *Besse and Courtillot*, 2002].

[54] The TPB rotation magnitude is also similar to the  $52^\circ \pm 8^\circ$  CCW rotation with respect to Africa documented by *Muttoni et al.* [1998] for the Epiligurian units unconformably resting upon Liguride nappes from the northern Apennines (Figure 1), yet its timing is different. In fact, *Muttoni et al.* [2000] proved that  $\sim 24^\circ$  rotation occurred in Oligo-Miocene times (thus possibly being related to the Corsica-Sardinia rotation), while the remaining  $28^\circ$  occurred during the Pliocene Apennine shortening episodes (in agreement with previous results from *Speranza et al.* [1997]).

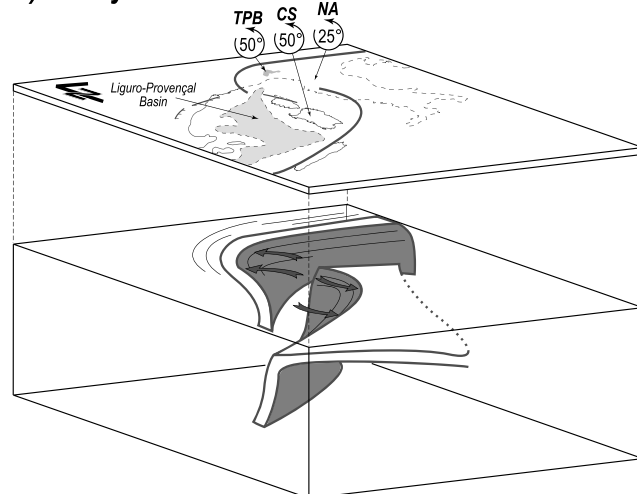
[55] Considering altogether, the paleomagnetic data from western Alps, Corsica-Sardinia, northern Apennines, and TPB, may support the following tectonic-rotational scenario (Figure 9). In the late Oligocene (Figure 9a), both the Alpine and the Apennine orogenic fronts roughly struck NE-SW; in the western Alps, east directed subduction lead to the closure of the oceanic domain and concomitant exhumation of HP units. At that time, the west directed Apennines-Calabria subduction process started migrating backward toward E-SE as attested by the initiation of the Liguro-Provençal-Balearic and Sardinia rift system [*Cherchi and Montadert*, 1982; *Gorini et al.*, 1993; *Séranne*, 1999; *Faccenna et al.*, 1997]. In early mid-Miocene times (between 20–21 and 15–16 Ma), the Corsica-Sardinia microplate drifted eastward (from the Provençal-Catalan margin) and contemporaneously rotated CCW by  $\sim 50^\circ$  (according to *Gattacceca et al.* [2007]) (Figure 9b). The TPB, located north of the (spreading) Liguro-Provençal Basin, also rotated  $\sim 50^\circ$  CCW, together with the underneath Alpine wedge, yielding a further tightening of the western Alpine Arc. Conversely, the Alpine nappes (including the Liguride units) located NE of Corsica-Sardinia underwent an intermediate ( $\sim 25^\circ$ ) CCW rotation, implying that they accommodated the excess Corsica-Sardinia rotation (and drift) by

internal deformation (through nappe stacking). Most likely, both the TPB and the Epiligurian units were passively carried (and rotated) by underneath rotational thrust sheet emplacement inducing belt bending (as also documented in

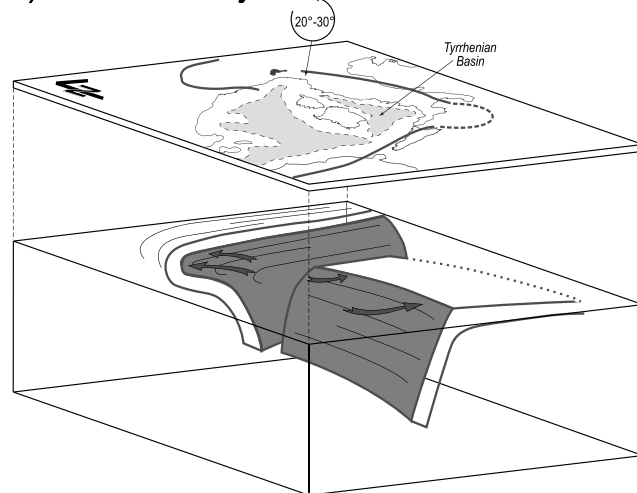
### A) Late Oligocene



### B) Early-Middle Miocene



### C) Pliocene-Today



the southern Apennines and Sicily [e.g., *Gattacceca and Speranza, 2002; Channell et al., 1990*]). Finally, thrust sheet emplacement caused a further  $20^{\circ}$ – $30^{\circ}$  CCW rotation during the Pliocene, but solely for the northern Apennines (Figure 9c). Here the remnants of the older chain (the Liguride stacks topped by the Epiligurian units) were passively carried (and further rotated) on top the northern Apennine nappes, recording the total  $\sim 50^{\circ}$  rotation documented by *Muttoni et al. [1998]*. Similarly stepwise increasing rotation values moving from the external to the internal nappes were shown in the Sicilian Maghrebides by *Channell et al. [1990]*, suggesting that the whole nappe pile accumulates the rotation associated to the activity of each thrust.

[56] Having found that the Alpine chain located below the TPB has been rotated along with Corsica-Sardinia, the question arises as to whether additional Alpine segments have undergone a similar rotational/geodynamic evolution. In Figure 1, we note that the CCW rotation values documented by *Thomas et al. [1999]*, *Aubourg and Chabert-Pelline [1999]*, and *Collombet et al. [2002]* at several western Alps localities vary between  $40^{\circ}$  and  $68^{\circ}$ , while the “Liguria” locality, located 20–30 km SW of the TPB has indeed rotated by  $117^{\circ}$  [*Collombet et al., 2002*]. The  $\sim 40^{\circ}$  rotation from the Subalpine Chain [*Aubourg and Chabert-Pelline, 1999*] is very difficult to constrain in time, because it postdates an overprint inferred as Neogene in age solely relying on the similarity of paleomagnetic inclination values with the expected European inclination value. Conversely, the  $47^{\circ}$ – $117^{\circ}$  rotations from the Briançonnais (Penninic) zone are certainly post-late Oligocene in age, as they were gathered from rocks undergoing greenschist metamorphism (thus certainly a magnetic overprint) in late Oligocene times (D3 phase according to *Collombet et al. [2002]*). Therefore the western Alpine rotations are synchronous with or younger than the rotations found for the TPB. This also implies that at the TPB we certainly do not “miss” any older Alpine rotation.

[57] Given the unconstrained rotational timing of the western Alps, several rotational scenarios can be inferred, yet among two basic end-members: (1) the  $50^{\circ}$ – $70^{\circ}$  CCW rotation of the western Alps occurred with different timing and geodynamics with respect the TPB, which escaped such rotation but rotated by  $\sim 50^{\circ}$  in early mid-Miocene along with Corsica-Sardinia (together with Liguria, which rotated by  $\sim 120^{\circ}$  as the sum of the two rotations); and (2) the whole western Alpine arc (including the TPB) rotated CCW by  $\sim 50^{\circ}$  in early mid-Miocene times together with Corsica-Sardinia, and Liguria underwent an additional  $\sim 70^{\circ}$  rotation for local (strike-slip fault shear?) tectonics. Further age constraints for the western Alpine rotation would be needed to discriminate between such two scenarios.

**Figure 9.** Schematic 3-D block diagram suggesting a possible kinematic reconstruction of the Alps-Apennines belt system since the late Oligocene. The evolution in time and space of both the Alpine and the Apennine orogenic fronts are correlated together with the deep subduction geometry. The mean paleomagnetic rotation values for each stage are also reported. (TPB) Tertiary Piedmont Basin, (CS) Corsica-Sardinia block, (NA) northern Apennines.

#### 7.4. No Paleomagnetic Rotation of Adria After Mid-Miocene Times

[58] The TPB lies on Alpine nappes stacked onto the Adriatic lithosphere along the Po Plain. Therefore our paleomagnetic data, along with previous results from *Carrapa et al.* [2003a], definitely prove that Adria has undergone no paleomagnetic rotation after mid-Miocene times. This finding concurs with paleomagnetic evidence gathered during the past 40 years at different peri-Adriatic localities [see *Van der Voo*, 1993; *Channell et al.*, 1992; *Channell*, 1996; *Muttoni et al.*, 2001], while is at odds with paleomagnetic data gathered from Istria and Dalmatia by *Márton et al.* [2003]. This also implies that the rotation of Adria cannot be considered (as suggested by *Collombet et al.* [2002]) as one of the possible causes for the CCW rotation documented along the western Alpine arc.

[59] There is now considerable evidence from both GPS and seismological data that Adria is rotating at Present with respect to both Africa and Europe [*Caporali and Martin*, 2000; *Calais et al.*, 2002; *Babbucci et al.*, 2004; *D'Agostino et al.*, 2006], but our data confirm that this rotation has not yet reached a paleomagnetically detectable value. Extrapolating in time the  $0.28^\circ/\text{Ma}$  present-day Adria versus Europe rotation rate recently proposed by *D'Agostino et al.* [2006], and assuming  $10^\circ$  as the minimum value of a paleomagnetically retrievable rotation, we find that the current Adria rotation cannot be older than  $\sim 35$  Ma ago (late Eocene). Obviously, this lower-bound age does not exclude that Adria started decoupling (and rotating) from Africa much more recently, few Ma (or even few hundreds of ka) ago.

#### 7.5. Enigmatic Nature of the TPB: Information From Anisotropy of Magnetic Susceptibility Data

[60] The magnetic fabric gathered from clayey sediments completely lacking visible strain markers has proven to serve as a valuable strain proxy [*Hrouda and Janák*, 1976]. Several studies carried out on clays from different Italian localities have found that the magnetic lineation trends parallel to the belt (and local fold) axis trend [*Averbuch et al.*, 1995; *Mattei et al.*, 1997; *Sagnotti et al.*, 1998; *Speranza et al.*, 1999], while it forms parallel to the stretching direction at extensional basins [*Sagnotti et al.*, 1994b; *Mattei et al.*, 1997, 1999; *Cifelli et al.*, 2004]. Moreover, it has been proven that the magnetic lineation of weakly deformed fine-grained terrigenous sediments trends approximately parallel or orthogonal to the local bed strike when forming after compressive or extensional tectonics, respectively, and that the magnetic fabric is particularly sensitive to synsedimentary tectonics [e.g., *Mattei et al.*, 1997; *Sagnotti et al.*, 1998]. Therefore, AMS data have the potential to provide relevant information to unravel the origin of basins characterized by a controversial tectonic setting, such as the TPB.

[61] AMS results from the TPB reveal a defined ( $e_{12} \leq 30^\circ$ , Table 2) magnetic lineation for 28 sites, while the remaining 6 sites display a purely sedimentary fabric, with the axis of maximum susceptibility scattered in the magnetic foliation plane, which is subparallel to the bedding plane (Figures 4b and 4c). The sites yielding a defined magnetic lineation are both Oligocene and Miocene in age (Table 2), suggesting that the TPB developed within a tectonic regime

acting synchronous to the deposition of the whole sedimentary succession. The in situ directions of the  $K_{\text{max}}$  axes substantially differ from the correspondent paleomagnetic declinations (their angle is  $>10^\circ$  for 24 out of 28 sites, and as high as  $37^\circ$  on average). This suggests that the preferred trend of the magnetic grains, thus the  $K_{\text{max}}$  orientation, was not primarily affected by the Earth magnetic field [see *Rochette et al.*, 1992].

[62] The great majority of the in situ magnetic lineations from 28 sites trend approximately N-S (from  $N30^\circ\text{E}$  to  $N50^\circ\text{W}$ , Figure 4c), i.e., roughly parallel to the local bed dips and orthogonal to the regional trend of the Alpine chain buried below the TPB. This suggests that the TPB formed in an extensional tectonic setting, characterized by a stretching direction perpendicular to the chain axis. Our lineation directions are in substantial agreement with those reported by *Carrapa et al.* [2003a], who studied the AMS of 22 lower Oligocene–Pliocene sites from the TPB [see *Carrapa et al.*, 2003a, Figure 14]. The structural information derived by AMS data is in agreement with *Mutti et al.* [1995], who proposed that the TPB formed in an extensional tectonic setting.

[63] Our AMS results also suggest that the sparse folds, thrusts, and other (mostly NW–SE oriented) compressive features documented so far at the TPB [*Perotti*, 1985; *Fossati et al.*, 1988; *Bernini and Zecca*, 1990; *Piana et al.*, 1997; *Gelati and Gnaccolini*, 1998; *Marroni et al.*, 2002; *D'Atri et al.*, 1997, 2002; *Carrapa et al.*, 2003a] either are sedimentary gravitational features, or are not due to synsedimentary shortening, but they are rather related to younger (post-late Miocene) compressive episodes, which did not affect the extensional magnetic fabric “frozen” during synsedimentary tectonics. Such late shortening events may be associated with the Pliocene thrust sheet emplacement documented by both seismic reflection and deep well data below the Po Plain, just north of the TPB [*Biella et al.*, 1988].

[64] Though the AMS data suggest that the TPB formed in an approximately N–S extensional regime (in present-day coordinates), the paleomagnetic data indicate that nappe stacking occurred below the basin itself during Aquitanian–Serravallian times. In fact, lacking regional strike-slip faults in the TPB, the sole viable mechanism yielding rotations within the belts is thrust sheet emplacement, as it has been already demonstrated for the northern Apennines [*Speranza et al.*, 1997; *Muttoni et al.*, 1998, 2000], the southern Apennines [*Gattacceca and Speranza*, 2002], and Sicily [*Channell et al.*, 1990; *Speranza et al.*, 1999, 2003]. This implies that stress layering along depth occurred in Aquitanian–Serravallian times and that a huge basin passively carried on top of displacing nappes may be dominantly characterized by extensional tectonics. Furthermore, the synsedimentary extension documented at the TPB, occurring above stacking nappes, is unlikely to be related to the spreading of the close Liguro-Provençal Basin, as suggested by *Mutti et al.* [1995].

[65] Since the magnetic lineation forms during (or soon after) sediment deposition, the pristine lineations (considered as a proxy for synsedimentary extensional directions) can be evaluated by back-rotating (according to local paleomagnetic rotation values, Table 1) the in situ lineation directions. After back rotation (Figure 10b), the Oligocene–Aquitanian sites define an approximately  $N20^\circ$  average trend,

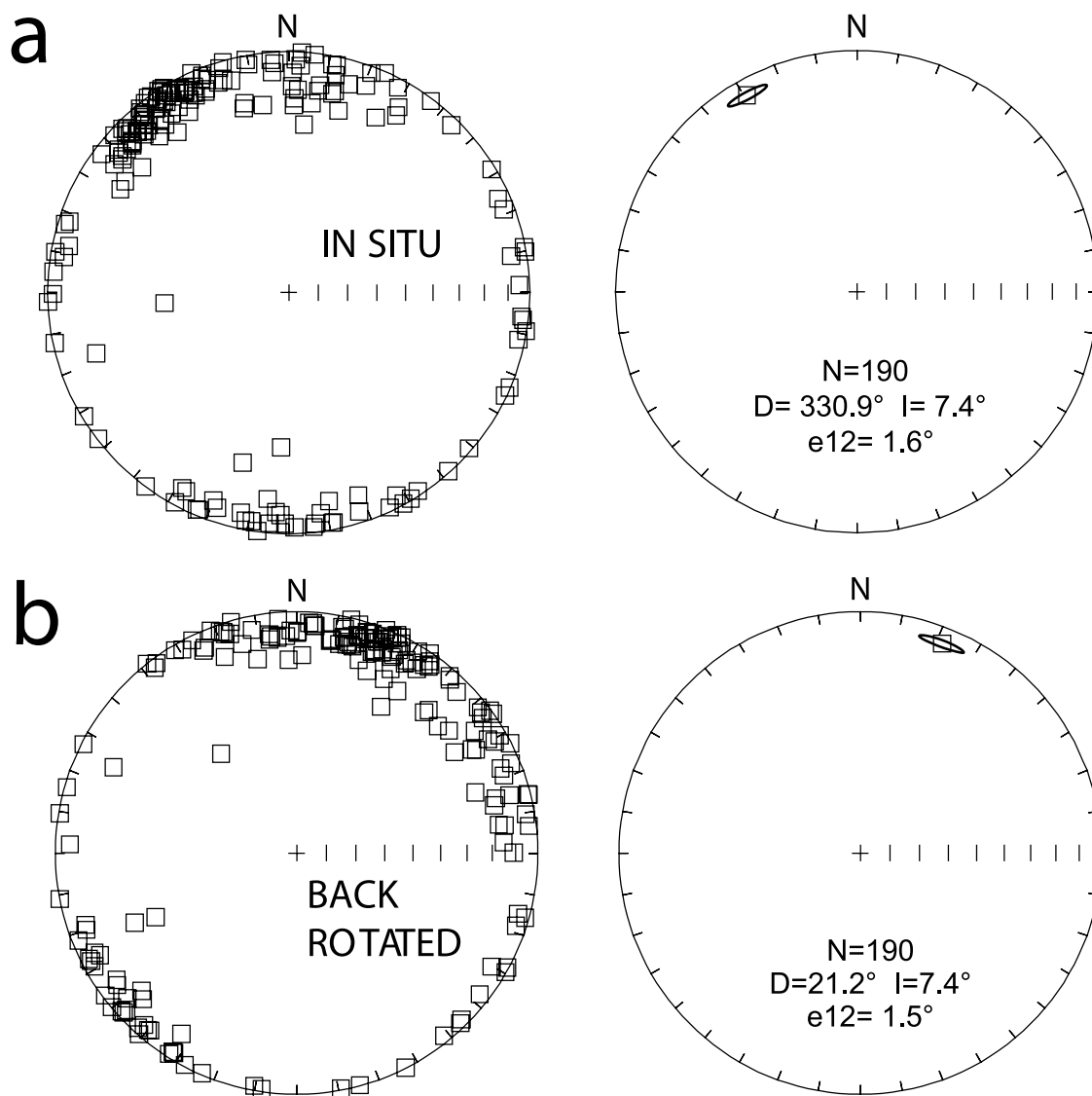


**Figure 10.** (a) Lower hemisphere equal-area projection of the in situ magnetic lineations ( $k_{\max}$ ) for 190 cores from not remagnetized Oligocene-Aquitainian sites with  $e_{12} < 30^\circ$  (see also Tables 1 and 2). (b) Same as in Figure 10a but with magnetic lineations back-rotated (Table 2) according to the respective site-mean paleomagnetic rotation values (Table 1).

which can be considered as a proxy for the Oligocene extensional direction, and approximately orthogonal to the regional direction of the Alpine chain buried below the TPB in Oligocene times, i.e., prior to the Corsica-Sardinia rotation. Tensorial statistics shows a similar scatter (as evaluated by the  $e_{12}$  values) of the lineation directions in situ, and back-rotated according to paleomagnetic data (Figure 10). This further proves that the magnetic lineation has not been acquired by late tectonic phases occurring after the basin rotation (i.e., after mid-Miocene times).

#### 7.6. Connection Between Alps and the Apennines: Insight Into the Mechanism of the Mediterranean Arc Formation

[66] The data set presented in this paper gives a first-order constraint on the timing and magnitude of formation of the western Alpine Arc. Its genesis, indeed, is strictly connected with the formation of Apennine-Calabrian Arc, as it devel-

ops during the fast rotation of the Sardinia-Corsica block related to the rollback of the Apennine slab. From a geodynamic point of view, this intimate relationship is not trivial. In fact, if the formation of the Apennine-Calabrian Arc is commonly related to the preexisting paleogeographic scenario (land-locked oceanic domain) controlling the width of the retreating panel [Malinverno and Ryan, 1986; Faccenna *et al.*, 2007], the formation of the Western Alpine Arc is commonly related to an opposite process related to the indentation of Adria microplate [Schmid and Kissling, 2000]. The other option is related to the possibility that also the western Alpine slab retreat backward (westward) during orogenic accretion, in a manner similar, although slower, to what observed for the Apennine slab. This mechanism could be also favorable for the exhumation of deep seated HP and UHP units [Rosenbaum *et al.*, 2002; Jolivet *et al.*, 2003; Rosenbaum and Lister, 2005; Brun and Faccenna, 2007]. If this is the case, then we are

left to imagine that both the Western Alpine and the Apennine slab start to migrate backward in opposite direction just after the onset of continental collision [Jolivet and Faccenna, 2000]. The mechanism of a concomitant process of two adjacent, but separated, slab is quite complex. One possible explanation could be related to displacement of mantle material during subduction. For the case of the Apennine-Calabrian slab, it has been so far proposed that its backward retreat could be driven by the consumption of the Liguro-Piedmont and Ionian oceanic crust. In this case it is possible that the backward retreat of the western alpine arc has been driven by the push of the mantle material displaced by the retreating Apenninic slab. Recent 3-D experiments of the behavior of retreating slabs show that near the lateral edge of the slab the asthenospheric material located below the slab escapes laterally inducing a toroidal component in the mantle flow [Funiello et al., 2006; Piromallo et al., 2006]. Asthenospheric material expelled from below the Apennine slab would then push the Alpine slab westward and force the subduction of continental material. The arcuate shape of the Alpine arc and the helicoidal shape of the Alps-Apennines belt would then essentially result from the geometry of the asthenospheric flow below Liguria and the Ligurian Sea. 3-D mantle convection experiments and seismic data (SKS splitting) are required to test this possible scenario.

## 8. Conclusions

[67] Our paleomagnetic data integrated with previous results from Kie [1988] and Carrapa et al. [2003a] show that the TPB, unconformably resting upon Alpine nappes (stacked in turn over Adriatic lithosphere), rotated  $\sim 50^\circ$  CCW with respect to major nearby plates during Aquitanian-Serravallian times. A very similar rotation magnitude and timing have been previously constrained (by a huge amount of paleomagnetic data) for the Corsica-Sardinia block, which drifted away from Europe during the spreading of the Liguro-Provençal Basin. This suggests that the Alpine wedge underlying the TPB rotated along with Corsica-Sardinia, inducing the tightening of the western Alpine arc. Previous results from the western Alps documented a  $47^\circ$ – $68^\circ$  ( $117^\circ$  at the Liguria locality) CCW rotation in the internal Penninic zone, occurring after a magnetic overprint surely postdating a late Oligocene greenschist metamorphism [Thomas et al., 1999; Collombet et al., 2002]. Therefore we are tempted to conclude that a regional  $\sim 50^\circ$  CCW rotation of the western Alps occurred synchronously with early mid-Miocene Corsica-Sardinia rotation, and that the additional  $\sim 70^\circ$  CCW rotation in Liguria has a local character. Unfortunately, the timing for the Penninic zone rotation is lacking, thus it cannot be excluded that the rotations at the western Alps arc and at the TPB were diachronous, and related in fact to different geodynamic processes.

[68] South of the TPB, the Liguride units (and their unconformably overlying Epiliguride cover) located on top of the northern Apennine units rotated CCW by only  $\sim 25^\circ$  during early mid-Miocene [Muttoni et al., 1998, 2000], the excess Corsica-Sardinian rotation likely being accommodated by internal tectonic imbrication of the chain. The Liguride units were subsequently rotated CCW by

additional  $20^\circ$ – $30^\circ$  in Pliocene times, while passively carried on top of the Apennine thrust sheets [Speranza et al., 1997; Muttoni et al., 2000].

[69] The synchronicity between the rotation/drift of the Corsica-Sardinia block (induced by eastward retreat of the Apenninic slab) and (further) bending of the western Alpine arc, strongly suggests a dynamic link. We speculate that the asthenosphere laterally escaping from the retreating Apenninic slab pushed the western Alpine slab, yielding its further retreat and bending.

[70] Finally, we find no paleomagnetic support for Adria rotation since at least late Miocene times, concurring with other paleomagnetic evidence formerly gathered at several peri-Adriatic localities [see, e.g., Van der Voo, 1993; Channell et al., 1992; Channell, 1996; Muttoni et al., 2001], which suggested an Adria-Africa coupling during Mesozoic-Tertiary drift. This implies that the formation of the western Alps arc has definitely not arisen from a Miocene (or younger) CCW Adria rotation, as suggested by Collombet et al. [2002]. We conclude that the present-day CCW rotation of Adria with respect to nearby plates, robustly documented by numerous GPS and seismological data, is a relatively recent (mid-late Tertiary, or younger) geodynamic feature of the Mediterranean domain, and has not yet become paleomagnetically detectable. N. D'Agostino and E. Boschi are thanked for providing information on Adria Plate motion and encouragement, respectively.

[71] **Acknowledgments.** We are grateful to R. Polino and R. Lanza for both the fruitful discussions on the TPB and the help given for the sampling campaign, as well as to B. Henry and an anonymous reviewer for their thoughtful remarks on our manuscript. Thanks also to the JGR Associate Editor S. Gilder and the Editor J.C. Mutter for carefully evaluating our work. Sampling facilities were kindly provided by M. Mattei.

## References

- Alvarez, W., F. G. Franks, and A. E. M. Nairn (1973), Paleomagnetism of Plio-Pleistocene basalts from NW Sardinia, *Nature*, **243**, 10–11.
- Alvarez, W., T. Coccozza, and F. C. Wezel (1974), Fragmentation of the Alpine orogenic belt by microplate dispersal, *Nature*, **248**, 309–314.
- Aubourg, C., and C. Chabert-Pelline (1999), Neogene remagnetization of normal polarity in the Late Jurassic black shales from the southern Subalpine Chains (French Alps). Evidence for late anticlockwise rotations, *Tectonophysics*, **308**, 473–486.
- Averbuch, O., M. Mattei, C. Kissel, D. Frizon de Lamotte, and F. Speranza (1995), Cinématique des déformations au sein d'un système chevauchant aveugle: L'exemple de la "Montagna dei Fiori" (front des Apennins centraux, Italie), *Bull. Soc. Geol. Fr.*, **5**, 451–461.
- Babbucci, D., C. Tamburelli, M. Viti, E. Mantovani, D. Albarello, F. D'Onza, N. Cenni, and E. Mugnaioli (2004), Relative motion of the Adriatic with respect to the confining plates: Seismological and geodetic constraints, *Geophys. J. Int.*, **159**, 765–775.
- Backman, J., and N. J. Shackleton (1983), Quantitative biochronology of Pliocene and early Pleistocene calcareous nanofossils from the Atlantic, Indian and Pacific oceans, *Mar. Micropaleontol.*, **8**, 141–170.
- Beccaluva, L., P. Brotzu, G. Macciotta, L. Morbidelli, G. Serri, and G. Traversa (1989), Cenozoic Tectono-magmatic evolution and inferred mantle sources in the Sardo-Tyrrhenian area, in *The Lithosphere in Italy: Advances in Earth Science Research*, edited by A. Boriani et al., pp. 229–248, Accad. Naz. dei Lincei, Rome.
- Bernini, M., and M. Zecca (1990), The deformations in the Oligocene–lower Miocene Molare and Rocchetta Formations, *Atti Tic. Sci. Terra*, **33**, 1–10.
- Besse, J., and V. Courtillot (2002), Apparent and true polar wander and the geometry of the geomagnetic field over the last 200 Myr, *J. Geophys. Res.*, **107**(B11), 2300, doi:10.1029/2000JB000050.
- Biella, G. C., R. Gelati, A. Lozej, P. M. Rossi, and I. Tabacco (1988), Sezioni geologiche nella zona limite Alpi occidentali-Appennino settentrionale ottenute da dati geofisici, *Rend. Soc. Geol. Ital.*, **11**, 287–292.

- Biella, G., R. Polino, R. de Franco, P. M. Rossi, P. Clari, A. Corsi, and R. Gelati (1997), The crustal structure of the western Po Plain: Reconstruction from integrated geological and seismic data, *Terra Nova*, 9, 28–31.
- Bogdanoff, S., and J. J. Schott (1977), Etude paleomagnetique et analyse tectonique dans les schistes rouges permien du sud de l'Argentera, *Bull. Soc. Geol. Fr.*, 7, 909–916.
- Bormioli, D., and R. Lanza (1995), Rotazioni antiorarie delle rocce terziarie delle Alpi Occidentali e dell'Appennino Settentrionale, in *Atti Convegno Rapporti Alpi-Appennino, Peveragno*, edited by R. Polino and R. Sacchi, pp. 277–289, Accad. Naz. delle Sci., Rome.
- Brun, J. P., and C. Faccenna (2007), Slab Roll back, back-arc extension and exhumation of HP rocks in the eastern-central Mediterranean, *Geophys. Res. Abstr.*, 9, 03025.
- Cairanne, G., C. Aubourg, and J. P. Pozzi (2002), Syn-folding remagnetization and the significance of the small circle test. Examples from the Vocontian trough (SE France), *Phys. Chem. Earth.*, 27, 1151–1159.
- Calais, E., J. M. Nocquet, F. Jouanne, and M. Tardy (2002), Current extension in the central part of the Western Alps from continuous GPS measurements, 1996–2001, *Geology*, 30(7), 651–654.
- Caporali, A., and S. Martin (2000), First results from GPS measurements on the present day alpine kinematics, *J. Geodyn.*, 30, 275–283.
- Caprara, L., E. Garzanti, M. Gnaccolini, and L. Mutti (1985), Shelf-basin transition: Sedimentology and petrology of the serravallian of the Tertiary Piedmont Basin (northern Italy), *Riv. Ital. Paleontol. Stratigr.*, 90, 545–564.
- Carrapa, B., and D. Garcia-Castellanos (2005), Western Alpine back-thrusting as subsidence mechanism in the Tertiary Piedmont Basin (western Po Plain, NW Italy), *Tectonophysics*, 406, 197–212.
- Carrapa, B., G. Bertotti, and W. Krijgsman (2003a), Subsidence, stress regime and rotation(s) of a sedimentary basin within the Western Alps: The Tertiary Piedmont Basin (Alpine domain, northwest Italy), in *Tracing Tectonic Deformation Using the Sedimentary Record*, edited by T. McCann and A. Santot, *Geol. Soc. Spec. Publ.*, 208, 205–227.
- Carrapa, B., J. Wijbrans, and G. Bertotti (2003b), Episodic exhumation in the Western Alps, *Geology*, 31(7), 601–604.
- Carrapa, B., J. Wijbrans, and G. Bertotti (2004), Detecting provenance variations and cooling patterns within the Western Alpine orogen through  $^{40}\text{Ar}/^{39}\text{Ar}$  geochronology on detrital sediments: The Tertiary Piedmont Basin, NW Italy, in *Detrital Thermochronology—Provenance Analysis, Exhumation and Landscape Evolution of Mountain Belts*, edited by M. Bernet and C. Spiegel, *Spec. Pap. Geol. Soc. Am.*, 378, 67–103.
- Cassano, E., L. Anelli, R. Fichera, and V. Cappelli (1986), Pianura Padana, interpretazione integrata di dati geofisici e geologici, paper presented at 73° Congresso della Società Geologica Italiana, Rome.
- Channell, J. E. T. (1996), Paleomagnetism and paleogeography of Adria, in *Paleomagnetism and Tectonics of the Mediterranean Region*, edited by A. Morris and D. H. Tarling, *Geol. Soc. Spec. Publ.*, 105, 119–132.
- Channell, J. E. T., J. S. Oldow, R. Catalano, and B. D'Argenio (1990), Paleomagnetically determined rotations in the western Sicilian folds and thrust belt, *Tectonics*, 9, 641–660.
- Channell, J. E. T., R. Brandner, A. Spieler, and J. S. Stoner (1992), Paleomagnetism and paleogeography of the Northern Calcareous Alps (Austria), *Tectonics*, 11, 792–810.
- Cherchi, A., and L. Mortadert (1982), Oligo-Miocene rift of Sardinia and the early history of the western Mediterranean Basin, *Nature*, 298, 736–739.
- Cifelli, F., M. Mattei, A. M. Hirt, and A. Günther (2004), The origin of tectonic fabrics in “undeformed” clays: The early stages of deformation in extensional sedimentary basins, *Geophys. Res. Lett.*, 31, L09604, doi:10.1029/2004GL019609.
- Cogné, J. P., and H. Perroud (1985), Strain removal applied to paleomagnetic directions in an orogenic belt: The Permian red slates of the Alps Maritimes, France, *Earth Planet. Sci. Lett.*, 72, 125–140.
- Collombet, M., J. C. Thomas, A. Chauvin, P. Tricart, J. P. Bouillin, and J. P. Gratier (2002), Counterclockwise rotation of the western Alps since the Oligocene: New insights from paleomagnetic data, *Tectonics*, 21(4), 1032, doi:10.1029/2001TC901016.
- Consiglio Nazionale delle Ricerche (1991), Progetto finalizzato geodinamica, Structural model of Italy map, scale 1:500,000, edited by G. Bigi et al., Rome.
- Cortesogno, L., and D. Haccard (1984), Note illustrative alla carta geologica della Zona Sestri-Voltaggio, *Mem. Soc. Geol. Ital.*, 28, 115–150.
- D'Agostino, N., G. Selvaggi, A. Avallone, D. Cheloni, E. D'Anastasio, and S. Mantenuto (2006), Present-day kinematics of Adria and its southern boundary, *Eos Trans. AGU*, 87(52), Fall Meet. Suppl., Abstract G42A-01.
- D'Atri, A. (1995), Biostatigrafia della Formazione di Visone (Miocene inferiore, Bacino terziario Ligure-Piemontese), *Boll. Mus. Reg. Sci. Nat. Torino*, 13(2), 345–375.
- D'Atri, A., F. Piana, S. Tallone, G. Bodrato, and M. Roz Gastaldi (1997), Tettonica oligo-miocenica nell'alto Monferrato (Bacino Terziario Piemontese) e nel settore nord-occidentale del gruppo di Voltri (Acqui Terme–Cassinelle, AI), *Atti Tic. Sci. Terra*, 5, 85–100.
- D'Atri, A., F. Dela Pierre, A. Festa, R. Gelati, M. Gnaccolini, F. Piana, P. Clari, and R. Polino (2002), Tettonica e sedimentazione nel “retroforeland alpino”, paper presented at 81° Riunione Estiva, Soc. Geol. Ital., Torino, Italy.
- Day, R., M. Fuller, and V. A. Schmidt (1977), Hysteresis properties of titanomagnetites: Grain size and composition dependence, *Phys. Earth Planet. Inter.*, 13, 260–267.
- Deamer, G. A., and K. P. Kodama (1990), Compaction induced inclination shallowing in synthetic and natural clay-rich sediments, *J. Geophys. Res.*, 95, 4511–4529.
- Dela Pierre, F., V. Mikhailov, and R. Polino (1995), The tectonosedimentary evolution of the tertiary basins in the western Po Plain: Kinematics inferred from subsidence curves, in *Atti del convegno rapporti Alpi-Appennino*, R. Polino, and R. Sacchi, pp. 129–146, Accad. Naz. delle Sci., Peveragno, Italy.
- Demarest, H. H. (1983), Error analysis of the determination of tectonic rotation from paleomagnetic data, *J. Geophys. Res.*, 88, 4321–4328.
- Dercourt, J., et al. (1986), Geological evolution of the Tethys belt from the Atlantic to the Pamirs since the Lias, *Tectonophysics*, 123, 241–315.
- Dunlop, D. J. (2002), Theory and application of the Day plot ( $M_r/M_s$  versus  $H_w/H_c$ ): 1. Theoretical curves and tests using titanomagnetite data, *J. Geophys. Res.*, 107(B3), 2056, doi:10.1029/2001JB000486.
- Dunlop, D. J., and Ö. Özdemir (1997), *Rock Magnetism: Fundamentals and Frontiers*, 573 pp., Cambridge Univ. Press, New York.
- Eldredge, S., V. Bachtadse, and V. Van der Voo (1985), Paleomagnetism and the orocline hypothesis, *Tectonophysics*, 119, 153–179.
- Enkin, R. J., and G. S. Watson (1996), Statistical analysis of paleomagnetic inclination data, *Geophys. J. Int.*, 126, 495–504.
- Faccenna, C., M. Mattei, R. Funicello, and L. Jolivet (1997), Styles of back-arc extension in the central Mediterranean, *Terra Nova*, 9, 126–130.
- Faccenna, C., T. W. Becker, F. P. Lucente, L. Jolivet, and F. Rossetti (2001), History of subduction and back-arc extension in the central Mediterranean, *Geophys. J. Int.*, 145, 809–820.
- Faccenna, C., O. Bellier, J. Martino, C. Piromallo, and V. Regard (2006), Slab detachment beneath eastern Anatolia: A possible cause for the formation of the North Anatolian fault, *Earth Planet. Sci. Lett.*, 242, 85–97.
- Faccenna, C., F. Funicello, L. Civetta, M. D'Antonio, M. Moroni, and C. Piromallo (2007), Slab disruption, mantle circulation, and the opening of the Tyrrhenian basins, in *Cenozoic Volcanism in the Mediterranean Area*, edited by L. Beccaluva, G. Bianchini, and M. Wilson, *Spec. Pap. Geol. Soc. Am.*, 41, 153–169, doi:10.1130/2007.2418(08).
- Federico, L., G. Capponi, L. Crispini, M. Scambelluri, and I. M. Villa (2005),  $^{40}\text{Ar}/^{39}\text{Ar}$  dating of high-pressure rocks from the Ligurian Alps: Evidence for a continuous subduction-exhumation cycle, *Earth Planet. Sci. Lett.*, 240, 668–680.
- Ferrandini, J., J. Gattacceca, M. Ferrandini, A. Deino, and M. C. Janin (2003), Chronostratigraphie et paléomagnétisme des dépôts oligo-miocènes de Corse: Implications géodynamiques pour l'ouverture du bassin liguro-provençal, *Bull. Soc. Geol. Fr.*, 174(4), 357–371.
- Fisher, R. A. (1953), Dispersion on a sphere, *Proc. R. Soc. London*, 217, 295–305.
- Fornaciari, E., and D. Rio (1996), Latest Oligocene to early Miocene quantitative calcareous nannofossil biostratigraphy in the Mediterranean region, *Micropaleontology*, 42, 1–36.
- Fornaciari, E., A. Distefano, D. Rio, and A. Negri (1996), Middle Miocene quantitative calcareous nannofossil biostratigraphy in the Mediterranean region, *Micropaleontology*, 42, 37–63.
- Fossati, A., C. R. Perotti, and P. L. Vercesi (1988), Deformazioni tettoniche al margine sud-orientale del Bacino Terziario Ligure-Piemontese, *Rend. Soc. Geol. Ital.*, 11, 305–308.
- Funicello, F., M. Moroni, C. Piromallo, C. Faccenna, A. Cenedese, and H. A. Bui (2006), Mapping mantle flow during retreating subduction: Laboratory models analyzed by feature tracking, *J. Geophys. Res.*, 111, B03402, doi:10.1029/2005JB003792.
- Gattacceca, J., and F. Speranza (2002), Paleomagnetism of Jurassic to Miocene sediments from the Apenninic carbonate platform (southern Apennines, Italy): Evidence for a 60° counterclockwise Miocene rotation, *Earth Planet. Sci. Lett.*, 201, 19–34.
- Gattacceca, J., A. Deino, R. Rizzo, D. S. Jones, B. Henry, B. Beaudoin, and F. Vadeboin (2007), Miocene rotation of Sardinia: New paleomagnetic and geochronological constraints and geodynamic implications, *Earth Planet. Sci. Lett.*, 258(3–4), 359–377.
- Gelati, R., and M. Gnaccolini (1982), Evoluzione tettonico-sedimentaria della zona limite tra Alpi ed Appennino tra l'inizio dell'Oligocene ed il Miocene medio, *Mem. Soc. Geol. Ital.*, 24, 183–191.
- Gelati, R., and M. Gnaccolini (1996), The stratigraphic record of the Oligocene–early Miocene events at the southwestern end of the Piedmont Tertiary Basin, *Riv. Ital. Paleontol. Stratigr.*, 102, 65–76.

- Gelati, R., and M. Gnaccolini (1998), Sedimentary tectonics and sedimentation in the Tertiary Piedmont Basin, north-western Italy, *Riv. Ital. Paleontol. Stratigr.*, *104*, 193–214.
- Gelati, R., M. Gnaccolini, P. Falletti, and D. Catrullo (1993), Stratigrafia sequenziale della successione Oligo-Miocenica delle Langhe, Bacino Terziario Ligure-Piemontese, *Riv. Ital. Paleontol. Stratigr.*, *98*, 425–452.
- Ghibaudo, G., P. Clari, and M. Perello (1985), Litostratigrafia, sedimentologia ed evoluzione tettonico-sedimentaria dei depositi miocenici del margine sud-orientale del Bacino Terziario Ligure-Piemontese (Valli Borbera, Scrivia e Lemme), *Boll. Soc. Geol. Ital.*, *104*, 349–397.
- Gnaccolini, M., R. Gelati, and P. Falletti (1998), Sequence stratigraphy of the “Langhe” Oligo-Miocene succession, Tertiary Piedmont Basin, northern Italy, in *Mesozoic and Cenozoic Sequence Stratigraphy of European Basins*, edited by P. C. De Graciansky et al., *SEPM Spec. Publ.*, *60*, 233–244.
- Gorini, C., A. Le Marrec, and A. Mauffret (1993), Contribution to the structural and sedimentary history of the Gulf of Lions (western Mediterranean), from the ECORS profiles, industrial seismic profiles and well data, *Bull. Soc. Geol. Fr.*, *164*(3), 353–363.
- Gradstein, F. M., J. G. Ogg, and A. G. Smith (2004), *A Geologic Time Scale 2004*, 589 pp., Cambridge Univ. Press, New York.
- Henry, B. (1973), Studies of microtectonics, anisotropy of magnetic susceptibility and paleomagnetism of the Permian Dome de Barrot (France): Paleotectonic and paleosedimentological implications, *Tectonophysics*, *17*, 61–72.
- Henry, B. (1976), Sur les propriétés magnétiques de laves spilitiques peu déformées de la bordure ouest du Pelvoux, *C.R. Soc. Phys. Hist. Nat. Geneve*, *11*, 105–110.
- Henry, B. (1980), Contribution à l'étude structurale des propriétés magnétiques de roches magmatiques des Alpes. Conséquences structurales, régionales et générales, thesis, Univ. Pierre et Marie Curie, Paris VI, Paris.
- Henry, B. (1992), Structural implications of paleomagnetic data from Pelvoux-Belledonne area (French Alps), *Tectonophysics*, *216*, 327–338.
- Hirt, A. M., and W. Lowrie (1988), Paleomagnetism of the Umbrian-Marches orogenic belt, *Tectonophysics*, *146*, 91–103.
- Hrouda, F. (1994), A technique for the measurement of thermal changes of magnetic susceptibility of weakly magnetic rocks by the CS-2 apparatus and KLY-2 Kappabridge, *Geophys. J. Int.*, *118*, 604–612.
- Hrouda, F., and F. Janák (1976), The changes in shape of the magnetic susceptibility ellipsoid during progressive metamorphism and deformation, *Tectonophysics*, *34*, 135–148.
- Istituto Nazionale di Geofisica e Vulcanologia, (2001), Italian magnetic network and geomagnetic field maps of Italy at year 2000, *Boll. Geod. Sci. Affini*, *60*.
- Jelinek, V. (1977), The statistical theory of measuring anisotropy of magnetic susceptibility of rocks and its application, report, 88 pp., Geofyzika, Brno, Czech Republic.
- Jelinek, V. (1978), Statistical processing of magnetic susceptibility on groups of specimens, *Stud. Geophys. Geod.*, *22*, 50–62.
- Jelinek, V. (1981), Characterization of the magnetic fabrics of rocks, *Tectonophysics*, *79*, 63–67.
- Jolivet, L., and C. Faccenna (2000), Mediterranean extension and the Africa-Eurasia collision, *Tectonics*, *19*, 1095–1106.
- Jolivet, L., C. Faccenna, B. Goffé, E. Burov, and P. Agard (2003), Subduction tectonics and exhumation of High-Pressure metamorphic rocks in the Mediterranean orogens, *Am. J. Sci.*, *303*, 353–409.
- Karlin, R. (1990a), Magnetic mineral diagenesis in suboxic sediments at Bettis site W-N, NE Pacific Ocean, *J. Geophys. Res.*, *95*, 4421–4436.
- Karlin, R. (1990b), Magnetite diagenesis in marine sediments from the Oregon continental margin, *J. Geophys. Res.*, *95*, 4405–4419.
- Karlin, R., and S. Levi (1983), Diagenesis of magnetic minerals in recent haemipelagic sediments, *Nature*, *303*, 327–330.
- Kastens, K., J. Masclé, and C. Aroux (1986), A microcosm of ocean basin evolution in the Mediterranean, *Nature*, *321*, 383–384.
- Katz, B., R. D. Elmore, M. Cogoini, M. H. Engel, and S. Ferry (2000), Association between burial diagenesis of smectite, chemical remagnetization and magnetite authigenesis in the Vocontian trough, SE France, *J. Geophys. Res.*, *105*, 851–869.
- Kechra, F., D. Vandamme, and P. Rochette (2003), Tertiary remagnetization of normal polarity in Mesozoic marly limestones from SE France, *Tectonophysics*, *362*, 219–238.
- Kie, H. T. (1988), Magnetotectonics in the Piemont Tertiary Basin, *Phys. Earth Planet. Inter.*, *52*, 308–319.
- Kirschvink, J. L. (1980), The least-squares line and plane and the analysis of palaeomagnetic data, *Geophys. J. R. Astron. Soc.*, *62*, 699–718.
- Kruiver, P. P., M. J. Dekkers, and C. G. Langereis (2000), Secular variation in Permian red beds from Dôme de Barrot, SE France, *Earth Planet. Sci. Lett.*, *179*, 205–217.
- Laubscher, H. P. (1988), The arc of the western Alps and the northern Apennines: An updated view, *Tectonophysics*, *146*, 67–78.
- Loneragan, L., and N. White (1997), Origin of the Betic-Rif mountain belt, *Tectonics*, *16*, 504–522.
- Lorenz, C. (1984), Evolution stratigraphique et structurale des Alpes Ligures depuis l'Éocène supérieur, *Mem. Soc. Geol. Ital.*, *28*, 211–228.
- Lucente, F. P., and F. Speranza (2001), Belt bending driven by lateral bending of subducting lithospheric slab: Geophysical evidences from the northern Apennines (Italy), *Tectonophysics*, *337*, 53–64.
- Lucente, F. P., C. Chiarabba, and G. B. Cimini (1999), Tomographic constraints on the geodynamic evolution of the Italian region, *J. Geophys. Res.*, *104*, 20,307–20,327.
- Malinverno, A., and W. B. F. Ryan (1986), Extension in the Tyrrhenian Sea and shortening in the Apennines as result of arc migration driven by sinking of the lithosphere, *Tectonics*, *5*, 227–245.
- Marroni, M., A. Cerrina Feroni, D. Di Biase, G. Ottria, L. Pandolfi, and A. Taini (2002), Polyphase folding at upper structural levels in the Borbera Valley (northern Apennines, Italy): Implications for the tectonic evolution of the linkage area between Alps and Apennines, *C. R. Geosci.*, *334*, 565–572.
- Martini, E. (1971), Standard Tertiary and Quaternary calcareous nannoplankton zonation, in *Proceedings of the 2nd International Conference on Planktonic Microfossils*, vol. 2, edited by A. Farinacci, pp. 739–785, Tecnosienze, Rome.
- Márton, E., K. Drobne, V. Cosovic, and A. Moro (2003), Palaeomagnetic evidence for Tertiary counterclockwise rotation of Adria, *Tectonophysics*, *337*, 143–156.
- Mattei, M., C. Kissel, and R. Funicello (1996), No tectonic rotation of the Tuscan Tyrrhenian margin (Italy) since late Messinian, *J. Geophys. Res.*, *101*, 2835–2845.
- Mattei, M., L. Sagnotti, C. Faccenna, and R. Funicello (1997), Magnetic fabric of weakly deformed clay-rich sediments in the Italian peninsula: Relationship with compressional and extensional tectonics, *Tectonophysics*, *271*, 107–122.
- Mattei, M., F. Speranza, A. Argentieri, F. Rossetti, L. Sagnotti, and R. Funicello (1999), Extensional tectonics in the Amantea basin (Calabria, Italy): A comparison between structural and magnetic anisotropy data, *Tectonophysics*, *307*, 33–49.
- McFadden, P. L. (1990), A new fold test for paleomagnetic studies, *Geophys. J. Int.*, *103*, 163–169.
- McFadden, P. L., and M. W. McElhinny (1990), Classification of the reversal test in paleomagnetism, *Geophys. J. Int.*, *130*, 725–729.
- Ménard, G. (1988), Structure et Cinématique d'une chaîne de collision, les Alpes Occidentales et Centrales, thèse de doctorat, Univ. Joseph Fourier, Grenoble I, Grenoble, France.
- Merabet, N., and L. Daly (1986), Détermination d'un pôle paléomagnétique et mise en évidence d'aimantations à polarité normale sur les formations du Permien supérieur du Massif des Maures (France), *Earth Planet. Sci. Lett.*, *80*, 156–166.
- Montigny, R., J. B. Edel, and R. Thuizat (1981), Oligo-Miocene rotation of Sardinia: K-Ar ages and paleomagnetic data of tertiary volcanics, *Earth Planet. Sci. Lett.*, *54*, 261–271.
- Mutti, E., L. Papani, D. Di Biase, G. Davoli, S. Mora, S. Segadelli, and R. Tinterri (1995), Il Bacino Terziario Epimesoalpino e le sue implicazioni sui rapporti tra Alpi ed Appennino, *Mem. Sci. Geol. Padova*, *47*, 217–244.
- Muttoni, G., A. Argnani, D. V. Kent, N. Abrahamsen, and U. Cibin (1998), Paleomagnetic evidence for Neogene tectonic rotations in the northern Apennines, Italy, *Earth Planet. Sci. Lett.*, *154*, 25–40.
- Muttoni, G., L. Lanci, A. Argnani, A. M. Hirt, U. Cibin, N. Abrahamsen, and W. Lowrie (2000), Paleomagnetic evidence for a Neogene two-phase counterclockwise tectonic rotation in the northern Apennines (Italy), *Tectonophysics*, *326*, 241–253.
- Muttoni, G., E. Garzanti, L. Alfonsi, S. Cirilli, D. Germani, and W. Lowrie (2001), Motion of Africa and Adria since the Permian: Paleomagnetic and paleoclimatic constraints from northern Libya, *Earth Planet. Sci. Lett.*, *192*, 159–174.
- Nicolosi, I., F. Speranza, and M. Chiappini (2006), Ultrafast oceanic spreading of the Marsili Basin, southern Tyrrhenian Sea: Evidence from magnetic anomaly analysis, *Geology*, *34*, 717–720.
- Patacca, E., R. Sartori, and P. Scandone (1990), Tyrrhenian basin and Apenninic arcs: Kinematic relations since late Tortonian times, *Mem. Soc. Geol. Ital.*, *45*, 425–451.
- Perotti, C. R. (1985), Analisi mesostrutturale della formazione delle marne di Rigoroso fra il T. Lemme ed il T. Scrivia (margine sud-orientale del Bacino Terziario Ligure-Piemontese), *Rend. Soc. Geol. Ital.*, *8*, 53–56.
- Piana, F., and R. Polino (1995), Tertiary structural relationships between Alps and Apennines: The critical Torino Hill and Monferrato area, north-western Italy, *Terra Res.*, *7*, 138–143.

- Piana, F., A. D'Atri, and P. Orione (1997), The Visone Formation, a marker of the early Miocene tectonics in the Alto Monferrato Domain (Tertiary Piemonte Basin, NW Italy), *Mem. Soc. Geol. Ital.*, **49**, 145–162.
- Piana, F., S. Tallone, S. Cavagna, and A. Conti (2006), Thrusting and faulting in metamorphic and sedimentary units of Ligurian Alps: An example of integrated field work and geochemical analyses, *Int. J. Earth Sci.*, **95**, 413–430.
- Piomallo, C., and A. Morelli (2003), P wave tomography of the mantle under the Alpine-Mediterranean area, *J. Geophys. Res.*, **108**(B2), 2065, doi:10.1029/2002JB001757.
- Piomallo, C., T. W. Becker, F. Funicello, and C. Faccenna (2006), Three-dimensional instantaneous mantle flow induced by subduction, *Geophys. Res. Lett.*, **33**, L08304, doi:10.1029/2005GL025390.
- Platt, J. P., J. H. Behrmann, P. C. Cunningham, J. F. Dewey, M. Helman, M. Parish, M. G. Shepley, S. Wallis, and P. J. Weston (1989), Kinematics of the Alpine arc and the motion history of the Adria, *Nature*, **337**, 158–161.
- Polino, R., V. Dal Piaz, and G. Gosso (1990), Tectonic erosion at the Adria margin and accretionary processes for the Cretaceous orogeny of the Alps, in *Deep Structure of the Alps*, edited by F. Roure, P. Heitzmann, and R. Polino, *Mem. Soc. Geol. Fr.*, **156**, 345–367.
- Polino, R., P. Clari, L. Crispini, A. D'Atri, F. Dela Pierre, A. Novaretti, F. Piana, R. Ruffini, and M. Timpanelli (1995), Relazioni tra zone di taglio crostali e bacini sedimentari: L'esempio della giunzione alpino-appenninica durante il terziario. Guida all'escursione in Monferrato e nella Zona Sestri-Voltaggio, in *Rapporti Alpi-Appennino*, edited by R. Polino and R. Sacchi, 593 pp., Accad. Naz. delle Sci., Peveragno, Italy.
- Rio, D., I. Raffi, and G. Villa (1990), Pliocene-Pleistocene calcareous nanofossil distribution patterns in the western Mediterranean, *Proc. Ocean Drill. Program Sci. Results*, **107**, 513–533.
- Rochette, P. (1987), Magnetic susceptibility of the rock matrix related to magnetic fabric studies, *J. Struct. Geol.*, **9**, 1015–1020.
- Rochette, P., M. Jackson, and C. Aubourg (1992), Rock magnetism and the interpretation of anisotropy of magnetic susceptibility, *Rev. Geophys.*, **30**, 209–226.
- Rosenbaum, G., and G. S. Lister (2005), The Western Alps from the Jurassic to Oligocene: Spatio-temporal constraints and evolutionary reconstructions, *Earth Sci. Rev.*, **69**(3–4), 281–306.
- Rosenbaum, G., G. S. Lister, and C. Duboz (2002), Reconstruction of the tectonic evolution of the western Mediterranean since the Oligocene, *J. Virtual Explor.*, **8**, 107–126.
- Roure, F., R. Polino, and R. Nicolich (1990), Early Neogene deformation beneath the Po Plain: Constraints on the post-collisional Alpine evolution, in *Deep Structure of the Alps*, edited by F. Roure, P. Heitzmann, and R. Polino, *Mem. Soc. Geol. Fr.*, **156**, 309–322.
- Sagnotti, L., M. Mattei, C. Faccenna, and R. Funicello (1994a), Paleomagnetic evidence for no tectonic rotation of the central Italy Tyrrhenian margin since upper Pliocene, *Geophys. Res. Lett.*, **21**, 481–484.
- Sagnotti, L., C. Faccenna, R. Funicello, and M. Mattei (1994b), Magnetic fabric and structural setting of Plio-Pleistocene clayey units in an extensional regime: The Tyrrhenian margin of Central Italy, *J. Struct. Geol.*, **16**, 1243–1257.
- Sagnotti, L., F. Speranza, A. Winkler, M. Mattei, and R. Funicello (1998), Magnetic fabric of clay sediments from the external northern Apennines (Italy), *Phys. Earth Planet. Inter.*, **105**, 73–93.
- Schmid, S. M., and E. Kissling (2000), The arc of the western Alps in the light of geophysical data on deep crustal structure, *Tectonics*, **19**, 62–85.
- Schumacher, M. E., and H. P. Laubscher (1996), 3D crustal architecture of the Alps-Apennines join: A new view on seismic data, *Tectonophysics*, **260**, 349–363.
- Schwartz, S. Y., and R. Van der Voo (1983), Paleomagnetic evaluation of the orocline hypothesis in the central and southern Appalachians, *Geophys. Res. Lett.*, **10**, 505–508.
- Selvaggi, G., and C. Chiarabba (1995), Seismicity and P-wave velocity image of the southern Tyrrhenian subduction zone, *Geophys. J. Int.*, **122**, 818–826.
- Séranne, M. (1999), The Gulf of Lions continental margin (NW Mediterranean) revisited by IBS: An overview, in *On the Mediterranean Basins: Tertiary Extension Within Alpine Orogen*, edited by B. Durand et al., *Geol. Soc. Spec. Publ.*, **156**, 15–36.
- Servizio Geologico d'Italia (1969), Foglio 70 (Alessandria), Rome, Italy.
- Servizio Geologico d'Italia (1970a), Foglio 69 (Asti), Florence, Italy.
- Servizio Geologico d'Italia (1970b), Foglio 81 (Ceva), Rome, Italy.
- Servizio Geologico d'Italia (1970c), Foglio 92–93 (Albenga-Savona), Bergamo, Italy.
- Servizio Geologico d'Italia (1971), Foglio 82 (Genova), Rome, Italy.
- Speranza, F., L. Sagnotti, and M. Mattei (1997), Tectonics of the Umbria-Marche-Romagna Arc (central northern Apennines, Italy): New paleomagnetic constraints, *J. Geophys. Res.*, **102**, 3153–3166.
- Speranza, F., R. Maniscalco, M. Mattei, A. Di Stefano, R. W. H. Butler, and R. Funicello (1999), Timing and magnitude of rotations in the frontal thrust systems of southwestern Sicily, *Tectonics*, **18**, 1178–1197.
- Speranza, F., I. Villa, L. Sagnotti, F. Florindo, D. Cosentino, P. Cipollari, and M. Mattei (2002), Age of the Corsica-Sardinia rotation and Liguro-Provençal Basin spreading: New paleomagnetic and <sup>40</sup>Ar/<sup>39</sup>Ar evidence, *Tectonophysics*, **347**, 231–251.
- Speranza, F., R. Maniscalco, and M. Grasso (2003), Pattern of orogenic rotations in central-eastern Sicily: Implications for the timing of spreading in the Tyrrhenian Sea, *J. Geol. Soc.*, London, **160**, 183–195.
- Stacey, F. D., and S. K. Banerjee (1974), *The Physical Principles of Rock Magnetism*, 195 pp., Elsevier, New York.
- Stephenson, A. (1980), A gyroremanent magnetization in anisotropic magnetic minerals, *Nature*, **284**, 49–51.
- Tapponnier, P. (1977), Evolution tectonique du système alpin en Méditerranée: Poinçonnement et écrasement rigide-plastique, *Bull. Soc. Geol. Fr.*, **139**, 437–460.
- Thomas, J. C., M. E. Claudel, M. Collombet, P. Tricart, A. Chauvin, and T. Dumont (1999), First paleomagnetic data from the sedimentary cover of the French penninic Alps: Evidence for Tertiary counterclockwise rotations in the western Alps, *Earth Planet. Sci. Lett.*, **171**, 561–574.
- Vandenberg, J. (1979), Preliminary results of a paleomagnetic research on Eocene to Miocene rocks of the Piemonte basin (N. W Apennines, Italy), *Geol. Ultraiectina*, **20**, 147–153.
- Van den Ende, C. (1977), Paleomagnetism of Permian red beds of the Dome de Barrot (S. France), Ph.D. thesis, 170 p., Univ. of Utrecht, Utrecht, Netherlands.
- Van der Voo, R. (1993), *Paleomagnetism of the Atlantic, Tethys, and Iapetus Oceans*, 411 pp., Cambridge Univ. Press, New York.
- Vanossi, M., L. Cortesogno, B. Galbiati, B. Messiga, G. Piccardo, and R. Vannucci (1984), Geologia delle Alpi Liguri: Dati, problemi, ipotesi, *Mem. Soc. Geol. Ital.*, **28**, 5–75.
- Vignaroli, G. (2006), Structural-metamorphic evolution of the Voltri Massif (Ligurian Alps, Italy). Tectonic implications for the Alps-Apennines linkage, Ph.D. thesis, 166 pp., Univ. of Roma Tre, Rome.
- Vignaroli, G., F. Rossetti, and C. Faccenna (2008), Retrogressive fabric development during exhumation of the Voltri Massif (Ligurian Alps, Italy): Arguments for an extensional origin and implications for the Alps-Apennine linkage, *Int. J. Earth Sci.*, in press.
- Westphal, M. (1973), Etudes paléomagnétiques de quelques formations permienne et triassiques dans les Alpes occidentales (France), *Tectonophysics*, **17**, 323–335.
- Westphal, M. (1976), Contribution du paléomagnétisme à l'étude des déplacements continentaux autour de la Méditerranée occidentale, thèse, Univ. of Strasbourg, Strasbourg, France.
- Wortel, M. J. R., and W. Spakman (2000), Subduction and slab detachment in the Mediterranean-Carpathian region, *Science*, **290**, 1910–1917.
- Zijderveld, J. D. A. (1967), A. C. demagnetization of rocks: Analysis of results, in *Methods in Palaeomagnetism*, edited by D. W. Collinson, K. M. Creer, and S. K. Runcorn, pp. 254–286, Elsevier, New York.

A. Cascella, Istituto Nazionale di Geofisica e Vulcanologia, Via della Faggiola, 32, I-56126, Pisa, Italy. (cascella@ingv.it)

C. Faccenna and G. Vignaroli, Dipartimento di Scienze Geologiche, Università degli studi Roma Tre, L.go San L. Murialdo, 1, I-00146, Rome, Italy. (faccenna@uniroma3.it; vignaroli@uniroma3.it)

M. Maffione, L. Sagnotti, and F. Speranza, Istituto Nazionale di Geofisica e Vulcanologia, Via di Vigna Murata, 605, I-00143, Rome, Italy. (maffione@ingv.it; sagnotti@ingv.it; speranza@ingv.it)

## **CHAPTER 2**

### ***The Bolivian Orocline***

**Bending of the Bolivian orocline and growth of the Central Andean plateau:  
paleomagnetic and structural constraints from the Eastern Cordillera (22-24°S, NW  
Argentina) (\*)**

**(\*) Manuscript submitted to *Tectonics* (\*\*).**

**(\*\*) Revised version under review.**

Marco Maffione<sup>1,3</sup>, Fabio Speranza<sup>1</sup>, Claudio Faccenna<sup>2</sup>

<sup>1</sup>Istituto Nazionale di Geofisica e Vulcanologia, Rome, Italy.

<sup>2</sup>Dipartimento di Scienze Geologiche, Università di Roma Tre, Rome, Italy.

<sup>3</sup>Dipartimento di Fisica, Università di Bologna, Bologna, Italy.

**Abstract**

We report new paleomagnetic and structural data from late Cretaceous to Mio-Pliocene continental sandy/silty sedimentary rocks from the Eastern Cordillera (Central Andes). Here, N-S to NNE-SSW ridges hosting Paleozoic basement and upper Cretaceous continental red beds overthrust thick adjacent Cenozoic basins. Pre-tilting (and likely primary) reliable directions gathered at 15 sites document  $45.9^{\circ} \pm 9.4$ ,  $30.1^{\circ} \pm 23.9^{\circ}$ , and  $15.4^{\circ} \pm 19.3^{\circ}$  clockwise (CW) rotations with respect to South America occurring after the late Cretaceous (~80 Ma), Oligo-Miocene (20-30 Ma), and late Miocene-Pliocene (5-10 Ma), respectively. Conversely, four upper Cretaceous sites from the walls of a N-S left-lateral strike-slip fault (Yavi-Abra Pampa fault) yield a null rotation. About 20 km to the

west, flower structures and subvertical syn-tectonic strata dated at  $14.26 \pm 0.19$  Ma are exposed along the subparallel Abra Moreta left-lateral strike-slip fault. Relying on data from the literature on the period when deformation began, we suggest that since Eo-Oligocene times (30-40 Ma) the Eastern Cordillera has undergone a regional CW rotation of  $40^\circ$ - $50^\circ$ , synchronous with crustal shortening and large-scale bending of the Andean salient. The CW rotation is possibly still active today, as documented by regional GPS data from the Andes. Since  $\sim 15$  Ma ago, the activity of N-S left-lateral strike-slip faults induced counterclockwise rotations along the fault zone, locally annulling the regional CW rotation. In agreement with a previous model, we speculate that mid-Miocene strike-slip activity accommodated the progressive southward spreading of the Altiplano-Puna high-altitude plateau, laterally migrating from the overthickened crustal region of the salient apex.

## 1. Introduction

High plateaus are the ultimate product of plate convergence. These remarkable structures are characterized by internally drained flat surfaces standing at high elevation over a thick and warm crust. The Altiplano-Puna plateau is located in the Central Andean Cordillera between  $15^\circ$  and  $28^\circ$ S (Figure 1), standing at a mean elevation of  $\sim 4000$  m over a 60-70 km thick crust [Isacks, 1988; Wigger *et al.*, 1994; Beck *et al.*, 1996]. The plateau widens up to  $\sim 200$  km in the area where the Cordillera axis is deflected by  $55^\circ$  along the “Bolivian Orocline” or “Arica Deflection” [Carey, 1955; Isacks, 1988]. Here, in the centre of the elbow, horizontal shortening is at a maximum [Isacks, 1988; Allmendinger *et al.*, 1997; Kley and Monaldi, 1998; Kley *et al.*, 1999; McQuarrie, 2002; Müller *et al.*, 2002], progressively decreasing towards the north and the south [e.g., Kley and Monaldi, 1998;

McQuarrie *et al.*, 2005, 2008]. The along-strike gradient of crustal shortening is considered to be the leading mechanism for the formation of the Bolivian orocline [e.g., Isacks, 1988; MacFadden *et al.*, 1995; Riller and Oncken, 2003; Rouse *et al.*, 2003].

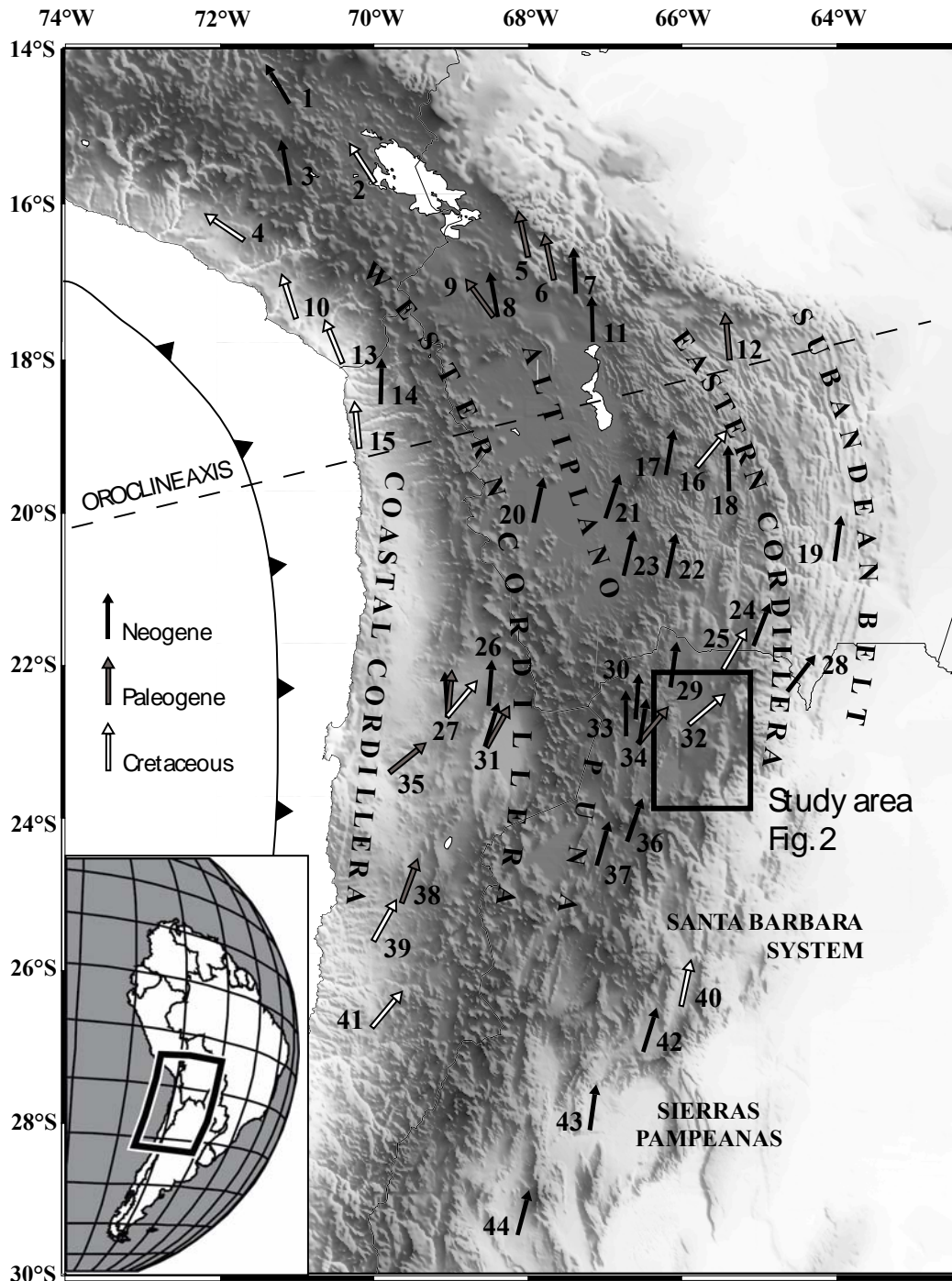


Figure 1. Digital elevation model of the Central Andes, showing the main morphotectonic domains and paleomagnetic directions from selected previous studies (arrows). The numbers adjacent to the arrows refer to the reference list of Table 1.

The deflection of the orogenic axis in the Bolivian orocline is accompanied by the “Central Andes rotation pattern” (CARP of *Somoza et al.*, [1996]), showing a general counterclockwise (CCW) rotation in the northern arc limb (Peru and northern Bolivia), and a clockwise (CW) rotation in the southern limb (southern Bolivia, Chile and northwestern Argentina, Figure 1 and Table 1). While shortening in the Andes has been ongoing since the late Cretaceous, the uplift of the plateau probably initiated in the Miocene during thrusting and consequent crustal thickening, reaching an elevation of up to 1.5-2.5 km [*Isacks*, 1988; *Hoke and Garzzone*, 2008]. In a later stage (probably from 10 to 6 Ma), during the thrusting of the Eastern Cordillera over the Brazilian Shield [*Isacks*, 1988; *Gubbels et al.*, 1993; *Wigger et al.*, 1994], the plateau reached its present-day elevation [e.g., *Isacks*, 1988; *Hoke and Garzzone*, 2008]. The growth and uplift of the Altiplano thus appears to be related, at least during its first phases, to the formation of the Bolivian orocline and to progressive crustal shortening. Transpression and strike-slip faulting have also been documented on both branches of the orocline. This pattern of deformation is regionally significant, and has been related to different mechanisms, such as a bending mechanism (i.e., saloon door) [e.g., *Isacks*, 1988; *MacFadden et al.*, 1995; *Müller et al.*, 2002], slip-partitioning due to the oblique convergence [*Randall et al.*, 1996; *Abels and Bischoff*, 1999; *Arriagada et al.*, 2000, 2003], compression-related block faulting, a lateral ramp accommodating panels of different shortening rates [*Somoza et al.*, 1996; *Prezzi and Vilas*, 1998; *Prezzi and Alonso*, 2002], or the lateral expansion of the plateau, similar to the Tibetan Plateau [*Riller and Oncken*, 2003]. While the overall structural pattern of the Cordillera has been well-established in terms of large-scale rotations and the tectonics of the salient limbs, the tectonics active during bending and growth of the belt are still poorly documented.

This study focuses on the deformation occurring during the formation of the orocline and the growth of the plateau. We selected a key site located in the Eastern Cordillera, at the margin of the Puna plateau (22-24°S, Figure 1), where thrusting, strike-slip deformation and rotations are expected to be particularly evident [*Allmendinger et al.*, 1997; *Müller et al.*, 2002]. We carried out detailed structural mapping and paleomagnetic investigation of Cretaceous to Mio-Pliocene continental sedimentary rocks in order to unravel the timing and the tectonic style active during the formation of the central Andean salient. Our data document a different rotational pattern related to thrust and strike-slip tectonics. In particular, we find that a strike-slip tectonic regime was active for a brief time interval after thrusting and during the uplift of the Altiplano. This deformation subsequently constrained the growth modes of the Central Andean plateau.

## **2. Background**

### **2.1. Regional geology**

The Central Andes are characterized by several morphotectonic domains, from west to east: the forearc (Coastal Cordillera and Precordillera), the Western Cordillera, the Altiplano-Puna plateau, the Eastern Cordillera, and the easternmost belt, the latter represented (from north to south) by the Subandean belt, the Santa Barbara system and the Sierras Pampeanas (Figure 1) (for a comprehensive review see *Isacks* [1988] and *Allmendinger et al.* [1997]).

The Altiplano-Puna plateau, an internally drained plateau 300 km wide, 2000 km long, and characterized by an average elevation of nearly 4000 m [*Isacks*, 1988], is located between the Western and Eastern Cordillera. It is characterized by a basin-and-range morphology, where ranges (predominantly hosting Paleozoic metasedimentary rocks) rise

up to 1000 m above the valley floors, mostly filled by continental Tertiary sediments and covered by Quaternary alluvium. The Eastern Cordillera consists of two tectonic domains: a back-thrust belt, located at the border with the Altiplano-Puna plateau (i.e., Falla San Vicente, *Baby et al.*, [1990]), and an east-verging thrust belt at its easternmost margin, comprising two main thrust systems (Cabalgamiento Andino Principal and Cabalgamiento Frontal Principal [*Sempere et al.*, 1990; *Kley et al.*, 1997; *Baby et al.*, 1992]). Finally, the Subandean belt is a classic east-verging thin-skinned fold and thrust belt [*Mingramm et al.*, 1979; *Baby et al.*, 1992].

## **2.2. Timing of deformation within the Eastern Cordillera and the surrounding regions**

In late Cretaceous times, while the first contractional deformation events occurred in northern Chile and western Peru, more easterly regions underwent subsidence related to the sag phase of the Salta rift [*Salfity*, 1982; *Galliski and Viramonte*, 1988; *Marquillas et al.*, 2005; *Monaldi et al.*, 2008]. In Eocene times (45-35 Ma), northern Chile and western Peru were affected by the Incaic tectonic phase [*Steinmann*, 1929], which later propagated eastward, probably through one or two basement megathrusts [*McQuarrie and DeCelles*, 2001; *McQuarrie*, 2002] involving the present day Eastern Cordillera at the border with the Altiplano-Puna plateau [*Kennan et al.*, 1995; *Sempere et al.*, 1990, 1997; *Horton*, 1998; *Coutand et al.*, 2001; *Müller et al.*, 2002; *DeCelles and Horton*, 2003; *Carrapa et al.*, 2005; *Deeken et al.*, 2006; *Hongn et al.*, 2007; *Carrapa and DeCelles*, 2008]. During the Oligocene (30-27 Ma), shortening and uplift also affected the Bolivian Altiplano [*Sempere et al.*, 1990; *McQuarrie and DeCelles*, 2001; *Horton et al.*, 2001, 2002; *DeCelles and Horton*, 2003], in addition to the Eastern Cordillera [*Marshall and Sempere*, 1991; *Allmendinger et al.*, 1997].

Within the northern Puna plateau and the adjacent Eastern Cordillera at 22-25°S, the timing of deformation initiation and uplift of the plateau is not yet fully constrained. A widely accepted model postulates that shortening started in the middle Miocene (17-15 Ma) [Coira *et al.*, 1982; Allmendinger, 1986; Isacks, 1988; Cladouhos *et al.*, 1994; Marrett *et al.*, 1994; Allmendinger *et al.*, 1997; Jordan *et al.*, 1997; 2001]. However, other studies have proposed older (Eo-Oligocene) compressive deformation [Boll and Hernández, 1986; Coutand *et al.*, 2001; Carrapa *et al.*, 2005; Carrapa and DeCelles, 2008].

The end of major shortening in the Bolivian Altiplano and Eastern Cordillera is generally constrained at ~9 Ma by undeformed tuffaceous strata covering a regionally extensive, widely recognized, high level geomorphic surface called the San Juan del Oro surface [Servant *et al.*, 1989; Gubbels *et al.*, 1993]. However, relying on seismic and structural data, Oncken *et al.* [2006] and Elger *et al.* [2005] proposed that shortening continued in the Eastern Cordillera until recent times. Paleomagnetic data are not univocal, thus cannot be used to evaluate this hypothesis. In fact, no tectonic rotation was documented in the northern Puna plateau (22.5-23.1°S) since the late Miocene (9-10 Ma) [Somoza *et al.*, 1996; Prezzi and Alonso, 2002], while a post-13 Ma 10-18° CW rotation was reported in the Eastern Cordillera (~19.5°S) [MacFadden *et al.*, 1990; Barke *et al.*, 2007] (see Table 1 and Figure 1).

Nevertheless, it must be kept in mind that the deformation within the Puna plateau seems to have shifted southward over time. In fact, structural [Allmendinger, 1986; Marrett *et al.*, 1994] and paleomagnetic [Somoza *et al.*, 1996; Aubry *et al.*, 1996] data indicate that deformation and uplift of the southern margin of the Puna plateau began 5-10 Ma and continued, with minor intensity, until the Quaternary.

Finally, the last 10 Ma were characterized by the development of the Subandean fold-and-thrust belt [*Allmendinger et al.*, 1983; *Sempere et al.*, 1990; *Baby et al.*, 1992; *Kley et al.*, 1996; *Moretti et al.*, 1996].

### **2.3. Previous paleomagnetic studies from the Central Andes and their tectonic implications**

During the last 20 years, a wealth of paleomagnetic data has been collected from the Central Andes (Figure 1 and Table 1) [*MacFadden et al.*, 1990, 1993, 1995; *Roperch and Carlier*, 1992; *Butler et al.*, 1995; *Somoza et al.*, 1996, 1999; *Aubry et al.*, 1996; *Beck*, 1998, 2004; *Coutand et al.*, 1999; *Roperch et al.*, 2000; *Arriagada et al.*, 2000, 2003, 2006; *Lamb*, 2001a; *Randall et al.*, 2001; *Somoza and Tomlinson*, 2002; *Prezzi and Alonso*, 2002; *Gilder et al.*, 2003; *Prezzi et al.*, 2004; *Richards et al.*, 2004; *Rousse et al.*, 2005; *Taylor et al.*, 2005, 2007; *Barke et al.*, 2007]. A vertical axis rotation pattern (Central Andes rotation pattern (CARP) of *Somoza et al.* [1996]) with the following features has been documented:

1. Mesozoic to Cenozoic rocks from the northern and southern limbs of the orocline underwent a regional CCW and CW (respectively) rotation of some tens of degrees (Figure 1). Along the orocline axis, paleomagnetic rotations of variable sign are observed, and a clear border between the opposite rotating limbs cannot be discerned.
2. Over a given region, the magnitude of rotations from coeval rocks may be considerably scattered.
3. A debate exists as to the existence of a correlation between the amount of rotation and distance from the plate boundary (compare for instance *Beck* [1998] and *Prezzi and Alonso* [2002]).

4. The magnitudes of the rotations are not clearly correlated with the ages of the rocks, and a temporal progression in the amount of rotation is not observed. This observation suggests that the tectonic rotation(s) occurred during rather short tectonic phase(s).

The CARP has been explained by two end-member models: (1) oroclinal bending [Isacks, 1988; Butler *et al.*, 1995; MacFadden *et al.*, 1995; Rouse *et al.*, 2003; Barke *et al.*, 2007] induced by an along-strike gradient of crustal shortening, and (2) in-situ block rotations [Hartley *et al.*, 1992; Somoza *et al.*, 1996, 1999; Randall, 1998; Randall *et al.*, 2001; Somoza and Tomlinson, 2002; Beck, 2004] associated with the evolution of the Central Andean megasalient, where the rotations occur in a domino-style manner as a consequence of the transpression due to the oblique subduction (especially in the forearc regions) [Randall *et al.*, 1996; Abels and Bischoff, 1999], or in the vicinity of a regional shear zone [Prezzi and Alonso, 2002]. Among these, a “composite model” has also been put forward, where oroclinal bending and small-block rotations are thought to occur concurrently [MacFadden *et al.*, 1995; Beck *et al.*, 1994; Butler *et al.*, 1995; Lamb, 2001a; Riller and Oncken, 2003].

***Previous paleomagnetic data from the Puna Plateau-Eastern Cordillera (latitude 21-24°S)***

Predominant CW rotations have been documented from the Puna Plateau and Eastern Cordillera (Figure 1, Table 1). Between latitude 21 and 24°S, paleomagnetic evidence from volcanic and sedimentary rocks just west of our study area suggest that the northern Puna underwent a post-Eocene CW rotation of ~40° that ended in late Miocene times [Somoza *et al.*, 1996; Prezzi and Alonso, 2002]. Conversely, data from the Eastern Cordillera reveal that significant tectonic rotations continued after mid-late Miocene times.

In fact, *MacFadden et al.* [1990] and *Coutand et al.* [1999] documented a post-13 Ma CW rotation of  $\sim 18^\circ$  at Quebrada Honda ( $22^\circ\text{S}$ ), and a post-10 Ma CW rotation of  $\sim 20^\circ$  from lava flows at Negro de Chorrillos-San Geronimo ( $24.2^\circ\text{S}$ ). *Coutand et al.* [1999] also reported post-late Cretaceous ( $\sim 80$  Ma) CW rotations of  $30^\circ$  and  $50^\circ$  (as re-evaluated by us considering updated South American poles from *Besse and Courtillot* [2002]) at the Siete Hermanos ( $22.2^\circ\text{S}$ ) and Abra Pampa ( $22.8^\circ\text{S}$ ) localities, respectively. These authors related some of the observed rotations to a scissoring mechanism along major reverse faults. Finally, *Prezzi et al.* [2004] measured a small ( $\sim 8^\circ$ ) CW rotation in middle Miocene volcanic rocks (12-13 Ma) from the Laguna de Pozuelos basin ( $22.4^\circ\text{S}$ ), within our study area.

### 3. Geological setting of the study area

#### *Tectonics*

The study area is located in the Eastern Cordillera adjacent to the northern Puna, though several previous studies (i.e., *Coutand et al.* [1999, 2001], *Marrett et al.* [1994], and *Cladouhos et al.* [1994]) have considered this region as belonging to the northern Puna (Figures 1 and 2). The Eastern Cordillera in the study area is controlled by N-S to NNE-SSW striking reverse and thrust faults bounding deep Tertiary basins [*Coira*, 1979; *Coira et al.*, 1982; *Marrett et al.*, 1994; *Cladouhos et al.*, 1994; *Coutand et al.*, 1999, 2001]. The distance between ranges is on the order of ten kilometers and the predominant dips of reverse faults are at high angles, likely because of the reactivation of Cretaceous normal faults. Specifically, the Cangrejos-Tres Cruces ridge is bounded to the west by the Yavi-Abra Pampa fault (Figure 2), interpreted as a Miocene low-angle east-verging thrust fault

[Bianucci *et al.*, 1987], and locally reactivated by Quaternary oblique dextral extensional kinematics [Cladouhos *et al.*, 1994].

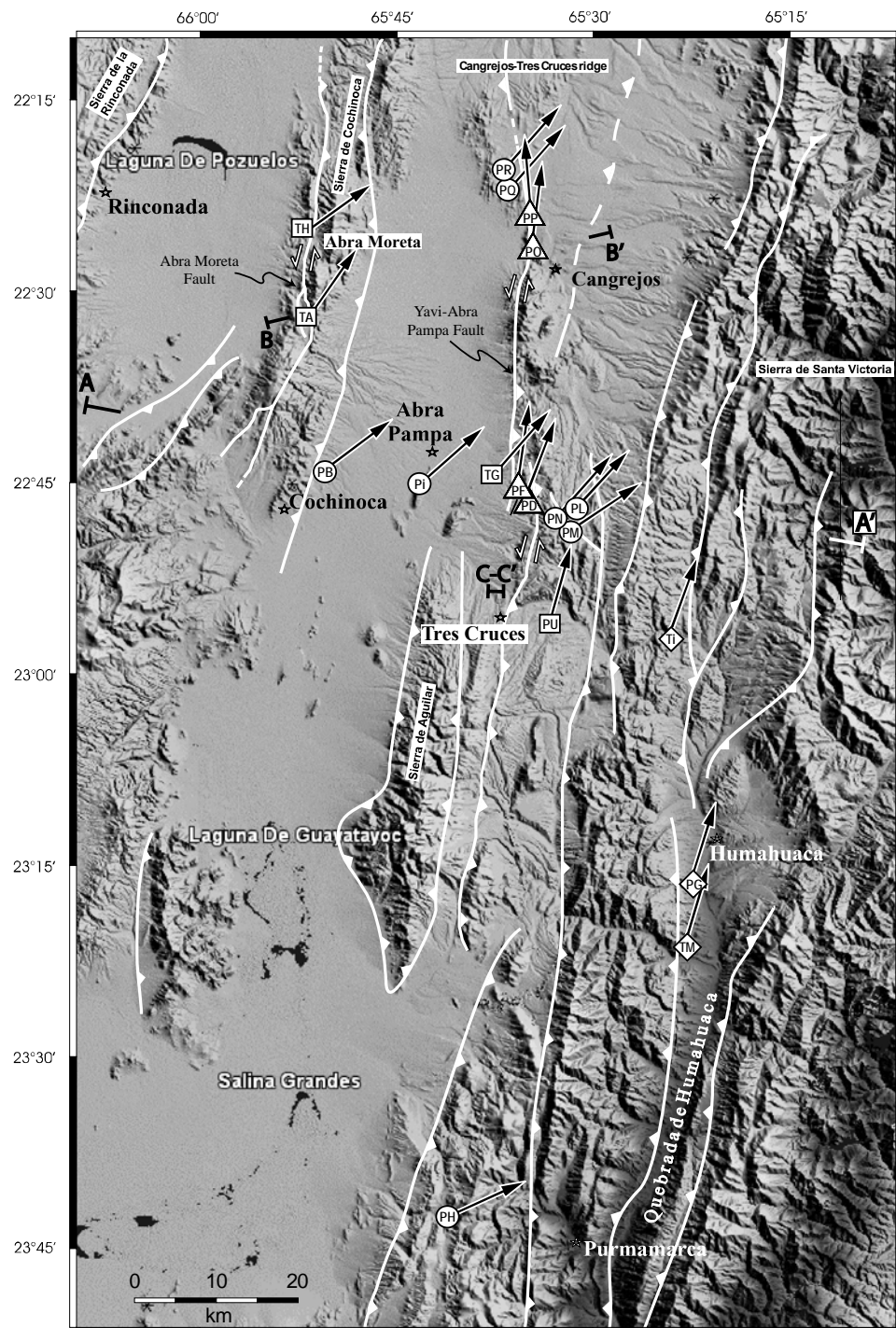


**Figure 2.** Digital elevation model and main tectonic features of the study area (see Figure 1 for location). Symbols for sampled sites are as in Figure 5. Black arrows represent site-mean rotations from this study calculated with respect to stable South America (see Table 2). AA', BB' and CC' are the traces of the geological cross sections of Figure 8.

Here, the Miocene reverse faults are truncated by the San Juan del Oro unconformity, which in turn is covered by a volcanic deposit dated at  $8.78 \pm 0.17$  Ma [Gubbels *et al.*, 1993; Cladouhos *et al.*, 1994]. Kinematic indicators and stratigraphic offset at several subvertical fault scarps recognized by Cladouhos *et al.* [1994] here and on the western flank of the Cochinoa and Rinconada ranges are suggestive of recent (probably Quaternary) right-lateral strike-slip tectonics.

Previous structural studies carried out in this region have yielded evidence for a WNW-ESE ( $110^\circ$ - $120^\circ$ ) regional shortening direction during the Miocene tectonic phase [Cladouhos *et al.*, 1994; Marrett *et al.*, 1994; Coutand *et al.*, 2001] postdating, or in some cases predating, the strike-slip tectonics [Baby *et al.*, 1990; Barrios, 1991; Cladouhos *et al.*, 1994; Hérail *et al.*, 1996; Müller *et al.*, 2002]. Regardless of the sense of shear, the significance and interpretation of the strike-slip structures have remained elusive so far. The outward descent to the thin-skinned foreland belt (Subandean) initiates east of Tres Cruces (i.e., the Quebrada de Humahuaca, Figure 2), where the dominantly east-verging thick-skinned thrust system of the Eastern Cordillera involved Precambrian metasediments and Cretaceous cover [Rodríguez Hernández *et al.*, 1999; Kley, 1996; Kley *et al.*, 1997].

### ***Stratigraphy***

The most widely exposed rocks on the Eastern Cordillera are Ordovician metasediments (Acoite formation) of the uppermost unit of the Santa Victoria Group [Turner, 1979; Coira, 1979, 1982]. During the Cretaceous rifting phase, regional-scale continental units (“Salta Group”) were deposited in the Salta Rift [Salfity, 1982; Galliski and Viramonte, 1988; Marquillas *et al.*, 2005; Monaldi *et al.*, 2008]. The first syn-rift deposits are represented by the Pirgua Subgroup (Aptian-Maastrichtian), a continental unit

comprising reddish conglomerates, sandstones, and shales from alluvial fan, fluvial, eolian, and lacustrine environments, with rare intercalations of volcanic rocks (basalts and trachytes) [Coira, 1979; Galliski and Viramonte, 1988]. In the study area, the Pirgua Subgroup reaches an average thickness of 700 m [Marquillas *et al.*, 2005], and is overlain by Maastrichtian to Eocene post-rift sequences (Balbuena and Santa Barbara Subgroup) [Moreno, 1970; Salfity, 1980; Salfity and Marquillas, 1994].

Both the Paleozoic basement and the sedimentary rocks from the Salta Group are unconformably covered by a thick package of continental clastic deposits, mainly showing westerly detrital sources [Jordan and Alonso, 1987; Marshall and Sempere, 1991]. Because of the paucity of fossils, their age has usually been inferred through regional correlation and/or radiometric dating on intercalated volcanic deposits (where present). In the western part of the study area, the oldest exposed continental deposits (besides the Salta Group) are represented by the Moreta and the Candado formations, a ~2000 m thick (in total) clastic sequence made of red conglomerates and sandstones [Coira, 1979]. Coutand *et al.* [2001] suggest that the Candado formation could be slightly older than the Moreta formation (see their Figure 4), while Coira [1979] considers them as coeval. Since volcanic rocks from the Moreta formation have been dated at  $28\pm 3$  and  $20\pm 2$  Ma [Linares, 1979; Linares *et al.*, 1987] we assume a 20-30 Ma age for the Moreta/Candado deposits. At the Abra Moreta locality (Figure 2) a mainly conglomeratic deposit called the “Cara Cara strata” [see Cladouhos *et al.*, 1994] has been dated at  $14.26\pm 0.19$  Ma using  $^{40}\text{Ar}/^{39}\text{Ar}$  on biotite from an intercalated tuff. This deposit was previously identified by Coira [1979] as the Sijes formation, and was correlated to the Chaco formation exposed near Tres Cruces, at the eastern flank of the Sierra de Aguilar (Figure 2).

Finally, within the eastern part of the study area, along the Quebrada de Humahuaca, the syn-orogenic deposits, directly lying upon the Ordovician basement, are represented by the Miomará formation [*Ramos et al.*, 1967; *Salfity et al.*, 1984], a thick continental clastic sequence composed of loose red-pinkish quartzitic sandstones of late Miocene-early Pliocene age (5-10 Ma).

#### **4. Sampling and methods**

We collected sandy to silty samples from the Pirgua, Moreta/Candado and Miomará formations at 32 localities (Figure 2, Table 2), predominantly using a petrol-powered portable drill cooled by water (oriented hand samples were gathered at only three sites). At each site we collected 6-16 cores (11 on average), spaced in at least two outcrops in order to try to average out secular variation of the geomagnetic field. In total, 325 cores and 15 hand samples were recovered. All samples were oriented using a magnetic compass, corrected to account for the local magnetic field declination value at the sampling area (about  $-6^{\circ}$  according to NOAA's National Geophysical Data Center [<http://www.ngdc.noaa.gov>]). We also performed structural analysis on small-scale brittle faults at nine localities, mostly coinciding with paleomagnetic sites.

After cutting the sampled cores into standard cylindrical specimens of 22 mm height, one pilot specimen per site was thermally demagnetized in 14 steps up to  $680^{\circ}\text{C}$  in order to select the most effective thermal steps to isolate the characteristic remanent magnetization (ChRM). Afterwards, all samples were thermally demagnetized through 11-12 steps up to  $680^{\circ}\text{C}$ . Preliminary laboratory analyses on the pilot specimens were carried out in the paleomagnetic laboratory of the Universidad de Buenos Aires (UBA, Buenos Aires, Argentina), while all the other measurements were completed in the paleomagnetic

laboratory of the Istituto Nazionale di Geofisica e Vulcanologia (INGV, Rome, Italy). The natural remanent magnetization (NRM) of the specimens was measured in the magnetically shielded room of the paleomagnetic laboratory of INGV with a DC-SQUID cryogenic magnetometer (2G Enterprises, USA). Magnetic mineralogy analyses were carried out to identify and characterize the main magnetic carriers. These analyses included:

- the measurement of the hysteresis properties, the acquisition of an isothermal remanent magnetization (IRM) and its subsequent back-field demagnetization with a Micromag Alternating Gradient Magnetometer (AGM, model 2900) with a maximum applied field of 1.4 T;
- the investigation of the thermal change of the magnetic susceptibility during a heating-cooling cycle from room temperature to 700°C, using an AGICO CS-3 apparatus coupled to the KLY-3 bridge;
- the thermal demagnetization of a three-component IRM imparted on the specimen axes, according to the method of *Lowrie* [1990]. Fields of 2.7, 0.6 and 0.12 T were successively imparted on the z, y, and x sample axes (respectively) with a Pulse Magnetizer (Model 660, 2G Enterprises).

## **5. Results**

### **5.1. Magnetic mineralogy**

Hysteresis measurements invariably indicate the presence of a high-coercivity fraction. All specimens show well-developed hysteresis loops that do not saturate at the maximum applied field of 1.4 T (Figures 3a-3b). The matrix is predominantly

paramagnetic (Figure 3a), though diamagnetic behavior is observed for the most quartz-rich samples (Figure 3b).

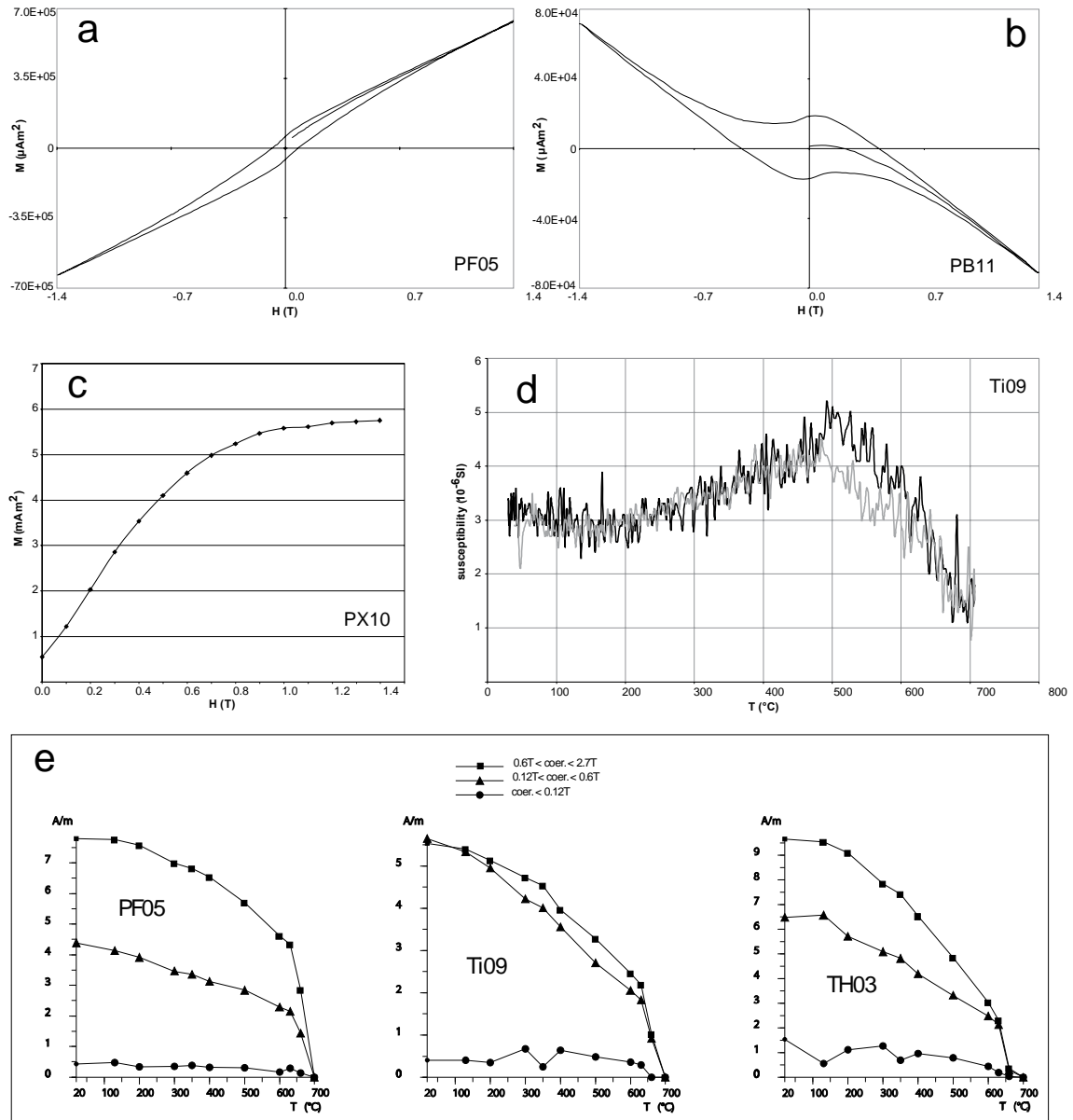


Figure 3. Results from magnetic mineralogy analyses from representative samples. (a, b) Hysteresis loops for (a) a typical and (b) a quartz-rich sample from the Pirgua formation. (c) Isothermal remanent magnetization (IRM) acquisition curve for a representative sample from the Pirgua formation. (d) Thermal variation of the low-field magnetic susceptibility during a heating and cooling cycle (black and grey lines, respectively). (e) Thermal demagnetization of a three-component IRM according to the method of *Lowrie* [1990] for three representative specimens from the Pirgua, Moreta and Miomarà formations.

Specimens were not saturated (except for the two sites PX and TM, Figure 3c) during the acquisition of the IRM up to 1.4 T. Thermomagnetic curves (Figure 3d) show a rather

linear decrease of the magnetic susceptibility from 500 to 700°C, suggesting that hematite is the predominant magnetic carrier. Finally, the thermal demagnetization of a three-component IRM (Figure 3e) confirms that both the medium-coercivity and the hard fractions are represented by hematite (demagnetized at about 700°C), while a soft component is virtually absent. In conclusion, magnetic mineralogy analyses point to hematite (of variable grain sizes) as the unique magnetic carrier of all Cretaceous-Pliocene samples gathered from the Eastern Cordillera.

## 5.2. Paleomagnetic characteristic directions

Thermal demagnetization data were plotted on orthogonal diagrams [*Zijderveld*, 1967], and the magnetization components were isolated by principal component analysis [*Kirschvink*, 1980]. Only 24 (out of 32) sites yielded reproducible directions during cleaning, while the remaining eight sites showed scattered demagnetization diagrams (Figure 4 and Table 2). For 18 sites, a ChRM was isolated between 400 and 680°C (Figure 4a-4n). Conversely, six sites revealed two magnetization components, a low temperature (LT) component between room temperature and 590°C, and a high temperature (HT) component removed at approximately 680°C (Figure 4o-4q).

The site-mean directions, for both LT and HT components, were evaluated by *Fisher's* [1953] statistics. Only two out of the six site-mean LT components showed an  $\alpha_{95}$  value less than 20.0° (Table 2) (fixed by us as the threshold value to discriminate between paleomagnetically reliable and scattered sites), and were thus discarded from further consideration. Conversely, 20 out of the 24 ChRMs and HT components yielded an  $\alpha_{95}$  value below 20.0°, and were used to infer on the paleomagnetism of the study area. Of the 20 sites revealing a reliable paleomagnetic direction, site PE was discarded, as it is the sole

site from the Pirgua Formation yielding a northeastward-directed, downward (and thus aberrant) paleomagnetic direction (Table 2).

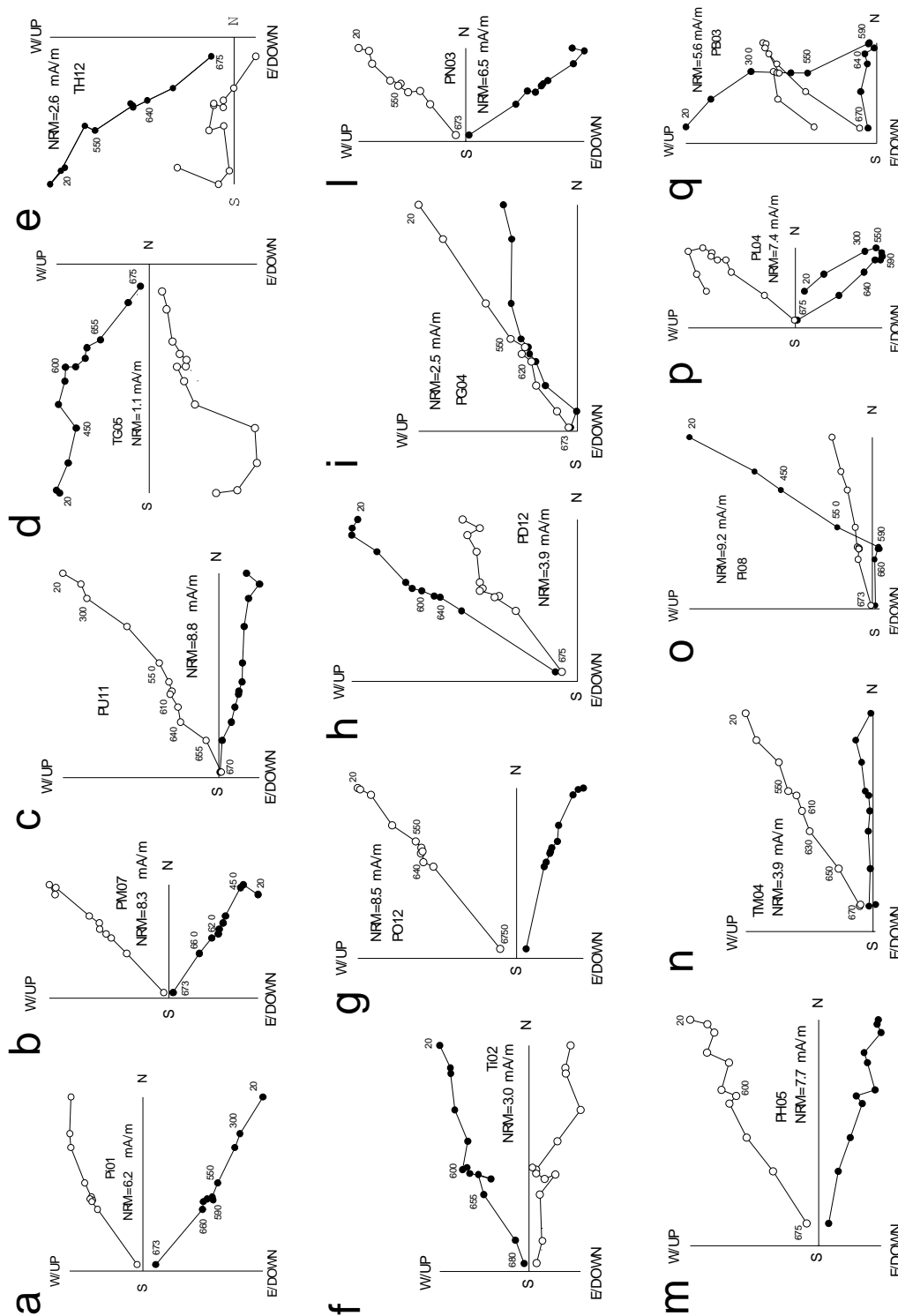
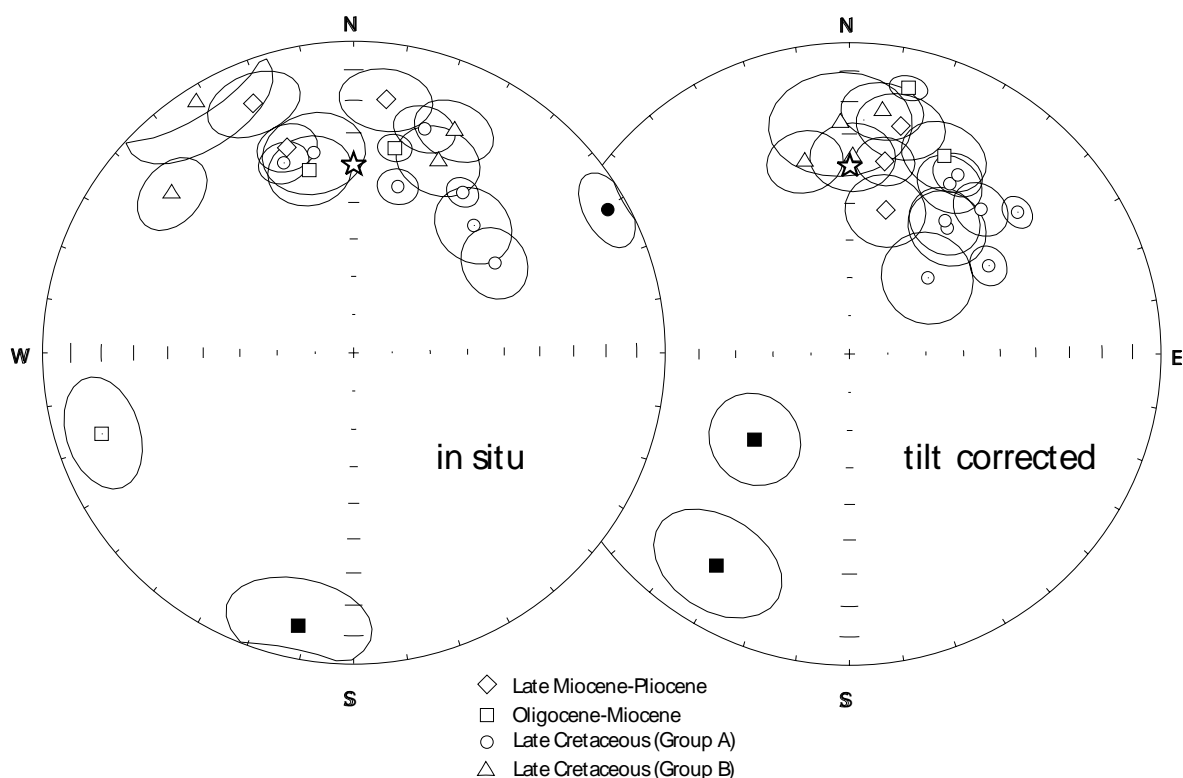


Figure 4. Orthogonal vector diagrams of typical demagnetization data, in situ coordinates, showing representative samples carrying single (a-n) and multiple (o-q) magnetization components. Solid and open dots represent projections on the horizontal and vertical planes, respectively. Demagnetization step values are in °C.

Only two Candado/Moreta Oligo-Miocene sites out of the 19 reliable site-mean directions showed a reverse polarity (Figure 5 and Table 2). The systematic normal polarity of all 12 upper Cretaceous samples taken from sites of the Pirgua Formation suggests that they may have been deposited during the Long Normal Cretaceous Superchron, as advocated by *Aubry et al.* [1996] and *Valencio et al.* [1977]. All sites show northeastward-directed (in the normal polarity state) paleomagnetic directions, except for four sites from the Pirgua Formation (PD, PF, PO, PP) sampled adjacent to the Yavi-Abra Pampa fault (Figures 2 and 5).



**Figure 5.** Equal-area projections of the site mean paleomagnetic directions from the studied area. Solid (open) symbols represent projection onto the lower (upper) hemisphere. Open ellipses are the projections of the  $\square 95$  cones about the mean directions. The star represents the mean normal polarity geocentric axial dipole (GAD) field direction ( $D=0^\circ$ ,  $I=-40^\circ$ ) for the study area. Groups A and B from the upper Cretaceous Pirgua Formation refer to CW rotated and non-rotated sites sampled adjacent to the Yavi-Abra Pampa fault, respectively (see text).

Therefore we calculated mean paleomagnetic directions for groups of sites sharing similar ages, but for the Pirgua formation we evaluated two mean directions, one for the four sites yielding northward “anomalous” directions (“group B”), and another for the remaining eight sites (“group A”, Table 3). The rotation and flattening values with respect to South America for the individual sites and the mean regional directions (Table 2 and Table 3, respectively) were evaluated according to *Demarest* [1983], using the reference paleopoles from *Besse and Courtillot* [2002].

The [*McFadden*, 1990] fold test, separately applied to Cretaceous (distinguishing A and B groups) and Tertiary sites, systematically yielded a positive result at the 95% confidence level (Table 4). The reversal test (according to *McFadden and McElhinny* [1990]), solely performed on the Tertiary sites (Cretaceous sites were invariably of normal polarity), was indeterminate.

In conclusion, the results from the fold test, along with the evidence that all the in-situ paleomagnetic directions are far from the geocentric axial dipole field direction for the study area (Figure 5), indicate that 19 sites from the Eastern Cordillera host a pre-tilting (and likely primary) remanent magnetization.

### **5.3. Structural analysis**

We measured 70 striated small-scale brittle fault planes (and relative kinematic indicators, if present) from late Cretaceous to Miocene sedimentary rocks at nine localities (Figure 6). For each fault plane we recorded the dip and strike, the direction and plunge (or the pitch, where more convenient) of the slickensides, and the sense of slip (if recognizable). Quartz or calcite steps, Riedel shear and SC-structures were the most commonly identified fault kinematic indicators.

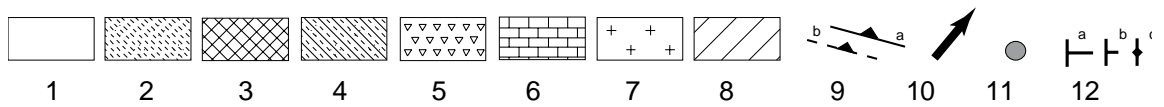
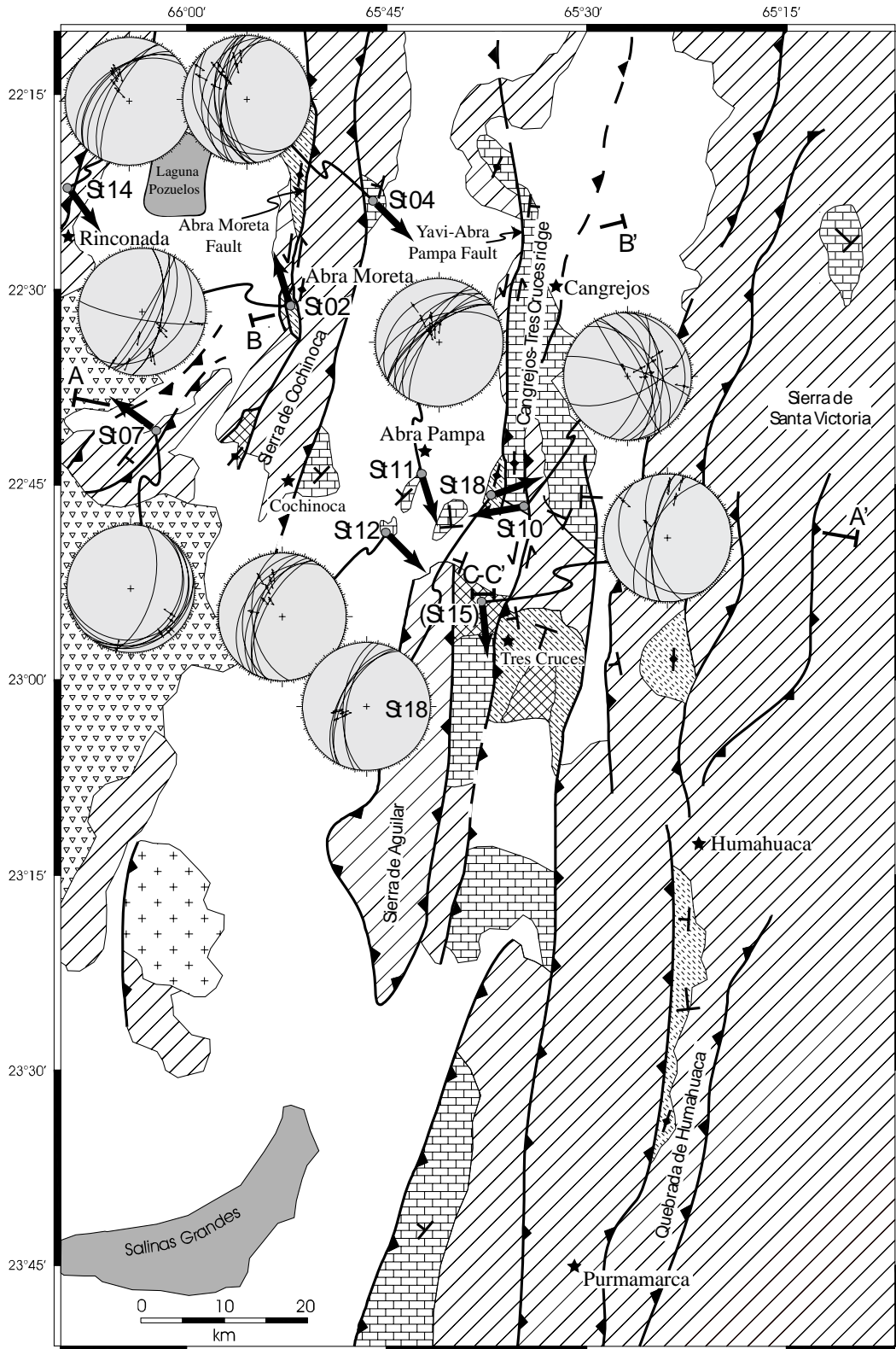


**Figure 6. Structural and geological map of the study area, showing at each measurement site the stereographic projections of the fault planes and relative slickensides. AA', BB' and CC' are the traces of the geological cross sections of Figure 8. 1, Recent alluvial and colluvial deposits [Quaternary]; 2, Miomará formation [late Miocene-Pliocene]; 3, Sijes/Chaco formation [middle-late Miocene]; 4, Moreta/Candado formation [Oligocene-Miocene]; 5, basic and acid volcanics [Neogene]; 6, Pirgua formation [Aptian-Maastrichtian]; 7, granitoides [Cretaceous]; 8, Acoite formation [Ordovician] and pre-Cretaceous formations; 9, main exposed (a) and buried (b) thrust faults; 10, site-mean direction of the slip vector and sense of displacement at reverse brittle faults; 11, structural analysis site; 12, bedding attitude for 0°-35° (a), 35°-70° (b), and ~90° (c) dipping strata.**

---

At each locality, we measured at least five fault planes in order to obtain a significant fault population. The average strike of the slip vector and the sense of displacement at each site is derived by contouring the slickensides density. Figure 6 shows the results of the structural analysis: at each site we show the stereonet of fault planes and the relative slickensides (Schmidt's lower hemisphere equal area projection) along with the arrows showing the relative motion of the hanging wall block, deduced by the average strike and sense of the slip vector. For reverse faults with a pure dip-slip component, this vector is roughly parallel to the shortening direction.

Measured fault planes strike roughly NNE-SSW on average, in agreement with the regional trend of the major structures, and show dual vergence with a predominance of west-dipping planes (Figure 6, 7a). Contouring of the slickensides density from all sites (Figure 7b) reveals two main clusterings at about 270° and 330°. This indicates an average regional strike of the slip vectors of ~N130°, as observed at the Abra Moreta, Abra Pampa, and Rinconada sites (sites St04, 07, 11, 12, 14, Figure 6). The sense of shear on reverse faults is only locally dip-slip (on NE-SW fault planes, i.e., near site St07 and 11) but predominantly oblique on NS to NNE-SSW planes, yielding an overall left-lateral transpressive regime (Figure 6). The E-W direction of the slip vectors was noted at two sites adjacent to the Yavi-Abra Pampa fault (St10 and 18), and its possible significance will be discussed below. The high angle of some reverse fault planes (Figure 7b) again suggests a reactivation of pre-existing structures.

The Sierra de Cochinoa structure constitutes a fault-bounded ridge bringing Pirgua and Paleozoic units on top of Tertiary ones [Coutand *et al.*, 2001]. On its western margin, a 40 km long strike-slip fault zone is characterized by the occurrence of subvertical strata, strike-slip duplexes and flower structures involving Tertiary formations. At Abra Moreta (site St02, Figure 6), the Moreta formation is exposed in a tectonic slice squeezed by the Paleozoic Acoite formation, forming a typical flower structure (Figure 8, cross section B-B' and Figure 9e).

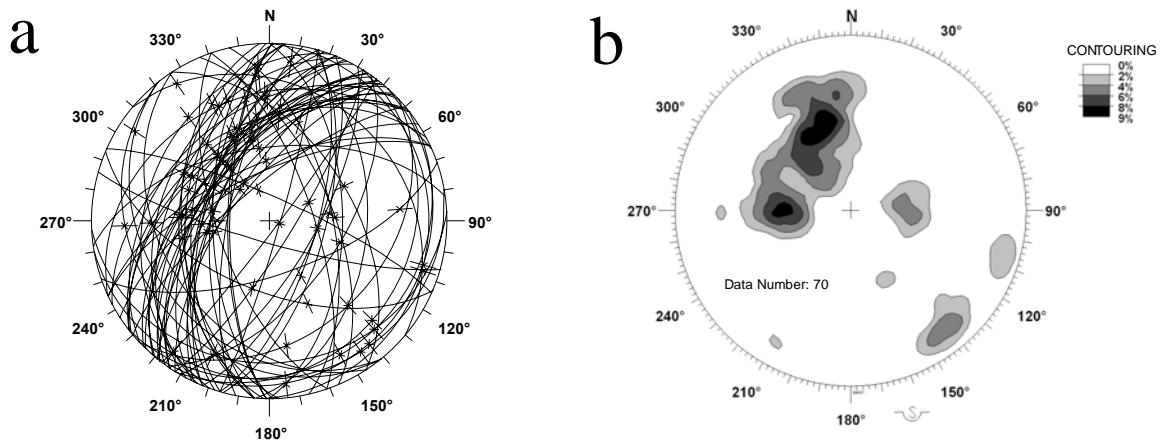


**Figure 7. Kinematic indicators from 70 fault planes. Lower-hemisphere stereographic projections of (a) fault planes directions, and individual slickenside direction and sense, and (b) slickenside density.**

Close to the flower structure, the Paleozoic Acoite formation thrusts over the Moreta formation, with left-lateral oblique motion (Figure 9d). To the west, the Sijes/Chaco formation shows subvertical N-S beds and is cut by N-S left-lateral strike-slip faults along almost the entire ~1 km long outcrop (Figure 8, 9b and 9c). Progressive unconformities mark a gradual decrease in bedding dip towards the west (Figure 8, 9a), revealing typical “growth strata” pointing to a syn-tectonic origin for this deposit. Thus, the age of this syn-tectonic deposit ( $14.26 \pm 0.19$  Ma, according to Cladouhos *et al.* [1994]) may constrain the age of the strike-slip tectonics in this sector of the Eastern Cordillera.

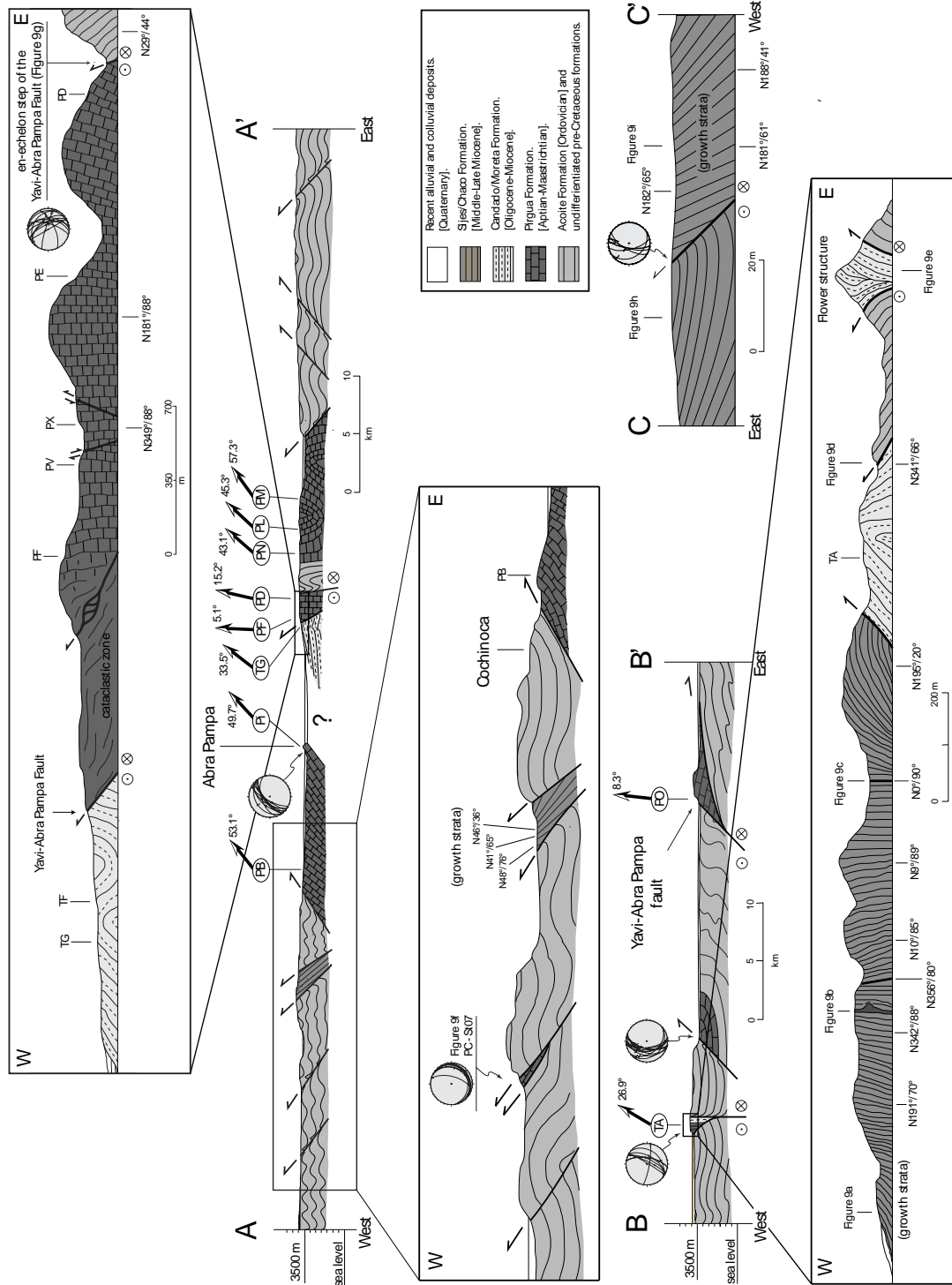


**Figure 8.** Geological cross sections from the study area. See Figures 2 and 6 for location. The arrows and respective numbers indicate the paleomagnetic rotation values with respect to South America at the sampling sites, according to Table 2. The stereographic projections of the fault plane directions at the measurement sites are shown as in Figure 6.

This pattern of deformation and sedimentation has also been observed northward at paleomagnetic site TH, where the Moreta/Candado formation shows sub-vertical beds. Growth strata with progressive unconformities within the Sijes/Chaco formation were also observed west of Cochinoqa (Figure 8, cross section AA'), and near Tres Cruces (Figure 8, cross section CC', and Figures 9h and 9i).

East of the Yavi-Abra Pampa fault, at the latitude of Abra Pampa, the Pirgua strata are remarkably subvertical along a 3.5 km long outcrop (Figure 8, cross section AA'), before coming into tectonic contact with the Acoite formation along a roughly N-S sinistral transpressive-trending fault zone (Figure 9g). In map view, this fault is en echelon arranged with the Yavi-Abra Pampa fault (Figures 2 and 6). The structural analysis carried out along the whole outcrop (St10, Figure 6), reveals the presence of mainly N-S trending east-dipping reverse and strike-slip faults.

To the west, the hanging wall of the Yavi-Abra Pampa fault is composed of a pervasively cataclastic Pirgua Formation for some hundreds of meters (Figure 8, cross section AA'). The fault itself cuts through the pre-existing thrust structures with a set of east-dipping (close to Abra Pampa) and west-dipping (Cangrejos locality, see *Bianucci et al.*, [1987]) reverse splays. This change in dip and vergence within a short distance along the same fault seems to be a common structural feature of this region (compare *Coutand et al.* [1999] and *Kley et al.* [2005]). Just west of the main faults, the Candado/Moreta formation is exposed along a N-S anticline-syncline couplet (Figure 8, cross section AA'). Moreover, at the Tres Cruces locality, N-S folds in the Cenozoic sequence plunge abruptly southward, possibly because of the interplay between thrust-related folding and strike-slip shear along the Yavi-Abra Pampa fault [e.g., *Kley et al.*, 2005].

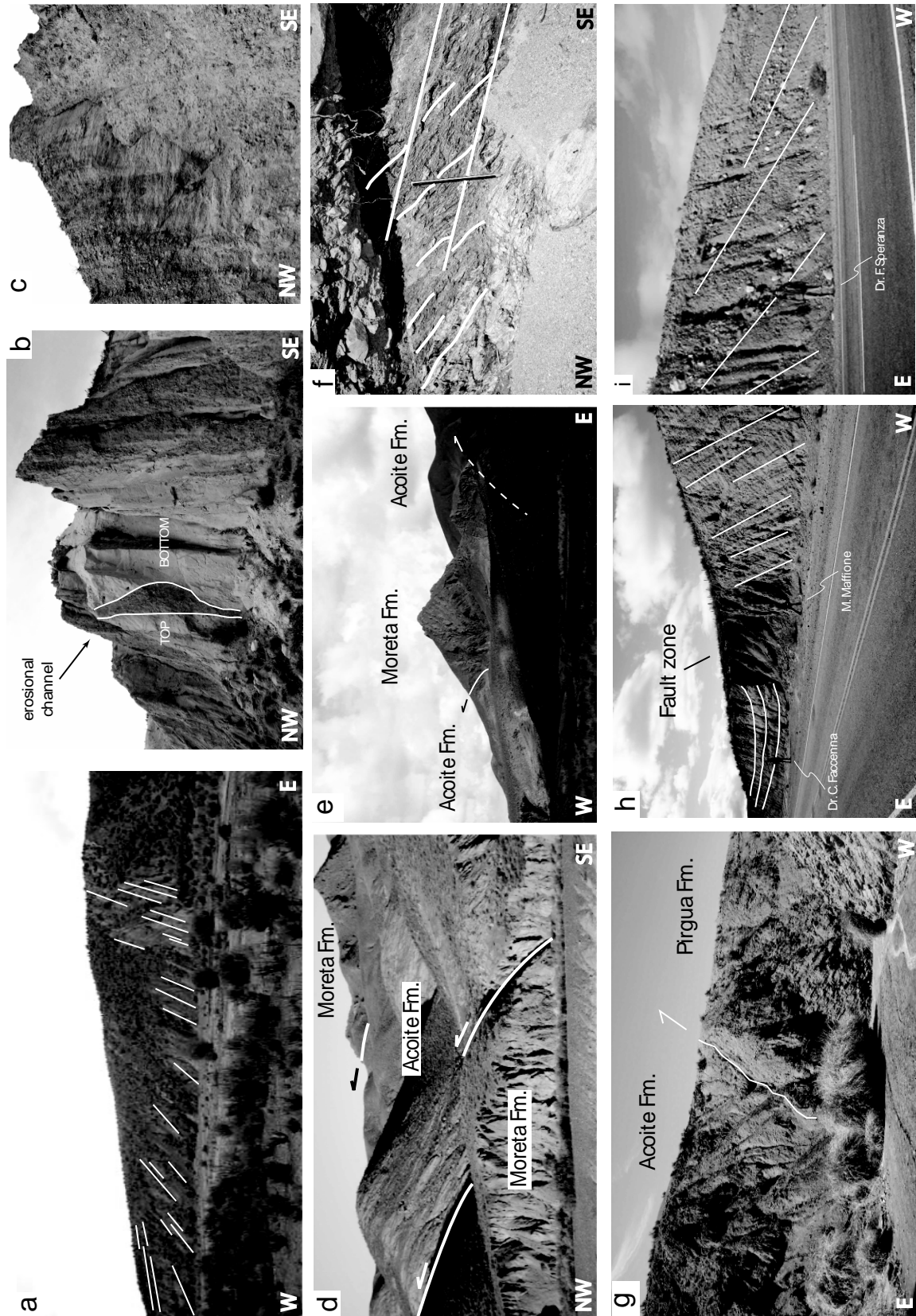


Figure 9. Main structural features from the study area. See Figure 8 for location. (a,h,i) Growth strata in the Sijes/Chaco formation. (b) Erosional channel in the “Cara Cara strata” revealing the bedding polarity. (c) Strike-slip fault plane. (d,e) Thrust faults of the flower structure at Abra Moreta. (f) SC-

**structure indicating a top-to-the-NW shear. (g) High angle reverse fault between Pirgua and Acoite formation.**

---

Summing up, the tectonic setting of this sector of the Eastern Cordillera is characterized by a set of reverse and thrust faults, possibly re-activating Cretaceous extensional faults, carrying Pirgua and pre-Cretaceous formations on top of Tertiary basins. The regional mean direction of the slip vectors (roughly NW-SE) is predominantly oblique on N-S to NNE-SSW fault planes, producing an overall sinistral transpressive regime. Perhaps the most impressive feature of the area is represented by the tens of kilometer-scale strike-slip features. Their activity is marked not only by important damage zones, duplexes and flower structures, but also by the deposition of a thick pack of clastic deposits that grew as their dip became sub-vertical. This supposition is clearly attested by the presence of growth strata (Figure 9a, and 9i).

The discharge of huge clastic deposits indicates that deformation occurred during a phase of intense erosion, possibly related to the uplift of the structures. Growth strata within the Sijes/Chaco formation indicate that the strike-slip deformation was active in mid Miocene times.

The transition between thrusting and strike-slip tectonics probably occurred under a similar tectonic regime. In fact, this transition is possible during mountain building, as the minimum compressional axis (which is vertical) gets larger with the increasing gradient of potential energy (due to the uplift). Therefore, we may imagine that the tectonic regime progressively shifted from compressive to strike-slip during the uplift of the belt.

## **6. Discussion**

### **6.1. Paleomagnetic rotation pattern from the Eastern Cordillera**

Our paleomagnetic data document that the Eastern Cordillera between 22° and 24°S has undergone  $45.9^{\circ} \pm 9.4^{\circ}$  (Cretaceous sites, group A),  $30.1^{\circ} \pm 23.9^{\circ}$ , and  $15.4^{\circ} \pm 19.3^{\circ}$  CW rotations with respect to South America after the late Cretaceous (~80 Ma), Oligo-Miocene (20-30 Ma), and late Miocene-Pliocene (5-10 Ma), respectively (Table 3). Such rotation values are fully consistent with previous results from the Pirgua Formation in Abra Pampa [Coutand *et al.*, 1999], indicating at three sites a mean  $49.7^{\circ}$  post-Cretaceous CW rotation (Figure 1 and Table 1).

Error bars on our rotation values do not allow us to statistically discriminate whether the rotation started before (or after) 20-30 Ma, nor can we determine whether part of the rotation occurred as recently as after 5-10 Ma. As a consequence, though our data indicate that the Eastern Cordillera of northwestern Argentina rotated CW by about 45° with respect to the foreland during the orogenic episodes, and that (a part of) the rotation certainly occurred after 20-30 Ma, the rotation timing may be solely inferred considering other paleomagnetic data and both local and regional geological-geophysical evidence.

Relying on the systematic (though not statistically significant) decrease of the mean paleodeclination values over time (Figure 5), and on the timing of the shortening episodes in this region previously documented by *Boll and Hernández* [1986] *Coutand et al.* [2001], *Carrapa et al.* [2005] and *Carrapa and DeCelles* [2008], we suggest that the rotation started during the first Eo-Oligocene (30-40 Ma) tectonic episodes (Incaic phase) affecting the Eastern Cordillera, and that the roughly 45° rotation was completed after the deposition of the Miomarà Formation (5-10 Ma). Thus, a gross 1°/Ma Tertiary rotation rate can be calculated, though it is not possible to discriminate whether the rotation was steady over time or episodic. A rotation ending no earlier than late Miocene-Pliocene times is consistent with previous data from the Eastern Cordillera, documenting a post-7-15 Ma

15°-18° CW rotation [MacFadden *et al.*, 1990, 1995], and a post-2-13 Ma 10° CW rotation [Barke *et al.*, 2007] (Figure 1 and Table 1). Conversely, the lack of post-late Miocene rotations (reported by Somoza *et al.* [1996] and Prezzi and Alonso [2002] from Puna volcanic and sedimentary rocks west of our study area) might be related to a different rotational behavior of the central Puna with respect to the Eastern Cordillera domain. Other Neogene volcanics from the Puna and the Altiplano (SW and NW of the study area, respectively) document small (yet systematic) CW rotations [Prezzi *et al.*, 1996; Lamb, 2001a; MacFadden *et al.*, 1995; Roperch *et al.*, 2000; Prezzi *et al.*, 2004], though rocks from these studies in some cases are older than 10 Ma (i.e., the age of the supposed ending of the major deformation phase in the Altiplano-Eastern Cordillera). In any case, given the normal confidence cones of both site-mean and regional-mean paleomagnetic directions (5°-15°, for the most favorable cases), it is almost impossible to assess the statistical significance of small-magnitude (10°-15°) rotations from recent rocks. This limitation is inherent to the paleomagnetic technique.

Nevertheless, independent geophysical evidence strongly supports the hypothesis that the Andean salient has indeed undergone further rotations during the last 5-10 Myrs. In fact, GPS data document that CCW and CW rotations are presently occurring north and south (respectively) of the orocline axis [Allmendinger *et al.*, 2005, 2007], perfectly mirroring the paleomagnetic rotation pattern averaged over the geological past. This strongly suggests that the Andean tectonics have not significantly changed during the last tens of millions of years, and that the present-day tectonic regime may be extrapolated into the geological past, as previously proposed by Hindle *et al.* [2002].

Paleomagnetic directions from four sites from the Pirgua Formation (group B) located adjacent to the Yavi-Abra Pampa fault fall roughly 40° apart from the remaining

eight coeval sites (group A), and are roughly concordant with the cratonic South American paleofield (Figures 2 and 5; Tables 2 and 3). We think that this peculiar behavior of sites from group B has a local origin linked to the Yavi-Abra Pampa fault system. Neutral rotations were already demonstrated to occur near N-S striking left-lateral strike-slip faults from the southern central Andes by *Riller and Oncken* [2003], and interpreted as the result of local shear-induced rotations. Furthermore, the average strike of the slip vectors evaluated at two stations (St18 and St10) close to the Yavi-Abra Pampa fault are rotated about 60° CCW with respect to those observed at the remaining sites far from the fault (Figure 6). As CCW (CW) rotations in the vicinity of a strike-slip fault are definitely induced by a left-lateral (right-lateral) shear [*Sonder et al.*, 1986, 1994], we suggest that the Yavi-Abra Pampa fault had a dominant left-lateral displacement that induced along the fault wall a roughly 40° CCW rotation, almost annulling the 40°-50° regional CW rotation observed elsewhere in upper Cretaceous strata. Also, the average strike of the slip vectors at sites adjacent to the Yavi-Abra Pampa fault zone, which differs from those evaluated at other sites far from the fault, would be the result of this local CCW rotation.

This mechanism, previously recognized in the Luracatao and Calchaqui valleys (24°-27°S) by *Riller and Oncken* [2003], could also explain why *Coutand et al.* [1999] observed a mean 29.7° CW rotation in strata from the Pirgua Formation exposed a few kilometers to the north at Siete Hermanos, along the northward prosecution of the Yavi-Abra Pampa fault, while the same formation at Abra Pampa, far from faults, yielded an average 49.7° CW rotation.

Finally, we may also rule out the possibility that the last Quaternary right-lateral strike-slip fault activity documented in the area by *Cladouhos et al.* [1994] has significantly influenced the paleomagnetic rotational pattern.

## 6.2. Oroclinal test: implications for the structural style and deformation timing

We have performed an “oroclinal” test [e.g., *Schwartz and Van der Voo, 1983; Eldredge et al., 1985; Hirt and Lowrie, 1988*] on our paleomagnetic data, to verify whether in the Eastern Cordillera a statistically significant rotational difference (i.e., “oroclinal bending”) exists at sites characterized by different structural attitude. In Figure 10, we compare the site mean paleomagnetic declinations (in tilt corrected coordinates) to the local bed strikes, considered as proxies of structural directions.  $D_0=25^\circ$  and  $S_0=20^\circ$  were adopted as reference paleodeclination and structural direction values, respectively (reference values are trivial for the test result).

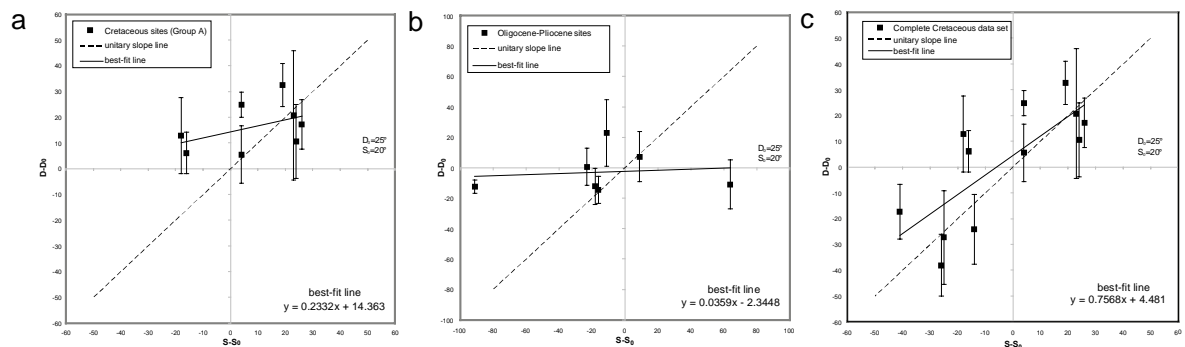


**Figure 10.** Paleomagnetic declination deviations versus relative strike of beds’ deviations for (a) late Cretaceous “group A” sites (see text), (b) Oligocene-Pliocene sites, and (c) the complete late Cretaceous data set [e.g., *Schwartz and Van der Voo, 1983*].  $D$  is the observed paleomagnetic declination at a site,  $D_0$  is the reference declination value.  $S$  is the observed bed strike at a site and  $S_0$  the reference bedding strike. Error bars for declination data are the respective  $\alpha_{95}/\cos(I)$  values.

We separately performed the oroclinal test on the Cretaceous sites of group A (i.e., without the four non-rotated sites adjacent to the Yavi-Abra Pampa fault (group B), Figure 10a), the Oligocene-Pliocene sites (Figure 10b), and the complete Cretaceous data set (Figure 10c). The slope of the best-fit line indicates the degree of correlation between paleomagnetic declinations and structural trends. A zero and a unitary slope of the best-fit

line imply that structural trend variability is not and is (respectively) due to paleomagnetic rotations. The statistical  $t$ -test (according to *Hirt and Lowrie* [1988]) is used to verify whether the slope values of the best-fit line calculated from our data set are statistically different from zero (indicating no paleomagnetic vs. structural correlation).

The  $t$ -test on the slope of the regression lines compared to zero slope gives  $t = 1.34$  and  $t = 0.28$  for the diagrams in Figure 10a and 10b, respectively. Both values are smaller than the critical  $t$  value at the 99% significance level ( $t_{99} = 2.99$  and  $t_{99} = 3.14$ , respectively), implying that the best-fit lines are statistically indistinguishable from zero-slope. Conversely, when the whole Cretaceous data set is considered (Figure 10c), the  $t$ -test yields  $t = 3.72$ , which is greater than the critical value at the 99% significance level ( $t_{99} = 2.71$ ). The result of the  $t$ -test for Figure 10c when the best-fit line is compared to the unitary-slope line ( $t = 1.20$ ) implies that both lines are statistically indistinguishable.

The tectonic implications of the results from the oroclinal test are twofold: first, thrust-fold structures from the Eastern Cordillera showing variable orientation (i.e., N-S to NE-SW) underwent an uniform regional CW rotation, with no oroclinal bending mechanism at the scale of our study area; second, oroclinal bending occurred at the four polyphase-rotated sites located adjacent to the Yavi-Abra Pampa fault (group B), when the entire Cretaceous data set (group A + group B) is considered. This implies that the local CCW rotation at sites located adjacent to the Yavi-Abra Pampa fault (inferred to be related to the strike-slip shear along this fault) occurred after the structural grain of the orogen was acquired, i.e., it postdates the onset of the deformation in the Eastern Cordillera of 30-40 Ma (according to *Bool and Hernández* [1988]; *Coutand et al.* [2001], *Carrapa et al.* [2005] and *Carrapa and DeCelles* [2008]). This time relationship among tectonic episodes is confirmed by the evidence that the strikes of the slip vectors along reverse faults evaluated

at two stations near the Yavi-Abra Pampa fault (St10 and St18, Figure 6) are rotated about 60° CCW with respect to those from other stations located far from major tectonic structures.

### **6.3. Style and timing of deformation in the Eastern Cordillera: interplay between compressive and strike-slip tectonics**

The paleomagnetic and structural evidence gathered at the Eastern Cordillera allows us to reconstruct the local tectonic history for the pre- and syn-orogenic episodes characterizing the deformation and uplift of the Central Andes (Figure 11). The deposition of the continental units of the Salta group started in Cretaceous times (Figure 11a) in the Salta Rift system. The inversion of pre-existing normal faults in Eo-Oligocene times (30-40 Ma) marked the onset of the Andean shortening in this sector (coeval to or a little later than the Incaic event in the internal part of the orogen). The end of the compressive tectonic phase is difficult to constrain, although several reverse faults are sealed by late Miocene deposits (around 10 Ma) further north.

The shortening stage was accompanied by a roughly 45° CW rotation, recorded along a thick yet discontinuous pile of continental sedimentary sequences (Pirgua, Moreta/Candado, and Miomarà formations). Approximately 30 degrees of rotation occurred during the Eocene to mid-Miocene interval (Figure 11b, the mean rotation values from the Pirgua and Miomarà formations are statistically different, see Table 3).

The slip vectors, as inferred by structural analysis of slickenside directions, are on average NW-SE striking (indicating a predominant SE-ward sense of displacement), though reverse and thrust fronts strike N-S to NNE-SSW (i.e., not orthogonal to the strike of the slip vectors).

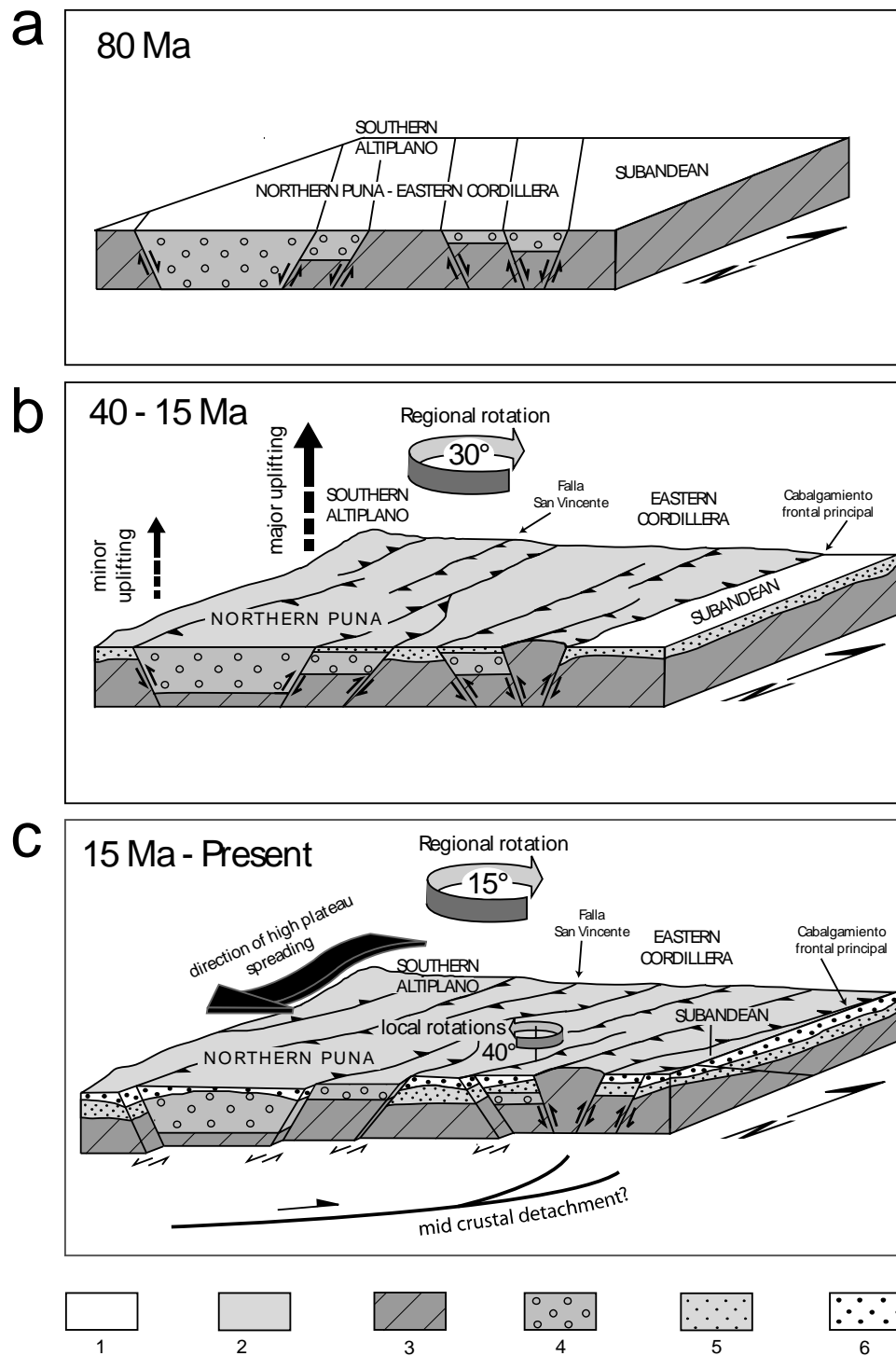


**Figure 11.** Schematic 3D-block diagram showing the proposed post-late Cretaceous evolution of the northern Puna-Eastern Cordillera-Subandean domain. 1, Undeformed domains. 2, Deformed domains. 3, Acoite formation [Ordovician]. 4, Salta group sedimentary rocks [upper Cretaceous-Eocene]. 5, Moreta/Candado formation [Oligocene-Miocene]. 6, Syn-tectonic deposits (Sijes/Chaco and Miomara formation [middle Miocene-Pliocene]). (a) During the late Cretaceous (~80 Ma), elongated NW-SE depressions limited by normal faults developed in the frame of the regionally extensive Salta rift, guiding the deposition of the syn/post-rift continental units of the Salta group. (b) Between ~40 and 15 Ma thrust-sheet emplacement in the southern Altiplano, northern Puna, and Eastern Cordillera, frequently inverting inherited extensional structures, accounted for part (~30°) of the total CW

**rotation recorded by the Cretaceous sedimentary rocks. Uplifting of the plateau occurred by the early Miocene (when it attained no more than a third of its modern elevation), and was more enhanced in the north, near the orocline apex. (c) At about 15 Ma ~N-S left-lateral strike-slip faults accommodated the southward spreading of the Central Andes plateau, and locally inducing up to 40° CCW rotations at the fault walls. Moreover, since 10-15 Ma to Present, a further regional ~15° CW rotation affected the Eastern Cordillera.**

---

Obliquity between slip vectors and major reverse and thrust faults suggests that compressive tectonics reactivated late Cretaceous normal faults trending not orthogonal to the mean regional shortening direction (which is roughly NW-SE according to previous studies [*Cladouhos et al.*, 1994; *Marrett et al.*, 1994; *Urreiztieta et al.*, 1996; *Coutand et al.*, 2001; *Riller and Oncken*, 2003]), yielding sinistral transpression on N-S striking faults. Structural, stratigraphic, and paleomagnetic evidence from the study area have shown that left-lateral strike-slip tectonics played a significant role in the evolution of this sector of the Andean belt. Map view structural relationships between thrust/reverse and strike-slip structures, the results of the oroclinal test, and the rotation of the thrusting-related directions of the slip vectors along the Yavi-Abra Pampa fault, strongly suggest that the mid-late Miocene left-lateral strike-slip tectonics postdate thrust-sheet emplacement. The age of the strike-slip activity along the N-S faults is constrained by a growing clastic sequence of the Sijes/Chaco formation (14.26±0.19 Ma, <sup>40</sup>Ar/<sup>39</sup>Ar age on reworked biotite, *Cladouhos et al.* [1994]) deposited during ongoing deformation. The lateral displacement of this fault should have been large enough to produce a local 40° CCW rotation along the Yavi-Abra Pampa fault (Figure 11c), as documented by paleomagnetic data and local deflection of slip vectors (Figures 2 and 6).

Evidence of orogen-parallel sinistral strike-slip faults is fairly well documented in the southern Central Andes. North of the investigated region, near Tupiza (22°S-21°S), *Herail et al.* [1996] and *Müller et al.*, [2002] reported sinistral N-S strike-slip to transpressional tectonics active from the end of the Oligocene to the late Miocene. Orogen-

parallel sinistral strike-slip faults have also been documented south of the studied area (24°-27°S), in the Luracatao and Calchaqui valleys [Riller and Oncken, 2003], the Santa Maria valley [Strecker *et al.*, 1989], and at the Olcapato-El Toro fault [Allmendinger *et al.*, 1983; Riller *et al.*, 2001]. These structures, associated with NE-striking fault zones, formed rhomb-shaped deformation domains, giving rise to internally drained sub-basins within the south-central Andes [Ramos, 1977; Riller and Oncken, 2003].

Generally, the transition from a compressive to a strike-slip regime is indeed expected if the strike-slip regime activated during uplift of the belt, as the minimum compressional axis (which is vertical in a compressive regime) gets larger with the increasing gradient of potential energy (i.e., mountain building and uplift). The linkage between strike-slip tectonics and uplift is supported by the syn-tectonic deposition of thick clastic wedges at ridge sides, attesting to a strong erosion episode also driven by uplift. Paleoelevation data indeed agree in documenting that this portion of the belt acquired the significant elevation of 1.5-2 km around the middle-late Miocene [Gregory-Wodzicki, 2000; Hoke and Garzzone, 2008].

Our paleomagnetic data collected in the Humahuaca valley (sites Ti, PG, and TM, Figure 2) also indicate that while strike-slip was active to the west, the shortening focused frontward, where upper Miocene-lower Pliocene deposits show an average 15° CCW rotation (Figure 11c). These results, along with GPS data documenting that the northern and southern Central Andes are presently undergoing CCW and CW rotations (respectively), mirroring the paleomagnetic rotation pattern [Allmendinger *et al.*, 2005, 2007], support the hypothesis that rotation and bending processes could continue until recent times. If so, we speculate that the presence of rotations within the Eastern Cordillera in absence of major faulting since ~9 Ma could be explained by the existence of a deep-

crustal shear zone or basement mega-thrust (as proposed by *McQuarrie and DeCelles* [2001] and *McQuarrie* [2002]) over which these domains have been passively shifted eastward and rotated with no significant internal deformation.

Earlier works [e.g., *Marrett et al.* 1994; *Cladouhos et al.* 1994; *Lamb* 2001a, 2001b] have described N-S to NNE-SSW striking Quaternary right-lateral strike-slip faults as the most recent tectonic feature in the Puna plateau and Eastern Cordillera. Within our study area, we have found no evidence of such kinematics, which in principle should postdate the structural evolution we have documented here.

#### **6.4. A southward lateral growth of the Puna plateau?**

The relevance of the strike-slip tectonics in the growth and deformation of the Central Andean plateau emerges only from a few studies and remains controversial. Previous models include: (i) strike-slip deformation between individual thrust sheets, sinistral in the south and dextral in the north, similar to flexural slip folding [*Müller et al.*, 2002]; (ii) strain partitioning related to shortening oblique to the strike of the orogen [*Randall et al.*, 1996; *Abels and Bischoff*, 1999]; (iii) sinistral shear on orogen-parallel deformation zones linked to tectonic segmentation into rhomb-shaped domains (longitudinally southward propagating), controlled by the gradient of crustal shortening [*Riller and Oncken*, 2003].

Here we suggest a “composite” rotational model, where large-scale oroclinal bending and local small-block rotations occur concurrently, as also previously proposed for the Andean belt by several other authors [*Beck et al.*, 1994; *Butler et al.*, 1995; *Lamb*, 2001a; *Riller and Oncken*, 2003]. Relying on our paleomagnetic data and interpretation, regional CW rotations related to the development of the Andean arcuate belt occurred in

the Eastern Cordillera from 30-40 Ma to Present, as GPS data suggest [*Allmendinger et al.*, 2005, 2007]. Accordingly, an average rotation rate of about  $1^\circ/\text{Myr}$  can be calculated, though obviously both a quasi-continuous rotation through time, and distinct episodes of rotations separated by intervals of “rotational quiescence”, are compatible with paleomagnetic data. Conversely, the strike-slip tectonics and (associated) CCW rotations that we document have only occurred in the past 15 Ma, and are coeval with a relatively recent regional-scale tectonic event. In fact, the strong uplift of the Altiplano-Puna plateau up to the remarkable height of 4000 m observed today is thought to have occurred mostly during the Neogene (last 10 Ma) [e.g., *Gregory-Wodzicki*, 2000; *Riller et al.*, 2001; *Hartley*, 2003; *Hoke and Garzzone*, 2008]. In contrast to the composite rotational models put forward in the past, and in agreement with the model by *Riller and Oncken* [2003], we suggest that the development of N-S strike-slip activity (and related local rotations) in the Eastern Cordillera (at the border with the Altiplano-Puna plateau) is related to the major uplifting phase of the plateau, and thus not directly linked to the large-scale development of the Andean salient (which started earlier).

According to this hypothesis, the onset of the strike-slip activity would be linked to the lateral (southward) growth of the Central Andean plateau. The plateau uplift started in the central part of the Andean salient, where the shortening amount was greater [e.g., *Kley and Monaldi*, 1998; *McQuarrie et al.*, 2005, 2008]. This may have induced a compressive stress (related to body forces) at the plateau margins, and progressive spreading of the plateau toward its northern and southern margins. Recent work by *Riller and Oncken* [2003] strongly supports the southward growth of the Puna plateau. They propose that the southward decrease in (I) thickness of Cenozoic foreland deposits, (II) width of the eastern fold-and-thrust belt, (III) age of coarse conglomerates at the eastern margin of the Puna,

and (IV) age of the intra-orogenic sub-basins, are the consequence of continuous southward growth of the plateau.

Present-day GPS rotations are almost ubiquitous over both internal and external Andean belt sectors [Allmendinger *et al.*, 2005, 2007], consequently they (as well as older paleomagnetic rotations) should be driven by a deep crustal shear zone (whose existence has been put forward by McQuarrie and DeCelles [2001] and McQuarrie [2002]) finally merging eastward into the surface thrust structures along the external Subandean Belt. Conversely, the local CCW rotations related to left-lateral strike-slip activity are a local phenomenon accommodating the southward plateau spreading, and occurred in a peculiar moment within the long-lasting formation of the Bolivian orocline. Thus, strike-slip tectonics in the Eastern Cordillera may represent a second-order effect of the huge crustal thickening kinematically requested at the apex of a 3000 km long salient undergoing progressive bending during the last 40 Myrs.

## 7. Conclusions

New paleomagnetic and structural evidence from the Eastern Cordillera at 22°-24°S reveals the relative timing and geometric-rotational characteristics for the interplay of thrust tectonics and strike-slip activity. These data may also suggest a novel interpretation for the geodynamics of this structural system.

The paleomagnetism of sandy-silty continental sedimentary rocks yields  $45.9^{\circ} \pm 9.4^{\circ}$ ,  $30.1^{\circ} \pm 23.9^{\circ}$ , and  $15.4^{\circ} \pm 19.3^{\circ}$  CW rotations with respect to South America occurring after the late Cretaceous (~80 Ma), Oligo-Miocene (20-30 Ma), and late Miocene-Pliocene (5-10 Ma), respectively. After considering previous paleomagnetic results from adjacent Andean sectors, ages for onset of tectonic deformation, and regional

GPS evidence from the Andes, we infer that a regional-scale CW rotation of about 45° occurred along with shear along reverse and thrust faults from the Eo-Oligocene (30-40 Ma) to Present, at an average rotation rate of roughly 1°/Myr. Since the major deformation phase ceased in the Eastern Cordillera at ~9 Ma, the recent and possibly present-day rotation was likely driven by a deep shear zone, merging further east with the active Andean thrust front.

Since about 15 Ma, N-S left-lateral strike-slip faults reactivated late Cretaceous normal faults (previously also inverted as reverse faults), and locally induced up to 40° CCW rotations at the fault walls, virtually annulling (along the faults) the regional CW rotation. The occurrence of strike-slip faulting was practically synchronous with the uplift of the Puna plateau. Thus, we propose, in agreement with the model by *Riller and Oncken* [2003], that strike-slip activity accommodated the southward spreading of the high-altitude Puna plateau. This tectonic process represented a second order effect of the large-scale development of the Andean salient, and occurred only after the crust had been overthickened by large shortening at the rear of the arc apex.

## **8. Acknowledgements**

The inception and completion of this work owes much to Ruben Somoza, who receives our deep gratitude for both his generosity and scientific integrity. Many thanks to B. Coira and A. Perez for both the fruitful discussions on the geology of the studied area, and the logistic support given for the sampling campaign at Abra Pampa. MM gratefully acknowledges a Marco Polo grant from the Bologna University, and financial support from the Italian Ministry for Foreign Affairs, awarded by the Official responsible for scientific cooperation G. Paparo.

**Table 1.** Previous paleomagnetic data from Cretaceous to Neogene rocks from Central Andes <sup>a</sup>

Label	Locality/Formation	Age (Ma)	Coordinate (Lat °S/Long °W)	D (deg)	I (deg)	$\alpha_{95}$ (deg)	R $\pm$ $\Delta$ R (deg)	Reference
1	Descanso	18.6-12.1	14.5/71.4	146.6	32.3	11.9	-31.0 $\pm$ 11.6	<i>Rousse et al.</i> [2005]
2	Umayo	58-75	15.8/70.1	319.0	-24.0	10.0	-33.0 $\pm$ 9.0	<i>Butler et al.</i> [1995]
3	Huacochullo	26.5-12.1	16.0/70.5	166.4	25.8	6.5	-11.3 $\pm$ 6.4	<i>Rousse et al.</i> [2005]
4	Aréquipa	100	16.5/71.8	300.0	-47.0	15.0	-56.0 $\pm$ 18.0	<i>Roperch and Carlier</i> [1992]
5	Viacha	25-35	16.8/68.5	169.0	32.0	11.0	-12.0 $\pm$ 11.0	<i>Roperch et al.</i> [2000]
6	Salla	26	17.2/67.7	353.0	-37.0	5.0	-12.0 $\pm$ 15.0	<i>MacFadden et al.</i> [1990]
7	Micaña	8-6	17.5/67.0	355.2	-25.8	5.9	-4.8 $\pm$ 5.2	<i>MacFadden et al.</i> [1990]
8	Totora Formation	14-9	17.5/68.3	347.0	-22.0	3.0	-10.2 $\pm$ 3.3	<i>Roperch et al.</i> [1999]
9	North Chuquichambi	41	17.5/68.3	329.0	-27.0	8.0	-36.0 $\pm$ 16.0	<i>Roperch et al.</i> [1996]
10	Ilo, Peru	ca. 80	17.5/71.4	331	-40.0	9.0	-18.0 $\pm$ 9.0	<i>Roperch and Carlier</i> [1992]
11	Mor-Eucalyptus	13-5	17.8/67.3	355.9	-34.3	18.6	-1.4 $\pm$ 18.3	<i>Barke et al.</i> [2007]
12	Tiupampa	58-60	18.0/65.5	167.2	38.1	7.9	-5.3 $\pm$ 8.9	<i>Butler et al.</i> [1995]
13	La Yarada	80	18.1/70.7	331.0	-38.0	6.0	-22.0 $\pm$ 8.0	<i>Roperch and Carlier</i> [1992]
14	Arica	ca. 19	18.5/70.0	358.0	-34.0	8.0	1.3 $\pm$ 7.9	<i>Roperch et al.</i> [1999]
15	Camaraca Formation	143	19.2/70.3	351.0	-40.0	7.0	-6.0 $\pm$ 8.0	<i>Scanlan and Turner</i> [1992]
16	La Palca	60-71	19.5/65.8	212.9	42.1	4.4	40.6 $\pm$ 6.0	<i>Butler et al.</i> [1995]
17	Los Frailes	13-2	19.5/66.3	6.7	-43.3	6.9	9.9 $\pm$ 7.7	<i>Barke et al.</i> [2007]
18	Inchasi	4-3	19.7/65.3	356	-31.1	5.6	-1.1 $\pm$ 5.6	<i>MacFadden et al.</i> [1993]
19	Quehua	13-7	20.0/67.0	15.3	-37.9	9.3	15.3 $\pm$ 9.5	<i>MacFadden et al.</i> [1995]
20	Altiplano volcanics	14-7	20.0/68.0	9.5	-47.2	11.6	12.5 $\pm$ 13.9	<i>Lamb</i> [2001a]
21	Monteagudo	15-25	20.5/64.0	5.0	-32.0	7.0	8.0 $\pm$ 6.9	<i>Lamb</i> [2001a]
22	Cerdas	16	20.8/66.3	10.0	-39.0	7.0	12.0 $\pm$ 8.0	<i>MacFadden et al.</i> [1995]
23	Cerdas	16-15	21.0/66.0	10.1	-39.1	7.0	10.1 $\pm$ 7.2	<i>MacFadden et al.</i> [1995]
24	Quebrada Honda	13-12	22.0/65.0	17.8	-40.7	3.9	17.8 $\pm$ 4.1	<i>MacFadden et al.</i> [1990]
25	Siete Hermanos	ca. 80	22.2/65.5	22.3	-22.4	12	29.7 $\pm$ 11.6 <sup>b</sup>	<i>Coutand et al.</i> [1999]
26	El Loa	11.3	22.3/68.6	1.0	-46.0	7.0	4.3 $\pm$ 8.3	<i>Somoza et al.</i> [1999]
27	Purilactis Formation	75-115	22.3/68.3	36.0	-40.7	4.1	~35	<i>Somoza and Tomlinson</i> [2002]
27	El Loa Formation	10	22.3/69.0	354.4	-36.0	4.9	-3.5 $\pm$ 6.6	<i>Somoza and Tomlinson</i> [2002]
27	San Pedro Formation	30	22.4/68.1	6.2	-38.0	6.7	5.4 $\pm$ 7.8	<i>Somoza and Tomlinson</i> [2002]
28	Bermejo	20-30	22.4/64.5	35.0	-44.0	19.0	38.0 $\pm$ 21.6	<i>Lamb</i> [2001a]
29	Laguna de Pozuelos basin	12	22.4/66.0	5.4	-45.9	6.1	7.6 $\pm$ 7.8	<i>Prezzi et al.</i> [2004]
30	Lipiyoc	9	22.5/67.0	1.0	-46.0	7.0	4.0 $\pm$ 8.3	<i>Somoza et al.</i> [1996]
30	Paciencia Group	28-17	22.6/68.3	20.0	-27.0	13.5	17.0 $\pm$ 13.0	<i>Harley et al.</i> [1992]
31	Purilactis Formation	65-55	22.8/68.4	41.0	-36.0	9.0	29.0 $\pm$ 10.0	<i>Harley et al.</i> [1992]
32	Abra Pampa	ca. 80	22.8/65.7	42.3	-47.7	19.0	49.7 $\pm$ 7.8 <sup>b</sup>	<i>Coutand et al.</i> [1999]
33	Morro Blanco	10	23.0/66.5	356.1	-41.1	2.7	-0.6 $\pm$ 3.3	<i>Prezzi and Alonso</i> [2002]
33	Lomo Blanca mine	7	23.1/66.4	1.3	-41.6	12.7	9.0 $\pm$ 6.8	<i>Prezzi and Alonso</i> [2002]
34	Coranzuli	52	23.1/66.4	216.4	38.4	9.5	39.8 $\pm$ 8.4	<i>Prezzi and Alonso</i> [2002]
35	Baquedano, Chile	45	23.4/69.8	56.0	-41.0	9.0	51 $\pm$ 19	<i>Dupont-Nivet et al.</i> [1996]

Label	Locality/Formation	Age (Ma)	Coordinate (Lat °S/Long °W)	D (deg)	I (deg)	$\alpha_{95}$ (deg)	R $\pm$ $\Delta$ R (deg)	Reference
36	Negro de Chorrillos-S. Geronimo	10	24.2/66.4	17.0	-31.9	14	19.5 $\pm$ 13.5	<i>Coutand et al.</i> [1999]
37	Puna Salteña	17	24.6/67.1	14.0	-41.0	5.0	16 $\pm$ 8	<i>Prezzi et al.</i> [1996]
38	Volcanics, Chile	51.5	25.2/69.7	25.0	-50.0	6.0	20 $\pm$ 18	<i>Dupont-Nivet et al.</i> [1996]
39	Volcanics, Chile	105	25.6/70.1	26.0	-46.0	19.0	29 $\pm$ 23	<i>Dupont-Nivet et al.</i> [1996]
40	Pirgua group	96	26.5/66.0	4.0	-45.0	6.0	12 $\pm$ 9	After <i>Aubry et al.</i> [1996]
41	Remolino Pluton Dykes	126	26.7/70.2	37.0	-39.0	12.0	40 $\pm$ 13	<i>Randall et al.</i> [1996]
42	Hualfin-Santa Maria	13	27.0/66.5	15.0	-37.0	11.0	17 $\pm$ 13	After <i>Aubry et al.</i> [1996]
43	Tinogasta	13	28.1/67.3	6.0	-37.0	9.0	8 $\pm$ 11	After <i>Aubry et al.</i> [1996]
44	Huaco-Mogna	13	29.6/68.1	13.0	-44.0	10.0	15 $\pm$ 13	After <i>Aubry et al.</i> [1996]

<sup>a</sup> See Figure 1.

<sup>b</sup> Recalculated using paleopoles from *Besse and Courtillot [2002]*.

Label refers to numbers in Figure 1. D and I, tilt-corrected declination and inclination;  $\alpha_{95}$ , statistical parameter after *Fisher [1953]*; R $\pm$  $\Delta$ R, rotation value and respective error with respect to stable South America, reported from *Lamb [2001a]*, *Prezzi and Alonso [2002]*, and *Barke et al. [2007]*.

**Table 2.** Paleomagnetic results from the Eastern Cordillera.

Site	Formation	Geographic coordinates		Age	Age (Ma)	Bedding (°)	Low temperature component							High temperature component/ChRM											
		Latitude S	Longitude W				Tilt corrected		In situ			Tilt corrected		In situ			k	$\alpha_{95}(\circ)$	n/N	R (°)	$\Delta R (\circ)$	F (°)	$\Delta F (\circ)$		
							D(°)	I(°)	D(°)	I(°)	k	$\alpha_{95}(\circ)$	n/N	D(°)	I(°)	D(°)								I(°)	
PA	Pirgua	22°25.41'	65°46.61'	Late Cretaceous	~80	284 - 43	-	-	-	-	-	-	-	-	-	-	-	-	-	-	-	-	-	-	-
PB	Pirgua	22°44.43'	65°50.96'	Late Cretaceous	~80	313 - 51	-	-	-	-	-	-	-	45.7	-61.3	348.7	-34.7	15.2	12.1	11/14	53.1	21.0	26.1	12.4	-
PC	Pirgua	22°42.26'	66°03.05'	Late Cretaceous	~80	129 - 61	-	-	-	-	-	-	-	-	-	-	-	-	-	-	-	-	-	-	-
PD	Pirgua	22°45.32'	65°34.38'	Late Cretaceous	~80	249 - 97	349.0	-19.2	318.6	-7.0	17.8	22.4	4/5	7.7	-22.2	311.2	-23.3	20.4	9.8	12/14	15.2	10.0	-13.0	11.1	-
PE *	Pirgua	22°45.42'	65°34.79'	Late Cretaceous	~80	265 - 85	-	-	-	-	-	-	-	41.6	12.4	17.3	-43.5	44.6	10.1	6/6	46.6	8.5	-35.0	8.7	-
PF	Pirgua	22°44.77'	65°35.92'	Late Cretaceous	~80	265 - 85	-	-	-	-	-	-	-	357.7	-26.4	327.9	-5.5	12.4	16.3	8/10	5.1	15.3	-8.8	15.1	-
PG	Miomarà	23°17.96'	65°21.83'	Miocene-Pliocene	10-5	274 - 40	-	-	-	-	-	-	-	10.4	-37.1	342.0	-31.3	51.7	7.2	9/10	12.6	7.6	-8.9	6.3	-
PH	Pirgua	23°41.80'	65°41.02'	Late Cretaceous	~80	309 - 40	-	-	-	-	-	-	-	57.6	-46.1	14.9	-44.0	111.2	5.8	7/8	65.1	8.7	9.5	9.1	-
PI	Pirgua	22°45.77'	65°42.89'	Late Cretaceous	~80	316 - 40	23.9	-36.7	6.3	-15.3	13.2	21.9	5/12	42.2	-37.3	17.6	-25.5	30.7	7.6	13/15	49.7	9.4	2.1	10.0	-
PL	Pirgua	22°46.79'	65°32.08'	Late Cretaceous	~80	92 - 7	223.1	28.3	225.6	23.6	47.9	9.8	6/6	37.8	-47.5	43.3	-43.1	46.0	10.0	6/6	45.3	12.9	12.2	11.2	-
PM	Pirgua	22°49.00'	65°31.38'	Late Cretaceous	~80	294 - 24	-	-	-	-	-	-	-	49.8	-30.1	34.2	-37.7	256.1	4.2	6/7	57.3	6.9	-5.2	8.7	-
PN	Pirgua	22°47.29'	65°32.49'	Late Cretaceous	~80	134 - 21	-	-	-	-	-	-	-	35.6	-46.3	57.6	-45.3	24.6	9.9	10/11	43.1	12.6	11.0	11.2	-
PO	Pirgua	22°26.19'	65°34.49'	Late Cretaceous	~80	96 - 32	-	-	-	-	-	-	-	0.9	-36.7	23.8	-33.0	19.0	10.8	11/12	8.3	12.0	1.9	11.7	-
PP	Pirgua	22°23.44'	65°34.15'	Late Cretaceous	~80	84 - 60	-	-	-	-	-	-	-	346.9	-36.6	24.4	-22.6	50.1	9.6	6/7	-5.7	11.0	1.9	11.1	-
PQ	Pirgua	22°22.98'	65°34.52'	Late Cretaceous	~80	114 - 93	-	-	-	-	-	-	-	30.5	-36.7	60.6	7.0	108.1	8.9	4/8	37.9	10.4	2.0	10.7	-
PR	Pirgua	22°21.55'	65°35.09'	Late Cretaceous	~80	274 - 65	-	-	-	-	-	-	-	31.1	-33.2	339.8	-35.2	57.9	6.8	9/9	38.5	8.5	-1.4	9.7	-
PS	Pirgua	22°25.20'	65°10.82'	Late Cretaceous	~80	314 - 32	-	-	-	-	-	-	-	-	-	-	-	-	-	-	-	-	-	-	-
PT *	Candado	22°54.95'	65°33.79'	Oligocene-Miocene	30-20	170 - 38	-	-	-	-	-	-	-	192.3	-13.9	193.3	21.3	11.6	28.2	4/4	-165.0	23.1	-35.7	22.3	-
PU	Candado	22°55.26'	65°33.48'	Oligocene-Miocene	30-20	199 - 20	-	-	-	-	-	-	-	12.5	-13.5	11.4	-33.3	207.5	4.2	7/11	13.8	5.8	-33.7	5.9	-
PV *	Pirgua	22°44.95'	65°35.74'	Late Cretaceous	~80	170 - 68	-	-	-	-	-	-	-	17.2	3.8	39.2	-53.0	7.4	20.3	9/10	-157.8	16.2	-37.0	16.2	-
PW	Pirgua	23°34.30'	65°25.88'	Late Cretaceous	~80	109 - 78	-	-	-	-	-	-	-	-	-	-	-	-	-	-	-	-	-	-	-
PX *	Pirgua	22°44.89'	65°35.52'	Late Cretaceous	~80	184 - 72	10.5	5.4	19.9	-65.7	11.9	20.2	6/11	12.6	2.6	27.3	-67.7	10.9	24.3	5/9	-162.4	19.2	-39.8	19.3	-
PY	Pirgua	23°34.30'	65°25.88'	Late Cretaceous	~80	284 - 132	-	-	-	-	-	-	-	-	-	-	-	-	-	-	-	-	-	-	-
TA	Moreta	22°31.73'	65°51.95'	Oligocene-Miocene	30-20	267 - 52	-	-	-	-	-	-	-	25.6	-30.2	346.4	-39.5	28.4	10.6	8/10	26.9	10.7	-16.6	9.7	-
TB	Candado	22°55.04'	65°35.66'	Oligocene-Miocene	30-20	262 - 67	-	-	-	-	-	-	-	-	-	-	-	-	-	-	-	-	-	-	-
TE	Moreta	22°31.73'	65°51.94'	Oligocene-Miocene	30-20	254 - 65	-	-	-	-	-	-	-	-	-	-	-	-	-	-	-	-	-	-	-
TF*	Candado	22°44.12'	65°36.84'	Oligocene-Miocene	30-20	104 - 100	332.4	13.8	4.4	-42.6	16.6	17.0	6/6	243.7	24.5	220.0	-49.1	7.5	23.7	7/8	69.2	20.4	-24.8	19.2	-
TG	Candado	22°44.12'	65°36.84'	Oligocene-Miocene	30-20	299 - 64	-	-	-	-	-	-	-	212.2	20.7	191.5	11.6	16.3	15.4	7/9	33.5	13.7	-26.3	13.0	-
TH	Moreta	22°25.78'	65°51.21'	Oligocene-Miocene	30-20	99 - 85	343.8	12.1	353.5	-23.4	3.6	29.8	10/12	228.0	56.1	252.2	-16.1	12.4	12.2	13/17	49.3	18.0	9.5	10.7	-
Ti	Miomarà	22°57.50'	65°23.27'	Miocene-Pliocene	10-5	272 - 78	-	-	-	-	-	-	-	12.7	-25.9	338.1	-14.7	17.5	10.7	12/12	14.9	9.7	-19.7	8.9	-
TL	Miomarà	22°57.61'	65°23.13'	Miocene-Pliocene	10-5	289 - 68	-	-	-	-	-	-	-	-	-	-	-	-	-	-	-	-	-	-	-
TM	Miomarà	23°21.87'	65°22.42'	Miocene-Pliocene	10-5	354 - 33	-	-	-	-	-	-	-	14.1	-50.7	7.3	-19.0	44.4	10.2	6/7	16.3	13.0	4.6	8.5	-

\*Discarded sites (see text). The geographic coordinates are referred to WGS84 datum. Age in Ma is from the geologic timescale of *Gradstein et al.* [2004]. Bedding is expressed in dip azimuth-dip values. D and I are site mean declination and inclination calculated before and after tectonic correction for the low and high temperature components and the characteristic remanent magnetization direction (ChRM). k and  $\alpha_{95}$  are statistical parameters after *Fisher* [1953]. n/N is number of samples giving reliable results/number of studied samples at a site. Site mean Rotation (R) and Flattening (F) values, and relative errors ( $\Delta R$  and  $\Delta F$ ) (according to *Demarest* [1983]) are relative to coeval D and I South American values expected at the sampling area considering South American paleopoles from *Besse and Courtillot* [2002].

**Table 3.** Mean paleomagnetic directions for sites of similar age.

Age	Age (Ma)	Formation	N	In situ				Tilt corrected				R (°)	$\Delta R$ (°)	F (°)	$\Delta F$ (°)
				D(°)	I(°)	k	$\alpha_{95}$ (°)	D(°)	I(°)	k	$\alpha_{95}$ (°)				
Late Cretaceous (group A)*	~80	Pirgua	8	25.0	-36.0	7.5	21.7	40.9	-42.6	43.9	8.4	45.9	9.4	-0.9	7.5
Late Cretaceous (group B)*	~80	Pirgua	4	350.7	-24.6	5.1	45.4	358.6	-30.7	60.5	11.9	3.6	11.3	-12.8	10.0
Oligocene-Miocene	30-20	Moreta/Candado	4	341.8	-35.3	2.7	70.4	27.4	-30.5	13.7	25.7	30.1	23.9	-19.2	20.5
late Miocene-Pliocene	10-5	Miomarà	3	349.2	-22.2	22.5	26.6	12.3	-37.9	42.2	19.2	15.4	19.3	-5.2	15.2

\*See text for definition of groups A and B. N, number of sites. Legend as in Table 2.

**Table 4.** Results of the fold test (according to *McFadden* [1990]) for sites of similar age.

Age	N	In situ statistics					Unfolded statistics					$\xi_{95\%}$
		D(°)	I(°)	k	$\alpha_{95}$ (°)	$\xi$	D(°)	I(°)	k	$\alpha_{95}$ (°)	$\xi$	
Oligocene-Pliocene	7	6.1	-21.9	5.6	28.0	5.783	21.1	-34.0	18.8	14.3	1.791	3.086
Late Cretaceous (group A)*	8	25.0	-36.0	7.4	21.7	4.701	40.9	-42.6	43.9	8.5	1.232	3.298
Late Cretaceous (group B)*	4	350.7	-24.6	5.1	45.4	3.849	358.9	-30.9	61.8	11.8	1.475	2.335

\* See text for definition of groups A and B. N, number of sites. D and I are mean declination and inclination, respectively. K and  $\alpha_{95}$  are the *Fisher's* [1953] statistical parameters.  $\xi$  and  $\xi_{95\%}$  are the statistical scos parameter and its 95% critical value, respectively (see *McFadden* [1990]).

## **CHAPTER 4**

### ***The Patagonian Orocline***

**Paleomagnetic evidence for a pre-early Eocene (~50 Ma) bending of the Patagonian orocline (Tierra del Fuego, Argentina): paleogeographic and tectonic implications. (\*)**

**(\*) Manuscript submitted to *Earth and Planetary Science Letters*.**

Marco Maffione,<sup>1,4</sup> Fabio Speranza<sup>1</sup>, Claudio Faccenna<sup>2</sup>, Eduardo Rossello<sup>3</sup>

<sup>1</sup>Istituto Nazionale di Geofisica e Vulcanologia, Rome, Italy.

<sup>2</sup>Dipartimento di Scienze Geologiche, Università di Roma Tre, Rome, Italy.

<sup>3</sup>CONICET, Departamento de Ciencias Geológicas, FCEN, Universidad de Buenos Aires, Buenos Aires, Argentina.

<sup>4</sup>Dipartimento di Fisica, Università di Bologna, Bologna, Italy.

**Abstract**

The southernmost segment of the Andes of southern Patagonia and Tierra del Fuego forms a ~700 km long orogenic re-entrant with an interlimb angle of ~90° known as Patagonian orocline. No reliable paleomagnetic evidence has been gathered so far to assess whether this great orogenic bend is a primary arc formed over an articulated paleomargin, or is due to bending of a previously less curved (or rectilinear) chain. Here we report on an extensive paleomagnetic and anisotropy of magnetic susceptibility (AMS) study carried out on 22 sites (298 oriented cores), predominantly sampled in Eocene marine clays from the external Magallanes belt of Tierra del Fuego. Five sites containing magnetite and subordinate iron sulphides yield a positive fold test at the 99% significance level, and

document no significant rotation since ~50 Ma. Thus, the Patagonian orocline is either a primary bend, or an orocline formed after Cretaceous-earliest Tertiary rotations. Our data imply that the opening of the Drake Passage between South America and Antarctica (probably causing the onset of Antarctica glaciation and global climate cooling), was definitely not related to the formation of the Patagonian orocline, but was likely the sole consequence of the  $32\pm 2$  Ma Scotia plate spreading. Well-defined magnetic lineations gathered at 18 sites from the Magallanes belt are sub-parallel to (mostly E-W) local fold axes, while they trend randomly at two sites from the Magallanes foreland. Then AMS data show that the Fuegian Andes were characterized by a N-S compression and northward displacing fold-thrust sheets during Eocene (50-35 Ma), an unexpected kinematics considering coeval South America-Antarctica relative motion. Both paleomagnetic and AMS data reveal no significant influence from the E-W left-lateral Magallanes-Fagnano strike-slip fault system (MFFS), running few kilometres south of our sampling sites. We conclude that strike-slip activity in the Fuegian Andes postdated the Eocene thrust tectonics, and that strike-slip fault offset may range in the lower bound values (~20 km) among those proposed so far. In any case our data exclude any influence of strike-slip tectonics on the genesis of the great orogenic bend called Patagonian orocline.

**Keywords:** paleomagnetism, tectonics, Patagonian orocline, Fuegian Andes, Drake Passage, Magallanes belt.

## 1. Introduction

The Andean Cordillera is one of the longest mountain belts of the Earth, spanning the entire Pacific margin of South America. Below 50°S, the trend of the southernmost

Andean belt decidedly changes from ~N-S (Patagonian Andes) to ~E-W (Fuegian Andes), forming a regional orogenic re-entrant arc commonly referred to as the Patagonian orocline (Carey, 1958; Figure 1). This arcuate structure forms at the intersection between the South America, Scotia, and Antarctica plates (Figure 1).

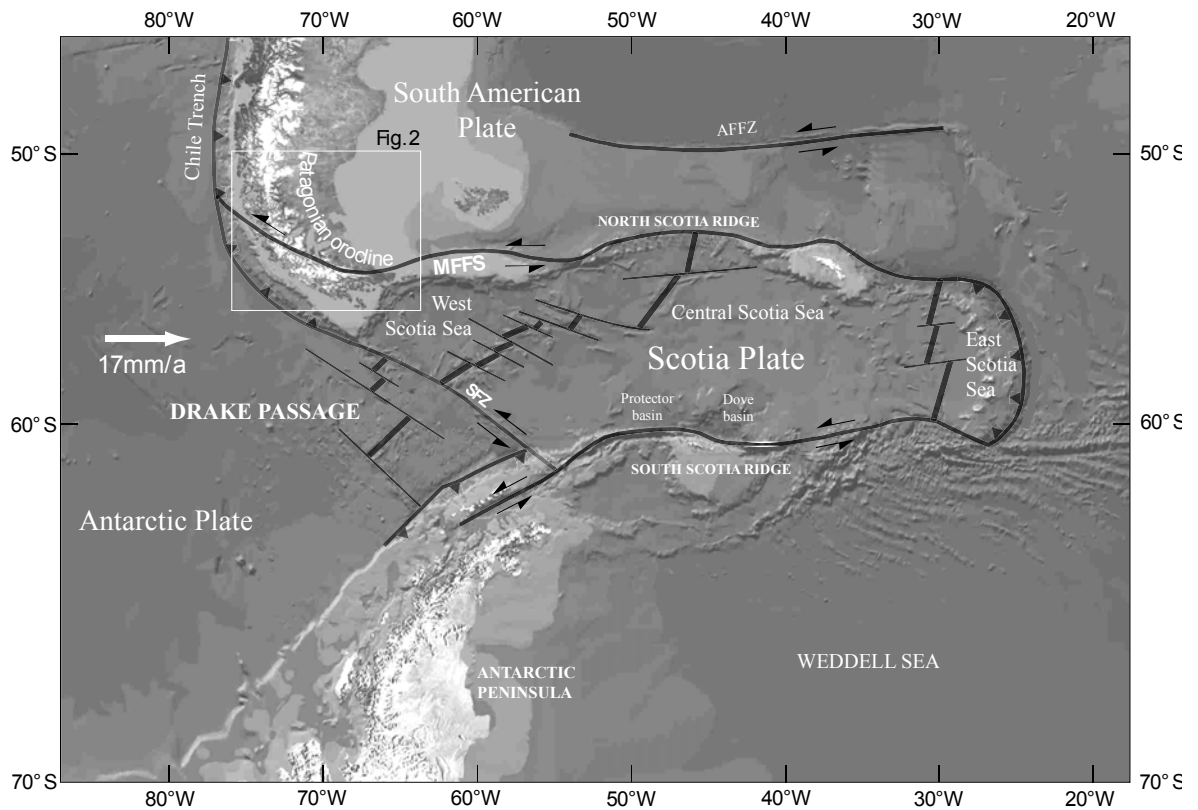


**Figure 1. Digital elevation model of the Scotia plate and surrounding regions from the General Bathymetric Chart of the Oceans (GEBCO). Lines with triangles and thicker black lines indicate trench zones and oceanic ridges, respectively. White arrow indicates the movement of the Antarctic plate with respect to South America, according to DeMets *et al.* (1990). SFZ, Shackleton Fracture Zone. AFFZ, Agulhas Falkland Fracture Zone. MFFS, Magallanes-Fagnano fault system.**

The Scotia plate with its deep-sea pathway (Drake Passage) separating the South American and Antarctic continents (Barker, 2001; Eagles *et al.*, 2005; Livermore *et al.*, 2005; Lodolo *et al.*, 1997, 2006) is thought to have caused first-order outcomes in the global paleoclimate. In fact, the formation of a deep water “gateway” between South America and Antarctica determined the onset of the Antarctic Circumpolar Current (ACC)

(Lawver and Gahagan, 2003; Barker et al., 2007a), which is considered one of the main causes for the developing of extensive ice sheets in the Antarctic continent (Barker et al., 2007b) and the onset of global climate cooling at the Eocene/Oligocene boundary (Zachos et al., 2001).

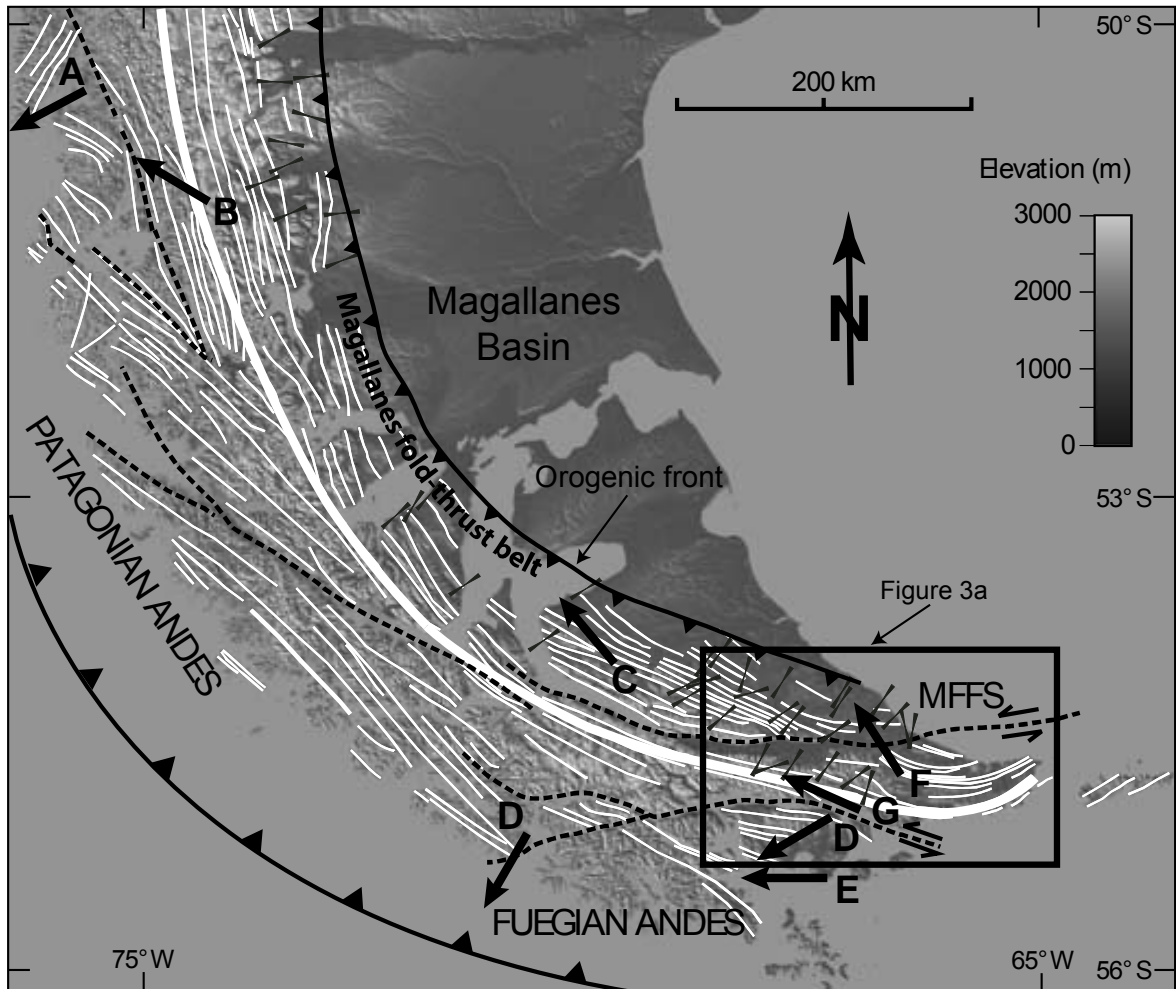


**Figure 2.** Digital elevation model of the southernmost Andes, redrawn from Ghiglione and Cristallini (2007), showing orogenic structural trends (thin solid white lines), major strike-slip faults (dashed black lines), basement thrust front (thick solid white line), strikes of shortening axes (black bars) according to Diraison et al. (2000), and previous paleomagnetic directions from igneous or metamorphic rocks (A=Rapalini et al., 2001; B=Rapalini et al., 2004; C=Burns et al., 1980; D=Dalziel et al., 1973; E=Cunningham et al., 1991; F=Baraldo et al., 2002; G=Rapalini et al., 2005). MFFS, Magallanes-Fagnano fault system. Location is in Figure 1.

The opening of the Drake passage is commonly related to the spreading of the Scotia Sea, where oceanic anomalies from the West Scotia ridge have been dated back to 34-28 Ma (*Lawver and Gahagan, 2003; Livermore et al., 2005; Lodolo et al., 2006*), but its tectonic relationships with the symmetrical curved margins of the Patagonian orocline and the Antarctic Peninsula, are still unclear.

Though a wealth of geological and geophysical data have documented ongoing tectonic deformation in the Patagonian and Fuegian Andes since ~100 Ma to Present [*Dalziel and Palmer, 1979; Winslow, 1982; Cunningham, 1993, 1994, 1995; Kohn et al., 1995; Diraison et al., 2000; Lodolo et al., 2003, 2006; Kraemer, 2003; Ghiglione and Ramos, 2005*], the kinematics and timing for the formation of the Patagonian orocline are unknown. Recently, a non-rotational origin for the Patagonian orocline was proposed, and its curved shape was related to the tectonic heritage from an original articulated paleomargin [*Ramos and Aleman, 2000; Diraison et al., 2000; Ghiglione, 2003; Ghiglione and Ramos, 2005; Ghiglione and Cristallini, 2007*]. However, paleomagnetic investigations of metamorphic and igneous rocks from the Fuegian Andes [*Dalziel et al., 1973; Burns et al., 1980; Cunningham et al., 1991; Roperch et al., 1997; Beck et al., 2000; Rapalini et al., 2001, 2004, 2005; Baraldo et al., 2002; Iglesia Llanos et al., 2003*] have systematically revealed so far northwestward-directed paleodeclinations (Figure 2), which conversely seem to indicate that the orogenic bend formed after rotations of mountain belt segments with respect to South America. The problem with the available paleomagnetic data is that both igneous and metamorphic rocks lack paleo-horizontal indicators (implying possible significant biases on the declination values), and the age of magnetization acquisition (related to the last metamorphic peak) is questionable (see *Rapalini, 2007* for an updated review). Therefore, both the rotational vs. non-rotational character of the

Patagonian orocline and the rotation timing (if existing) are paleomagnetically unconstrained at present.

The most external part of the Patagonian orocline is represented by the thin-skinned Magallanes fold and thrust belt (Figure 2), where upper Cretaceous to Miocene marine and continental sediments are exposed along folds and thrust sheets sub-parallel to the large-scale orogenic bend [Winslow, 1982; Olivero *et al.*, 2001, 2003; Ghiglione *et al.*, 2002; Ghiglione, 2002; Olivero and Malumiàn, 2008]. The 7 km-thick sedimentary succession exposed in the Magallanes belt of Tierra del Fuego offers in principle the opportunity to paleomagnetically document with great accuracy the magnitude and timing of vertical axis rotations in the southernmost Andes, overcoming the problem of a safe paleo-horizontal evaluation for metamorphic and igneous rocks.

In this paper we report the results of an extensive paleomagnetic study of Eocene to early Miocene marine and continental sedimentary rocks from the southeastern Magallanes fold and thrust belt of Tierra del Fuego. Our data represent the first reliable paleomagnetic constraint on the formation of the Patagonian orocline, and document that no vertical axis rotations occurred since early Eocene times (~50 Ma). A pre-existing Patagonian orocline since at least 50 Ma implies that the significantly younger (~32 Ma) opening of the Drake Passage was not influenced by Andean tectonics, but was rather the exclusive consequence of the Scotia Sea spreading onset.

## **2. Background**

### **2.1. Geology of the Patagonian and Fuegian Andes, and structural setting of the Magallanes belt of Tierra del Fuego**

From southwest to northeast, five broad morphostructural provinces parallel to the arc can be recognized in the southernmost Andes: (1) a coastal magmatic arc (Patagonian batholith), (2) a marginal basin assemblage (Rocas Verdes basin), (3) a metamorphic core zone (Cordillera Darwin), (4) a fold and thrust belt (Magallanes fold and thrust belt), and (5) an undeformed foreland basin (Magallanes (or Austral) basin). The Magallanes basin is composed by a thick (~7 km) succession of marine and continental sedimentary units ranging from Jurassic to Miocene age [Thomas, 1949; Winslow, 1982; Olivero and Malumián, 1999, 2008; Olivero et al., 2001, 2003; Ghiglione et al., 2002; Ghiglione and Ramos, 2005; Malumián and Olivero, 2006; Rossello et al., 2008].

The southern part of the Patagonian orocline is also cut by the Magallanes-Fagnano fault system (MFFS), a roughly E-W en-echelon left-lateral strike-slip fault array running for more than 600 km from the Atlantic to the Pacific coast of South America, and considered the present-day South America-Scotia plate boundary [Cunningham, 1993, 1995; Barker, 2001; Lodolo et al., 2003; Eagles et al., 2005; Rossello, 2005]. The total displacement of the MFFS, as well as the age of its formation are still a matter of debate [Cunningham, 1995; Olivero and Martinioni, 2001; Lodolo et al., 2003; Rossello et al., 2004a; Eagles et al., 2005; Torres-Carbonell et al., 2008a], whereas its present-day activity is substantiated by both GPS [Smalley et al., 2003] and seismological [Pelayo and Wiens, 1989] evidence.

Fold axes and thrust faults from Tierra del Fuego strike from NW-SE in the inner sectors, to E-W and ENE-WSW along the Atlantic coast [Ghiglione et al., 2002; Ghiglione, 2002; Ghiglione and Ramos, 2005; Torres-Carbonell et al., 2008b] (Figures 2 and 3). Folds are usually asymmetric with axes predominantly plunging westward [Ghiglione et al., 2002; Torres-Carbonell et al., 2008b]. According to Diraison et al.

[2000], the shortening directions (as inferred by 1600 striated fault planes from the Mesozoic-Cenozoic sedimentary cover of the fold-thrust belt) are not always perfectly orthogonal to the main structures, and progressively rotate from N75° to N43° from the Patagonian to the Fuegian Andes, respectively (Figure 2). Finally, some NNE-trending right-lateral strike-slip faults (i.e., Fueguina fault, Figure 3b) have been interpreted as R' Riedel shear zones associated to the major MFFS [Ghiglione *et al.*, 2002].

The first orogenic episodes at the southern margin of South America were triggered by the mid to late Cretaceous inversion and closing of the back-arc Rocas Verdes marginal basin [Dalziel *et al.*, 1974; Cunningham, 1994, 1995], yielding shortening, ductile deformation, and regional metamorphism, with peak metamorphism occurring between 100 and 90 Ma [Kohn *et al.*, 1995; Cunningham, 1995]. A first episode of rapid uplift and cooling of the metamorphic core between 90 and 70 Ma [Kohn *et al.*, 1995] predated the late Campanian (~70 Ma) northward propagation of compression in the Magallanes basin [Winslow, 1982; Ghiglione *et al.*, 2002]. At least four main compressive events, related to an equivalent number of unconformities recorded by the sedimentary successions, occurred in the Magallanes belt in late Paleocene (61-55 Ma), early-middle Eocene (50-43 Ma), early Oligocene (~33 Ma), and early Miocene (~21 Ma) times [Olivero and Malumiàn, 1999; Ghiglione *et al.*, 2002; Kraemer, 2003; Ghiglione and Ramos, 2005; Malumiàn and Olivero, 2006; Torres-Carbonell *et al.*, 2008b]. Virtually undeformed post-early Miocene sedimentary rocks testify the end of tectonic shortening in the southern Magallanes basin [Ghiglione, 2002; Ghiglione *et al.*, 2002]. The tectonic history of the Magallanes basin has been interpreted as related to either compressive [Ghiglione and Ramos, 2005] or extensional [Ghiglione *et al.*, 2008] tectonics of Eocene age, followed by an Oligocene-early Miocene episode in which wrench tectonics dominated.

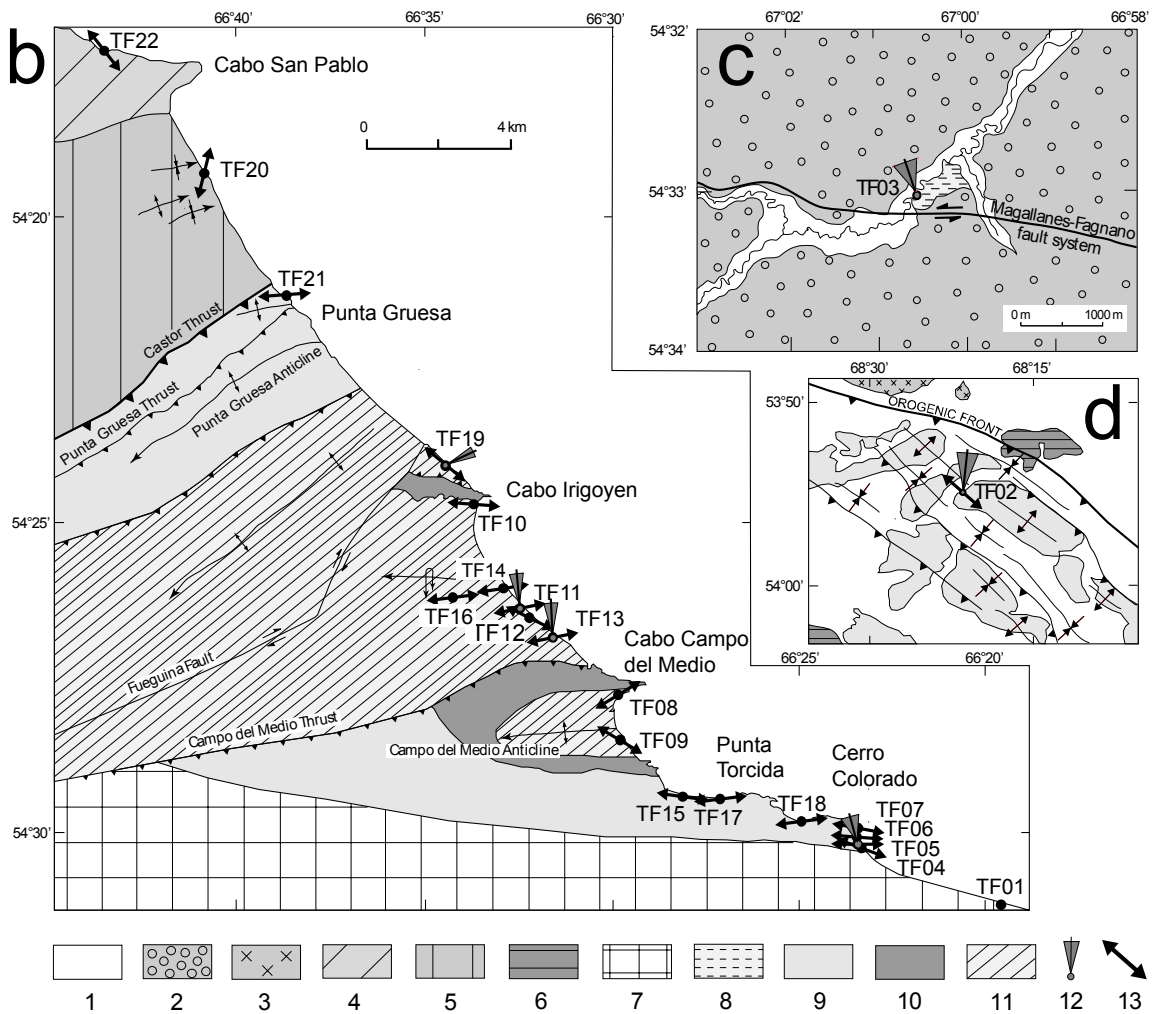
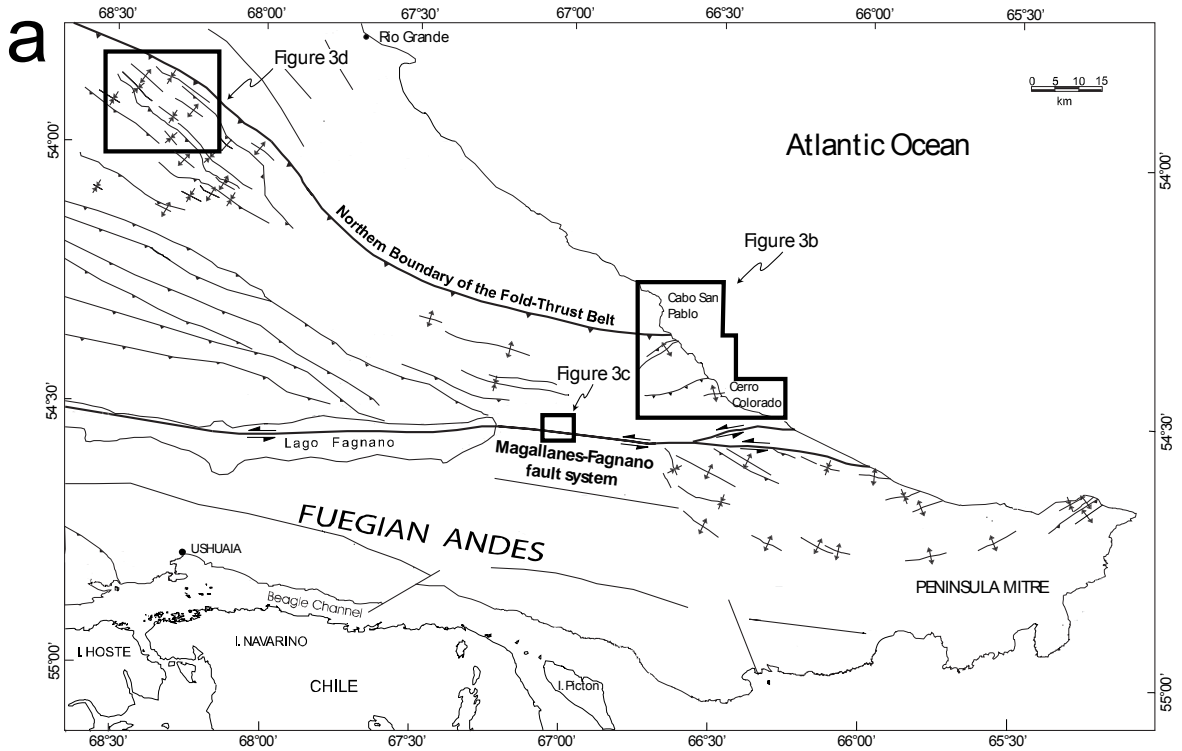


**Figure 3. Structural and geological maps of the study areas, redrawn from *Ghiglione et al.* (2002) (Figure 3b, 3c, 3d). Legend: 1, Alluvial sediments (Quaternary). 2, Glacial deposits (Quaternary). 3, Carmen Silva formation (middle Miocene). 4, Capas de Cabo San Pablo (early Miocene). 5, Desdemona formation (late Oligocene-early Miocene). 6, Cabo Domingo group (Oligocene-Miocene). 7, Capas de la Estancia Maria Cristina (earliest Oligocene). 8, Sloggett formation (late Eocene-early Oligocene). 9, Cerro Colorado formation (upper middle to late Eocene). 10, Leticia formation (upper middle Eocene). 11, Punta Torcida formation (early Eocene). 12, Site-mean rotation with respect to South America with respective rotation error (grey cone). 13, Direction of the (in situ) site-mean magnetic lineation ( $K_{\max}$ ).**

---

## **2.2. Previous paleomagnetic data from the Patagonian orocline and the Antarctic Peninsula**

Though *Carey* [1958] first proposed that the abrupt curvature of the southernmost Andes could be due to oroclinal bending of an initially straight orogen, paleomagnetic evidence from the southernmost Andes has been gathered only since the 1970s [*Dalziel et al.*, 1973; *Burns et al.*, 1980; *Cunningham et al.*, 1991; *Roperch et al.*, 1997; *Beck et al.*, 2000; *Rapalini et al.*, 2001, 2004, 2005; *Baraldo et al.*, 2002; *Iglesia Llanos et al.*, 2003]. These studies indicate significant post-late Cretaceous counterclockwise (CCW) rotations (up to 118°) affecting the internal southern Andes below latitude 48°S (Figure 2). It is likely that (at least part of) the largest magnitude rotations arise from local tectonic effects linked to thrusting [*Iglesia Llanos et al.*, 2003], or strike-slip faulting [*Rapalini et al.*, 2001].

However, the earliest paleomagnetic studies [*Dalziel et al.*, 1973; *Burns et al.*, 1980] do not pass modern reliability criteria of laboratory procedures [e.g., *Beck*, 1988], while all data from Patagonian and Fuegian Andes, were invariantly gathered from igneous or metamorphic rocks, thus suffer of significant uncertainties on the paleo-horizontal surface and age of magnetization, as well as of possible incomplete averaging of the paleosecular variation of the geomagnetic field.

In detail, three localities from the southern Patagonian Andes at a 47°S latitude do not show any significant rotation, thus defining the northern limit of the CCW-rotating domain [Roperch *et al.*, 1997; Beck *et al.*, 2000; Iglesia Llanos *et al.*, 2003]. To the south, a post-late Jurassic CCW rotation of 39°, 57°, and 62° has been documented from sedimentary and igneous rocks at Lago San Martin north (49°S, 72.2°W), Lago San Martin south (49.1°S, 72.5°W), and Lago Argentino (50.2°S, 72.8°W), respectively [Iglesia Llanos *et al.*, 2003]. Further south, Rapalini *et al.* [2001] have evidenced a post-early Cretaceous CCW rotation of 118° from basalts and lavas at the Madre de Dios Archipelago (50.4°S, 75.4°W, Figure 2), while Rapalini *et al.* [2004] have documented a 59° post-late Cretaceous CCW rotation from ophiolites at the southernmost Patagonian Andes (51.7°S, 73.6°W). An extensive paleomagnetic study carried out by Burns *et al.* [1980] on volcanic and metamorphic rocks throughout the Patagonian and Fuegian Andes revealed post-late Jurassic-early Cretaceous 27-40° CCW rotations. Conversely, igneous rocks of the Navarino Island and adjacent regions of Chile yielded post-94 and post-77 Ma 150° and 120° CCW rotations, respectively [Dalziel *et al.*, 1973], while a 90° post-late Cretaceous CCW rotation was obtained from volcanic and sedimentary rocks [Cunningham *et al.*, 1991]. Igneous rocks sampled by Baraldo *et al.* [2002] and Rapalini *et al.* [2005] in the inner part of the orogenic belt from Tierra del Fuego documented a 33° to 66° post-late Cretaceous CCW rotation.

Finally, the arcuate shape of the Antarctic Peninsula, mirroring to the Patagonian orocline, could suggest a related tectonic evolution. The paleomagnetic data from the Antarctic Peninsula [Grunow, 1993, and references therein] documented two distinct phases of rotation, clockwise (CW) with respect to East Antarctica between 175 and 155

Ma, due to the early opening in the Weddell Sea basin, and CCW with respect to West Antarctica in the 155-130 Ma time interval.

### 3. Sampling and methods

In December 2007 we performed an extensive paleomagnetic sampling campaign within the southeastern part of the Magallanes belt of Tierra del Fuego (Figures 2 and 3). Because of the widespread cover of glacial deposits and the scarce road network, most of the samples (except for sites TF02 and TF03) were collected along the cliffs of the Atlantic coast between Cabo San Pablo and Cerro Colorado (Figure 3). Lower Eocene to lower Miocene marine fine-grained sediments (siltstones and mudstones) were systematically sampled (only at site TF03 continental clays were gathered).

The oldest sampled marine sediments are those from the Punta Torcida Fm. (early Eocene, *Olivero and Malumiàn, 1999, 2008*), a major ~400 m thick regressive unit dominated by dark-grey mudstones with scarce intercalations of light-grey fine sandstones. This formation is unconformably covered by the upper middle Eocene Leticia Fm., consisting of grey and greenish fine, bioturbated, glauconitic, tuffaceous or lithic sandstones with subordinated fine conglomerates, mudstones and tuffaceous sandstones. The Leticia Fm. is followed by the upper middle to late Eocene Cerro Colorado Fm., a major transgressive-regressive sequence consisting of a vertical stacking of four coarsening- and thickening-upwards sequences with a very high sedimentation rate. Each member is composed by dark-grey mudstones at the base, intercalation of mudstones and light-grey sandstones in the middle part, and thick grey or yellowish fine to coarse sandstones at the top. Finally, the younger sampled rocks are those from the Capas de la Estancia Maria Cristina (earliest Oligocene, *Malumiàn and Olivero, 2006*) and the Cabo

Domingo Group, in turn including the Desdemona (late Oligocene-early Miocene, *Ghiglione, 2002; Malumiàn and Olivero, 2006*), the Capas de Cabo San Pablo (early Miocene, *Malumiàn and Olivero, 2006*), and the Carmen Silva (middle Miocene, *Codignotto and Malumiàn, 1981*) Formations.

The continental deposits of the Sloggett Fm. (late Eocene-early Oligocene, *Rossello et al., 2004b; Olivero and Malumiàn, 2008*) sampled at site TF03 are conglomerates and sandstones grading laterally and vertically to mudstones and coal measures, including large trees.

In total, we collected 298 cylindrical oriented samples at 22 sites (Tables 1 and 2) using a petrol-powered portable drill cooled by water. Site distribution within the sedimentary succession is as follows (Table 1): eight sites were sampled from the early Eocene Punta Torcida Fm., ten sites from the upper middle-late Eocene Cerro Colorado Fm., one site from the late Eocene-early Oligocene Sloggett Fm., one site from the earliest Oligocene Capas de la Estancia Maria Cristina, one site from the late Oligocene-early Miocene Desdemona Fm., and one site from the early Miocene Capas de Cabo San Pablo Fm. At each site we gathered 9-18 cores (14 on average), spaced in at least two outcrops in order to try to average out the secular variation of the geomagnetic field.

All samples were oriented in situ using a magnetic compass, corrected to account for the local magnetic field declination value at the sampling area ( $\sim 12^\circ$  during the sampling campaign period, according to NOAA's National Geophysical Data Centre (<http://www.ngdc.noaa.gov>)).

Once selected the most effective temperature steps through the use of pilot specimens, one sample from each core was thermally demagnetized in eight-nine steps up to  $360^\circ\text{C}$ . All natural remanent magnetization (NRM) measurements were carried out in the

magnetically shielded room of the paleomagnetic laboratory of the Istituto Nazionale di Geofisica e Vulcanologia (INGV, Rome, Italy), using a DC-SQUID cryogenic magnetometer (2G Enterprises, USA). Demagnetization data were plotted on orthogonal diagrams [Zijderveld, 1967], and magnetization components were isolated by principal component analysis [Kirschvink, 1980]. Rotation and flattening values with respect to stable South America for the individual sites were evaluated according to *Demarest* [1983], using reference South American paleopoles from *Besse and Courtillot* [2002].

The low-field anisotropy of magnetic susceptibility (AMS) of all specimens was investigated by a KLY-3 bridge (AGICO), while magnetic mineralogy experiments were only performed on selected specimens from each site. We studied the hysteresis properties and the acquisition of an isothermal remanent magnetization (IRM) up to 500 mT, using a Micromag Alternating Gradient Magnetometer (AGM, model 2900). We also investigated the thermal change of the magnetic susceptibility during a heating-cooling cycle from room temperature to 700°C, using an AGICO CS-3 apparatus coupled to the KLY-3 bridge, and the thermal demagnetization of a three-component IRM imparted on the specimen axes, according to *Lowrie* [1990]. Fields of 2.7, 0.6 and 0.12 T were successively imparted on the z, y, and x sample axes (respectively) with a Pulse Magnetizer (Model 660, 2G Enterprises).

## **4. Results**

### **4.1. Magnetic mineralogy**

Hysteresis measurements consistently indicate the predominance of a paramagnetic fraction (likely clayey minerals) in the induced magnetization, being the hysteresis loops represented by lines passing very close to the axes origin (Figure 4a). The few

“ferromagnetic” (sensu lato) fraction shows saturation remanence ( $M_{rs}$ ) values of  $\sim 2$   $nAm^2$ , and coercivity of remanence ( $B_{cr}$ ) in the range of 28-33 mT (Figure 4b).

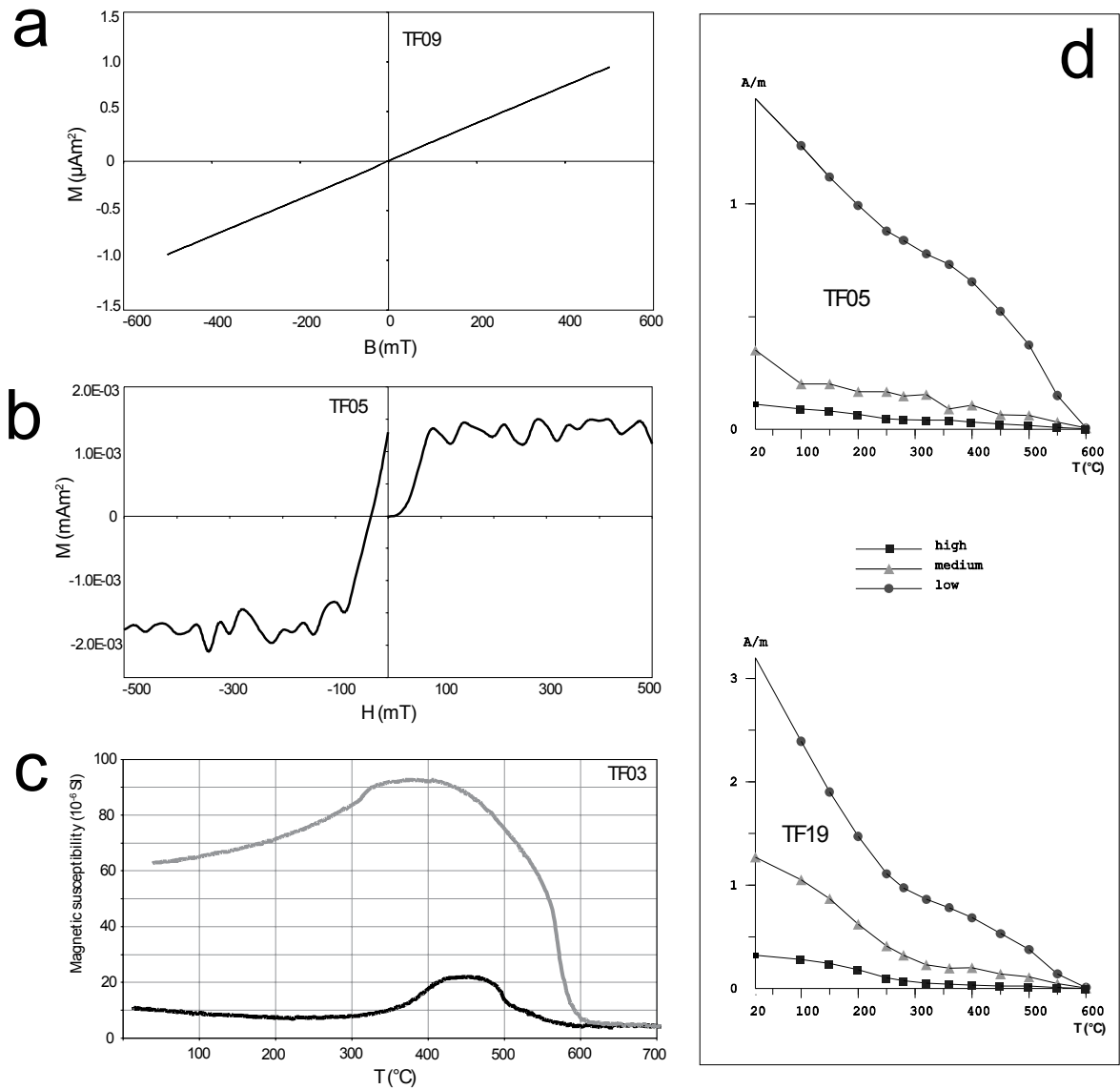


**Figure 4. Results of the magnetic mineralogy analyses for representative samples. (a) Hysteresis cycle, (b) isothermal remanent magnetization (IRM) acquisition curve, (c) thermal variation of the low-field magnetic susceptibility during a heating-cooling cycle (black and grey line, respectively), and (d) thermal demagnetization of a three-component IRM according to the method of Lowrie [1990].**

Thermomagnetic curves (Figure 4c) yield a hyperbolic trend up to  $\sim 300^{\circ}C$  during heating, thus confirming the predominant contribution of the paramagnetic fraction to the low-field susceptibility (i.e., Hrouda, 1994). A susceptibility increase between 350 and

520°C and the path of the cooling curve (revealing a Curie temperature of ~580°C), suggest the formation of new magnetite from the paramagnetic matrix. Finally, the thermal demagnetization of a three-component IRM (Figure 4d) reveals that the “ferromagnetic” minerals are represented by a largely predominant soft fraction demagnetized between 550 and 600°C. At sites TF02 and TF19 the soft and the intermediate coercivity fraction also undergo a significant drop between 300 and 400°C.

In summary, the magnetic mineralogy experiments reveal that paramagnetic clayey minerals dominate the low-field susceptibility, while a small amount of “ferromagnetic” fraction is generally represented by magnetite, and by a mixture of magnetite and iron sulphides at sites TF02 and TF19.

#### **4.2. Anisotropy of magnetic susceptibility**

The AMS parameters at both the specimen and the site levels were evaluated using Jelinek statistics [*Jelinek*, 1977, 1978], and are reported in Table 1. The site-mean susceptibility values, ranging from 126 to 302 x 10<sup>-6</sup> SI (205 x 10<sup>-6</sup> SI, on average), confirm the predominant contribution of the paramagnetic clayey matrix on both the low-field susceptibility and AMS [e.g., *Rochette*, 1987; *Averbuch et al.*, 1995; *Sagnotti et al.*, 1998; *Speranza et al.*, 1999). The shape of the AMS ellipsoid is predominantly oblate, with a mean value of the shape factor (T) of 0.47 (Table 1), suggesting a prevailing sedimentary fabric [*Hrouda and Janàk*, 1976]. In addition, the low values of the P' parameter (1.030-1.070) indicate that the sediments underwent mild deformation. The magnetic foliation (given by the clustering of the K<sub>min</sub> axes) is well defined at all sites except for sites TF01 and TF03 (Figure 5), and it is always parallel to the local bedding plane, confirming that the sediments host a predominant sedimentary-compactional magnetic fabric.

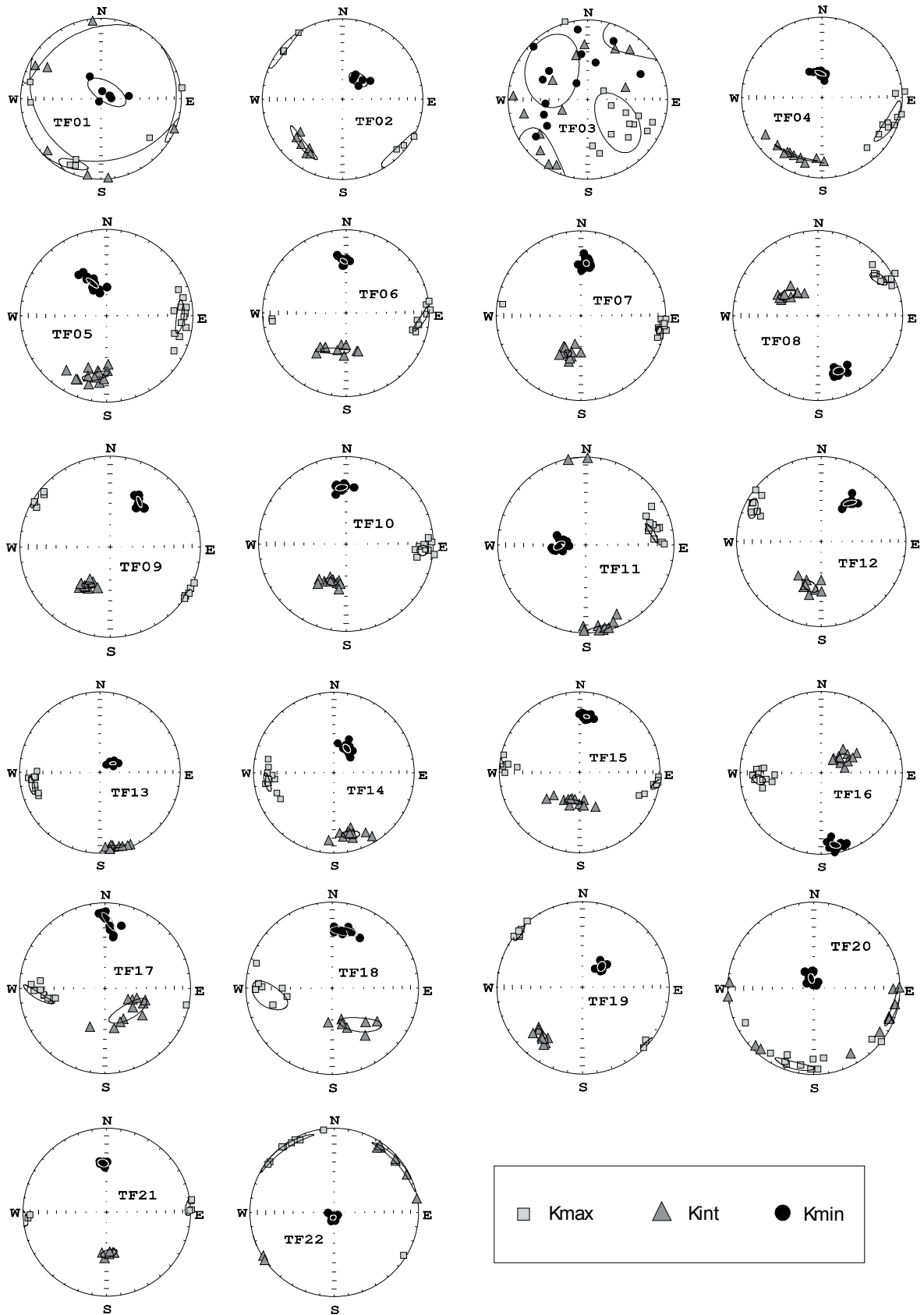


Figure 5. Schmidt equal-area projections, lower hemisphere, of the (in-situ coordinates) principal axes of the AMS ellipsoid and their respective 95% confidence ellipse, for all sampled sites (see Table 1).

The sites yielding a well-defined magnetic fabric are also characterized by a well-developed magnetic lineation, as documented by the clustering of  $K_{\max}$  axes from the individual specimens (12 and 8 sites display an  $e_{12}$  value lower than  $10^\circ$  and  $24^\circ$ , respectively, Table 1). Magnetic lineations trend roughly E-W (on average) in the Magallanes belt (i.e., sub-parallel to local fold axes and thrust fault trends, Figure 3b and 3d), while they are ~N-S oriented at two sites located in the foreland basin.

### 4.3. Paleomagnetism

Only eight (out of 22) sites yielded a measurable remanent magnetization, well above the noise level of the magnetometer ( $\sim 5 \mu\text{A/m}$ ). Their characteristic remanent magnetization directions (ChRMs) were isolated between  $120\text{-}210^\circ\text{C}$  and  $360^\circ\text{C}$ , after the removal of a scattered low temperature component (Figure 6). Site-mean directions (evaluated according to *Fisher* [1953]), are well defined, the  $\alpha_{95}$  values being comprised between  $9.7^\circ$  and  $19.9^\circ$  ( $13.5^\circ$  on average, Figure 7 and Table 2). Two out of the eight magnetized sites (TF08 and TF09) were discarded because of their sub-horizontal paleomagnetic directions (while a  $-75^\circ$  inclination is expected at the sampling localities considering the 50 Ma paleopole for South America). The remaining six reliable paleomagnetic sites are equally distributed into the normal and reverse polarity state, and yield, except for site TF19, NNW-directed directions (when considered in the normal polarity state).

There are three lines of evidence which support the primary nature of the ChRMs evaluated for the six reliable sites from Tierra del Fuego: (1) both the in-situ and tilt-corrected directions are far from the local geocentric axial dipole (GAD) field direction ( $D=0^\circ$ ,  $I=-70.0^\circ$ ; Figure 7), thus excluding a magnetic overprint; (2) dual paleomagnetic

polarities suggest magnetization acquisition during at least two magnetic polarity chrons;  
 (3) the McFadden's (1990) fold test performed on five out of six sites (excluding the scattered site TF19) is positive at the 99% significance level ( $\xi_{in situ}=4.2$ ;  $\xi_{unfolded}=0.8$ ;  $\xi_{99\%}$  critical value=3.6), thus supporting a pre-tilting magnetization acquisition.

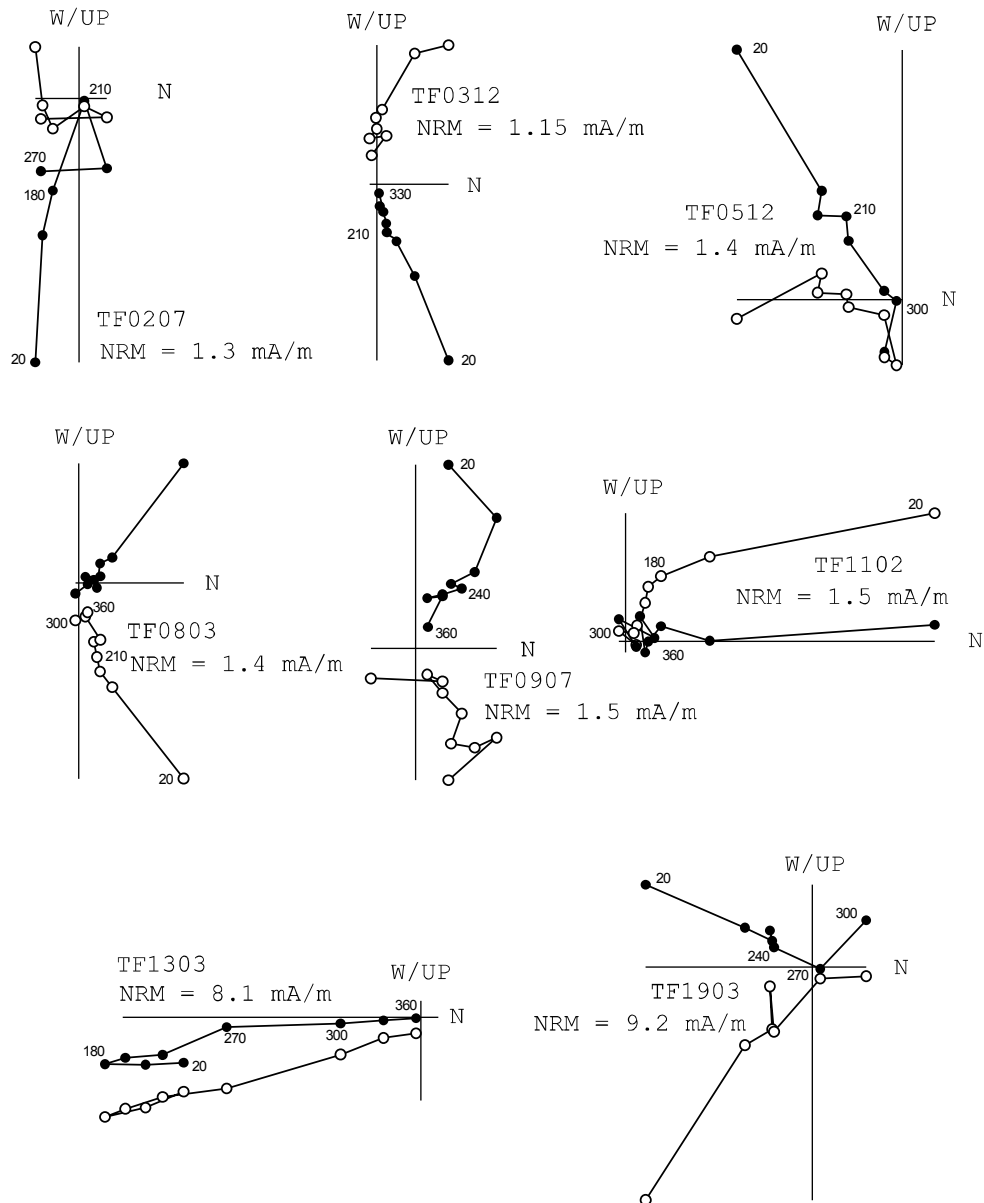


**Figure 6. Orthogonal vector diagrams of demagnetization data (in situ coordinates) for the 8 sites yielding a measurable remanence. Solid and open dots represent projection on the horizontal and vertical planes, respectively. Demagnetization step values are in °C.**

Since the ages of the rocks (predominantly early to late Eocene) are very close to age of regional tectonic deformation and strata tilting (early-middle Eocene to early Oligocene), a positive fold test is virtually the proof for the primary nature of the measured magnetization.

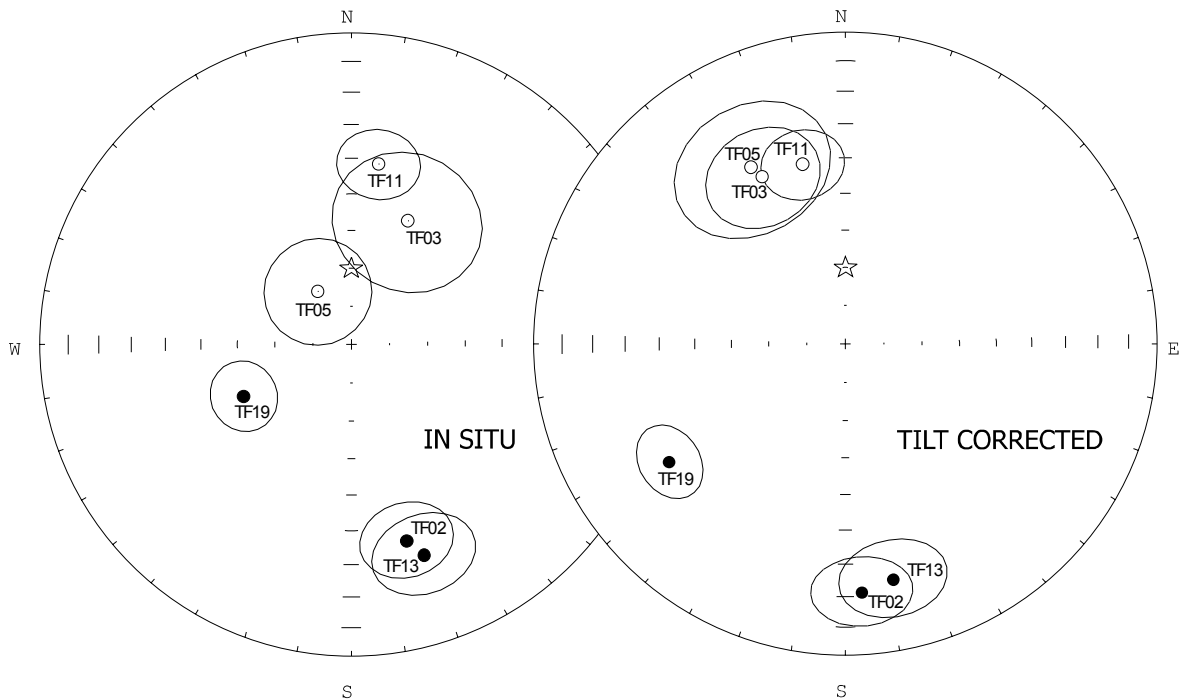


**Figure 7.** Equal-area projections of the site-mean paleomagnetic directions. Open (solid) symbols represent projection onto the upper (lower) hemisphere. Open ellipses are the projections of the  $\alpha_{95}$  cones about the mean directions. The star represents the normal polarity geocentric axial dipole (GAD) field direction ( $D=0^\circ$ ,  $I=-70.0^\circ$ ) for the study area.

Site-mean flattening values with respect to South America are always negative, and range between  $-33.8^\circ$  and  $-54.2^\circ$  (Table 2). Such “shallowing” of the paleomagnetic directions can be explained considering the effects of diagenesis and compaction on clayey sediments [e.g., *Deamer and Kodama, 1990*], as already observed for similar deposits sampled elsewhere [*Speranza et al., 1997; Maffione et al., 2008*]. The five clustered sites yield no significant rotation of the Magallanes belt of Tierra del Fuego with respect to

South America ( $-7.8^{\circ} \pm 10.4^{\circ}$ ) since at least early Eocene times ( $\sim 50$  Ma). Conversely, the scattered TF19 site yields a  $63.9^{\circ} \pm 11.1^{\circ}$  CW rotation (Figure 3 and Table 2).

## 5. Discussion

### 5.1. Rotational nature of the Patagonian orocline, and relations with Scotia plate spreading and Drake Passage opening

Our data represent the first paleomagnetic evidence from sedimentary sequences exposed in the northern foothills of the Fuegian Andes, and support that the curved shape of the orogen was already fully acquired at  $\sim 50$  Ma. Therefore the Patagonian orocline might be in principle the result of one of the two following kinematics: (1) it is a non-rotational (or primary) arc (*sensu Marshak* [1988]), resulting from the tectonic deformation of an original curved paleo-margin affected by radial shortening directions; (2) it is an orocline, formed after rotations older than 50 Ma. The first scenario has been proposed in several recent papers [*Ramos and Aleman*, 2000; *Diraison et al.*, 2000; *Ghiglione*, 2003; *Ghiglione and Ramos*, 2005; *Ghiglione and Cristallini*, 2007], though none is based upon proper paleomagnetic evidence. Conversely, this hypothesis mostly relies upon sand-box analogue models results, indicating how an opportune changing through time in the South America-Antarctica relative plate motion can account for all features observed in the Patagonian arc (i.e., shape of the curvature, pattern and amount of the shortening directions).

However, when the overall paleomagnetic data set from the Patagonian orocline is considered, all previous results from the Fuegian Andes systematically yield a post-160 to 100 Ma CCW rotation with respect of South America, though the igneous and metamorphic nature of the studied rocks may imply first-order flaws on both data quality

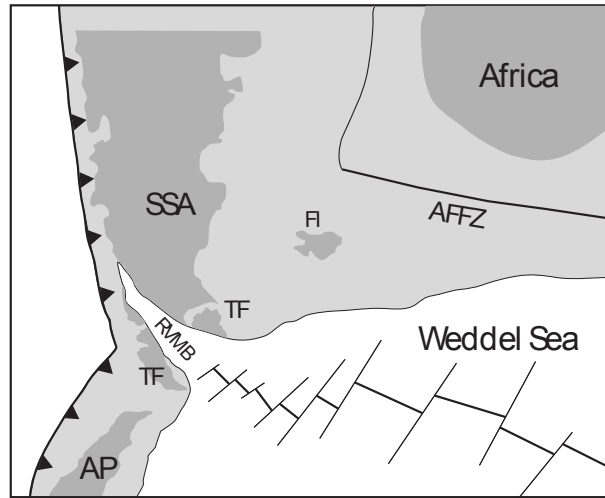
and magnetization age. We conclude that further paleomagnetic investigations of the pre-lower Eocene sequences from the Magallanes belt of the Tierra del Fuego are surely needed to properly understand the rotational nature of the Patagonian orocline. Yet, the available paleomagnetic data set is indeed suggestive of an orogenic bend formed after rotations occurring before 50 Ma, in late Mesozoic-earliest Paleogene times.

A candidate yielding the possible pre-50 Ma oroclinal bending of the Fuegian Andes is the inversion and closure of the Rocas Verdes marginal basin during mid-late Cretaceous times. *Kraemer* [2003] demonstrated that the closure of the Rocas Verdes basin could have produced a maximum regional CCW rotation of  $30^\circ$ , assuming a reasonable basin width of 25 km. Therefore, we speculate that about  $60^\circ$  of the entire  $90^\circ$  orogenic trend change observed along the Patagonian orocline could be related to a pre-existing articulated paleomargin, while further  $30^\circ$  were possibly acquired during the mid-late Cretaceous closure of the Rocas Verdes basin (Figure 8).

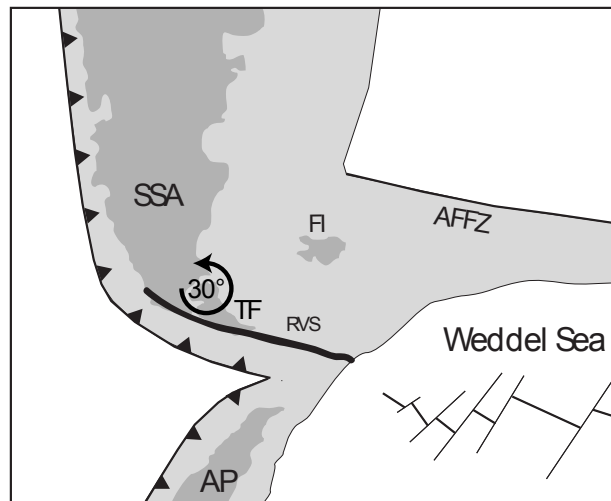
Thus the final configuration of the Patagonian orocline was completed well before than the onset of the Scotia plate spreading at  $\sim 32$  Ma [*Barker*, 2001; *Lawver and Gahagan*, 2003; *Eagles et al.*, 2005; *Livermore et al.*, 2005; *Lodolo et al.*, 2006]. This implies that the opening of the Drake Passage deep-sea pathway at the Eocene-Oligocene boundary [*Barker*, 2001; *Eagles et al.*, 2005; *Livermore et al.*, 2005; *Lodolo et al.*, 1997, 2006], likely determining first-order outcomes in the global paleoclimate [*Lawver and Gahagan*, 2003; *Barker et al.*, 2007a, 2007b], was decidedly unrelated to the evolutionary history of the Patagonian orocline, and most likely the sole consequence of the Scotia plate spreading.

Resting apart from the five non-rotated sites, site TF19 yields a  $\sim 60^\circ$  CW rotation (Figures 3 and 7).

120 Ma



100 Ma



50 Ma

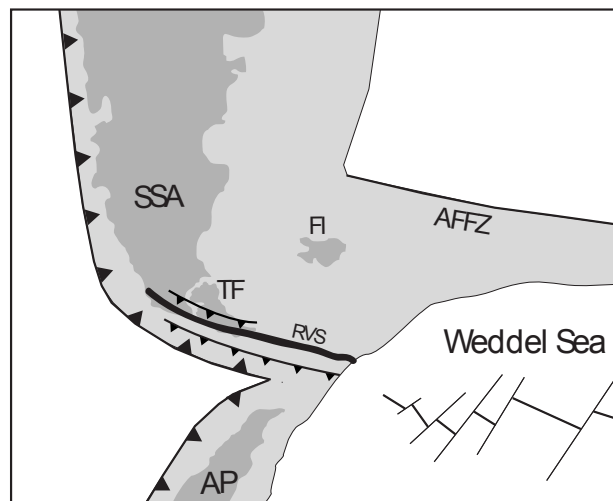


Figure 8. Tectonic reconstruction of the South America-Antarctica plate boundary since 120 to 50 Ma. 120 Ma, extensional episode related to the opening of the Rocas Verdes marginal basin (RVMB). 100 Ma, inversion and closure of the RVMB, probably accompanied by a CCW rotation of the Fuegian Andes. 50 Ma, northward thrust-sheet emplacement in the Fuegian Andes. SSA southernmost South America; AFFZ, Agulhas Falkland Fracture Zone; TF, Tierra del Fuego; FI, Falkland (Malvinas) Islands; AP, Antarctic Peninsula; RVS, suture of the Rocas Verdes marginal basin.

This site is located in proximity of the Fueguina fault (Figure 3), a right-lateral strike-slip fault interpreted as an R' Riedel shear fracture associated to the major left-lateral MFFS [Ghiglione *et al.*, 2002]. Thus we interpret this large-magnitude CW rotation as a local effect related to right-lateral displacement along the Fueguina fault, consistently with paleomagnetic evidence gathered from other strike-slip faults exposed elsewhere [e.g., Sonder *et al.*, 1986].

## **5.2. Unravelling the relative relevance and timing of thrust vs. strike-slip tectonics in the Fuegian Andes: evidence from magnetic fabric**

The well-defined magnetic lineations gathered at 20 out of 22 sites from Tierra del Fuego offer the opportunity to unravel with great accuracy the finite deformation pattern of the Magallanes belt of the Fuegian Andes. In fact there is wide evidence from other orogens that AMS of fine-grained sediments represents a valuable strain proxy, even in absence of other visible strain markers [e.g., Sagnotti *et al.*, 1998; Maffione *et al.*, 2008]. The magnetic lineation gathered from a fold belt normally trends sub-parallel to the local fold axis, or anyway parallel to the maximum elongation axis ( $\epsilon_1$ ) of the strain ellipsoid.

Along the Atlantic coast between Cabo San Pablo and Cerro Colorado, the magnetic lineations from Tierra del Fuego consistently define the extent the external orogen, where they trend roughly E-W sub-parallel to local fold axes, while they are N-S (on average) at two northernmost sites located in the undeformed foreland (Figure 3 and Figure 5). At site TF19, the magnetic lineation trends NW-SE, thus confirming the significant CW rotation with respect to other neighbour sites evidenced by paleomagnetic data, likely due to the Fueguina fault activity. Apart from the sites located along the Atlantic coast, magnetic lineation is oriented NW-SE at site TF02, again sub-parallel to local fold axes (Figure 3).

The general E-W trending of the magnetic lineations between Capo San Pablo and Cerro Colorado, coupled with the lack of paleomagnetic rotations, proves that a roughly N-S directed compressive tectonic regime was active in the southern Magallanes basin synchronous with sedimentation. In fact, it has been shown that the magnetic fabric is mostly sensitive to the pristine tectonic regime, acting during sedimentation or shortly after, prior to complete sediment lithification [e.g., *Sagnotti et al.*, 1998; *Faccenna et al.*, 2002]. Therefore, our AMS data from the Atlantic coast support a N-S oriented shortening acting during sediment deposition (i.e., during Eocene, 50-35 Ma).

The origin of this tectonic regime is not completely clear. A N-S compression in the Magallanes basin of Tierra del Fuego is in apparent contrast with the relative motion between Antarctica and South America, which was characterized from 46 Ma by a WNW-ESE oriented sinistral component, changing to a clear E-W direction since ~20 Ma [*Livermore et al.*, 2005]. Alternatively, Eocene N-S shortening might be related to the vanishing activity of the southeastern tip of the Andean subduction zone. Within this frame, the Magellan basin could be directly interpreted as a flexural-related basin developing during the formation of the orogenic belt. Further data on the deep belt structure are needed to fully understand the tectonic setting.

AMS data may also serve to evaluate the relative relevance of thrust vs. strike-slip tectonics in the Fuegian Andes, where both the displacement and onset age of the MFFS strike-slip fault system are a matter of debate. Variable displacement amounts of some tens of kilometres have been postulated so far (20-30 km, *Olivero and Martinioni* [2001]; 40 Km, *Lodolo et al.* [2003]; 48 Km, *Torres-Carbonell et al.* [2008a]; 55 km, *Rossello et al.* [2004a]), while ages of the onset of the MFFS activity vary between 100 and 7 Ma [*Cunningham et al.*, 1995; *Torres-Carbonell et al.*, 2008a]. The magnetic fabric of the

sampled rocks reveals a N-S compression acting during the Eocene (50-35 Ma) at sites along the Atlantic coast, which is incompatible with left-lateral strike-slip shear along the E-W segment of the MFFS located ~10 km south of the sampling area. Conversely, this tectonics is compatible with the roughly N40° direction of maximum shortening inferred from brittle fault populations in Tierra del Fuego by *Diraison et al.* [2000] (Figure 2). Therefore we may suppose that the apparent discrepancy between the shortening direction inferred by magnetic fabric and structural analysis is related to the evolution of the tectonic regime with time. We suggest that most of the brittle faults measured by *Diraison et al.* [2000] formed synchronous to a post-early Oligocene (~30 Ma) onset of wrench tectonics in the southern Magallanes basin (in agreement with *Ghiglione and Ramos* [2005]), while the older Eocene (50-35 Ma) tectonics was characterized by a pure N-S compression related to thrust tectonics. The Oligocene (and/or younger) strike-slip tectonic regime has not overprinted the magnetic fabric of Eocene sedimentary rocks, as also observed elsewhere in case of evolving tectonic stresses of mild intensity (i.e., not yielding new schistosity, e.g., *Faccenna et al.* [2002]). We speculate that the onset of strike-slip tectonics may be related as well to the opening of the Scotia plate, determining the superposition of a strike-slip regime on a pre-existing orogenic bend characterized by almost pure thrust tectonics.

Sites from Cerro Colorado and site TF03 are located ~5 km and ~200 m (respectively) from the MFFS, thus their paleomagnetic directions and magnetic lineation trends can be used to assess whether left-lateral strike-slip activity has caused local CCW rotations [e.g., *Sonder et al.*, 1986]. We note that rotation values from sites TF03-TF05 are not significantly different from those at sites TF11-TF13, located several km more distant from the MFFS, and magnetic lineations from Cerro Colorado are not CCW rotated with respect

to sites located further north along the external orogen sector (Figure 3). Therefore we conclude that strike-slip shear along the MFFS has not caused large-magnitude rotations in the Fuegian Andes, and displacement along the fault is likely in the lower bound among those put forward in the past (~20 km, according to *Olivero e Martinioni* [2001]). In any case, there is surely no influence of strike-slip tectonics for the formation of the Patagonian orocline (see “strike-slip orogen” model by *Cunningham* [1993]).

## 6. Conclusions

Five lower Eocene-lower Oligocene paleomagnetic sites from the Magallanes belt of Tierra del Fuego consistently yielding a positive fold test indicate a lack of paleomagnetic rotations in the Fuegian Andes since ~50 Ma. Further data from older sediments are needed to assess whether the Patagonian orocline is a primary arc developed above an articulated paleomargin, or it formed after rotations older than 50 Ma. However, previous paleomagnetic evidence from metamorphic and igneous rocks (even if not fully reliable) from the internal part of the orogenic bend may suggest that the arc is mostly primary (i.e., developed above an articulated paleomargin), and that a further 30° CCW rotation occurred in mid-late Cretaceous times during the closure of the Rocas Verdes marginal basin. A pre-existing Patagonian orocline at 50 Ma implies that opening of the Drake Passage at ~32 Ma was the exclusive consequence of the Scotia plate spreading, where 32±2 Ma oceanic anomalies are documented.

A well-developed magnetic fabric from 20 sites, coupled with paleomagnetic evidence, documents an Eocene (50-35 Ma) N-S shortening in the Magallanes belt of Tierra del Fuego associated to northward fold-and-thrust belt propagation. Both paleomagnetic and

AMS data do not reveal any significant influence from the postulated left-lateral shear along the E-W MFFS.

We conclude that strike-slip tectonics postdated the Eocene north-verging thrust tectonics (i.e., is younger than 35 Ma), and that the horizontal displacement along the MFFS may range in the lower bound values (~20 km) among the estimates put forward so far. In any case, our data indicate that strike-slip tectonics has not contributed at all to the genesis of the great orogenic re-entrant known as Patagonian orocline.

## **7. Acknowledgements**

MM gratefully acknowledges H. Soloaga, L. Waltter, and F. Oliva (Inspector and Sergeants of the Police Department in Tolhuin) for their logistic support given for the sampling campaign at Cabo San Pablo. G. González Bonorino and Emilio Saez helped us for lodgement in CADIC (Ushuaia) and in the Panaderia La Union (Tolhuin), respectively. Many thanks to E. Boschi for encouraging this work, and to F. Florindo and R. Somoza for fruitful discussions on the Drake Passage opening and Andean tectonics, respectively. MM and FS were funded by INGV, while CF and ER were supported by the Università di Roma Tre.

**Table 1.** Anisotropy of magnetic susceptibility results from Tierra del Fuego.

Site	Formation	Latitude °S	Longitude °W	Age	Age (Ma)	n/N	Km	L	F	T	P'	D(°)	I(°)	e <sub>12</sub> (°)
TF01	Capas E. Maria Cristina	54.50819	66.30651	Earliest Oligocene	30-34	-	-	-	-	-	-	-	-	-
TF02	Cerro Colorado	53.91318	68.36002	U. Middle-Late Eocene	34-40	6/11	264	1.023	1.056	0.376	1.084	311.4	-1.3	18
TF03	Sloggett	54.55055	67.00568	L. Eocene-E. Oligocene	28-37	-	-	-	-	-	-	-	-	-
TF04	Cerro Colorado	54.49756	66.37447	U. Middle-Late Eocene	34-40	10/11	179	1.007	1.045	0.731	1.057	110.6	10.8	19
TF05	Cerro Colorado	54.49685	66.37592	U. Middle-Late Eocene	34-40	13/13	202	1.010	1.040	0.564	1.057	90.8	15.5	13
TF06	Cerro Colorado	54.49291	66.38249	U. Middle-Late Eocene	34-40	11/13	243	1.020	1.026	-0.01	1.035	94.6	9.1	14
TF07	Cerro Colorado	54.49213	66.38316	U. Middle-Late Eocene	34-40	14/14	302	1.013	1.028	0.441	1.042	281	-6.4	4
TF08	Punta Torcida	54.45557	66.49070	Early Eocene	49-56	10/11	244	1.018	1.045	0.429	1.067	58.6	17.2	9
TF09	Punta Torcida	54.46647	66.48586	Early Eocene	49-56	10/12	194	1.010	1.036	0.603	1.049	301.6	1.7	5
TF10	Punta Torcida	54.40377	66.55741	Early Eocene	49-56	10/11	128	1.016	1.050	0.521	1.070	94.8	13.1	6
TF11	Punta Torcida	54.43650	66.52520	Early Eocene	49-56	11/11	177	1.005	1.022	0.565	1.028	79.5	24.3	10
TF12	Punta Torcida	54.43860	66.51984	Early Eocene	49-56	8/9	150	1.008	1.036	0.618	1.047	115.9	-11.3	8
TF13	Punta Torcida	54.44307	66.50858	Early Eocene	49-56	10/13	170	1.014	1.027	0.293	1.041	79	-14.9	7
TF14	Punta Torcida	54.42979	66.53755	Early Eocene	49-56	11/13	187	1.008	1.023	0.662	1.030	81.8	-17.4	8
TF15	Cerro Colorado	54.48060	66.45114	U. Middle-Late Eocene	34-40	13/13	214	1.011	1.036	0.621	1.052	278.4	-2.4	9
TF16	Cerro Colorado	54.43369	66.54663	U. Middle-Late Eocene	34-40	12/13	177	1.012	1.021	0.342	1.033	83.8	-23.9	8
TF17	Cerro Colorado	54.48033	66.44112	U. Middle-Late Eocene	34-40	11/11	264	1.015	1.040	0.451	1.058	84	-21.5	18
TF18	Cerro Colorado	54.48695	66.40784	U. Middle-Late Eocene	34-40	7/9	278	1.009	1.055	0.715	1.070	82.8	-26.6	20
TF19	Punta Torcida	54.39883	66.56378	Early Eocene	49-56	8/10	195	1.018	1.022	0.112	1.040	310.4	1.1	7
TF20	Desdemona	54.31318	66.69111	L. Oligocene – E. Miocene	20-25	12/13	212	1.004	1.055	0.774	1.065	14.2	-8.4	15
TF21	Cerro Colorado	54.35286	66.64365	U. Middle-Late Eocene	34-40	6/15	126	1.017	1.046	0.007	1.054	266.3	-0.2	8
TF22	Capas Cabo San Pablo	54.27540	66.73711	Early Miocene	16-20	9/9	185	1.007	1.048	0.759	1.060	322	3.4	24

The geographic coordinates are referred to WGS84 datum. Age in Ma is from the geologic timescale of *Gradstein et al.* [2004]. n/N, number of samples giving reliable results/number of studied samples at a site.  $K_m$ , mean susceptibility in  $10^{-6}$  SI. L, F, T and P' are magnetic lineation ( $k_{max}/k_{int}$ ), magnetic foliation ( $k_{int}/k_{min}$ ), shape factor and corrected anisotropy degree, respectively, according to *Jelinek* [1981]. D and I are in situ site mean declination and inclination, respectively, of the maximum susceptibility axis.  $e_{12}$  is semi-angle of the 95% confidence ellipse around the mean  $K_{max}$  axis in the  $K_{max}$ - $K_{int}$  plane.

**Table 2.** Paleomagnetic results from Tierra del Fuego.

Site	Formation	Geographic coordinates		Age	Age (Ma)	Bedding (°)	Tilt corrected		In situ				R (°)	ΔR (°)	F (°)	ΔF (°)	
		Latitude °S	Longitude °W				D(°)	I(°)	D(°)	I(°)	k	α <sub>95</sub> (°)					n/N
<b>TF02</b>	Cerro Colorado	53.91318	68.36002	U. Middle - Late Eocene	34-40	229-26	176.2	21.1	164.2	34.8	19.7	11.9	9/11	6.3	15.9	-54.2	9.9
<b>TF03</b>	Sloggett	54.55055	67.00568	L. Eocene - E. Oligocene	28-37	106-50	331.9	-35.9	24.5	-54.0	7.7	19.9	9/14	-19.2	20.7	-37.9	15.7
<b>TF05</b>	Cerro Colorado	54.49685	66.37592	U. Middle - Late Eocene	34-40	157-34	333.6	-39.8	327.6	-73.6	10.7	14.0	12/17	-16.7	19.2	-36.0	11.4
<b>TF08*</b>	Punta Torcida	54.45557	66.49070	Early Eocene	49-56	339-70	328.6	-1.3	312.1	66.4	16.3	11.2	12/12	-23.6	10.9	-72.9	8.9
<b>TF09*</b>	Punta Torcida	54.46647	66.48586	Early Eocene	49-56	213-50	261.8	2.3	275.4	32.0	9.0	18.7	9/13	89.6	16.0	-71.9	14.7
<b>TF11</b>	Punta Torcida	54.43650	66.52520	Early Eocene	49-56	89-25	346.6	-40.4	8.6	-41.0	58.8	10.4	4/13	-5.6	12.5	-33.8	8.3
<b>TF13</b>	Punta Torcida	54.44307	66.50858	Early Eocene	49-56	235-16	168.5	23.8	160.9	29.2	18.8	12.2	9/13	-3.7	12.3	-50.4	9.7
<b>TF19</b>	Punta Torcida	54.39883	66.56378	Early Eocene	49-56	223-27	236.1	32.4	244.3	58.5	23.1	9.7	11/11	63.9	11.1	-41.7	7.8

**\*Discarded sites (see text). Bedding is expressed in dip azimuth-dip values. D and I are site mean declination and inclination calculated after and before tectonic correction. k and α<sub>95</sub> are statistical parameters after Fisher [1953]. n/N is number of samples giving reliable results/number of studied samples at a site. Site mean Rotation (R) and Flattening (F) values, and relative errors (ΔR and ΔF) (according to Demarest [1983]) are relative to coeval D and I South American values expected at the sampling area considering South American paleopoles from Besse and Courtillot [2002].**

# **PART III**

## **CONCLUSIONS**

## **CHAPTER 5**

*Results, implications,  
and concluding remarks*

## 1. Main results and implications from the studied curved belts

The first part of my study has dealt with the bending of the Western Alpine Arc. The bending of the Alps in this region has been investigated so far using different approaches, though few based on reliable paleomagnetic data. Paleomagnetic data from this study reveal that the Western Alpine Arc is a primary bend formed along the irregular paleomargin of the European plate, that has been tightened by further  $\sim 50^\circ$  during Aquitanian-Serravallian times. The formation of the further  $50^\circ$  of curvature occurred during the rollback of the Apenninic slab and related back-arc spreading of the Liguro-Provençal Basin and drift of the Corsica-Sardinia block. Possible toroidal components in the mantle flow near the lateral edge of the Apenninic slab could have triggered a common dynamics driving both the Alpine and the Apennine slab motions, and resulting in a synchronous opening of the Liguro-Provençal basin and rollback of Alpine slab, with following bending of the belt.

This study revealed that the Western Alpine Arc is a complex bend formed during a multiphase deformation, and controlled by different geodynamic mechanisms, mainly linked to the subduction of the Apenninic-Alpine slab.

The second study has been carried out in a specific sector of the southern limb of the Central Andean megasalient, using paleomagnetism and structural analysis integrated with previous geological and geophysical data. This study provided a contribution to the understanding of the timing of deformation in a specific area of the Andean chain. Relying on our and past evidence, the Bolivian Orocline, erroneously called “orocline” by *Carey* [1955], would represent a progressive bend [sensu *Weil and Sussman*, 2004] whose arcuate shape was controlled by the along-strike gradient of crustal shortening. Actually, rotations occurred synchronous with thrusting, and the acquisition of the curvature was coeval to the

main deformation phase. Clockwise rotations up to  $\sim 45^\circ$  documented from our study are compatible with a secondary-bending type mechanism occurred after Eocene-Oligocene times (30-40 Ma), and their nature is probably related to the widespread shearing taking place between zones of differential shortening. Beginning from  $\sim 15$  Ma ago, the activity of N-S left-lateral strike-slip faults in the Eastern Cordillera at the border with the Altiplano-Puna plateau induced up to  $\sim 40^\circ$  counterclockwise rotations along the fault zone, locally annulling the regional clockwise rotation. We suggested that mid-Miocene strike-slip activity developed in response of a compressive stress (related to body forces) at the plateau margins, caused by the progressive lateral (southward) growth of the Altiplano-Puna plateau, laterally spreading from the overthickened crustal region of the salient apex. The growth of plateaux by lateral spreading seems to be a mechanism common to other major plateaux in the Earth (i.e., Tibetan plateau).

Nevertheless, how did rotations occur in the Central Andes still remain the main debated issue about the Bolivian Orocline bending. In fact, a progressive shear model like that proposed for the developing of the megasalient, would produce rigid block rotations along vertical axis of both thrust sheets and bounding fault planes. This would imply a  $\sim$ NW-SE direction of the original structural grain of the orogen in this sector before deformation. Conversely, rotations could also have occurred by diffuse shear internal to the rock, without implying a rotation of the fault planes. In this case, the strike of the present structural features (fault traces and fold axes) would have not changed during the arc formation. The depth of the detachment zone allowing rotation is another strongly debated issue. According to the model by *McQuarrie* [2002] and *McQuarrie et al.* [2005], rotations in the Eastern Cordillera may have occurred above a mid-crustal megathrust, over which the entire sector would have passively transported onto the foreland and rotated.

Therefore, despite the very numerous studies carried out in the Central Andes, the problem of the bending of the Bolivian Orocline remain not still fully resolved.

The study of the Patagonian Orocline, in the southernmost Andes, though based on a small number of paleomagnetic data, represents the first reliable constraint to the timing of the bending in the southern tip of South America. The importance of this study is in the fact that the bending of the Patagonian Orocline is strictly linked to the opening of the Drake Passage between South America and Antarctica, which is thought to have caused first-order outcomes in the global paleoclimate. Our data indicate that the Patagonian Orocline did not undergo any significant rotation since early Eocene times (~50 Ma), implying that it may represent either a primary bend, or an orocline formed during late Cretaceous-early Eocene deformation phase.

Our data imply that the opening of the Drake Passage at ~32 Ma was definitely not related to the formation of the Patagonian orocline, but was likely the sole consequence of the Scotia plate spreading.

## **2. Concluding remarks about curved mountain belts and their study**

In this study, different types of orogenic bends from various geologic and geodynamic settings have been investigated. Some important implications can be inferred from the paleomagnetic and structural investigations from this study, in addition to the various examples of arcuate systems reported in Part I of this thesis. These are the followings:

- a. Bends are common features to numerous orogenic chains in the Earth. Their evolution, both at small and big scales, is strictly related to the general processes leading to the growth of mountain belts. Therefore, unravelling the evolution of specific orogenic

bends can allow us to understand, with major detail, the general mechanisms governing mountain building.

- b. Besides the geometric similarities shown by several arcuate systems, they can deeply differ by each other depending on both tectonics and kinematics, thus on mechanisms governing their formation.
- c. An integrated paleomagnetic and structural analysis is required to unravel the timing and kinematic evolution of a curved orogen. In fact, only a comprehensive multidisciplinary study can allow us to discern between primary, progressive and secondary arcs, and document their tectonic evolution.
- d. A rigid classification of curved belts in primary, progressive, or secondary arcs could be, in some cases, too simplistic. In fact, many orogenic bends are the result of a long and complex geologic history, controlled by different geodynamic mechanisms that can change with time, or act simultaneously.

# REFERENCES

- Abels, A., L. Bischoff (1999). Clockwise block rotations in northern Chile: Indications for a large-scale domino mechanism during the middle-late Eocene. *Geology*, 27, 751-754.
- Aller, J., J. Gallastegui (1995). Analysis of kilometric-scale superposed folding in the Central Coal Basin (Cantabria zone, NW Spain). *J. Struct. Geol.*, 17, 961-969.
- Allerton, S. (1994). Vertical axis rotation associated with folding and thrusting: An example from the eastern Subbetic, southern Spain. *Geology*, 22, 1039-1042.
- Allerton, S. (1998). Geometry and kinematics of vertical-axis rotations in fold and thrust belts. *Tectonophysics*, 299, 15-30.
- Allerton, S., Lonergan, L., Platt, J.P., Platzman, E.S., McClelland, E. (1993). Palaeomagnetic rotations in the eastern Betic Cordillera, southern Spain. *Earth Planet. Sci. Lett.*, 119, 225-242.
- Allmendinger, R.W. (1986). Tectonic development, southeastern border of the Puna Plateau, northwestern Argentine Andes. *Geol. Soc. Am. Bull.*, 97, 1070-1082.
- Allmendinger, R.W., V.A. Ramos, T.E. Jordan, M. Palma, B.L. Isacks (1983). Paleogeography and Andean structural geometry, NW Argentina. *Tectonics*, 2, 1-16.
- Allmendinger, R.W., T.E. Jordan, S.M. Kay, B.L. Isacks (1997). The evolution of the Altiplano–Puna Plateau of the Central Andes. *Annu. Rev. Earth Planet. Sci.*, 25, 139-174.
- Allmendinger, R.W., R. Smalley, M. Bevis, H. Caprio, B. Brooks (2005). Bending the Bolivian orocline in real time. *Geology*, 33, 905-908.
- Allmendinger, R.W., R. Reilinger, J. Loveless (2007). Strain and rotation rate from GPS in Tibet, Anatolia, and the Altiplano. *Tectonics*, 26, TC3013, doi:10.1029/2006TC002030.
- Alonso, J.L., J.A. Pulgar, J.C. Garcia-Ramos, P. Barba (1996). Tertiary basins and Alpine tectonics in the Cantabria Mountains (NW Spain). In: Tertiary Basins of Spain, P.F. Friend, C. Dabrio (Eds.), pp. 214-227, Cambridge Univ. Press, New York.
- Anderson, H., J.A. Jackson (1987). Active tectonics in the Adriatic region. *Geophys. J. R. Astron. Soc.*, 91, 937-983.
- Argand, E. (1924). La tectonique de l'Asie. In: 13th International Geological Congress Conf. Proceedings, Brussels, p. 171.
- Arriagada, C., P. Roperch, C. Mpodozis (2000). Clockwise block rotations along the eastern border of the Cordillera de Domeyko, northern Chile (22°45'–23°30'S). *Tectonophysics*, 326, 153-171.
- Arriagada, C., P. Roperch, C. Mpodozis, G. Dupont-Nivet, P. R. Cobbold, A. Chauvin, J. Cortés (2003). Paleogene clockwise tectonic rotations in the forearc of central Andes, Antofagasta region, northern Chile. *J. Geophys. Res.*, 108(B1), 2032, doi:10.1029/2001JB001598.
- Arriagada, C., P. Roperch, C. Mpodozis, R. Fernandez (2006). Paleomagnetism and tectonics of the southern Atacama Desert (25–28°S), northern Chile. *Tectonics*, 25, TC4001, doi:10.1029/2005TC001923.

- Arthaud, F., P. Matte (1977). Late Paleozoic strike-slip faulting in southern Europe and north Africa; results of a right lateral shear zone between the Appalachians and the Urals. *GSA Bull.*, 88, 1305-1328.
- Aubry, L., P. Roperch, M. de Urreiztieta, E. Rossello, A. Chauvin (1996). Paleomagnetic study along the south-eastern edge of the Altiplano-Puna Plateau: Neogene tectonic rotations. *J. Geophys. Res.* 101, 17883–17899.
- Averbuch, O., Mattei, M., Kissel, C., Frizon de Lamotte, D., Speranza, F., (1995). Cinématique des déformations au sein d'un système chevauchant aveugle: l'exemple de la "Montagna dei Fiori" (front des Apenins centraux, Italie). *Bull. Soc. Géol. France*, 5, 451–461.
- Baby, P., T. Sempere, J. Oller, L. Barrios, G. Hérail, R. Marocco (1990). A late Oligocene–Miocene intermountain foreland basin in the southern Bolivian Altiplano. *C. R. Acad. Sci., Ser., II*, 311, 341-347.
- Baby, P., G. Hérail, R. Salinas, T. Sempere (1992). Geometry and kinematic evolution of passive roof duplexes deduced from cross section balancing: example from the foreland thrust system of the southern Bolivian Subandean Zone. *Tectonics*, 11, 523-536.
- Bachtadse, V., and R. Van der Voo (1986). Paleomagnetic evidence for crustal and thin-skinned rotations in the European Hercynides. *Geophys. Res. Lett.*, 13, 161-164.
- Balla, Z. (1987). Tertiary paleomagnetic data for the Carpatho–Pannonian region in the light of Miocene rotation kinematics. *Tectonophysics*, 139, 67-98.
- Baraldo, A., Rapalini, A., Tassone, A., Lippai, H., Menichetti, M., Lodolo, E. (2002). Estudio paleomagnético del intrusivo del cerro Hewhoepen, Tierra del Fuego, y sus implicancias tectónicas. 15° Congreso Geológico Argentino, El Calafate, Actas 1, 285-290.
- Barke, R., S. Lamb, and C. MacNiocaill (2007). Late Cenozoic bending of the Bolivian Andes: New paleomagnetic and kinematic constraints. *J. Geophys. Res.*, 112, B01101, doi:10.1029/2006JB004372.
- Barker, P.F. (2001). Scotia Sea regional tectonic evolution: implications for mantle flow and palaeocirculation. *Earth Sci. Rev.*, 55, 1-39.
- Barker, P.F., Filippelli, G.M., Florindo, F., Martin, E.E., Scher, H.D. (2007a). Onset and role of the Antarctic Circumpolar Current. *Deep-Sea Research II*, 54, 2388-2398.
- Barker, P.F., Diekmann, B., Escutia, C. (2007b). Onset of Cenozoic Antarctic glaciation. *Deep-Sea Research II*, 54, 2293-2307.
- Barrios, L. (1991). Analisis tectónico de la estructura de Pululus: Altiplano sur. *Rev. Tec. YPFB*, 12(2), 275-284.
- Bazhenov, M.L., V.S. Burtman, M. Sandulescu (1993). Paleomagnetism of the upper cretaceous rocks and its bearing on the origin of the Romanian Carpathian arc. *Rom. J. Tecton. Reg. Geol.*, 75, 9-14.
- Beck, M.E. Jr. (1976). Discordant paleomagnetic pole position as evidence of regional shear in the western Cordillera of North America. *Am. J. Sci.*, 276, 694-712.
- Beck, M.E. Jr. (1988). Block rotations in continental crust: examples from Western North America, in: C. Kissel, C. Laj (Eds.), *Paleomagnetic Rotations and Continental Deformation*, Kluwer Academic, Dordrecht.

- Beck, M.E. Jr. (1998). On the mechanism of crustal block rotations in the central Andes. *Tectonophysics*, 299, 75-92.
- Beck, M.E. Jr. (2004). The central Andean rotation pattern: Another look. *Geophys. J. Int.*, 157, 1348-1358.
- Beck, M.E. Jr., R.F. Burmester, R.E. Drake, P. Riley (1994). A tale of two continents: Some tectonic contrasts between the central Andes and the North American Cordillera, as illustrated by their paleomagnetic signatures. *Tectonics*, 13, 215-224.
- Beck, M.E. Jr., Burmester, R., Cembrano, J., Drake, R., García, A., Hervé, F., Munizaga, F. (2000). Paleomagnetism of the North Patagonian Batholith, southern Chile. An exercise in shape analysis. *Tectonophysics*, 326(1-2), 185-202.
- Beck, S.L., G. Zandt, S.C. Myers, T.C. Wallace, P.G. Silver, L. Drake (1996). Crustal thickness variations in the Central Andes. *Geology*, 24, 407-410.
- Besse, J., and V. Courtillot (2002). Apparent and true polar wander and the geometry of the geomagnetic field over the last 200 Myr. *J. Geophys. Res.*, 107(B11), 2300, doi: 10.1029/2000jb000050.
- Beutner, E.C. (1977). Causes and consequences of curvature in the Sevier orogenic belt, Utah to Montana. In *Rocky Mountain Thrust Belt, Geology and Resources*, Guideb. Wyo. Geol. Assoc. Annu. Field Conf., 29, 353-365.
- Bianucci, H.A., C.A.F. Garrasino, and E.G. Sanchez (1987). Corrimiento de bajo angulo entre La Quiaca y Abra Pampa (Provincia de Jujuy, Argentina), *Decimo Congr. Geol. Arg., San Miguel de Tucuman*, Actas I, 165-168.
- Boll, A. and R.M. Hernández (1986). Interpretación estructural del área Tres Cruces, Provincia de Jujuy, Argentina. *Boletín de Informaciones Petroleras*, II (7), 2-14.
- Bonardi, G., W. Cavazza, V. Perrone, S. Rossi (2001). Calabria Peloritani Terrane and Northern Ionian Sea, in *Anatomy of an Orogen: The Apennines and Adjacent Mediterranean Basins*, G.B. Vai, I.P. Martini (Eds), pp. 287-306, Kluwer Acad., Dordrecht, Netherlands.
- Box, S.E. (1985). Early Cretaceous orogenic belt in northwestern Alaska: Internal organization, lateral extent, and tectonic interpretation, in: D.G. Howell (Ed.), *Tectonostratigraphic Terranes of the Circum-Pacific Region*, Earth Science Series 1, Circum-Pacific Council for Energy and Mineral Resources, Houston, TX, 1985, pp. 137-145.
- Boyer, S.E. (1995). Sedimentary basin taper as a factor controlling the geometry and advance of thrust belts. *Am. J. Sci.*, 295, 1220-1250.
- Burbank, D.W., Engesser, B., Matter, A., Weidmann, M. (1992). Magnetostratigraphic chronology, mammalian faunas, and stratigraphic evolution of the Lower Freshwater Molasse, Haute-Savoie, France. *Eclogae geologicae Helvetiae*, 85, 399-431.
- Burchfiel, B.C. (1980). Eastern Alpine System and the Carpathian Orocline as an example of collision tectonics. *Tectonophysics*, 63, 31-62.
- Burkhard, M. (1990). Aspects of the large scale Miocene deformation in the most external part of the Swiss Alps (Subalpine Molasse to the Jura fold belt). *Eclogae Geologicae Helvetiae*, 83, 559-583.

- Burkhard, M., Sommaruga, A. (1998). Evolution of the Western Swiss Molasse Basin structural relations with the Alps and the Jura belt. In: Mascle, A., Puigdefabregas, C., Luterbacher, H.P., Fernandez, M. (Eds.), *Cenozoic Foreland Basins of Western Europe* (134). *Geological Society Special Publications*, London, pp. 279-298.
- Burns, K.L., Rickard, M.J., Belbin, L., Chamalaun, F. (1980). Further paleomagnetic confirmation of the Magallanes orocline. *Tectonophysics*, 63, 75-90.
- Butler, R.F. (2004). *Paleomagnetism: Magnetic Domains to Geologic Terranes*. Electronic Editions, University of Portland, Portland, Oregon, pp.238.
- Butler, R.F., D. Richards, T. Sempere, L. Marshall (1995). Paleomagnetic determinations of vertical-axis tectonic rotations from Late Cretaceous and Paleocene strata of Bolivia. *Geology*, 23, 799-802.
- Carey, S. W. (1955). The orocline concept in geotectonics. *Proc. R. Soc. Tasmania*, 89, 255– 288.
- Carey, S.W. (1958). The tectonic approach to continental drift, in *Continental Drift: A symposium*, Geology Department, Univ. Tasmania, Hobart, Tasmania, 177-355.
- Carrapa, B., D. Adelman, G.E. Hilley, E. Mortimer, E.R. Sobel, M.R. Strecker (2005). Oligocene range uplift and development of plateau morphology in the southern central Andes. *Tectonics*, 24, TC4011, doi:10.1029/2004TC001762.
- Carrapa, B., P.G. DeCelles (2008). Eocene exhumation and basin development in the Puna of northwestern Argentina. *Tectonics*, 27, TC1015, doi:10.1029/2007TC002127.
- Channell, J.E.T, W. Lowrie, F. Medizza, W. Alvarez (1978). Paleomagnetism and tectonics in Umbria, Italy. *Earth Planet. Sci. Lett.*, 39, 199-210.
- Channell, J.E.T., B. D'Argenio, F. Horvath (1979). Adria, the African promontory in Mesozoic Mediterranean paleogeography. *Earth Sci. Rev.*, 15, 213-292.
- Channell, J.E.T., R. Catalano, B. D'Argenio (1980). Paleomagnetism and deformation of the Mesozoic continental margin of Sicily. *Tectonophysics*, 61, 391– 407.
- Channell, J.E.T., J.S. Oldow, R. Catalano, B. D'Argenio (1990). Paleomagnetically determined rotations in the western Sicilian fold and thrust belt. *Tectonics*, 9, 641–660.
- Cifelli, F., F. Rossetti, M. Mattei, A. M. Hirt, R. Funicello, L. Tortorici (2004). An AMS, structural and paleomagnetic study of quaternary deformation in eastern Sicily. *J. Struct. Geol.*, 26, 29-46.
- Cifelli, F., M. Mattei, F. Rossetti (2007). Tectonic evolution of arcuate mountain belts on top of a retreating subduction slab: The example of the Calabrian Arc. *J. Geophys. Res.*, 112, doi:10.1029/2006JB004848.
- Cladouhos, T.T., R.W. Allmendinger, B. Coira, E. Farrar (1994). Late Cenozoic deformation in the Central Andes: Fault kinematics from the northern Puna, northwest Argentina and southwest Bolivia. *J. S. Am. Earth Sci.*, 7, 209-228.
- Codignotto, J.O., Malumián, N. (1981). Geología de la región al Norte del paralelo 54 S. de la Isla Grande de Tierra del Fuego. *Rev. Asoc. Geol. Argentina*, 36, 44-88.

- Coira, B. L. (1979). Descripción geológica de la Hoja 3c, Abra Pampa, Provincia de Jujuy. *Bol. Serv. Geol. Nac. Argent.*, 170, 1-90.
- Coira B, J. Davidson, C. Mpodozis, V.A. Ramos (1982). Tectonic and magmatic evolution of the Andes of northern Argentina and Chile. *Earth Sci. Rev.*, 18, 303-332.
- Costa, E., F. Speranza (2003). Paleomagnetic analysis of curved thrust belts reproduced by physical models. *J. Geodynamics*, 36, 633-654.
- Coutand, I., P. Roperch, A. Chauvin, P.R. Cobbold, P. Gautier (1999). Vertical axis rotations across the Puna plateau (northwestern Argentina) from paleomagnetic analysis of Cretaceous and Cenozoic rocks. *J. Geophys. Res.*, 104, 22,965-22,984.
- Coutand, I., P.R. Cobbold, M.de Urreiztita, P. Gautier, A. Chauvin, D. Gapais, E. Rossello (2001). Style and history of Andean deformation, Puna plateau, northwestern Argentina. *Tectonics*, 20(2), 210-234.
- Csontos, L., A. Voros (2004). Mesozoic plate tectonic reconstruction of the Carpathian region. *Palaeogeogr. Palaeoclimatol. Palaeoecol.*, 210, 1-56.
- Cunningham, W.D. (1993). Strike-slip faults in the southernmost Andes and development of the Patagonian orocline. *Tectonics*, 12(1), 169-186.
- Cunningham, W.D. (1994). Uplifted ophiolitic rocks on Isla Gordon, southernmost Chile: implications for the closure history of the Rocas Verdes marginal basin and the tectonic evolution of the Beagle Channel region. *J. South Am. Earth Sci.* 7(2), 135-147.
- Cunningham, W.D. (1995). Orogenesis at the southern tip of the Americas: the structural evolution of the Cordillera Darwin metamorphic complex, southernmost Chile. *Tectonophysics*, 244, 197-229.
- Cunningham, W.D., Klepeis, K.A., Gose, W.A., Dalziel, I.W.D. (1991). The Patagonian orocline: new paleomagnetic data from the Andean magmatic arc in Tierra del Fuego, Chile. *J. Geophys. Res.* 96(B10), 16061-16067.
- Dahlen, F.A. (1990). Critical taper model of fold-and-thrust belts and accretionary wedges. *Ann. Rev. Earth Planet. Sci.*, 18, 55– 99.
- Dalziel, I.W.D., Palmer, K.F. (1979). Progressive deformation and orogenic uplift at the southernmost extremity of the Andes. *Geol. Soc. Am. Bull.* 90, 259-280.
- Dalziel, I.W.D., Kligfield, T., Lowrie, W., Opdyke, N.D. (1973). Paleomagnetic data from the southernmost Andes and the Antarctic Andes. In: Tarling, D.H., Runcorn, S.K., (Eds), *Implication of Continental Drift to the Earth Sciences*. Vol. 1, Academic Press, London, pp. 37-101.
- Dalziel, I.W.D., De Wit, M.F., Palmer, K.F. (1974). Fossil marginal basin in the southern Andes. *Nature*, 250, 291-294.
- Davy, P. P.R. Cobbold, (1988). Indentation tectonics in nature and experiment. 1. Experiments scaled for gravity. *Bull. Geol. Inst. University of Uppsala*, N.S. 14, 129-141.
- Deamer, G.A., Kodama, K.P. (1990). Compaction induced inclination shallowing in synthetic and natural clay-rich sediments. *J. Geophys. Res.* 95(B4), 4511-4529.
- DeCelles, P. G., and B. K. Horton (2003). Early to middle Tertiary foreland basin development and the history of Andean crustal shortening in Bolivia. *Geol. Soc. Am. Bull.*, 115, 58–77.

- Deeken, A., R.S. Edward, I. Coutand, M. Haschke, U. Riller, M.R. Strecker (2006). Development of the southern Eastern Cordillera, NW Argentina, constrained by apatite fission track thermochronology: From early Cretaceous extension to middle Miocene shortening. *Tectonics*, 25, TC6003, doi:10.1029/2005TC001894.
- Demarest, H.H. (1983). Error analysis of the determination of tectonic rotation from paleomagnetic data. *J. Geophys. Res.*, 88, 4321–4328.
- DeMets, C., Gordon, R.G., Argus, D.F., Stein, S. (1990). Current plate motions. *Geophys. J. Int.*, 101, 425-478.
- Diraison, M., Cobbold, P.R., Rossello, E.A., Amos, A.J. (1998). Neogene dextral transpression due to oblique convergence across the Andes of northwestern Patagonia, Argentina. *J. South Am. Earth Sci.*, 11 (6), 519-532.
- Diraison, M., Cobbold, P.R., Gapais, D., Rossello, E.A. (2000). Cenozoic crustal thickening, wrenching and rifting in the foothills of the southernmost Andes. *Tectonophysics*, 316, 91-119.
- Drake, C.L., and H.P. Woodward (1963). Appalachian curvature, wrench faulting, and offshore structures. *Trans. N.Y. Acad. Sci.*, 26, 48-63.
- Duermeijer, C., Krijgsman, W., Langereis, C., Ten Veen, J.H. (1998). Post-early Messinian counterclockwise rotations on Crete: implications for Late Miocene to Recent kinematics of the southern Hellenic arc. *Tectonophysics*, 298, 177-189.
- Dupont-Nivet, G., P. Roperch, P. Gautier, A. Chauvin, M. Gérard, G. Carlier (1996). Clockwise rotations in northern Chile: oroclinal bending and in situ tectonic rotations?. *3rd Int. Symp. Andean Geodynamics*, ORSTOM, St. Malo, 355-358.
- Dupont-Nivet, G., I. Vasiliev, C.G. Langereis, W. Krijgsman, C. Panaiotu (2005). Neogene tectonic evolution of the southern and eastern Carpathians constrained by paleomagnetism. *Earth Planet. Sci. Lett.*, 236, 374-387.
- Eagles, G., Livermore, R.A., Fairhead, J.D., Morris, P. (2005). Tectonic evolution of the west Scotia Sea. *J. Geophys. Res.* 110, B02401, doi:10.1029/2004JB003154.
- Eldredge, S., V. Bachtadse, and R. Van der Voo (1985). Paleomagnetism and the orocline hypothesis. *Tectonophysics*, 119, 153-179.
- Elger, K., Oncken, O., and Glodny, J. (2005). Plateau-style accumulation of deformation, southern Altiplano. *Tectonics*, 24, TC4020, doi: 10.1029/2004TC001675.
- England, P., Housemann, G. (1989). Extension during continental convergence, with application to the Tibetan Plateau. *J. Geophys. Res.*, 94, 17,561-17,579.
- England, P., Molnar, P. (1997). Active deformation of Asia: from kinematics to dynamics. *Science*, 278, 647– 650.
- Evans, M.A. (1994). Joints and décollement zones in Middle Devonian shales: Evidence for multiple deformation events in the central Appalachian Plateau. *GSA Bull.*, 106, 447-460.
- Faccenna, C., M. Mattei, R. Funiciello, L. Jolivet (1997). Styles of back-arc extension in the Central Mediterranean, *Terra Nova*, 9, 126–130.

- Faccenna, C., Speranza, F., D'Ajello Caracciolo, F., Mattei, M., Oggiano, G. (2002). Extensional tectonics on Sardinia (Italy): insights into the arc-back-arc transitional regime. *Tectonophysics*, 356, 213-232.
- Faure, S., Tremblay, A., Angelier, J. (1996). Alleghanian paleostress reconstruction in the northern Appalachians: Intraplate deformation between Laurentia and Gondwana. *GSA Bull.*, 108, 1467-1480.
- Fisher, R.A. (1953). Dispersion on a sphere. *Proc. R. Soc. London*, 217, 295-305.
- Frank, F.C. (1968). Curvature of island arc. *Nature*, 220, p. 363.
- Frank, F.C. (1972). Plate tectonics, the analogy with glaciers flow, and isostasy, flow and fracture of rocks. *Geophysical Monograph*, 16, 285-292.
- Galliski, M.A., J.G. Viramonte (1988). The Cretaceous paleorift in northwestern Argentina: a petrologic approach. *J. S. Am. Earth Sci.*, 1, 329-342.
- Gattacceca, J., Speranza, F. (2002). Paleomagnetism of Jurassic to Miocene sediments from the Apenninic carbonate platform (southern Apennines, Italy): evidence for a 60° counterclockwise Miocene rotation. *Earth Planet. Sci. Lett.*, 201, 19-34.
- Gautier, P., Brun, J.P. (1994). Crustal-scale geometry and kinematics of late-orogenic extension in the central Aegean (Cyclades and Evvia Island). *Tectonophysics*, 238, 399-424.
- Gautier, P., J.P. Brun, R. Moriceau, D. Sokoutis, J. Martinod, L. Jolivet (1999). Timing, kinematics and cause of Aegean extension: a scenario based on a comparison with simple analogue experiments. *Tectonophysics*, 315, 31-72.
- Gehring, A.U., Keller, P., Heller, F. (1991). Paleomagnetism and tectonics of the Jura arcuate mountain belt in France and Switzerland. *Tectonophysics*, 186, 269-278.
- Ghiglione, M.C. (2002). Diques clásticos asociados a deformación transcurrente en depósitos sinorogénicos del Mioceno inferior de la Cuenca Austral. *Rev. Asoc. Geol. Argentina*, 57, 103-118.
- Ghiglione, M.C. (2003). Estructura y evolución tectónica del Cretácico-Terciario de la costa Atlántica de Tierra del Fuego [Ph.D. thesis]: Buenos Aires, Universidad de Buenos Aires, pp. 150.
- Ghiglione, M.C., Ramos, V.A. (2005). Progression of deformation in the southernmost Andes. *Tectonophysics*, 405, 25-46.
- Ghiglione, M.C., Cristallini, E.O. (2007). Have the southernmost Andes been curved since Late Cretaceous time? An analog test for the Patagonian Orocline. *Geology*, 35(1), 13-16.
- Ghiglione, M.C., Ramos, V.A., Cristallini, E.O. (2002). Estructura y estratos de crecimiento en la faja plegada y corrida de los Andes fueguinos. *Rev. geol. Chile*, 29(1), 17-41.
- Ghiglione, M.C., Yagupsky, D., Ghidella, M., Ramos, V.A. (2008). Continental stretching preceding the opening of the Drake Passage: Evidence from Tierra del Fuego. *Geology*, 36(8), 643-646.
- Gilder, S., S. Rouse, D. Farber, B. McNulty, T. Sempere, V. Torres, O. Palacios (2003). Post-Middle Oligocene origin of paleomagnetic rotations in Upper Permian to Lower Jurassic rocks from northern and southern Peru. *Earth Planet. Sci. Lett.*, 210, 233-248.
- Gradstein, F.M., J.G. Ogg, A.G. Smith (2004). A Geologic Time Scale 2004. Cambridge University Press, pp. 589.

- Graham, R.H. (1978). Wrench faults, arcuate fold patterns and deformation in the southern French Alps. *Proc. Geol. Assoc.*, 89, 125-142.
- Gray, M.B., G. Mitra (1993). Migration of deformation fronts during progressive deformation: Evidence from detailed structural studies in the Pennsylvania Anthracite region, U.S.A. *J. Struct. Geol.*, 15, 435-449.
- Gray, M.B., J. Stamatakos (1997). New model for evolution of fold and thrust belt curvature based on integrated structural and paleomagnetic results from the Pennsylvania salient. *Geology*, 25, 1067-1070.
- Gregory-Wodzicki, K. M. (2000). Uplift history of the central and northern Andes: A review. *GSA Bull.*, 112, 1091–1105.
- Grubbs, K.L., R. Van der Voo (1976). Structural deformation of the Idaho-Wyoming overthrust belt (USA), as determined by triassic paleomagnetism. *Tectonophysics*, 33, 321-336.
- Grunow, A.M. (1993). New paleomagnetic data from the Antarctic Peninsula and their tectonic implications. *J. Geophys. Res.* 98, 13,815-13,833.
- Gubbels T, B. Isacks, E. Farrar (1993). High level surfaces, plateau uplift, and foreland development, Bolivian central Andes. *Geology*, 21, 695-698.
- Gürsoy, H., Piper, J.D.A., Tatar, O., Temiz, H. (1997). A paleomagnetic study of the Sivas basin, Central Turkey: crustal deformation during lateral extrusion of the Anatolian block. *Tectonophysics*, 271, 89– 105.
- Hartley, A , E. Jolly, P. Turner (1992). Paleomagnetic evidence for rotation in the Precordillera of northern Chile: Structural constraints and implications for the evolution of the Andean forearc. *Tectonophysics*, 205, 49-64.
- Hartley, A. (2003). Andean uplift and climate change. *J. Geol. Soc. London*, 160, 7-10.
- Hérail, G, J. Oller, P. Baby, J. Blanco, M.G. Bonhomme, P. Soler (1996). The Tupiza, Nazareno and Estarca basins (Bolivia): strike-slip faulting and related basins in the Cenozoic evolution of the southern branch of the Bolivian Orocline. *Tectonophysics*, 259, 201-212.
- Hindle, D., O. Bessonb, M. Burkhard (2000). A model of displacement and strain for arc-shaped mountain belts applied to the Jura arc. *Journal of Structural Geology*, 22, 1285-1296.
- Hindle, D., J. Kley, E. Klosko, S. Stein, T. Dixon, E. Norabuena (2002). Consistency of geologic and geodetic displacements during Andean orogenesis. *Gephys. Res. Lett.*, 29(8), doi:10.1029/2001GL013757.
- Hirt, A.M., W. Lowrie (1988). Paleomagnetism of the Umbrian-Marches orogenic belt. *Tectonophysics*, 146, 91-103.
- Hobbs, W.H. (1914). Mechanics of formation of arcuate mountain belts. *Journal of Geology*, 22, 72-90.
- Hoke, G., C. Garziona (2008). Paleosurfaces, paleoelevation, and the mechanisms for the late Miocene topographic development of the Altiplano plateau. *Earth Planet. Sci. Lett.*, 271, 192-201.
- Hongn, F., C. del Papa, J. Powell, I. Petrinovic, R. Mon, V. Deraco (2007). Middle Eocene deformation and sedimentation in the Puna–Eastern Cordillera transition (23°–26°S): Control by preexisting heterogeneities on the pattern of initial Andean shortening. *Geology*, 35(3), 271-274.

- Horberg, L., V. Nelson, V. Church (1949). Structural trends in central western Wyoming. *Geol. Soc. Am. Bull.*, 60, 183-216.
- Horton, B.K. (1998). Sediment accumulation on top of the Andean orogenic wedge: Oligocene to late Miocene basins of the Eastern Cordillera, southern Bolivia. *Geol. Soc. Amer. Bull.*, 110, 1174-1192.
- Horton, B.K., B.A. Hampton, G.L. Waanders (2001). Paleogene synorogenic sedimentation in the Altiplano Plateau and implications for initial mountain building in the Central Andes. *Geol. Soc. Amer. Bull.*, 113, 1387-1400.
- Horton, B.K., B.A. Hampton, B.N. LaReau, E. Baldellon (2002). Tertiary provenance history of the northern and central Altiplano (central Andes, Bolivia): a detrital record of plateau-margin tectonics. *J. Sediment. Res.*, 72, 711-726.
- Hrouda, F. (1994). A technique for the measurement of thermal changes of magnetic susceptibility of weakly magnetic rocks by the CS-2 apparatus and KLY-2 Kappabridge. *Geophys. J. Int.*, 118, 604-612.
- Hrouda, F., Janák, F. (1976). The changes in shape of the magnetic susceptibility ellipsoid during progressive metamorphism and deformation. *Tectonophysics*, 34, 135-148.
- Iglesia Llanos, M.P., Lanza, R., Riccardi, A.C., Geuna, S., Laurenzi, M.A., Ruffini, R. (2003). Palaeomagnetic study of the El Quemado complex and Marifil formation, Patagonian Jurassic igneous province, Argentina. *Geophys. J. Int.* 154, 599-617.
- Irving, E., P.J. Wynne (1991). Paleomagnetism: Review and tectonic implications, Chapter 3. In: H. Gabrielse, C.J. Yorath (Eds.), *Geology of the Cordilleran Orogen in Canada*, Geological Survey of America, Denver, CO, pp. 61-86.
- Isacks, B.L. (1988). Uplift of the central Andean plateau and bending of the Bolivian orocline. *J. Geophys. Res.*, 93, 3211– 3231.
- Jackson, J. (1994). Active tectonics of the Aegean region. *Annu. Rev. Earth Planet. Sci.*, 22, 239-271.
- Jelinek, V. (1977). The statistical theory of measuring anisotropy of magnetic susceptibility of rocks and its application. *Geofyzika*, Brno, pp. 88.
- Jelinek, V. (1978). Statistical processing of magnetic susceptibility on groups of specimens. *Stud. Geophys. Geod.*, 22, 50-62.
- Johnstone, S.T. (2001). The Great Alaskan Terrane Wreck: reconciliation of paleomagnetic and geological data in the northern Cordillera. *Earth Planet. Sci. Lett.*, 193, 259-272.
- Jolivet, L., J.-P. Brun, P. Gautier, S. Lallemand and M. Patriat (1994). 3D-kinematics of extension in the Aegean region from the Early Miocene to the Present: insights from the ductile crust. *Bull. Geol. Soc. Fr.*, 165, 195-209.
- Jordan, T.E., R.N. Alonso (1987). Cenozoic stratigraphy and basin tectonics of the Andes Mountains, 20–28 south latitude. *AAPG Bull.*, 71, 49-64.
- Jordan, T.E., J.H. Reynolds, J.P. Erikson (1997). Variability in age of initial shortening and uplift in the central Andes, 16–33°30'S. In: Ruddiman, W.F. (Ed.), *Tectonic Uplift and Climate Change*. Plenum Press, New York, pp. 41- 61.

- Jordan, T. E., M. Burns, R. Veiga, F. Pangaro, S. Kelley, C. Mpodozis (2001). Extension and basin formation in the southern Andes caused by increased convergence rate: A mid-Cenozoic trigger for the Andes. *Tectonics*, 20, 308-324.
- Kempf, O., Schlunegger, F., Strunck, P., Matter, A. (1998). Paleomagnetic evidence for late Miocene rotation of the Swiss Alps: results from the north Alpine foreland basin. *Terra Nova*, 10, 6-10.
- Kennan, L., S.H. Lamb, C. Rundle (1995). K–Ar dates from the Altiplano and Cordillera Oriental of Bolivia: implications for Cenozoic stratigraphy and tectonics. *J. S. Am. Earth Sci.*, 8, 163-186.
- Kent, D.V. (1988). Further paleomagnetic evidence for oroclinal rotation in the Central folded Appalachians from the Bloomsburg and the Mauch Chunk Formations. *Tectonics*, 7, 749-759.
- Kimura, G. (1986). Oblique subduction and collision: Forearc tectonics of the Kuril arc. *Geology*, 14, 404–407.
- Kirschvink, J.L. (1980). The least-squares line and plane and the analysis of paleomagnetic data. *Geophys. J. R. astr. Soc.*, 62, 699-718.
- Kissel, C., Laj, C. (1988). The Tertiary geodynamical evolution of the Aegean arc: a paleomagnetic reconstruction. *Tectonophysics*, 146, 183–201.
- Kissel, C., Speranza, F. (1995). Paleomagnetism of external southern and central Dinarides and northern Albanides: implications for the Cenozoic activity of the Scutari-Pec Transverse zone. *J. Geophys. Res.*, 100, 14999-15007.
- Kissel, G., C., Kissela, C. Laja, A. Poissonb, N. Görür (2003). Paleomagnetic reconstruction of the Cenozoic evolution of the Eastern Mediterranean. *Tectonophysics*, 362, 199-217.
- Kley, J. (1996). Transition from basement-involved to thin-skinned thrusting in the Cordillera Oriental of southern Bolivia. *Tectonics*, 15, 763-775.
- Kley, J., C.R. Monaldi (1998). Tectonic shortening and crustal thickness in the Central Andes: how good is the correlation? *Geology*, 26(8), 723-726.
- Kley, J., A.H. Gangui, D. Kruger (1996). Basement involved blind thrusting in the eastern Cordillera Oriental, southern Bolivia: evidence from cross-sectional balancing, gravimetric and magnetotelluric data. *Tectonophysics*, 259, 179-184.
- Kley, J., J. Mqller, S. Tawackoli, V. Jacobshagen, E. Manutsoglu (1997). Pre-Andean and Andean-age deformation in the Eastern Cordillera of southern Bolivia. *J. S. Am. Earth Sci.* 10, 1-19.
- Kley, J., C.R. Monaldi, J.A. Salfity (1999). Along-strike segmentation of the Andean foreland: causes and consequences. *Tectonophysics*, 301, 75-94.
- Kley, J., C. R. Monaldi, E. Rossello, and B. Habighorst (2005). Seismic and field evidence for selective inversion of Cretaceous normal faults, Salta rift, northwest Argentina. *Tectonophysics*, 399, 155-172.
- Kohn, M.J., Spear, F.S., Harrison, T.M., Dalziel, I.D.W. (1995).  $^{40}\text{Ar}/^{39}\text{Ar}$  geochronology and P-T-t paths from the Cordillera Darwin metamorphic complex, Tierra del Fuego, Chile. *J. Metam. Geol.*, 13, 251-270.
- Kraemer, P.E. (2003). Orogenic shortening and the origin of the Patagonian orocline (56 degrees S. Lat). *J. South Am. Earth Sci.*, 15, 731-748.

- Lamb, S. (2001a). Vertical axis rotation in the Bolivian orocline, South America. 1. Paleomagnetic analysis of Cretaceous and Cenozoic rocks. *J. Geophys. Res.*, 106, 26,605-26,632.
- Lamb, S. (2001b). Vertical axis rotation in the Bolivian orocline, South America. 2. Kinematic and dynamical implications. *J. Geophys. Res.*, 106, 26,633-26,653.
- Laubsher, H.P. (1972). Some overall aspects of Jura dynamics. *Am. J. Sci.*, 272, 293-304.
- Laubscher, H.P. (1992). Jura kinematics and the Molasse basin. *Eclogae geologicae Helvetiae*, 85, 653-676.
- Lawver, L.A., Gahagan, L.M. (2003). Evolution of Cenozoic seaways in the circum-Antarctic region. *Palaeogeography Palaeoclimatology Palaeoecology*, 198, 11-38.
- Le Pichon, X. (1982). Landlocked ocean basins and continental collision: the eastern Mediterranean as a case example. In: Hsu, K. (Ed.), Mountain building processes. London Academic press, 201-211.
- Lee, J., G.S. Lister (1992). Late Miocene ductile extension and detachment faulting, Mykonos, Greece. *Geology*, 20, 121-124.
- Lefort, J.P., and Van der Voo, R. (1981). A kinematic model for the collision and complete suturing between Gondwanaland and Laurussia in the Carboniferous. *J. Geol.*, 89, 537-550.
- Lickorish, W.H., Grasso, M., Butler, R.W.H., Argnani, A., Maniscalco, R. (1999). Structural styles and regional tectonic setting of the "Gela Nappe" and frontal part of the Maghrebian thrust belt in Sicily. *Tectonics*, 18, 655-668.
- Lickorish, W.H., M. Ford, J. Bürgisser, P.R. Cobbold (2002). Arcuate thrust systems in sandbox experiments: A comparison. *GSA Bull.*, 114, 1089-1107.
- Linares, E. (1979). Catálogo de edades radiométricas realizadas por INGEIS y sin publicar II. Años 1975-1976. Publicaciones Especiales de la Asociación Geológica Argentina. Serie "B", Didáctica y Complementaria, 6, 32 p., Buenos Aires.
- Linares, E., Parica, C. A., Parica, P. D. (1987). Catálogo de edades radiométricas realizadas por INGEIS y sin publicar IV. Años 1979-1980. Publicaciones Especiales de la Asociación Geológica Argentina. Serie "B", Didáctica y Complementaria, 15, 49 p., Buenos Aires.
- Linzer, H.G. (1996). Kinematics of retreating subduction along the Carpathian Arc, Romania. *Geology*, 24(2), 167-170.
- Linzer, H.G., W. Frisch, P. Zweigel, R. Girbacea, H.-P. Hann, F. Moser (1998). Kinematic evolution of the Romanian Carpathians. *Tectonophysics*, 297, 133-156.
- Livermore, R., Nankivell, A., Eagles, G., Morris, P. (2005). Paleogene opening of Drake Passage. *Earth Planet. Sci. Lett.* 236, 459-470.
- Lodolo, E., Coren, F., Schreider, A.A., Ceccone, G. (1997). Geophysical evidence of a relict oceanic crust in the southwestern Scotia Sea. *Mar. Geophys. Res.*, 19, 439-450.
- Lodolo, E., Menichetti, M. Bartole, R., Ben-Avraham, Z., Tassone, A., Lippai, H. (2003). Magallanes-Fagnano continental transform fault (Tierra del Fuego, southernmost South America). *Tectonics*, 22(6), 1076, doi:10.1029/2003TC001500.
- Lodolo, E., Donda, F., Tassone, A. (2006). Western Scotia Sea margins: Improved constraints on the opening of the Drake Passage. *J. Geophys. Res.*, 111, B06101, doi:10.1029/2006JB004361.

- Lowrie, W. (1990). Identification of ferromagnetic minerals in a rock by coercivity and unblocking temperature properties. *Geophys. Res. Lett.*, 17(2), 159-162.
- Lowrie, W., A.M. Hirt (1986). Paleomagnetism in arcuate mountain belts. In: The orogin of Arcs. Developments in geotectonics, vol. 21, Elsevier, Amsterdam, pp. 141-158.
- Lowrie, W., A.M. Hirt, and R. Kligfield (1986). Effects of tectonic deformation on the remanent magnetization of rocks. *Tectonics*, 5(5), 713-722.
- Lu, C.Y. and Malavieille, J. (1994). Oblique convergence, indentation and rotation tectonics in Taiwan Mountain belt: Insights from experimental modelling. *Earth Planet. Sci. Lett.*, 121, 477-494.
- Lucente, F.P., C. Chiarabba, G.B. Cimini, D. Giardini (1999). Tomographic constraints on the geodynamic evolution of the Italian region. *J. Geophys. Res.*, 104, 20,307– 20,327.
- MacDonald, W.D. (1980). Net tectonic rotation, apparent tectonic rotation, and structural tilt correction in paleomagnetic studies. *J. Geophys. Res.*, 85, 3659-3669.
- Macedo, J., S. Marshak (1999). Controls on the geometry of fold-thrust belt salients, *GSA Bulletin*, 111(12), 1808–1822.
- MacFadden, B.J., F. Anaya, H. Perez, C.W. Naeser, P.K. Zeitler, K.E. Campbell (1990). Late Cenozoic paleomagnetism and chronology of Andean basins of Bolivia: Evidence for possible oroclinal bending. *J. Geol.*, 98, 541–555.
- MacFadden, B.J., F. Anaya, J. Argollo (1993). Magnetic polarity stratigraphy of Inchasi: A Pliocene mammal-bearing locality from the Bolivian Andes deposited just before the Great American Interchange. *Earth Planet. Sci. Lett.*, 114, 229–241.
- MacFadden, B.J., F. Anaya, C.C. Swisher III (1995). Neogene paleomagnetism and oroclinal bending of the central Andes of Bolivia. *J. Geophys. Res.*, 100, 8153– 8167.
- Maffione, M., Speranza, F., Faccenna, C., Cascella, A., Vignaroli, G., Sagnotti, L. (2008). A synchronous Alpine and Corsica-Sardinia rotation. *J. Geophys. Res.*, 113, B03104, doi:10.1029/2007JB005214.
- Maffione, M., Speranza, F., Faccenna. Bending of the Bolivian orocline and growth of the Central Andean plateau: paleomagnetic and structural constraints from the Eastern Cordillera (22-24°S, NW Argentina). Submitted to *Tectonics*, 2008.
- Maffione, M., Speranza, F., Faccenna, E.A. Rossello. Paleomagnetic evidence for a pre-early Eocene (~50 Ma) bending of the Patagonian orocline (Tierra del Fuego, Argentina): paleogeographic and tectonic implications. Submitted to *Eart Planet. Sci. Lett.*, 2009.
- Malinverno, A., W.B.F. Ryan (1986). Extension in the Tyrrhenian Sea and shortening in the Apennines as result of arc migration driven by sinking of the lithosphere. *Tectonics*, 5, 227 – 245.
- Malumián, N., Olivero, E.B. (2006). El Grupo Cabo Domingo, Tierra del Fuego: Bioestratigrafía, paleoambientes y acontecimientos del Eoceno-Mioceno marino. *Rev. Asoc. Geol. Argentina*, 61(2), 139-160.
- Marques, F.O., P.R. Cobbold (2002). Topography as a major factor in the development of arcuate thrust belts: insights from sandbox experiments. *Tectonophysics*, 348, 247– 268.

- Marquillas, R. A., C. del Papa, I.F. Sabino (2005). Sedimentary aspects and paleoenvironmental evolution of a rift basin: Salta Group (Cretaceous-Paleogene), northwestern Argentina. *Int. J. Earth Sci.*, 94, 94-113.
- Marrett, R.A., R.W. Allmendinger, R.N. Alonso, R.E. Drake (1994). Late Cenozoic tectonic evolution of the Puna Plateau and adjacent foreland, northwestern Argentine Andes. *J. S. Am. Earth Sci.*, 7, 179-208.
- Marshak, S. (1988). Kinematics of orocline and arc formation in thin-skinned orogens. *Tectonics*, 7(1), 73-86.
- Marshak, S., M.S. Wilkerson (1992). Effects of overburden thickness on thrust belt geometry and development. *Tectonics*, 11, 560-566.
- Marshak, S., P.A. Geiser, W. Alvarez, T. Engelder (1982). Mesoscopic fault array of the northern Umbrian Apennine fold belt, Italy: Geometry of conjugate shear by pressure-solution slip. *Geol. Soc. Am. Bull.*, 93, 1013-1022.
- Marshak, S., P. Kwiecinski, D. McEachran, J. Tabor (1985). Structural geometry of the "orocline" in the Appalachian foreland, near Kingstone, New York. *Geol. Soc. Am. Abstr. Programs*, 17, 53.
- Marshak, S., Wilkerson, M.S., Hsui, A.T. (1992). Generation of curved fold-thrust belts: Insights from simple physical and analytical models. In *Thrust Tectonics*, K.R. McClay (Ed.), Chapman & Hall, London. pp. 83-92.
- Marshall, L.G., T. Sempere (1991). The Eocene to Pleistocene vertebrates of Bolivia and their stratigraphic context: a review. In *Fosiles y Facies de Bolivia. Vol. 1: Vertebrados*, (ed) R Suarez-Socuco, 12, 631-652. Santa Cruz, Bolivia: Rev. Tecnica Yacim. Petrol. Fisc. Boliv.
- Mañenco, L., Bertotti, G., Dinu, C. Cloetingh, S. (1997). Tertiary tectonic evolution of the external South Carpathians and the adjacent Moesian platform (Romania). *Tectonics*, 16, 869-911.
- Mattei, M., P. Cipollari, D. Cosentino, A. Argentieri, F. Rossetti, F. Speranza (2002). The Miocene tectonic evolution of the southern Tyrrhenian Sea: Stratigraphy, structural and paleomagnetic data from the on-shore Amantea basin (Calabrian Arc, Italy). *Basin Res.*, 14, 147-168.
- Mattei, M., V. Petrocelli, D. Lacava, M. Schiattarella (2004). Geodynamic implications of Pleistocene ultrarapid vertical-axis rotations in the southern Apennines, Italy. *Geology*, 32, 789-792.
- McFadden, P.L. (1990). A new fold test for paleomagnetic studies. *Geophys. J. Int.*, 103, 163-169.
- McFadden, P.L., M.W. McElhinny (1990). Classification of the reversal test in paleomagnetism. *Geophys. J. Int.*, 130, 725-729.
- McKenzie, D. (1972). Active tectonics of the Mediterranean region. *Geophys. J. R. Astron. Soc.*, 30, 109-185.
- McKenzie, D. (1978). Active tectonics of the Alpine-Himalayan belt; the Aegean Sea and surrounding regions. *Geophys. J. Royal Astr. Soc.*, 55, 217-254.
- McKenzie, D., Jackson, J. (1983). The relationship between strain rates, crustal thickening, palaeomagnetism, finite strain and fault movements within a deforming zone. *Earth Planet. Sci. Lett.*, 65, 182-202.
- McQuarrie, N., (2002). Building a high plateau: the kinematic history of the central Andean fold-thrust belt, Bolivia. *Geol. Soc. Amer. Bull.*, 114, 950-963.

- McQuarrie, N., DeCelles, P.G. (2001). Geometry and structural evolution of the central Andean Backthrust belt, Bolivia. *Tectonics*, 17, 203-220.
- McQuarrie, N., B. K. Horton, G. Zandt, S. Beck, DeCelles, P. G., (2005). Lithospheric evolution of the Andean fold-thrust belt, Bolivia, and the origin of the central Andean plateau. *Tectonophysics*, 399, 15-37.
- McQuarrie, N., J.B. Barnes, T.A. Ehlers (2008). Geometric, kinematic, and erosional history of the central Andean Plateau, Bolivia (15-17°S). *Tectonics*, 27, TC3007, doi:10.1029/2006TC002054.
- Miller, J.D., Kent D.V. (1986). Paleomagnetism of the upper Devonian Catskill Formation from the southern limb of the Pennsylvania salient: possible evidence of oroclinal rotation. *Geophys. Res. Lett.*, 13, 1173-1176.
- Mingramm, A, A. Russo, A. Pozzo, L. Casau (1979). Sierras subandinas. In *Segundo Simposio de Geología Regional Argentina*, pp. 95–138. Córdoba: Acad. Nac. Ciencias.
- Miser, H.D. (1932). Oklahoma structural salient of the Ouachita Mountains. *GSA Bull.*, 43, 138 p.
- Molnar, P., P. Tapponnier (1978). Active tectonics of Tibet. *J.Geophys. Res.*, 83, 5361-5375.
- Monaldi, C.R., J.A. Salfity, J. Kley (2008). Preserved extensional structures in an inverted Cretaceous rift basin, northwestern Argentina: Outcrop examples and implications for fault reactivation. *Tectonics*, 27, TC1011, doi:10.1029/2006TC001993.
- Moore, G.W. (1973). Westward tidal lag as the driving force of plate tectonics. *Geology*, 1, 99-100.
- Moreno, J.A. (1970). Estratigrafía y paleogeografía del Cretácico superior en la cuenca del noroeste argentino, con especial mención de los Subgrupos Balbuena y Santa Barbara. *Rev. Asoc. Geol. Arg.*, 24, 9-44.
- Moretti, I., P. Baby, E. Méndez, D. Zubieta (1996). Hydrocarbon generation in relation to thrusting in the Sub Andean Zone from 18 to 22°S, Bolivia. *Petroleum Geoscience*, 2, 17-28.
- Morley, C.K. (1996). Models for relative motion of crustal blocks within the Carpathian region, based on restorations of the outer Carpathians thrust sheets. *Tectonics*, 15, 885-904.
- Morris, A., Anderson, M. (1996). First paleomagnetic results from the Cycladic massif, Greece, and their implications for Miocene extension directions and tectonic models in the Aegean. *Earth Planet. Sci. Lett.* 142, 397-408.
- Mugnier, J.L., Guellec, S., Ménard, G., Roure, F., Tardy, M., Vialon, P. (1990). A crustal scale balanced cross-section through the external Alps deduced from the ECORS profile. In: Roure, F, Heitzmann, P, Polino, R (Eds.), Deep Structure of the Alps, vol. 1. *Mém. Soc. géol. suisse*, Zurich, pp. 203-216.
- Müller, J.P., J. Kley, V. Jacobshagen (2002). Structure and Cenozoic kinematics of the Eastern Cordillera, southern Bolivia (21°S). *Tectonics*, 21, doi:10.1029/2001TC001340.
- Muttoni, G., L. Lanci, A. Argnani, A.M. Hirt, U. Cibin, N. Abrahamsen, W. Lowrie (2000). Paleomagnetic evidence for a Neogene two-phase counterclockwise tectonic rotation in the Northern Apennines (Italy). *Tectonophysics*, 326, 241-253.
- Nur, A., R. Hagai, S. Oona (1986). Fault mechanics and the kinematics of block rotations. *Geology*, 14, 746-749.

- Olivero, E.B., Malumián, N. (1999). Eocene stratigraphy of southeastern Tierra del Fuego island, Argentina. *AAPG Bull.*, 83(2), 295-313.
- Olivero, E.B., Martinioni, D.R. (2001). A review of the geology of the Argentinian Fuegian Andes. *J. South Am. Earth Sci.*, 14, 175-188.
- Olivero, E.B., Malumián, N. (2008). Mesozoic-Cenozoic stratigraphy of the Fuegian Andes, Argentina. *Geologica Acta*, 6 (1), 5-18.
- Olivero, E.B., Malumián, N., Palamarczuk, S., Scasso, R.A. (2001). El Cretácico superior-Paleogeno del área del Río Bueno, costa atlántica de la Isla Grande de Tierra del Fuego. *Rev. Asoc. Geol. Argentina*, 57(3), 199-218.
- Olivero, E.B., Malumián, N., Palamarczuk, S. (2003). Estratigrafía del Cretácico superior-Paleoceno del área de bahía Thetis, Andes Fueguinos, Argentina: acontecimientos tectónicos y paleobiológicos. *Rev. Geol. Chile*, 30, 245-263.
- Oncken, O., D. Hindle, J. Kley, K. Elger, P. Victor, K. Schemmann (2006). Deformation of the Central Andean Upper Plate System - Facts, Fiction, and Constraints for Plateau Models. In: *Frontiers in Earth Science, The Andes*, Oncken, O., et al. (Eds), Springer Berlin Heidelberg, Part I, 3-27, doi.: 10.1007/978-3-540-48684-8\_1.
- Parés, J.M., R. Van der Voo (1992). Paleozoic paleomagnetism of Almaden, Spain: A cautionary note. *J. Geophys. Res.*, 97, 9353-9356.
- Parés, J.M., Van der Voo, R., Stamatakos, J.A., Pérez-Estaún, A. (1994). Remagnetization and post-folding oroclinal rotations in the Cantabrian/Asturian arc, northern Spain. *Tectonics*, 13, 1461-1471.
- Pătrașcu, St., Panaiotu, C., Seclaiaman, M. Panaiotu, C.E. (1994). Timing of rotational motion of Apuseni Mountains (Romania): Paleomagnetic data from Tertiary magmatic rocks. *Tectonophysics*, 233, 163-176.
- Pavoni, N. (1986). Regularities in the pattern of major fault zones of the Earth and the origin of arcs, in Wezel, F. C., ed., *The origin of arcs*: Amsterdam, Elsevier, p. 63-78.
- Pelayo, A.M., Wiens, D.A. (1989). Seismotectonics and relative plate motion in the Scotia Sea region. *J. Geophys. Res.* 94, 7293-7320.
- Perroud, H., (1982). Relations paléomagnétisme et déformation: Exemple de la région de Cabo de Peñas (Espagne). *Comptes rendus de l'Académie des sciences. Série II, Sciences de la terre et des planètes*, 294, 45-48.
- Perroud, H., (1983). Paleomagnetism of Paleozoic rocks from the Cabo de Peñas, Asturia, Spain. *Geophysical Journal of the Royal Astronomical Society*, 75, 201-215.
- Perroud, H., (1985). Paléomagnétisme dans l'arc ibéro-armoricain et l'orogénèse Varisque en Europe occidentale. Ph.D. thesis, Univ. de Rennes I, Rennes, France.
- Perroud, H., (1986). Paleomagnetic evidence for tectonic rotations in the Variscan Mountain Belt. *Tectonics*, 5, 205-214.
- Perroud, H., N. Bonhomme (1981). Paleomagnetism of the Ibero-Armorican arc and the Hercynian orogeny in western Europe. *Nature*, 292, 445-448.

- Philippe, Y. (1994). Transfer zone in the Southern Jura Thrust Belt (eastern France): Geometry, development and comparison with analogue modelling experiments. In: Mascle, A. (Ed.), Hydrocarbon and Petroleum Geology of France (special issue). *European Association of Petroleum Geology Special Publication*, 4, 327-346.
- Philippe, Y. (1995). Rampes latérales et zones de transfert dans les chaînes plissées. Unpublished PhD thesis, Université de Savoie.
- Piper, J.D.A., Moore, J.M., Tatar, O., Gursoy, H., Park, R.G. (1996). Palaeomagnetic study of crustal deformation across an intracontinental transform: the North Anatolian Fault Zone in Northern Turkey. In: Morris, A., Tarling, D.H. (Eds.), Palaeomagnetism and Tectonics on the Mediterranean Region. *Geol. Soc. Spec. Publ.* 105, 299– 310.
- Piromallo, C., A. Morelli (2003). P wave tomography of the mantle under the Alpine-Mediterranean area. *J. Geophys. Res.*, 108(B2), 2065, doi:10.1029/2002JB001757.
- Platt, J.P., P.C. England (1994). Convective removal of lithosphere beneath mountain belts; thermal and mechanical consequences. *Am. J. Sci.*, 294, 307-336.
- Platzman, E.S., Tapirdamaz, C., Sanver, M. (1998). Neogene anticlockwise rotation of central Anatolia (Turkey): preliminary paleomagnetic and geochronological results. *Tectonophysics* 299, 175– 189.
- Prezzi, C., J. Vilas (1998). New evidence of clockwise vertical axis rotations south of the Arica elbow (Argentine Puna). *Tectonophysics*, 292, 85–100.
- Prezzi, C.B., R.N. Alonso (2002). New paleomagnetic data from the northern Argentine Puna: Central Andes rotation pattern reanalyzed. *J. Geophys. Res.*, 107(B2), 2041, doi:10.1029/2001JB000225.
- Prezzi, C.B., F.A. Vilas, A.M. Sinito (1996). Estudio paleomagnético de rocas sedimentarias terciarias de la Puna salteña: determinación de rotaciones horarias. *Rev. Assoc. Geol. Argent.*, 51(3), 261-273.
- Prezzi, C.B., P.J. Caffè, R. Somoza (2004). New paleomagnetic data from the northern Puna and western Cordillera Oriental, Argentina: a new insight on the timing of rotational deformation. *J. Geodynamics*, 38, 93-115.
- Ramos, V.A. (1977). Basement tectonics from landsat imagery in mining exploration. *Geologie en Mijnbouw*, 56(3) 243-252.
- Ramos, V.A., Aleman, A. (2000). Tectonic evolution of the Andes. In: Cordani, U., et al. (Eds.), Tectonic evolution of South America: Rio de Janeiro, Brazil. Proceedings of the 31<sup>o</sup> International Geological Congress, Rio de Janeiro, Brazil, In-folio Producao Editorial, 635-685.
- Ramos, V.A., M.A. Turic, and A.B. Zuzek (1967). Geología de las Quebradas de Huichaira-Pocoya, Purmamarca y Tumbaya Grande en el margen de la Quebrada de Humahuaca (provincia de Jujuy). *Rev. Asoc. Geol. Arg.*, XXII(3), 209-221.
- Ramsay, J.G. (1981). Tectonics of the Helvetic Nappes. *Spec. Pap. Geol. Soc. London*, 9, 293-309.
- Randall, D.E. (1998). A new Jurassic-Recent apparent polar wander path for South America and a review of central Andean tectonic models. *Tectonophysics*, 299, 49-74.
- Randall, D.E., G.K. Taylor, J. Grocott (1996). Major crustal rotations in the Andean margin: paleomagnetic results from the Coastal Cordillera of northern Chile. *J. Geophys. Res.*, 101(B7), 15783-15798.

- Randall, D.E., A. Tomlinson, G.K. Taylor (2001). Paleomagnetically defined rotations from the Precordillera of northern Chile: Evidence of localized in situ fault-controlled rotations. *Tectonics*, 20, 235-254.
- Rapalini, A.E. (2007). A paleomagnetic analysis of the Patagonian orocline. *Geologica Acta*, 5(4), 287-294.
- Rapalini, A.E., Hervé, F., Ramos, V.A., Singer, S. (2001). Paleomagnetic evidence of a very large counterclockwise rotation of the Madre de Dios archipelago, southern Chile. *Earth Planet. Sci. Lett.*, 184(2), 471-487.
- Rapalini, A.E., Calderón, M., Hervé, F., Cordani, U., Singer, S. (2004). First Paleomagnetic Results on the Sarmiento Ophiolite, Southern Chile: Implications for the Patagonian Orocline. Geosur 2004, Internat. Symp. on the Geology and Geophysics of the Southernmost Andes, the Scotia Arc and the Antarctic Peninsula, Buenos Aires, Bolletino de Geofisica Teórica ed Aplicata, 45, 246-249.
- Rapalini, A.E., Lippai, H., Tassone, A., Cerredo, M.E. (2005). An AMS and paleomagnetic study across the Andes in Tierra del Fuego. 6th International Symposium on Andean Geodynamics (ISAG 2005, Barcelona), Extended Abstracts, 596-599.
- Ratschbacher, L., Linzer, H.G., Moser, F., Strusievcz, R.O., Bedeleian, H., Har, N., Mogos, P.A. (1993). Cretaceous to Miocene thrusting and wrenching along the central South Carpathians due to a corner effect during collision and orocline formation. *Tectonics*, 12, 855-873.
- Richards, D.R., R.F. Butler, T. Sempere (2004). Vertical-axis rotations determined from paleomagnetism of Mesozoic and Cenozoic strata of the Bolivian Andes. *J. Geophys. Res.*, 109, B07104, doi:10.1029/2004JB002977.
- Ries, A.C., R.M. Shackleton (1976). Patterns of strain variation in arcuate fold belts. *Philos. Trans. R. Soc. London, Ser. A*, 283, 281-288.
- Ries, A. C., A. Richardson, R. M. Shackleton (1980). Rotation of the Iberian arc: Paleomagnetic results from north Spain. *Earth Planet. Sci. Lett.*, 50, 301-310.
- Riller, U., O. Oncken (2003). Growth of the central Andean Plateau by tectonic segmentation is controlled by the gradient in crustal shortening. *J. Geol.*, 111, 367-384.
- Riller, U., I. Petrinovic, J. Ramelow, M. Strecker, O. Oncken (2001). Late Cenozoic tectonism, collapse caldera and plateau formation in the central Andes. *Earth Planet. Sci. Lett.*, 188, 299-311.
- Rochette, P. (1987). Magnetic susceptibility of the rock matrix related to magnetic fabric studies. *J. Struct. Geol.*, 9, 1015-1020.
- Rodríguez Hernández, L.R., N. Heredia, R.E. Seggiaro, M.A. González (1999). Estructura andina de la Cordillera Oriental en el área de la Quebrada de Humahuaca, provincia de Jujuy, NO de Argentina. *Trabajos de Geología, Universidad de Oviedo*, 21, 321-335.
- Roperch, P., G. Carlier (1992). Palcomagnetism of Mesozoic rocks from the central Andes of southern Peru: Importance of rotations in the development of the Bolivian orocline. *J. Geophys. Res.*, 97, 17,233-17,249.
- Roperch, P., L. Aubry, G. Hérail, M. Fornari, A. Chauvin (1996). Magnetostratigraphy and paleomagnetic rotation of the North-Central Bolivian Altiplano Basin. *3rd Int. Symp. Andean Geodynamics*, ORSTOM, St. Malo, 477-480.

- Roperch, P., Chauvin, A., Calza, F., Palacios, C., Parraguez, G., Pinto, L., Goguitchaivilli, A. (1997). Paleomagnetismo de las rocas volcánicas del Jurásico tardío al Terciario temprano de la región de Aysén (Coyhaique-Cochrane). 8° Congreso Geológico Chileno, Antofagasta, Universidad Católica del Norte, Actas, 1, 236-240.
- Roperch, P., G. Hérail, M. Fornari (1999). Magnetostratigraphy of the Miocene Corque basin, Bolivia: Implications for the geodynamic evolution of the Altiplano during the late Tertiary. *J. Geophys. Res.*, 104, 20,415–20,429.
- Roperch, P., M. Fornari, G. Hérail, G.V. Parraguez (2000). Tectonic rotations within the Bolivian Altiplano: Implications for the geodynamic evolution of the central Andes during the late Tertiary. *J. Geophys. Res.*, 105, 795-820.
- Rossello, E.A. (2005). Kinematics of the Andean sinistral wrenching along the Fagnano-Magallanes Fault Zone (Argentina-Chile Fuegian Foothills). 6th International Symposium on Andean Geodynamics. Barcelona, Actas 623-626.
- Rossello, E.A., Haring, C.E., Nevistic A.V., Cobbold, P.R. (2004a). Wrenching along the Fagnano-Magallanes fault zone, northern foothills of the Fuegian Cordillera (Argentina-Chile): preliminary evaluation of displacements. 32° International Geological Congress, Firenze, CD-Room.
- Rossello, E.A., E.G. Ottone, C.E. Haring, V.A. Nevistic (2004b). Significado tectónico y paleoambiental de los niveles carbonosos paleógenos de Estancia La Correntina, Andes Fueguinos, Argentina. *Asoc. Geol. Argentina, Revista, Geología de la Patagonia (Buenos Aires)*. 59 (4), 778-784.
- Rossello, E.A., Haring, C.E., G. Cardinali, F. Suárez, G.A. Laffitte & A.V. Nevistic (2008). Hydrocarbons and petroleum geology of Tierra del Fuego, Argentina. *Tierra del Fuego Geology and Geophysics: New advances and perspective (Geosur 2004) Guest Editors Menichetti, M., Tassone, A. Geologica Acta (Barcelona, España)*. 6 (1), 69-83.
- Rossetti, F., B. Goffé, P. Monié, C. Faccenna, G. Vignaroli (2004). Alpine orogenic P-T-t-deformation history of the Catena Costiera area and surrounding regions (Calabrian Arc, southern Italy): The nappe edifice of north Calabria revised with insights on the Tyrrhenian-Apennine system formation. *Tectonics*, 23, TC6011, doi:10.1029/2003TC001560.
- Rousse, S., S. Gilder, D. Farber, B. McNulty, P. Patriat, V. Torres, T. Sempere (2003). Paleomagnetic tracking of mountain building in the Peruvian Andes since 10 Ma. *Tectonics*, 22(5), 1048, doi:10.1029/2003TC001508.
- Rousse, S., S. Gilder, M. Fornari, T. Sempere (2005). Insight into the Neogene tectonic history of the northern Bolivian Orocline from new paleomagnetic and geochronologic data. *Tectonics*, 24, TC6007, doi:10.1029/2004TC001760.
- Royden, L.H. (1993). Evolution of retreating subduction boundaries formed during continental collision. *Tectonics*, 12, 629-638.
- Rutten, M.G. (1969). *The geology of Western Europe*. Amsterdam. Elsevier, 520 pp.
- Sagnotti, L., Speranza, F., Winkler, A., Mattei, M., Funicello, R. (1998). Magnetic fabric of clay sediments from the external northern Apennines (Italy). *Phys. Earth Planet. Inter.*, 105, 73-93.

- Salfity JA (1982). Evolucion paleogeografica del Grupo Salta (Cretacico-Eogenico), Argentina, *Actas 5th Congr. Latinoam. Geol*, Buenos Aires, 1, 11-26.
- Salfity, J.A. (1980). Estratigrafia de la Formacion Lecho (Cretacico) en la Cuenca Andina del Norte Argentino. Tesis 1, Universidad Nacional de Salta, Publicacion Especial, 1-91.
- Salfity, J.A., E.M. Brandán, C.R. Monaldi, E.F. Gallardo (1984). Tectonica compresiva cuaternaria en la Cordillera oriental Argentina, latitud de Tilcara (Jujuy), *Noveno Congr. Geol. Arg.*, S.C. Bariloche, Actas II, 427-434.
- Salfity, J.A., R.A. Marquillas (1994). Tectonic and sedimentary evolution of the Cretaceous-Eocene Salta Group Basin, Argentina. In: Salfity JA (ed). *Cretaceous Tectonics of the Andes. Earth Evolution Sciences*, Friedr. Vieweg & Sohn, 266-315.
- Scheepers, P.J.J. (1992). No tectonic rotation for the Apulia-Gargano foreland in the Pleistocene. *Geophys. Res. Lett.*, 19, 2275–2278.
- Scheepers, P.J.J., C.G. Langereis (1994). Paleomagnetic evidence for counter-clockwise rotations in the southern Apennines fold-and-thrust belt during the late Pliocene and middle Pleistocene. *Tectonophysics*, 239, 43–59.
- Schellart, W.P. (2004). Kinematics of subduction and subduction-induced mantle flow in the upper mantle. *J. Geophys. Res.*, 109, B07401, doi: 10.1029/2004JB002970.
- Schellart, W.P., G.S. Lister (2004). Tectonic models for the formation of arc-shaped convergent zones and backarc basins. *GSA Spec. Paper*, 383, 237-258.
- Schlunegger, F., Burbank, D.W., Matter, A., Engesser, B., Moëdden, C. (1996). Magnetostratigraphic calibration of the Oligocene to Middle Miocene (30±15Ma) mammal biozones and depositional sequences of the Swiss Molasse Basin. *Eclogae geologicae Helveticae*, 89, 753-788.
- Schwartz, S.Y., R. Van der Voo (1983). Paleomagnetic evaluation of the orocline hypothesis in the central and southern Appalachians. *Geophys. Res. Lett.*, 10, 505–508.
- Schwartz, S.Y., R. Van der Voo (1984). Paleomagnetic study of thrust sheet rotation during foreland impingement in the Wyoming-Idaho overthrust belt. *J. Geophys. Res.*, 89, 10077-10086.
- Selvaggi, G., C. Chiarabba (1995). Seismicity and P-wave velocity image of the southern Tyrrhenian subduction zone. *J. Geophys. Int.*, 121, 818–826.
- Sempere, T., G. Hérail, J. Oller, M.G. Bonhomme (1990). Late Oligocene–early Miocene major tectonic crisis and related basins in Bolivia. *Geology*, 18, 946-949.
- Sempere, T., R.F. Butler, D.R. Richards, L.G. Marshall, W. Sharp, C.C. Wisher (1997). Stratigraphy and chronology of late Cretaceous–early Paleogene strata in Bolivia and northern Argentina. *Geol. Soc. Amer. Bull.*, 109, 709-727.
- Sengör, A.M.C., Yilmaz, Y. (1981). Tethyan evolution of Turkey: a plate tectonic approach. *Tectonophysics*, 75, 181-241.
- Sengör, A.M.C., B.A. Natal'in (2004). Tectonics of the Altai: an example of a Turkic-type orogen, in van der Pluijm, B.A., and Marshak, S. (eds), *Earth structure*, 2<sup>nd</sup> edition: New York, W.W. Norton and Co., 535-546.

- Servant, M., T. Sempere, J. Argollo, M. Bernat, G. Féraud, P. Lo Bello (1989). Morphogenèse et soulèvement de la Cordillère Orientale des Andes de Bolivie au Cénozoïque, *Académie des Sciences Comptes Rendus*, sér II, 309, p. 417-422.
- Shemenda, A.I. (1993). Subduction of the lithosphere and back arc dynamics; insight from physical modelling. *J. Geophys. Res.*, 98, 16,167-16,185.
- Siddans, A.W.B. (1979). Arcuate fold and thrust patterns in the subalpine chains of southeast France. *J. Struct. Geol.*, 1, 117-126.
- Smalley Jr, R., Kendrick, E., Bevis, M.G., Dalziel, I.W.D., Taylor, F., Lauria, E., Barriga, R., Casassa, G., Olivero, E.B., Piana, E. (2003). Geodetic determination of relative plate motion and crustal deformation across the Scotia-South America plate boundary in eastern Tierra del Fuego. *Geochemistry, Geophysics, Geosystems*, 4, 1-19.
- Somoza, R., A.J. Tomlinson (2002). Paleomagnetism in the Precordillera of northern Chile (22°30'S): Implications for the history of tectonic rotations in the central Andes. *Earth Planet. Sci. Lett.*, 194, 369–381.
- Somoza, R., S. Singer, B. Coira (1996). Paleomagnetism of upper Miocene ignimbrites at the Puna: An analysis of vertical-axis rotations in the Central Andes. *J. Geophys. Res.*, 101, 11,387-11,400.
- Somoza, R., S. Singer, A.J. Tomlinson (1999). Paleomagnetic study of upper Miocene rocks from northern Chile: Implications for the origin of late Miocene-Recent tectonic rotations in the southern central Andes. *J. Geophys. Res.*, 104, 22,923– 22,936.
- Sonder, L.J., P. England, G. Houseman (1986). Continuum calculations of continental deformation in transcurrent environments. *J. Geophys. Res.*, 91(B5), 4797-4810.
- Sonder, L.J., C.H. Jones, S.L. Salyards, K.M. Murphy (1994). Vertical-axis rotations in the Las Vegas Valley Shear Zone, southern Nevada: Paleomagnetic constraints on kinematics and dynamics of block rotations. *Tectonics*, 13 (4), 769-788.
- Speranza, F., Islami, I., Kissel, C., Hyseni, A. (1995). Paleomagnetic evidence for Cenozoic clockwise rotation of the external Albanides. *Earth Planet. Sci. Lett.* 129, 121-134.
- Speranza, F., L. Sagnotti, M. Mattei (1997). Tectonics of the Umbria-Marche-Romagna Arc (central northern Apennines, Italy): New paleomagnetic constraints. *J. Geophys. Res.*, 102(B2), 3153-3166.
- Speranza, F., Maniscalco, R., Mattei, M., Di Stefano, A., Butler, R.W.H., Funicello, R. (1999). Timing and magnitude of rotations in the frontal thrust systems of southwestern Sicily. *Tectonics*, 18(6), 1178-1197.
- Speranza, F., M. Mattei, L. Sagnotti, F. Grasso (2000). Paleomagnetism of upper Miocene sediments from Amantea basin (Calabria, Italy): Rotational differences between the northern and southern Tyrrhenian domains. *J. Geol. Soc. London*, 157, 327–334.
- Speranza, F., Maniscalco, R., Grasso, M. (2003). Pattern of orogenic rotations in central-eastern Sicily: implications for the timing of spreading in the Tyrrhenian Sea. *J. Geol. Soc. London*, 160, 183-195.
- Stamatakos, J., A.M. Hirt (1994). Paleomagnetic considerations of the development of the Pennsylvania salient in the central Appalachians. *Tectonophysics*, 231, 237-255.

- Stamatakos, J., A.M. Hirt, W. Lowrie (1996). The age and timing of folding in the central Appalachians from paleomagnetic results. *GSA Bull.*, 108, 815-829.
- Steinmann, G. (1929). *Geologie von Peru*, Karl Winter (Ed), Heidelberg, Germany. 448 pp.
- Strecker, M.R., P. Cerveny, A.L. Bloom, D. Malizia (1989). Late Cenozoic tectonism and landscape development in the foreland of the Andes: northern Sierras Pampeanas (26°-28° S), Argentina. *Tectonics*, 8, 517-534.
- Tait, J. (1999). New early Devonian paleomagnetic data from NW France: paleogeography and implication for the Armorican microplate hypothesis. *J. Geophys. Res.*, 104, 2831-2839.
- Tapponnier, P., and Molnar, P. (1976). Slip-line field theory and large-scale continental tectonics. *Nature*, 264, 319-324.
- Tapponnier, P., Peltzer, G., Le Dain, A. Y., Armijo, R. Cobbold, P. R. (1982). Propagating extrusion tectonics in Asia: New insights from simple experiments with plasticine. *Geology*, 10, 611-616.
- Tarling, D.H. (1983). *Paleomagnetism*. Chapman and Hall, London, 397 pp.
- Tauxe, L. (1998). *Paleomagnetic Principles and Practice*. Kluwer Academic Publishers, pp. 293.
- Taylor, G.K., B. Dashwood, J. Grocott (2005). The central Andean rotation pattern: Evidence of an anomalous terrane in the forearc of northern Chile from paleomagnetic rotations. *Geology*, 33, 777-780.
- Taylor, G.K., J. Grocott, B. Dashwood, M. Gipson, C. Arévalo (2007). Implications for crustal rotation and tectonic evolution in the central Andes fore arc: New paleomagnetic results from the Copiapo region of northern Chile, 26°–28°S, *J. Geophys. Res.*, 112, B01102, doi:10.1029/2005JB003950.
- Thomas, W.A. (1977). Evolution of Appalachian salients and recesses from reentrants and promontories in the continental margin. *American Journal of Science*, 277, 1233-1278.
- Torres-Carbonell, P.J., Olivero, E.B., Dimieri, L.V. (2008a). Control en la magnitud de desplazamiento de rumbo del Sistema Transformante Fagnano, Tierra del Fuego, Argentina. *Rev. Geol. Chile*, 35, 63-79.
- Torres-Carbonell, P.J., Olivero, E.B., Dimieri, L.V. (2008b). Structure and evolution of the Fuegian Andes foreland thrust-fold belt, Tierra del Fuego, Argentina: Paleogeographic implications. *J. South Am. Earth Sci.*, 25, 417-439.
- Tropeano, M., L. Sabato, P. Pieri (2003). Filling and cannibalization of a foredeep: The Bradanic Trough, southern Italy, in *Sediment Flux to Basins: Causes, Controls and Consequences*, edited by S. J. Jones and L. E. Frostick, *Geol. Soc. Spec. Publ.*, 191, 55-79.
- Turner, J.C.M., V. Méndez, C.S. Lurgo (1979). Geología de la region noroeste, provincias de Salta y Jujuy, Republica Argentina, *Actas 7th Congr. Geol. Arg.*, 1, 367-387.
- Urreiztieta, M. de, D. Gapais, C. Le Corre, P.R. Cobbold, E. Rossello (1996). Cenozoic dextral transpression and basin development at the southern edge of the Puna Plateau, northwestern Argentina. *Tectonophysics*, 254, 17-39.
- Van der Voo, R. (1969). Paleomagnetic evidence for the rotation of the Iberian peninsula. *Tectonophysics*, 7, 5-56.

- Van der Voo, R., Zijdeveld, J.D.A. (1969). Paleomagnetism in the western Mediterranean area. *Verh. K. Ned. Geol. Mijnbouwk. Genoot., Geol. Ser.*, 26, 121-138.
- Van der Voo, R., J.E.T. Channell (1980). Paleomagnetism in orogenic belts. *Rev. Geophys. Space Phys.*, 18, 455-481.
- Van der Voo, R., A.N. French, R.B. French (1979). A paleomagnetic pole position from the folded upper Devonian Catskill red beds, and its tectonic implications. *Geology*, 7, 345-348.
- Van der Voo, R., Stamatakos, J.A., Parés, J.M. (1997). Kinematic constraints on thrust-belt curvature from syndeformational magnetizations in the Lagos del Valle Syncline in the Cantabrian Arc, Spain. *J. Geophys. Res.*, 102, 10,105–10,119.
- Velencio, D.A., J.E. Mendia, A. Giudici, J.O. Gascon (1977). Paleomagnetism of the Cretaceous Pirgua Subgroup (Argentina) and the age of the opening of the South Atlantic. *Geophys. J. R. Astron. Soc.*, 51(1), 47-58.
- Walcott, C.R., S.H. White (1998). Constraints on the kinematics of post-orogenic extension imposed by stretching lineations in the Aegean region. *Tectonophysics*, 298, 155-175.
- Weil, A.B. (2006). Kinematics of orocline tightening in the core of an arc: Paleomagnetic analysis of the Ponga Unit, Cantabrian Arc, northern Spain. *Tectonics*, 25, TC3012, doi:10.1029/2005TC001861.
- Weil, A.B., A.J. Sussman (2004). Classifying curved orogens based on timing relationship between structural development and vertical-axis rotations. *Geol. Soc. Am. Spec. Paper*, 383, 1-15.
- Weil, A.B., Van der Voo, R., Van der Pluijm, B.A., Parés, J.M. (2000). The formation of an orocline by multiphase deformation: A paleomagnetic investigation of the Cantabria-Asturias Arc (northern Spain). *Journal of Structural Geology*, 22, 735–756.
- Weil, A.B., Van der Voo, R., Van der Pluijm, B.A. (2001). Oroclinal bending and evidence against the Pangea megashear: The Cantabria-Asturias Arc (northern Spain). *Geology*, 29, 991–994.
- Wigger P, M. Schmitz, M. Araneda, G. Asch, S. Baldzuhn, et al. (1994). Variation in the crustal structure of the southern Central Andes deduced from seismic refraction investigations. In: Reutter, K.J., Scheuber, E., Wigger, P.J. (Eds.), *Tectonics of Southern Central Andes: Structure and Evolution of an Active Continental Margin*. Springer-Verlag, New York, pp. 23– 48.
- Winslow, M.A. (1982). The structural evolution of the Magallanes Basin and Neotectonics in the Southernmost Andes. In: Craddock, C., (Ed.), *Antarctic Geoscience*, University of Wisconsin, Madison, pp. 143-154.
- Wortel, M.J.R., Spakman, W. (1992). Structure and dynamics of subducted lithosphere in the Mediterranean region. *Proc. K. Ned. Akad. Wetensch.* 95, 325–347.
- Zachos, J., Pagani, M., Sloan, L., Thomas, E., Billups, K. (2001). Trends, rhythms, and aberrations in global climate 65 Ma to present. *Science*, 292, 686–693.
- Zijdeveld, J.D.A. (1967). A.C. demagnetization of rocks: Analysis of results, In: *Methods in Palaeomagnetism*, Collinson, D.W., K.M. Creer, and S.K. Runcorn (Eds), Elsevier, New York, pp. 254–286.

- Zweigel, P. (1997). The Tertiary tectonic evolution of the Eastern Carpathians (Romania): Orogenic arc formation in response to microplate movements. *Tubinger Geowissenschaftliche Arbeiten, Series A*, 33, 1-158.
- Zweigel, P. (1998). Arcuate accretionary wedge formation at convex plate margin corners: results of sandbox analogue experiments. *J. Stru. Geol.*, 20, 1597-1609.
- Zweigel, P., L. Ratschbacher, W. Frisch (1998). Kinematics of an arcuate fold-thrust belt: the southern eastern Carpathians (Romania). *Tectonophysics*, 297, 177-207.